Universidade de Lisboa

Instituto de Geografia e Ordenamento do Território

Landforms and Geoecological Units of Pingo Canadian Landmark (Northwest Territories, Canada): A Remote Sensing-Based Approach

Daniel Luis Giestal Baptista

Mestrado em Geografia Física e Ordenamento do Território

Dissertação de Mestrado orientada pelo Doutor Gonçalo Brito Guapo Teles Vieira e pelo Doutor Pedro Miguel Berardo Duarte Pina

2024

Universidade de Lisboa
Instituto de Geografia e Ordenamento do Território

Landforms and Geoecological Units of Pingo Canadian Landmark (Northwest Territories, Canada): A Remote Sensing-Based Approach

Daniel Luis Giestal Baptista

Mestrado em Geografia Física e Ordenamento do Território

Dissertação de mestrado orientada pelo Doutor Gonçalo Brito Guapo Teles Vieira e pelo Doutor Pedro Miguel Berardo Duarte Pina

Júri:
Presidente: Doutor Sérgio Manuel Cruz de Oliveira, Professor Auxiliar do Instituto de Geografia e Ordenamento do Território da Universidade de Lisboa
Vogais:
- Doutor António Alberto Teixeira Gomes, Professor Associado da Faculdade de Letras da Universidade do Porto
- Doutora Paula Sofia Antunes Matos, Investigadora Júnior do Instituto de Geografia e Ordenamento do Território da Universidade de Lisboa

2024

Declaração de Autoria

Eu Daniel Luis Giestal Baptista, declaro que a presente dissertação de mestrado intitulada "*Landforms and Geoecological Units of Pingo Canadian Landmark (Northwest Territories, Canada): A Remote Sensing-Based Approach"*, é o resultado da minha investigação pessoal e independente. O conteúdo é original e todas as fontes consultadas estão devidamente mencionadas na bibliografia ou outras listagens de fontes documentais, tal como todas as citações diretas ou indiretas têm devida indicação ao longo do trabalho segundo as normas académicas.

ABSTRACT

Pingo Canadian Landmark (PCL) is a 16.6 km^2 protected coastal area located in the southwest region of Tuktoyaktuk Peninsula (Northwest Territories, Canada). PCL presents great geomorphological significance, containing characteristic permafrost landforms, such as pingos and tundra polygons. The scientific value of PCL gains even more relevance in a context of climate change, which is known to have particularly strong impacts on the Arctic (Cohen et al., 2014; Davy et al., 2018; Screen & Simmonds, 2010; Stjern et al., 2019). Much scientific evidence points to the increasing magnitude of coastal erosion and permafrost degradation, linked to higher air and sea temperatures, and marine storms, which may put the unique landforms of PCL at risk (Holland et al., 2023; Irrgang et al., 2018; Karjalainen et al., 2020; Lim et al., 2020a; Lim et al., 2020b; O'Rourke, 2017; Parker, 2021; Vermaire et al., 2013).

The focus of this dissertation is to present a very detailed analysis of the landscape of PCL, supported by high quality remote sensing data. This analysis primarily includes: a Geomorphological Map, based on an ultra-high resolution (10 cm) optical orthomosaic and Digital Surface Model, captured in July 2019 using Unmanned Aerial Vehicles; and a supervised classification Landcover Map, based on very-high resolution (46 cm) WorldView-2 satellite imagery from 2017. The combined interpretation of these results permitted the identification of homogeneous sectors in terms of geomorphology and vegetation within PCL (geoecological units). Additionally, historic data (archived aerial photographs from 1950 to 2004) are interpreted to identify general trends of coastal erosion in the study area, and areas with direct anthropogenic impacts on PCL's landscape are pointed out. The selected methodologies allowed to develop an unprecedentedly detailed and multifaceted diagnosis of PCL's landscape. Also, hopefully this study will aid in the management of PCL and the conservation of its geoheritage.

Keywords: Remote Sensing; Precision Cartography; Tundra Geomorphology; Tundra Geoecology; Pingos.

RESUMO

Pingo Canadian Landmark (PCL) é uma área costeira protegida com 16,6 km^2, gerida pelo Parks Canada, em conjunto com o Inuvialuit Land Administration e o povo de Tuktoyaktuk (uma aldeia localizada cerca de 5 km a nordeste da área protegida). PCL insere-se nos Territórios do Noroeste (Canadá), mais precisamente na região sudoeste da Península de Tuktoyaktuk, junto ao delta do Rio Mackenzie. Esta é a região do mundo com maior concentração de pingos (Mackay, 1979, 1998). Os pingos são formas de relevo periglaciais que correspondem a sobrelevações do terreno com núcleos de gelo no seu interior, tipicamente associadas a áreas de permafrost contínuo. O termo "periglacial" refere-se a ambientes frios, mas não glaciares, normalmente localizados na periferia das regiões glaciares. Resumidamente, pode-se dizer que nestes ambientes, a congelação e o degelo do solo, bem como os processos de ação do gelo, são as dinâmicas geomorfológicas dominantes que controlam a paisagem. Quanto ao termo "permafrost" (ou pergelissolo), pode ser genericamente definido como sendo solo que permanece congelado durante um período mínimo de 2 anos. Além dos pingos, outra forma de relevo periglacial também característico da paisagem de PCL são as extensas redes de polígonos de tundra. Estes têm origem na contração térmica do solo, provocada pelas contínuas baixas temperaturas que caracterizam as regiões polares. Essa contração resulta na formação de fendas no solo, que depois acabam por ser preenchidas durante os meses menos frios do ano por água no estado líquido precipitada. Esta água congela quando as temperaturas baixam novamente (formando o que normalmente é chamado de "cunha de gelo"), resultando no alargamento da fenda. Por sua vez, o alargamento da fenda traduz-se num aumento da sua capacidade de albergar água líquida durante as estações menos frias, sendo que esse maior volume de água irá depois congelar, resultando num processo cíclico de progressivo crescimento das cunhas de gelo ano após ano (French, 2007; Williams & Smith, 1989).

PCL apresenta um grande interesse ao nível geomorfológico, uma vez que as suas formas de relevo existem apenas em ambientes de permafrost e sob condições bastante específicas. Aliada ao seu valor científico, a paisagem de PCL é também de grande importância cultural para o povo Inuvialuit. Por exemplo, ainda hoje os pingos desempenham um papel prático na vida dos Inuvialuit, fornecendo pontos de vista estratégicos para a caça, ou funcionando como referências para a orientação ou navegação (Inuvialuit Regional Corporation, 2011, 2020). O valor científico, e cultural, associado a esta área de estudo ganha ainda mais relevância num contexto de alterações climáticas, que se sabe terem um impacto particularmente forte no Ártico (Cohen et al., 2014; Davy et al., 2018; Screen & Simmonds, 2010; Stjern et al., 2019). Muitas evidências científicas apontam para um aumento na

frequência e magnitude dos fenómenos de erosão costeira e degradação do permafrost no Ártico, ligados ao aumento das temperaturas do ar e do mar, e ao aumento das tempestades marinhas e costeiras, que podem colocar os pingos e outras formas de relevo de PCL em risco (Holland et al., 2023; Irrgang et al., 2018; Karjalainen et al., 2020; Lim et al., 2020a; Lim et al., 2020b; O'Rourke, 2017; Parker, 2021; Vermaire et al., 2013).

O foco principal desta dissertação é apresentar uma análise muito detalhada da paisagem recente de PCL, apoiada em dados de deteção remota de muito elevada resolução. Esta inovadora e abrangente avaliação da paisagem traduz-se principalmente nos seguintes dois objectivos: **(i)** Criar um Mapa Geomorfológico preciso, com base num ortomosaico ótico de ultra-alta resolução (10 cm) e num Modelo Digital de Superfície (MDS), captado no terreno em julho de 2019 por uma equipa composta por elementos do Centro de Estudo Geográficos (CEG) e Instituto de Geografia e Ordenamento do Território da Universidade de Lisboa (IGOT), bem como do Geological Survey of Canada (GSC), utilizando drones, ou veículos aéreos não tripulados (VANTs). Este mapa é composto por vinte classes e subclasses, todas elas digitadas manualmente por fotointerpretação, e cujas designações traduzidas podem ser as seguintes (subclasses em itálico): "Pingos"; "*Crateras dos Cumes dos Pingos e Fendas de Dilatação dos Pingos*"; "*Erosão Superficial em Pingos*"; "Polígonos de Tundra"; "Lagos e Charcos"; "Acumulações de Madeira"; "Antigas Bacias de Lago"; "Bacias de Lago Inundáveis"; "*Grandes Lagos e Charcos Isolados*"; "*Pantanais*"; "*Pantanais com Lagos e Charcos*"; "*Pantanais Secos*"; "*Pantanais Secos com Pequenos Lagos e Charcos*"; "Colinas de Gelo"; "Areia"; "Arribas Costeiras e Vertentes em Recuo devido ao Degelo"; Planícies de Tundra"; "Passadiço para Turistas"; "Linhas Sísmicas (Associadas à Exploração do Petróleo)"; e "Rastos de Viaturas". De entre estas classes e subclasses, verificou-se que as três com maior representatividade em PCL foram as "Planícies de Tundra" (correspondendo a 24,03% da área de estudo), "Polígonos de Tundra" (21,27%) e "Bacias de Lago Inundáveis" (11,59%). Já as classes e subclasses com menor representação foram "*Crateras dos Cumes dos Pingos e Fendas de Dilatação dos Pingos*" e "*Erosão Superficial em Pingos*" (cada uma com 0,19%), "Linhas Sísmicas (Associadas à Exploração do Petróleo)" (0,09%), e "Passadiço para Turistas" (0,01%). **(ii)** Criar um Mapa de Cobertura do Solo, através de uma classificação supervisionada aplicada a uma imagem captada pelo satélite comercial WorldView-2, de muito-alta resolução (1,84 m - 8 bandas multiespectrais, 46 cm - pancromática), e de 2017. Este mapa é composto por nove classes, cujas designações traduzidas podem ser as seguintes: "Vegetação Alta de Tundra"; "Vegetação Baixa de Tundra"; "Tundra Seca"; "Tundra Inundada"; "Solo Exposto"; "Areia"; "Areia Húmida e Lama"; "Acumulações de Madeira"; e "Estruturas Antrópicas". De entre elas, as três com maior presença em PCL são "Vegetação Baixa de Tundra" (correspondendo a 23,3% da área de estudo), "Vegetação Alta de Tundra"

(18,42%), e “Tundra Seca” (10,58%). As que revelaram ter menor presença são “Areia Húmida e Lama” (1,86%), “Estruturas Antrópicas” (1,3%) e “Areia” (0,85%). Convém também indicar que foi efetuada uma análise de desempenho da classificação supervisionada, nomeadamente através do cálculo da respetiva Matriz de Confusão, com uma Exatidão Média (Overall Accuracy) elevada, de 94,35%.

A interpretação combinada dos resultados anteriormente mencionados permitiu identificar cinco setores homogéneos em termos de vegetação e geomorfologia para PCL, designadas por unidades geoecológicas, podendo elas ter as seguintes traduções: “Pingos” (que abrange 1,99% da área de estudo, sendo a menos representativa); “Tundra Elevada” (24,35%, sendo a mais representativa); “Tundra Baixa” (21,79%); “Tundra Inundada” (12,76%); e “Tundra Costeira” (17,43%). Além disto, fotografias aéreas arquivadas que abrangem um intervalo temporal de 67 anos (pertencendo aos anos 1950, 1967, 1972, 1985, 2000 e 2004) foram interpretadas, incluindo a digitação da linha da costa em PCL para cada uma delas, e comparadas com a imagem WorldView-2 de 2017 (para a qual também foi digitada a linha de costa em PCL), com o intuito de identificar tendências gerais de erosão costeira na área de estudo ao longo desse período. Ainda, foram apontadas áreas dentro de PCL onde os impactos antrópicos diretos na paisagem são notórios, sendo que estes impactos estão predominantemente associados à circulação de veículos motorizados dentro dos limites de PCL, uma atividade que oficialmente está proibida nesta área protegida precisamente por razões de conservação da natureza.

Em suma, as metodologias selecionadas permitiram desenvolver um diagnóstico inédito, detalhado e multifacetado da paisagem de PCL do ponto de vista geoecológico. Além disso, espera-se que os resultados e conclusões alcançados ajudem na gestão do parque e na preservação do seu geopatrimónio.

Palavras-chave: Deteção Remota; Cartografia de Precisão; Geomorfologia de Tundra; Geoecologia de Tundra; Pingos.

ACKNOWLEDGEMENTS

First, I would like to acknowledge all the institutions and groups that are associated with this study. Thank you to the Nunataryuk project (funded by the European Union's Horizon 2020 Research and Innovation Programme under grant agreement no. 773421, and by the Climate Change Preparedness in the North Program of the Government of Canada). Several members of this project provided valuable insight into the scientific research of the arctic, and much appreciated advice regarding my work. Thank you to the Centro de Estudos Geográficos (CEG), Instituto de Geografia e Ordenamento do Território (IGOT), and to the Geological Survey of Canada (GSC), namely to the team comprised by members of these institutions that obtained the field data without which this research project would not be possible. Thank you to the people of Tuktoyaktuk, to the Hamlet of Tuktoyaktuk, and to Parks Canada for permitting and supporting the before mentioned field activities. Thank you to Natural Resources Canada, especially to Mr. Dustin Whalen, for also providing important data for this study. Also, thank you to the Portuguese Polar Program, the University of Lisbon's ZEPHYRUS research group, the University of Lisbon's POLAR2E College on Polar and Extreme Environments, and to HTC.

Next, I give great thanks to the supervisor of my dissertation, Professor Gonçalo Vieira. His valuable field expertise and knowledge regarding polar and periglacial sciences, and physical geography and GIS in general, were extremely helpful and inspiring. Additionally, his constant support and availability to talk, meet, and clarify any issues played a key role in the completion of this research project. All the same can be said of the co-supervisor of this dissertation, Professor Pedro Pina, to whom I also give great thanks. The elaboration of this study was a very long and laborious process, and both were always ready to help every step of the way, even at their own personal sacrifice.

Many thanks to my parents Rosa and Luis, for their incessant support and affection, without which the completion of this study would also not be possible. Thank you also to all my other family members that supported me and provided me with motivation. Thank you especially to my uncle João Manuel and my grandmother Maria Luísa, who always incentivized me to complete this study and my degree, but sadly never got to see it happen. Special thanks also to all my other loved ones who have passed, but that are certainly by my side in spirit.

Great thanks to my friends Álvaro, André, Gonçalo and Rita, for their much-appreciated comradery and kind-heartedness. Great thanks also to my friends and fellow colleagues from the POLAR2E College and Nunataryuk ULisbon group, Bernardo, Pedro, Rodrigue and Sofia, for their comradery and for sharing helpful knowledge and advice regarding polar studies.

Lastly, I thank all those who, in any way, inspired me to not give up in the face of adversity.

TABLE OF CONTENTS

LIST OF FIGURES

LIST OF TABLES

1 - INTRODUCTION

The Earth, and its climates, have been under continuous change ever since the planet formed, about 4600 Ma. Considering that Humankind's presence on Earth corresponds to only a very small fraction of the time that the Planet has existed, most of that change has no connection to Human behavior. However, though we have been here for such a short amount of time, that does not mean we haven't already made our mark. The Intergovernmental Panel on Climate Change (IPCC) has dedicated itself to making a scientifically substantiated case for this, namely through the six Assessment Reports it has already published, between 1990 to 2023. These Reports have presented evidence of humankind's impact on the global climate, with the most recent complete Assessment Report (from 2023) pointing out that anthropogenic greenhouse gas emissions and other anthropogenic forcing factors have unequivocally provoked global warming, especially since the 1950's (IPCC, 2023). In the sixth Assessment Report, human influence is referred to as the very likely (90-100% probability) main driver of the global retreat of glaciers since the 1990's, as well as of the reduction of Arctic Sea ice area during the periods of 1979-1988 and 2010-2019. This latest Report also points to, with a high level of confidence, the crucial relevance that ice sheet melting, as well as deep-ocean warming, have in the long-term perpetuation of sea-level rise (IPCC, 2021, 2023).

Truly, the effects of humankind's actions and climate change take a greater toll in some regions in comparison to others, and few regions on Earth are being affected as quickly and noticeably as the Arctic. The ratio that compares mean global temperature change with the mean temperature change of the Arctic, commonly referred to as the Arctic Amplification, has displayed values between 1.6 and 2.3 ºC in many studies, meaning that the Arctic has been warming roughly twice as fast as the rest of the world (Cohen et al., 2014; Davy et al., 2018; Screen & Simmonds, 2010; Stjern et al., 2019). However, some more recent studies point to an even more drastic scenario of the Arctic warming up to four times faster than the rest of the world (Rantanen et al., 2022; You et al., 2021). The rise of air, and consequently sea, temperatures can lead to the alteration of arctic landscapes, especially ones where coastal dynamics (e.g., marine storms and flooding) have a strong direct influence. In these locations, interactions between the atmosphere, the sea or ocean, and ground ice (including permafrost), can result in coastline change, through the degradation of sand spits, beaches or coastal permafrost bluffs, as well as of characteristic periglacial landforms, such as ice wedges (and the tundra polygon networks they are associated with), or pingos (Irrgang et al., 2018; Karjalainen et al., 2020). Studying these types of regions is therefore of great scientific interest, and much can be learned from them regarding the ways in which the Earth's changing climate is producing clearly perceptible changes on a number of its landscapes.

The study area that this dissertation focuses on is Pingo Canadian Landmark (PCL), a 16.56 km^2 protected coastal area located in the southwest region of Tuktoyaktuk Peninsula (Northwest Territories, Canada), near the Mackenzie River delta. With its diverse geoecological characteristics, the type of arctic coastal environment in which PCL's landscape is inserted presents many interesting features and dynamics that can be studied at several scales, both spatially and temporally, and the right resources are needed to correctly analyze them. In most cases, remote sensing is capable of corresponding to those needs, as, already for decades now, a multitude of remote sensing techniques have existed, allowing to continuously capture the state of landscapes around the globe, and making it so that they can be studied from practically any place. In addition, as remote sensing evolves, not only does the catalog of resources it has produced grow in quantity, but also, the remote sensing techniques and equipment themselves have become more and more impressive in terms of the quality of the data they can produce.

Characterizing the landscape of PCL, and understanding the geoecological dynamics of its landscape, primarily with the aid of ultra-high and very-high resolution remote sensing products, are two of the main goals of this study. To achieve these broad goals, several other, more specific, objectives were established: **(i)** Making a diagnosis and analysis of the current state of PCL's landscape, through the elaboration of a very detailed Geomorphological Map (focusing on permafrost features, and even some direct man-made changes to the park), produced by visual analysis of an ultra-high-resolution optical orthomosaic and Digital Surface Model (DSM), built with data captured in surveys carried out in July 2019 using Unmanned Aerial Vehicles (UAV); **(ii)** Creating a Landcover Map, based on a very-high-resolution commercial satellite (WorldView-2) scene from 2017, and using a supervised classification; **(iii)** After the conclusion and interpretation of the two previously mentioned maps, identifying homogeneous sectors within the park (in terms of geomorphology and vegetation), called geoecological units. Altogether, the work developed in this study will also hopefully provide valuable insight on how to best manage the park and assess the sensitivity of its geoheritage to climate change in the next decades.

This manuscript is divided into several chapters, with the first after this Introduction being dedicated to a Literature Review (Chapter 2), referring to several key topics associated with the dissertation's subject, namely about periglacial environments in general (Chapter 2.1), about the most prevalent periglacial landforms that can be found at Pingo Canadian Landmark (Chapter 2.2), and about some of the past studies and research concerning the park (Chapter 2.3). The next main chapter contains the Characterization of the Study Area (Chapter 3), including a framework of regional geology and geomorphology (Chapter 3.1.1), and climate and ocean dynamics (Chapter 3.1.2), as well as some information on the unique cultural

heritage of the region's Inuvialuit people (Chapter 3.2). Next, Chapter 4 will be dedicated to the explanation of the various Data used and Methods applied during the several practical procedures carried out in order to achieve the already mentioned objectives of this dissertation. Then, the results of those procedures will be presented in Chapter 5. Afterwards, a critical discussion of the results will be done in Chapter 6, which will include a final conjoined interpretation of the previously presented results (translated into the Geoecological Map), and a connection will be established between the results of this study and the context of climate change and man-induced impacts on the land. Some final considerations about this study, including limitations verified throughout its elaboration and recommendations for future research, as well as the central conclusions reached, will be presented in Chapter 7.

2 - LITERATURE REVIEW

2.1 – Permafrost and Periglacial Environments

The term “periglacial” refers to cold, but non-glacial, environments, normally located in the periphery of actual glacial regions. Summarily, it can be said that in these types of environments, ground freezing and thawing, as well as frost-action processes, are the commanding dynamics that transform the landscape (French, 2007).

In all biomes, the climate is one of the most important controlling factors on the landscape, and in periglacial environments, this is equally true. When we take into consideration several criteria that are intrinsically associated with climate, such as temperature, insolation and altitude, according to French (2007), we can discern a varied group of periglacial sub-climates.

One of those are the **high arctic climates** of the polar latitudes, which include for example Tuktoyaktuk Peninsula, which is where the study area of this dissertation is located, and Banks Island (both in the Northwest Territories, Canada), or Svalbard (an island of the Norwegian archipelago of Svalbard). These are characterized by their extremely cold winters (where temperatures may reach around -30 ºC), and less cold summers (where temperatures may rise to about +6 ºC). The summers are, however, short lasting (only 2 to 3 months long), though still, during them, the superficial layers of the soil tend to thaw. Therefore, it can be stated that this sub-climate is characterized by having a considerable seasonal variation in temperature, and also a strong seasonal variation in insolation (as during part of the year they undergo continuous darkness, and during another part continuous daylight). For the same reasons, they are characterized by a weak daily variation in both insolation and temperature. As for precipitation, it tends to be of low values, ranging from around 100 mm/year to 400 mm/year in more maritime locations. Despite this, since the very cold temperatures provide perfect conditions for the formation of a continuous, and mostly impervious, permafrost in the subsurface, the precipitated water tends to accumulate near the ground surface, which in the summer can lead to a humid, bog-like landscape (French, 2007).

There are also periglacial environments that have **continental** characteristics, which are commonly located at subarctic latitudes. This type of periglacial sub-climate can be found, for example, in Central Siberia and in the Canadian Yukon. Though these two already mentioned sub-climates have relatively similar mean annual air temperatures, the continental sub-climates have even greater seasonal variations in temperature in comparison to the high arctic ones, as their winters tend to be even colder (sometimes lower than -40 ºC), and their

summers quite warmer (reaching as high as +20 ºC in some locations) and longer lasting. The annual thermal amplitude is therefore very high in these continental areas. Since these regions are more frequently influenced by the Arctic and Polar Fronts, they are also characterized by higher precipitation rates than the high arctic climates (ranging from 250 mm to 600 mm/year, with a higher concentration in the summer). However, the warm summers also lead to higher evaporation rates (resulting in a drier landscape), and are not as favorable to the existence of surface-level permafrost. Thus, boreal forests or taiga commonly form, with arboreal species of the *Pinaceae* family, commonly denominated as pines, spruces and tamaracks (e.g., *Pinus silvestris, Picea glauca, Picea mariana* and *Larix dahurica*) or of the of *Betulaceae* family, namely the *Betuloideae* subfamily, commonly referred to as birches (e.g., *Betula pubescens*) (French, 2007).

Another type of periglacial sub-climate that can be identified is that of the **Tibet (Qinghai-Xizang) Plateau**. The unique characteristics of this region were considered distinct enough for it to deserve its own sub-climate, according to French (2007). In comparison to the previous two sub-climates, this one is located at much lower latitudes, conferring to it more balanced day-night and seasonal cycles. Therefore, aside from having large seasonal variations in insolation, these regions have great daily insolation variations too. Also, insolation becomes even more of an influential factor given the very high altitudes that can be reached in these regions (4200 to 4800 m). This has an important relationship with precipitation, as most of the 200 mm to 600 mm/year observed there are evaporated, which in return hinders vegetation development. Therefore, the landscapes of this part of the world are relatively barren, being characterized as “steppe-tundra”. Also, in these regions, mean annual air temperatures tend to be of around -2 ºC to -6 ºC, but do not deviate substantially from that average throughout the year. All these conditions, associated with insolation, temperature and elevation, result in this region being affected by a more frequent occurrence of thaw-freeze cycles throughout the year in comparison to the previously mentioned sub-climates.

There are also **alpine periglacial climates**. They occur at mid-latitudes, for example, in the Alps of Europe and in the Rockies of North America, above the tree lines of those mountain ranges, which can be located at 2000 m to 4000 m of altitude. They also can occur at much lower altitudes in areas where the tree line is also much lower, such as in Iceland or northern Scandinavia. They have some similarities with the previously mentioned region of the Tibet Plateau. For example, in both there is a high diurnal and seasonal variation in insolation, and in both there is a high frequency in the freeze-thaw cycle. However, of all the sub-climates so far mentioned, the periglacial Alpine climate is the one which has a less rigorous winter, and also that which has highest precipitation values (750 to 1200 mm/year), being that much of this precipitation occurs in the form of snow. Unlike the Tibet Plateau, however, evaporation

is not a strong factor here. The snow cover, which tends to be thick, combined with the lack of yearlong extreme cold, leads to these regions having discontinuous or no permafrost at all (French, 2007).

A final major periglacial sub-climate that can be identified are the so-called **climates of low annual temperature range**. The temperatures of these locations are low year-round, but they deviate very little from 0 ºC throughout the whole year (usually by no more than 5 to 10 ºC). Similar to the Tibet Plateau, and especially to the alpine periglacial climates, these areas display a high frequency of freeze-thaw cycles, which tend to have impact only up to shallow depths of ground. The areas where these characteristics occur are rather restricted in terms of geographic extent, and include a somewhat varied group of places, ranging from sub-arctic oceanic locations such as the Falkland Islands (where the surrounding ocean mitigates variations in the temperature), to the summits of low-latitude mountains or volcanoes, such as Hawaii's Mauna Loa (where seasonal variations are weak, leading to also weak variations in the temperature throughout the year) (French, 2007).

Still, French (2007) mentions an additional sixth sub-climate, and it corresponds to the small, arid, very cold, **ice-free areas that exist in peripheral parts of the Antarctic continent**, such as in southern and northern Victoria Land. These areas are affected by very strong katabatic winds, which are so intense that they do not allow the formation of perennial snow or ice. In sum, all six of the sub-climates that have just been characterized can be considered as periglacial, which leads to the conclusion that periglacial environments are quite diverse.

As seen in the previous descriptions of the several types of periglacial sub-climates, permafrost is undoubtedly an essential term to understand when characterizing periglacial environments. Traditionally, permafrost is a term used to refer to permanently, or perennially, frozen ground, with a more precise definition pointing out that the ground (soil and/or rock, possibly also including organic matter and/or ice content) must maintain itself at a temperature of, or lower than, 0 ºC for at least 2 consecutive years, to achieve the status of permafrost (Figure 1) (French, 2007; Williams & Smith, 1989). However, as mentioned in the literature, the commonly used description of permafrost as "perennially frozen ground" can be reductive. This is because the permafrost may not be entirely frozen. Due to factors such as the mineralogical composition of the soil and rocks (e.g., the presence of mineral salts), it is possible for unfrozen liquid water to exist in the ground even at below 0 ºC temperatures (French, 2007; Williams & Smith, 1989). Nevertheless, for the purpose of this study, the commonly used definition (ground that remains at ≤ 0°C during at least two consecutive years) shall be acknowledged as sufficient.

Figure 1 *- Permafrost (exposed as the result of erosion) in the Northwest Territories, Canada. Source: Rowley (2015).*

Permafrost landscapes, closely linked to periglacial environments as already mentioned, can be very complex, especially when we examine their constitution below the ground surface. An important way in which permafrost landscapes can be classified is by taking into account the spatial extent of the region that the permafrost occupies. According to this method of classification, areas with the presence of permafrost can assume one of the four following sub-types: Continuous permafrost areas, where the perennially frozen ground occupies 90 to 100% of the surface area; Discontinuous permafrost areas, where it covers 50 to 90% of the surface area; Sporadic permafrost areas, where only between 10 and 50% of the ground is perennially frozen; and Isolated permafrost areas, where less than 10% of the ground surface corresponds to permafrost (Barry & Gan, 2011; French, 2007). Also, despite being frozen ground, permafrost may vary greatly in terms of its temperature, with a distinction many times being made between “warm” and “cold” permafrost, with the first presenting temperatures closer to 0 ºC, and the latter presenting temperatures much lower than the freezing threshold. The colder the mean annual temperatures are, typically greater will be the extent of ground occupied by permafrost, as well as its thickness. There are regions of the world where, even with the seasonal variations of the temperatures, these very rarely go above 0 ºC, providing stable conditions for prolonged permafrost aggradation (increase in thickness or extent of the permafrost), and the formation of continuous permafrost (French, 2007; Williams & Smith, 1989). In these regions, permafrost may reach hundreds of meters of depth (sometimes, even more than a kilometer) and may have thousands, or even tens of thousands of years of age (Williams & Smith, 1989). On the other hand, there are regions where several factors may hinder the development of the permafrost. One of the most important of those factors is the type of soil cover, as, for example, the presence of vegetation or snow at the surface can shield the ground, inhibiting heat exchanges between it and the very cold atmosphere, and leading to the existence of discontinuous or sporadic permafrost. Naturally,

the effects associated with soil cover, as well as with variations in the actual air temperature, are more noticeable near the ground surface, and they gradually diminish in depth, where the annual thermal amplitude gets smaller. The level at which seasonal fluctuations in air temperature no longer have influence on the temperature of the ground, or in other words, where thermal annual amplitude is zero, is called the Depth of Zero Annual Amplitude, and it can be situated at 10 to 15 m deep, or deeper, in rock (French, 2007; Williams & Smith, 1989).

As has been explained, periglacial environments are not entirely composed of permafrost. In many periglacial regions, especially those where mean monthly temperatures tend to fluctuate around 0 ºC, the near-surface layer of soil, located above the permafrost, will seasonally thaw (typically in the summer) and re-freeze (typically in the autumn). This layer of soil is designated the "active layer" (French, 2007; Williams & Smith, 1989). The active layer is normally thinner (around 10 to 15 cm) in polar regions, and thicker (1 m or more) in subarctic regions, as the latter present greater seasonal variations in temperature (French, 2007; Williams & Smith, 1989). In addition to the active layer, the literature points out another ground layer typical of permafrost regions. It is called the "transient layer" and is usually defined as the layer of soil located between the active layer and the uppermost limit of the permafrost, characterized by being very rich in ice. It goes through freeze-thaw cycles that are longer than that of the active layer, but shorter than that of permafrost *per se*. These cycles may reach the decadal or even centurial scale, as it maintains itself frozen in colder years, and thaws in years where the temperatures are higher. This way, it would be correct to say that the transient layer can technically be considered permafrost, if it remains frozen for at least two consecutive years (French, 2007; French & Harbor, 2013).

It is not uncommon for there to exist areas of ground that are continuously unfrozen, but surrounded by permafrost. These are called "taliks", and their formation can be associated with continuous thermal disturbances at the surface (such as the presence of vegetation, snow, or, very frequently, bodies of water), properties of the soil and groundwater it contains, wildfires, or the construction and usage of infrastructures, (French, 2007; O'Neill et al., 2020). According to O'Neill et al. (2020), there are several types of taliks that can be distinguished, and they are divided into three main groups: Suprapermafrost taliks; Intrapermafrost taliks; and Open or Through taliks (Figure 2). **Suprapermafrost taliks** are those that exist close to the ground surface, between the active layer and the perennially frozen ground itself. It is frequent for these types of taliks to exist beneath a water body, such as a lake or river, due to the mitigation effect that water normally has on temperature variations, which in this case leads to a less noticeable decrease in ground temperatures underneath the water body. In the case of that water body disappearing, these taliks may refreeze. **Intrapermafrost taliks** are entirely surrounded by perennially frozen ground. Being confined by the permafrost, they are for the

most part hydraulically isolated, and any ground water they contain will also be confined. To the contrary, **Open or Through taliks** (sometimes also called “Through-going taliks”) are those that penetrate through the permafrost. Therefore, they correspond to sections of unfrozen ground that establish a connection between the surface and unfrozen areas that underlie the perennially frozen ground (or sub-permafrost areas) (French, 2007; O’Neill et al., 2020). Taliks, especially through taliks, play a crucial role in the distribution of groundwater in permafrost regions, and consequently, they also have an important connection to the way heat transfers take place beneath the ground (Williams & Smith, 1989).

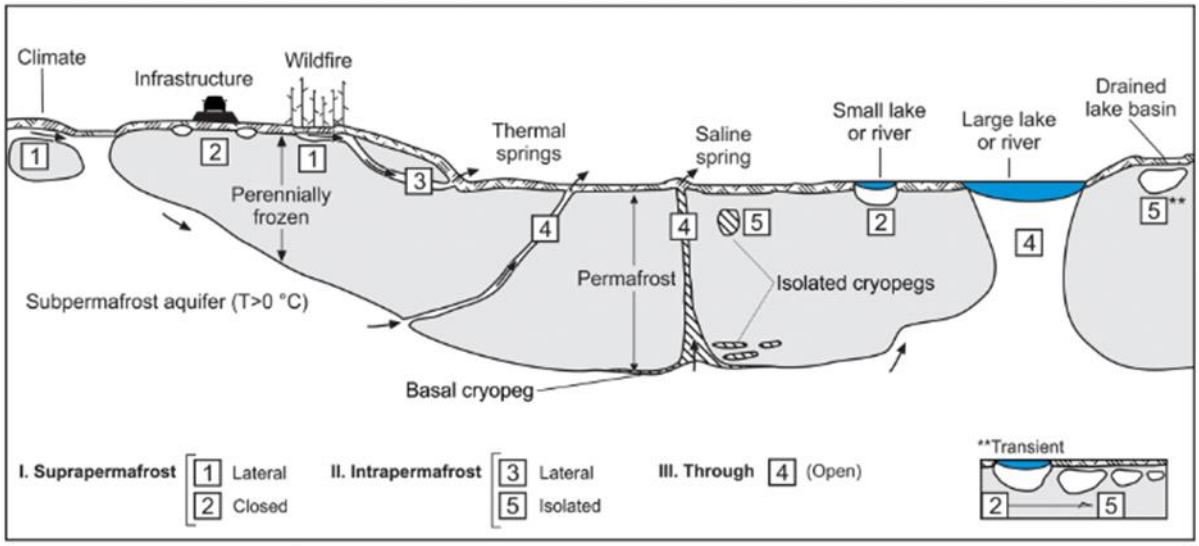

Figure 2 *- Talik configurations, hydraulic connectivity, and mechanisms/features associated with talik formation. Source: O’Neill (2020).*

It should be explained that it is incorrect to affirm that permafrost “melts”. As it is a composite of soil, rock, organic matter and groundwater, it is therefore more correct to say that it “thaws” (Grosse et al., 2010). However, in permafrost regions and periglacial environments, there is also pure ice in the ground. As commonly explained in the literature, four types of ground ice can be distinguished: pore ice, segregated ice, intrusive ice and vein ice (Barry & Gan, 2011; French, 2007; Harris et al., 1988; Mackay, 1979; Rowley et al., 2015; Sharma, 2010; Williams & Smith, 1989). Pore ice (or interstitial ice) is that which occupies the interstitial spaces between soil grains, cementing them together. It forms when pore water in the ground freezes *in-situ* (Figure 3). **Segregated ice** forms in layers or lenses in the soil, when pore water migrates in direction towards the 0 ºC freezing plane (Figure 4). **Intrusive ice** (sometimes called intrusion ice, or injection ice) is formed when groundwater is injected, usually due to upward pressures, into a perennially or seasonally frozen zone. There, confined by its enclosing sediments, it freezes, typically forming a clear and sharp contact with those enclosing sediments (Figure 5). **Vein ice** is associated with the infiltration of water (for example, melted snow) into small fissures at the surface-level of the ground, such as thermal

contraction fissures. This water later freezes, leading to the expansion of those fissures, many times forming what are called “ice wedges” (Figure 6).

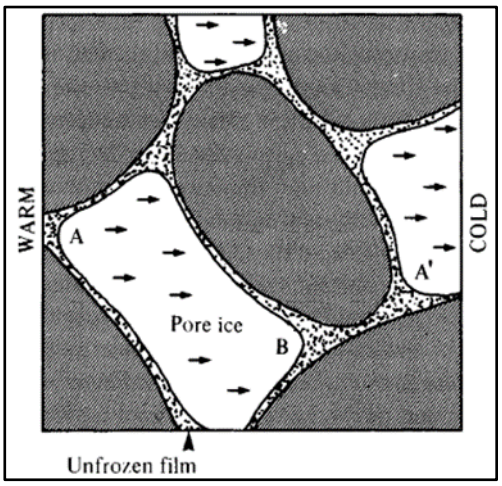

Figure 3 *- Pore ice, and series-parallel transport in a frozen non-colloidal soil. Source: Williams & Smith (1989).*

Figure 4 *- Segregated ice, formed slightly below the surface, pushing soil particles upwards. Note the slight mounding that is occurring. Source: Rowley (2015).*

Figure 5 *- Intrusive ice (the ground surface also shows abundant effects of seasonal frost heave). Source: Williams & Smith (1989).*

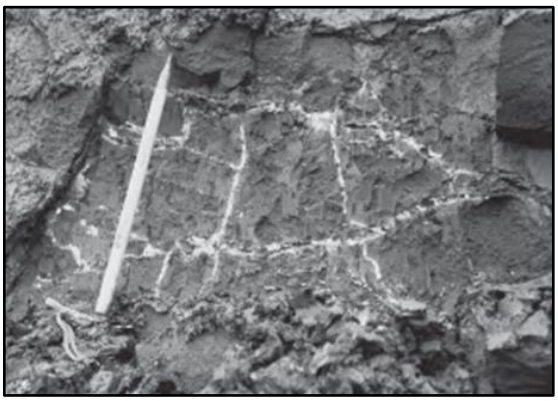

Figure 6 *- Network of vein ice, formed in a silty clay diamicton. Source: French (2007).*

It is important to remember that upon freezing, water’s volume expands by 9%, and, when subjected to temperatures of -22 ºC, the expansion reaches its maximum, of about 13.5%. At temperatures even lower than this, the frozen water will actually begin to contract (French, 2007; Sharma, 2010). This fact becomes very relevant when we try to understand the several ways in which freeze-thaw processes can have morphogenetic effects. Cryoturbation, permafrost creep, frost creep, gelifluction, gelivation, ice segregation and thermal contraction are some of the main processes that mold periglacial landscapes, and the last two of these processes lead to the formation of very characteristic periglacial landforms, pingos and tundra polygons, respectively, which are both present in PCL, the study area of this dissertation. These two types of periglacial landforms, and the mentioned processes that they are associated with, shall be addressed in the specific chapters that follow. Before that, a brief explanation of the other previously mentioned morphogenetic processes that are characteristic of periglacial environments will be done.

First, **cryoturbation** is a term that refers to several types of movements that may occur within a soil layer linked to frost-action (freeze-thaw) processes, for example, frost heave and thaw settlement, leading to the formation of small-scale landforms, such as hummocks (Figure 7) (Barry & Gan, 2011; French, 2007; Harris et al., 1988; Williams & Smith, 1989).

***Figure 7** - Examples of frost hummocks (also called "thufur"), occurring in deep seasonal frost. Source: French & Harbor (2013).*

Permafrost creep is a process that corresponds to the very slow displacement of frozen ground due to gravity, and it usually occurs in areas of ice-rich soils combined with steep slopes, especially those where temperatures tend to not be of extreme cold, leading to the existence of warm permafrost. The displacement happens when originally frozen pore water melts, migrates downslope, and then settles and freezes once again, with this process occurring repeatedly over time. Rock glaciers consist in an extreme example of permafrost creep (French, 2007).

As for **frost creep**, it's a similar process to permafrost creep, as it also involves the slow displacement of the ground in a downslope direction, but in this case that movement takes place due to the occurrence of frost heave (Figure 8). The volumetric expansion of water in the soil leads to the uplifting of some of the soil particles in a direction that is perpendicular to that of the slope, and those particles will later be deposited slightly downslope, due to the fact that the settlement occurs in a vertical downwards direction from the point where the frost heave had displaced them (French, 2007; Harris et al., 1988; Williams & Smith, 1989).

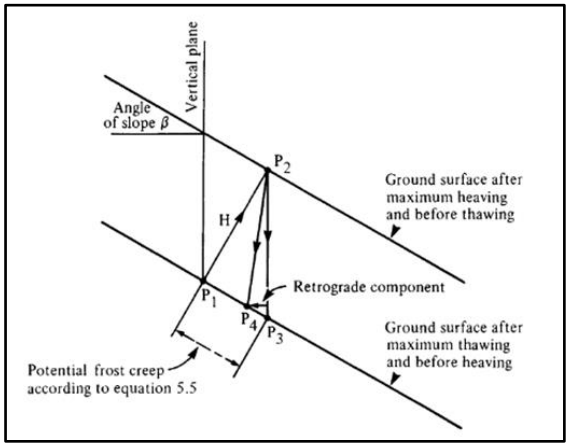

***Figure 8** – Diagram illustrating movements of a particle within a soil mass, as a result of heaving and subsequent consolidation, on a slope. Frost creep is shown. Source: Williams & Smith (1989).*

Gelifluction is yet another slow downslope mass movement. It usually takes place on slopes with underlying frozen ground (which impedes water percolation), after the melting of segregated ice (Figure 9). This makes the near-surface soil very saturated and not cohesive, leading to its flow, commonly in a laminar fashion, down the slope. The term "solifluction" is sometimes used interchangeably with the term "gelifluction". In truth, they designate very similar processes, being that gelifluction is typically attributed to sliding movements of the active layer (therefore being associated more exclusively with permafrost and periglacial regions) (French & Harbor, 2013; Harris et al., 1988; Rowley et al., 2015; Sharma, 2010; Williams & Smith, 1989).

Figure 9 *– Solifluction lobes show saturated conditions on this slope. Source: Rowley (2015).*

Gelivation, sometimes referred to as "congelifraction", "frost weathering", "frost-wedging" or "hydro-fracturing", is the process through which liquid water infiltrates into fissures in rock formations, and then, as it transitions into its solid frozen state and expands, leads to the widening of those fissures, and eventually, to the shattering of the rock (Figure 10). When taking place over large areas, this phenomenon can lead to the formation of blockfields (also called "felsenmeer") or blockslopes, which are accumulations of angular rock rubble (Allaby, 2015; French, 2007; French & Harbor, 2013; Harris et al., 1988).

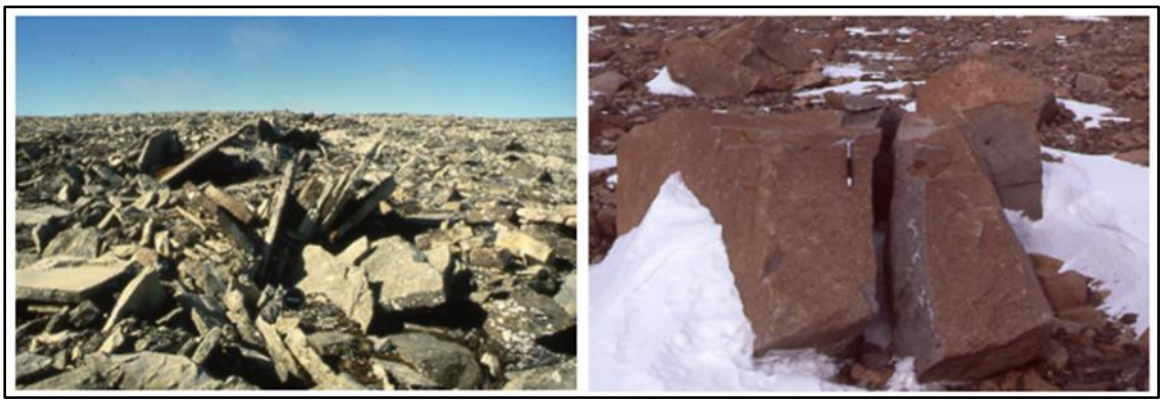

Figure 10 *– Examples of fracturing associated with frost-wedging. Source: French & Harbor (2013).*

Finally, one more term that is of great importance when describing periglacial environments is “thermokarst”. This term is used to describe landscape features formed by processes associated with the thaw of ice-rich ground, especially the degradation of ice-rich permafrost (Barry & Gan, 2011; French, 2007; French & Harbor, 2013; Harris et al., 1988; Rowley et al., 2015; Sharma, 2010; Williams & Smith, 1989). Besides high contents of ice, another characteristic that favors the development of thermokarst is the existence of unconsolidated sediment and non-resistant rock formations (French, 2007). There are several causes of the degradation of permafrost. They may be associated with geomorphic, vegetational or climatic triggers, and also, they may be of natural origin, or man-induced. For example, in terms of geomorphic triggers, naturally occurring standing water and vehicle movement both induce thermal disruptions at the ground surface, and consequently throughout time may lead to the thawing of the underlying frozen ground. Also, alterations in the vegetation coverage of the ground, may they be caused by man-induced actions (such as deforestation) or by a naturally occurring forest fire, can also give rise to permafrost degradation. Finally, changes in either regional climatic conditions, or in the characteristics of the global climate, which result from a combination of the Earth’s natural climate variation and anthropogenic forcing factors that accelerate climate change, are other major factors that originate thermokarst processes (French, 2007; French & Harbor, 2013; Rowley et al., 2015; Sharma, 2010). There are several types of changes that thermokarst processes may induce upon a periglacial landscape. For instance, when thawing of originally frozen ground occurs, the ground loses consistency, and when the excess water in the ground is removed by drainage or evaporation, subsidence is a frequently witnessed effect. Later, accumulation of water in the depression may even lead to the formation of thaw ponds or lakes, which further disturb the thermal equilibrium of the ground, accentuating the degradation of underlying frozen ground, and leading to the deepening of the depression (Barry & Gan, 2011; French, 2007; Rowley et al., 2015; Williams & Smith, 1989). Surface runoff water, for example, from snowmelt, rain, or from the thaw of permafrost itself, may also gather along ice wedges, leading to the transformation of the wedges into channel-like features (French, 2007; Williams & Smith, 1989). Furthermore, in fluvial and, especially, coastal regions (where tide dynamics and storm surge events are also a factor), thermokarst evolution can be greatly accelerated, something that can be reflected in the existence of rapidly retreating retrogressive thaw slumps (Figure 11) (French, 2007; French & Harbor, 2013; Williams & Smith, 1989). In sum, when attempting to understand the evolution of periglacial landscapes, it is key to consider thermokarst processes.

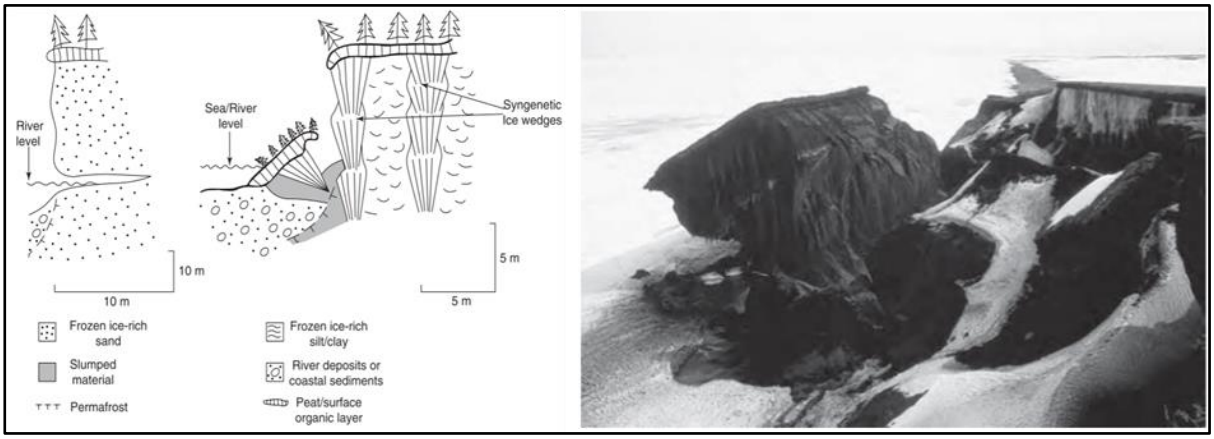

Figure 11 *– Forms of lateral and thermal riverbank and coastal erosion (Left). Example of coastal erosion by thermal-erosional undercutting and block collapse along ice wedges aligned parallel to the coast, in the Mackenzie River Delta region, Canada. Source: French (2007).*

2.2 - Characteristic Landforms of Periglacial Environments

2.2.1 - Pingo General Characteristics and Dynamics

Pingos are periglacial ice-cored hills, associated with the presence of permafrost. They originate with the growth and upheave of their ice-core and subsequent deformation of the land surface, normally into a conical shape. Pingos exist in central and northern Alaska, the Canadian arctic, the Russian arctic (Siberia), Greenland, Svalbard and Tibet (French, 2007; Karjalainen et al., 2020). Tuktoyaktuk Peninsula, in which the study area of this dissertation is inserted, is the region with the highest concentration of pingos in the world (Mackay, 1979, 1998).

Pingos can have a diameter that ranges from about 30 m to 600 m, and reach heights that go from just a few meters tall, up to around 50 m, such as in the case of the two tallest known pingos in the world, Ibyuk Pingo, which is located within PCL and is 49 m high (Figure 12), and Kadleroshilik Pingo, which is located 40 km southeast of Prudhoe Bay (Alaska, USA) and is 54 m high (Mackay, 1998; Wolfe et al., 2021). The diameter of a pingo, and consequently, its basal area, are established early in the pingos development, usually in its first years of growth. On the other hand, the height of pingos increases more gradually. For example, in Mackay (1979), growth rates ranging from 0.5 cm/year to 34 cm/year were mentioned amongst several pingos of Tuktoyaktuk Peninsula, being that maximum growth rates were normally reported at the pingo summits. As for their age, pingos can reach several thousands of years (French, 2007). For example, Ibyuk Pingo is reported to be from 1000 to 1300 years old (± 200 years) (Mackay, 1986a).

Figure 12 *- Ibyuk Pingo, located within Pingo Canadian Landmark. Note that here, it is the southern slopes of the landform that are viewed. Photo by Vieira (2019).*

As mentioned in chapter 2.1, ice segregation is a key process in the formation of pingos. It takes place when ground moisture that is adsorbed to soil particles migrates towards the freezing plane, then freezes to form originally thin layers, or lenses, of ice, along that plane. This "migration" is the result of a temperature gradient induced suction force, called "cryosuction". In fine-grained soil types, with a high number of capillaries, or interstices between its particles, cryosuction is especially facilitated (French, 2007; Williams & Smith, 1989). Keeping in mind that water undergoes a volumetric expansion when it transitions from liquid to solid state, at the same time as the ice lens is formed the overlying layers of soil are upheaved. With that said, pingos are not the only periglacial landforms that can be created by ice segregation. For example, palsas are small mounds (usually about 1 to 3 m in height, but sometimes reaching as high as 7 m, and with less than 100 m in diameter), which are composed of several alternating layers of segregated ice and peaty soil, and that typically exist in areas of discontinuous permafrost (French, 2007; Williams & Smith, 1989).

It is important to differentiate two main types of pingos, according to the different circumstances that result in the formation of the ice lens that will consequently lead to the formation of the pingo. Those two types are: open (or hydraulic) system pingos, and closed (or hydrostatic) system pingos (Figure 13).

Open, or hydraulic, system pingos, are associated with groundwater seepage. They form when sub-permafrost or inter-permafrost groundwater rises to the surface in a talik (due to artesian pressure), and freezes, forming an ice lens. This process is continuous, and as the lens grows, it heaves the soil of the active layer and forms a mound (Barry & Gan, 2011; French, 2007; Rowley et al., 2015; Sharma, 2010; Williams & Smith, 1989). Typically, these types of pingos are located in areas with some topographic relief, such as at valley bottoms, or are associated with geological faults (through which groundwater may rise). For example, water from the melting of the basal zones of glaciers may contribute to the growth of these types of pingos. They are reported to exist, for example, in East Greenland, Svalbard and

Tibet. According to French (2007), the growth of these types of pingos results from the combination of two processes: ice injection and ice segregation. The injection of groundwater corresponds to the main source of moisture fed to the underground lens, but since pingo growth depends on the combination of three separate main variables (water pressure, a factor determined by conditions external to the pingo; overburden strength, which can vary with time of year; and rate of freezing, which depends mainly upon temperature), it is unlikely that artesian pressures and ice injection alone can lead to the continuous and sustained formation of a well developed pingo, therefore emphasizing the importance of ice segregation, even in the development of these hydraulic system pingos.

Closed, or hydrostatic, system pingos are those that exist more commonly in the Tuktoyaktuk Peninsula area, and they also exist in other parts of the Canadian arctic, in northern Alaska and central Siberia (Mackay, 1979). As mentioned, waterbodies can shield the underlying ground from the extremely cold air temperatures that may affect periglacial regions. However, when those waterbodies cease to exist, their mitigating effect also ceases to occur. Therefore, in what was the bed of a currently drained lake, the saturated and sandy ground can freeze. Permafrost aggradation takes place and leads to a process known as pore water expulsion. This corresponds to when liquid pore water is forced to migrate due to the freezing and solidification of the surrounding soil. However, if that water has no unfrozen ground to drain to, it becomes confined into a water lens, and the development of hydrostatic pressures takes place (McRoberts & Morgenstern, 1975). This liquid water will then progressively freeze, forming a continuously growing ice lens by ice segregation. The large pressures which result from the drainage being blocked by permafrost aggradation, lead to the growing lens being heaved towards the surface, deforming the ground and progressively forming a mound (Barry & Gan, 2011; French, 2007; Mackay, 1979; Rowley et al., 2015; Sharma, 2010; Williams & Smith, 1989).

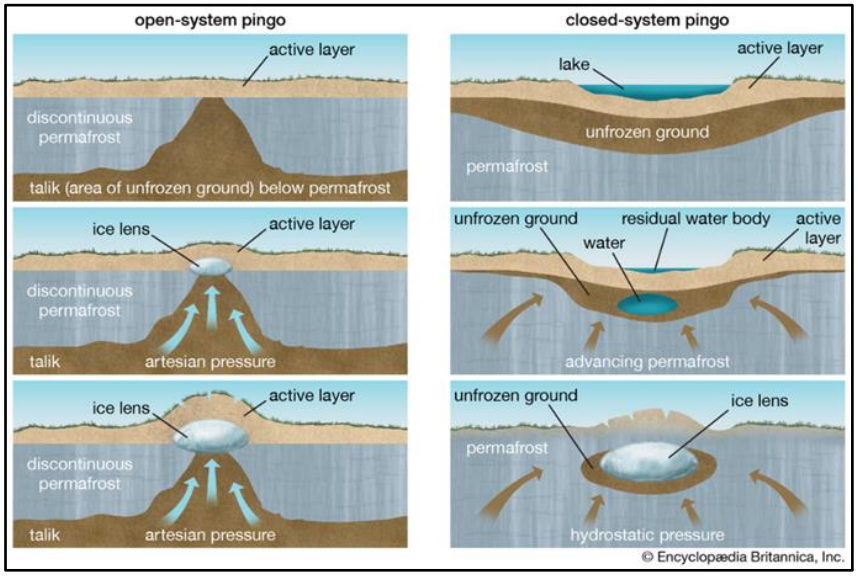

Figure 13 - *Diagram explaining the formation of open-system and closed-system pingos. Source: Encyclopedia Britannica (2016).*

As pingos grow and age, these landforms undergo a series of geomorphological dynamics: first, the progressive formation of dilation cracks (namely starting from the pingo summit) and erosion (also of the summit); then, gradual subsidence; and ultimately, collapse.

The layer of overburden soil and vegetation that covers the ice core of pingos, and which may vary in thickness from 1 to 10 m (French, 2007), protects the ice core and prevents it from melting. The thicker the overburden, the more protected the ice core will be (Mackay, 1979). However, as the ice core grows and is upheaved, the overburden can only be stretched to a certain point, after which dilation cracks are seen to form, typically originating from the pingo's summit, and sometimes extending all the way to its periphery (Figure 14). These cracks condition the further growth of pingos, as normally they expose their ice core and leave them vulnerable to erosion and thaw, especially on pingos that reach considerable heights, where meteorological weathering factors are usually harsher. Wind and precipitation, for example, erode the summits of pingos, widening the dilation cracks and degrading overburden soil and vegetation, and as those protective elements disappear, the erosion will only tend to intensify.

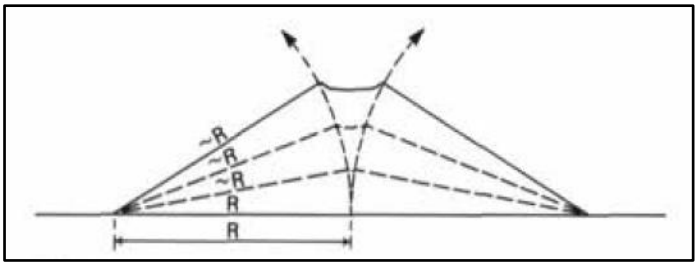

***Figure 14** - Schematic diagram of a pingo, where dilation from stretching is relieved by a summit dilation crack. Source: Mackay (1979).*

As mentioned, subsidence is another step in a pingo's evolution and normally occurs when water begins to stop being supplied to the sub-pingo lens. It is known that artificially perforating a sub-pingo water lens can lead to artesian flows and even geysers several meters high, especially under closed system pingos, where hydrostatic pressure accumulates. This was demonstrated in the field work conducted in Mackay (1978) and Mackay (1979), during which drilling with the objective of studying sub-pingo water pressures led to the subsidence of three pingos of the Tuktoyaktuk Peninsula (Figure 15). Just on a single drilling event in 1976 at one of those pingos, more than 5000 m^3 of water were released through a geyser, and, after another drilling event at that same pingo conducted in 1977, 60 cm of subsidence were reported, which corresponded to a loss of 10 years of growth according to the author (Mackay, 1979). However, just as this evidence shows that subsidence may occur after artificial flows are triggered, naturally occurring ruptures in the sub-pingo lens and spring flow may also lead to pingo subsidence. Another possible means of a sub-pingo water lens being drained is through a talik. In closed system pingos, as permafrost aggrades and the pingo grows, there is a substantial and increasing weight on the saturated soil that underlies the pingo. Originally,

it is from this soil that the sub-pingo water lens' moisture is fed, but later, if there is any unfrozen ground to which the moisture can drain to, the increasing weight may lead to drainage and water loss from the sub-pingo lens, and consequently, pingo subsidence (Mackay, 1979). Another geomorphic feature associated with pingo subsidence is the formation of a bulge around the pingo's periphery (Figure 16). As the pingo's overburden (which has been stretched by its growth) settles, this bulge is formed, due to the fact that it can no longer fit back into the space it once occupied (Mackay, 1979). Sometimes, "pulsating" patterns may be observed in the evolution of a pingo's height, with it increasing in height while its sub-pingo lens is still being fed, then subsiding during a period of time throughout which the lens ceases to be fed moisture, only to return to growth when the circumstances at the lens are favorable to that once again (French, 2007; Mackay, 1977, 1998; Williams & Smith, 1989).

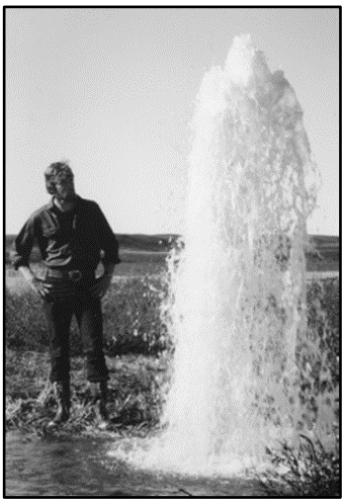

Figure 15 *– Drill-hole flow from a pingo studied in 1976, on behalf of Mackay (1979). The gusher that rose to a maximum of 2.6 m issued from a 7.5 cm diameter hole with a depth of 22 m. The water temperature was about -0.1º C. Source: Mackay (1998).*

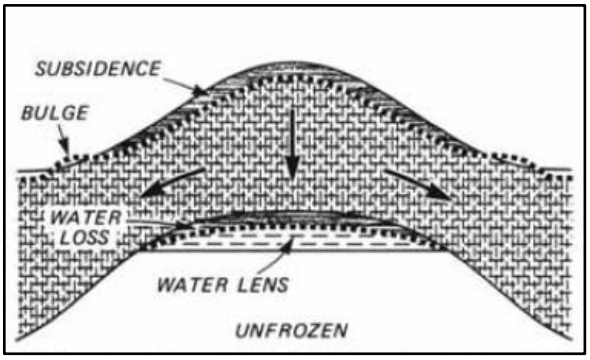

Figure 16 *- Schematic cross section, with greatly enlarged scale to illustrate subsidence from sub-pingo water loss and the formation of peripheral bulges. Source: Mackay (1979).*

The final stage in a pingo's evolution is its collapse and erosion (Figure 17). The main causes of this phenomenon are the cessation of the supply of moisture to a sub-pingo water lens (for example, after a rupture of the lens, leading to immense water loss), and the melting of a pingo's ice core (namely after it has been exposed by erosion). The first of those scenarios is more likely to affect pingos in an earlier stage of development, while the second more commonly affects older pingos. In the case of erosion of a pingo's summit and exposure of its ice core, it is common for a crater to begin to form at the top of the pingo. Many times, precipitation leads to the appearance of a pond in the crater depression. Also, especially in older pingos with steeper slopes, those slopes may be affected by permafrost creep or even larger magnitude mass wasting events, which will also contribute to the degradation of the pingo, and can accelerate its collapse. Eventually, prolonged thaw and disappearance of the ice core, and erosion of the pingo itself, will lead to only subtle remnants of the pingo being left behind. Being that pingos only exist in the presence of permafrost, the remnants of these

landforms found in regions where currently there is no permafrost are an important indicator that permafrost did in fact exist in those regions in the past (French, 2007; Mackay, 1986a, 1998).

Figure 17 *– Oblique air view of a pingo located on the Tuktoyaktuk Peninsula (Canada), showing exposure of its ice core and clear signs of subsidence (Left). Pingo showing advanced signs of erosion. The ice core is very clearly exposed, with seasonal-growth bands being visible (Right). Source: French (2007).*

2.2.2 - Tundra Polygon and Ice Wedge General Characteristics and Dynamics

Tundra polygons are a type of patterned ground landform, and correspond to the surface-level manifestation of a typical form of vein ice that can be found in permafrost regions, ice wedges. Ice wedges are wedge shaped ground ice formations, that form within thermal contraction cracks that can appear in permafrost (Figure 18). Due to their formation process, which is cyclical in nature as will be further explained, ice wedges are composed by vertically banded, or foliated, ice (French, 2007; Hargitai & Soare, 2014; Warburton, 2013). Tundra Polygons are amongst the most abundant landforms that can be found in permafrost and periglacial regions, being that well developed networks of these features can be found, for example, in central Alaska, the Canadian arctic, Siberia, Greenland, Iceland and Svalbard (French, 2007; Karjalainen et al., 2020).

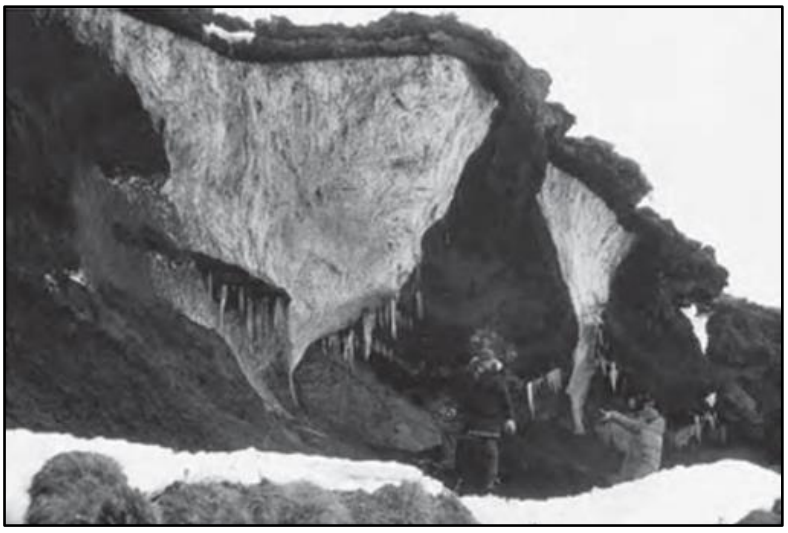

Figure 18 *– Large epigenetic ice wedges located near King Point, on the Yukon Coast (Canada), exposed by retrogressive thaw-slumping. Source: French (2007).*

As already mentioned, water's volume expands as it cools and turns into ice, but, when subjected to extreme below freezing temperatures, ice will contract. With that said, saturated soil, when also subjected to continuous below freezing temperatures, will contract as well. However, the thermal limit below which the soil will begin to contract rather than expand depends greatly on its water content. For example, ice formation, and then contraction, both tend to happen at lower temperatures for high porosity, fine-grained soils, in comparison to what happens with coarser grained soils (Williams & Smith, 1989).

During the coldest periods of the year, as this contraction occurs, fissures begin to open in the soil. These thermal contraction cracks are initially just a few millimeters wide, and several tens of centimeters to about a meter deep. However, normally starting in the Spring and then continuing during the Summer, these fissures are progressively filled with water (for example, resulting from the melting of snow) or sediments, and sometimes a combination of both (Barry & Gan, 2011; French, 2007; Williams & Smith, 1989). With the coming of the Winter, the water content in the fissure will freeze and expand, consequently acting as a wedge (i.e. an "ice wedge"), widening the fissure. Then, in the subsequent Spring and Summer, partial melting of the ice wedge will occur. With the crack now slightly widened, it will sustain an also slightly greater volume of water (and possibly sediment), which, consequently, upon freezing and expanding, will further widen the crack in a small proportion (Figure 19). This cycle continues year after year, with partial melting of the ice wedge and infilling of the crack occurring in the warmer seasons, and freezing of the infilling materials and widening of the crack taking place in the colder seasons, resulting in the progressive growth of the ice wedge (French, 2007; Williams & Smith, 1989). The presence of continuous permafrost corresponds to the ideal condition for the development of the ice wedges, as it will hinder drainage, and therefore most of the liquid water that has infilled the cracks will be retained there, and later contribute to the growth of the wedge upon freezing (French, 2007).

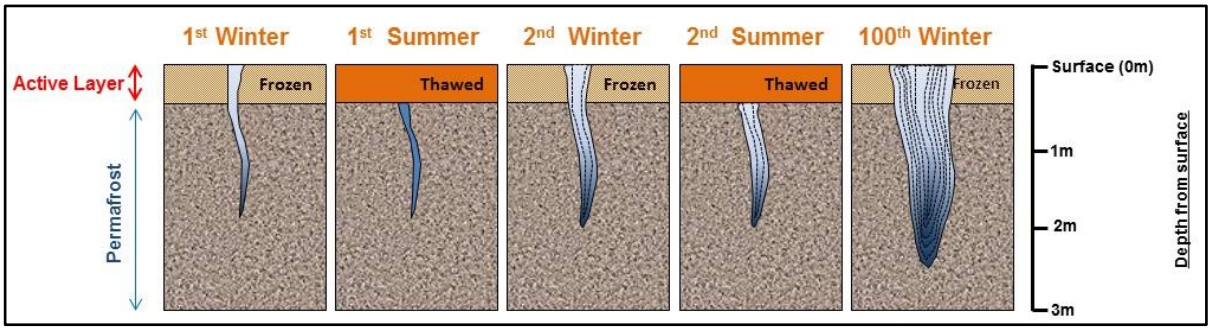

Figure 19 *- Diagram showing the cyclical formation process of ice wedges. Source: Gamesby (2012).*

Though ice wedges start small, they may attain widths of as much as 3 m, or slightly more. The widest portions of the wedge are those closest to the ground surface, being that they are narrower in depth. It is not uncommon for wedges to extend 10 m deep, and some have been known to reach as deep as 20 m (Harris et al., 1988). There are several ways in

which ice wedges may be classified. According to their stage of development, they may be categorized as active (if they are experiencing the growth cycles described before), inactive (if they are currently not growing, but could resume growth in the future), or relict (if they have long ceased growing, and can no longer resume growth) (French, 2007). Also, given that thermal contraction cracks may be infilled by sediments in addition to water, the resulting wedges may be classified according to their infill composition. This way, pure ice wedges, icy silt wedges, or even soil or sand wedges can be distinguished (French, 2007; Williams & Smith, 1989). Another distinction that can be made is between epigenetic, syngenetic and anti-syngenetic wedges (Figure 20). Epigenetic wedges (Figure 18) are those whose formation occurs at a later time than the permafrost in which they are located. In other words, the cracks that lead to their development form in pre-existing frozen ground. This type of wedge tends to grow wider rather than deeper (French, 2007; Harris et al., 1988). Syngenetic wedges (Figure 11) are those whose genesis is practically contemporary with that of its hosting sedimentary layers. As deposition occurs, and the ground surface rises, the wedge grows along with it in what can be described as an “upwards growth” process. Therefore, these wedges tend to have a greater vertical development than epigenetic wedges, achieving the greater values of depth that were mentioned before. Also, and unlike epigenetic wedges, syngenetic wedges many times develop into a more irregular form, somewhat differing from the typical wedge shape (French, 2007; Harris et al., 1988). As for anti-syngenetic wedges, their growth process is similar to that of syngenetic wedges, but it occurs in the inverse direction, and is associated with the removal of surface material, rather than its deposition. These wedges form on slopes that are experiencing erosion on their surface level, but, for them to form, the rate of thermal cracking must accompany the rate of the surface removal. At the same time as the surface layers are progressively eroded, the cracks also progressively grow in depth, and are infilled by water and possibly other materials, which then freeze. Therefore, there is a “downwards growth” of the ice wedge, perpendicular to the slope ground surface. However, any evidence of the formation of these wedges is very frequently covered by gelifluction (or similar mass movement processes), leading to them not being perceivable on the landscape (French, 2007).

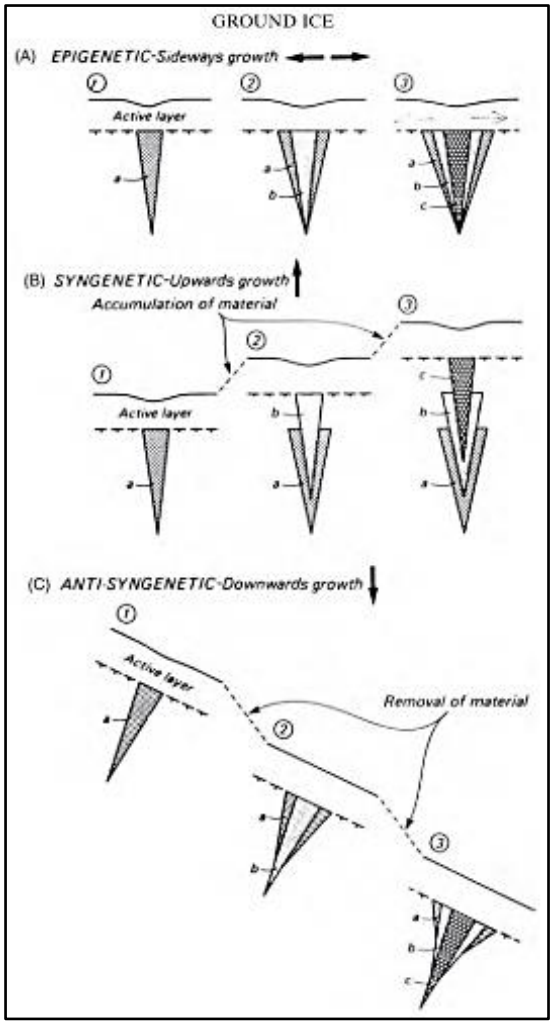

Figure 20 *– Schematic diagram showing the growth of epigenetic, syngenetic and anti-syngenetic wedges. Three growth stages are indicated for each. Source: French (2007).*

Almost always, ice wedges are non-isolated features. They form patterned ground landscapes or polygonal networks, with each wedge corresponding to a side in one (or several) polygons. These polygonal landforms go by several designations, such as “ice wedge polygons”, “thermal-contraction-crack polygons”, or “tundra polygons” (French, 2007), being that this last term will be the one most used throughout this dissertation. Tundra polygons can cover extensive areas, and there are as much as millions of square kilometers of arctic and sub-arctic landscape that are characterized by these distinctive landforms (French, 2007; Williams & Smith, 1989). The polygons vary greatly in terms of size, normally as a consequence of the underlying sediment in which the ice wedges form. In more consolidated substrates and bedrock, when they exist, polygon networks are smaller, as are the individual polygons themselves, normally ranging between 5 and 15 m across in size. On the other hand, with less consolidated underlying sediments, we can observe more developed and widespread networks, as well as larger individual polygons, which can reach average sizes of 15 to around 40 m (Barry & Gan, 2011; French, 2007).

An important distinction that can be made when characterizing tundra polygons is that between low-centered and high-centered polygons (Figures 21 and 22). Low-centered polygons are especially typical of poorly drained tundra areas, and are characterized by having a raised rim (often by 50 cm or more), sometimes called a “rampart” in the literature (French, 2007). This small elevation around the borders of the polygons is associated with the ice wedges which underlie each polygon border, as this upwards land deformation is due to the thermal expansion of the ice wedges, which, during their freezing process heave the ground above them. With the elevation of the rims of each polygon, the centers of those polygons will consist in a depression, where water will tend to accumulate (namely, from snowmelt), becoming very humid and sometimes hosting small lakes or ponds (French, 2007; Williams & Smith, 1989; Wolter et al., 2018). As they shield the ground from the extremely cold air temperatures, the existence of the waterbodies will at first favor the thaw of ice in the underlying soil of the polygon center, and, at a later stage, will also contribute to the thawing of the ice wedges which form the rims of the polygons. This effect, when combined with an increase in air temperatures, or also with water accumulation along the thermal contraction cracks (which can occur as the ice wedges grow wider, sometimes even forming channel like features), can lead to a clear top-down thawing of the ice-wedges, which are preserved only at the deeper (and colder) levels of ground. This leads to the disappearance of the before mentioned ramparts, and while those parts of the terrain are lowered, the same does not occur with the polygon centers. With this, a relief inversion progressively occurs, as the polygon centers, which once where concave land features, transform into convexities of the land surface. These elevated mounds are designated as high-centered polygons (French, 2007; Williams & Smith, 1989; Wolter et al., 2018). However, it should be mentioned that high-centered polygons can also be subjected to degradation, especially after vegetation present on their surfaces is negatively affected, for example, by coastal erosion, wind action and other weather processes, human activity, or animal activity (for example, animals can degrade the polygons by means of burrowing). Therefore, in time, high-centered polygons will transform into what are sometimes called “thermokarst polygons”, which can have degrading impacts on underlying permafrost (Eisner & Peterson, 1998; French, 2007; K. M. Peterson & Billings, 1980).

Figure 21 *– Low-centered tundra polygon landscape (Top) and high-centered tundra polygon landscape (Bottom). Both are viewed from several hundred meters of height. Source: Williams & Smith (1989).*

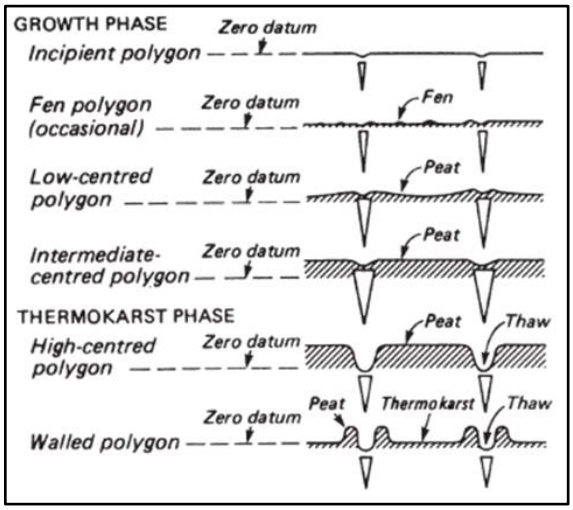

Figure 22 *– Stages of evolution of tundra polygon relief towards the formation of thermokarst polygons. Source: French (2007).*

It is also interesting to notice the patterns that the networks of tundra polygons form (Figure 23). As mentioned in French (2007), early and more theoretical studies, such as those of Lachenbruch (1962, 1966) and Grechishchev (1970) suggested that orthogonal networks were to be the most common, with the tundra polygons tending to be square or rectangular in shape, and with intersections of ice wedges forming angles of about 90º. These theories also suggested that the networks begin their formation with larger primary thermal contraction cracks, with the appearance of secondary cracks occurring at a later stage. However, throughout the decades, field studies have demonstrated that tundra polygons are frequently viewed having shapes that diverge from squares and rectangles. For example, hexagons and other more irregular shapes are frequent, in which cases ice wedge intersection angles tend to be closer to 120º rather than 90º. Also, in networks which are more hexagonal in nature, it is believed that all cracks throughout the network form at about the same time. Networks with 90º ice wedge intersection angles do exist, nevertheless. The polygons that comprise them are still many times irregular in shape, being that those networks are called “random orthogonal networks”. More regular orthogonal networks (where polygon shapes closer to squares and rectangles can be found) are called “oriented orthogonal networks”, and are typically associated with the presence of hydrological features which condition the distribution of the horizontal thermal regime through the terrain, such as large waterbodies or river channels. For

example, the theoretical explanations for the formation of oriented orthogonal networks proposed in Lachenbruch (1962), who stated that “where horizontal temperature changes are great, horizontal stress differences are likely to be also”, were confirmed in Mackay (1986b), who pointed out that cracks had this type of orientation between a cold old lake shore with very deep permafrost and a nearby residual pond without permafrost (with the study area of this work being located on Richards Island, Northwest Territories, Canada). Terrain inclination can also influence the form that tundra polygons will assume, with more steep values of slope being associated with more elongated polygons (up to 30º inclination, as patterned ground will not form on slopes steeper than that) (Sharma, 2010).

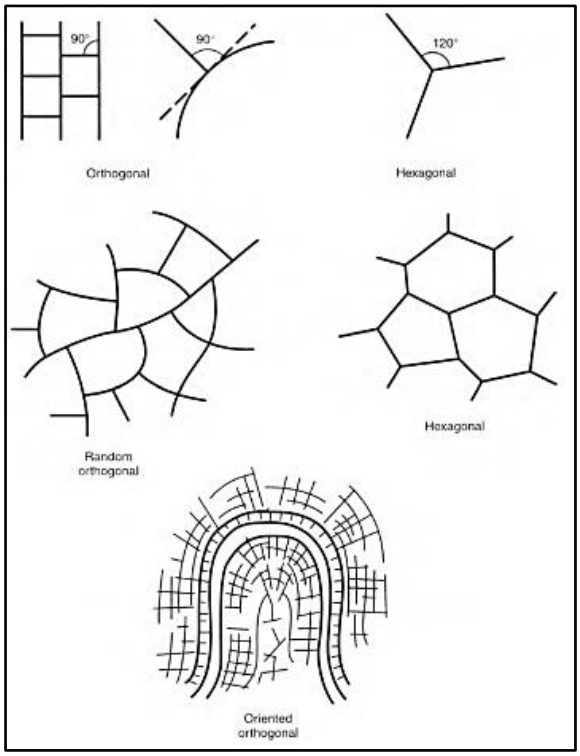

Figure 23 *– Types of polygonal networks in permafrost terrain. Source: French (2007).*

As has been described, tundra polygons simultaneously condition the evolution of the landscape, as well as they themselves are conditioned by the characteristics of the geomorphological and hydrological setting in which they are inserted. Ice wedges are commonly affected by thermokarst processes, and there is one type of setting in which this is particularly evident, and that is in coastal environments (such as that of the study area of this dissertation). The existence of tundra polygon networks in areas where tidal activity is very dynamic and coastal storms are prevalent can be a factor that promotes coastal erosion and retreat. This is due to the fact that these networks are typically associated with high ground ice contents, especially in networks where the ice wedges are well developed and comprised of pure or near-pure ice (French, 2007; Karjalainen et al., 2020; Williams & Smith, 1989). The ground ice (namely, the ice wedges themselves) is highly susceptible to thaw due to the action of saline water, as it is known that sodium chloride has the effect of lowering the melting point

of ice (Kim & Yethiraj, 2008). Therefore, marine waters accelerate the thaw of ice wedges on a chemical level, compromising the structural integrity of the substrate, and in addition to this, the mechanical action of tides, waves and storm surges cause further degradation of coastal tundra polygon networks. Tundra polygons are prone to breaking, especially along the ice wedges that correspond to their borders, which can lead to large sections of coastal tundra bluffs falling into the sea or onto any existing beach below, with those materials later being carried away by tidal activity or future storms (Figures 11 and 24) (French, 2007; French & Harbor, 2013; Sturtevant et al., 2004; Williams & Smith, 1989). In Costa (2022), a study of recent (1985 to 2020) coastal change along the Beaufort Sea coast on Tuktoyaktuk Peninsula (Northwest Territories, Canada), coastal regions with tundra polygon networks were amongst those where the highest coastal erosion rates were quantified.

Finally, it should be mentioned that rising air and sea temperatures are another factor that can contribute to the degradation of tundra polygons, as well as pingos (which are also prone to erosion by the chemical and mechanical degradation processes associated with coastal dynamics that were described in the previous paragraph, especially in the cases of coastal pingos with an exposed ice core). With this being said, tundra polygons and pingos are particularly at danger of degradation in the context of climate change, as not only air and sea temperatures rise, but also as increased coastal storm activity is verified (Irrgang et al., 2018; Karjalainen et al., 2020). Also still, in addition to creating favorable conditions for the degradation of existing tundra polygons and pingos, warming trends in global and regional (Arctic) climates will also hinder the formation and development processes of these periglacial landforms in the future, further contributing to their disappearance (Karjalainen et al., 2020).

Figure 24 *– Ice wedges, exposed by coastal erosion (Yukon Coast, Canada). Photo by Vieira (2018).*

2.3 – Pingo Canadian Landmark in the Literature

Due to its “outstanding, exceptional, unique, and rare” features, PCL was appointed as a site of Canadian national significance in 1978, and in 1984 it was officially declared as a Canadian National Landmark, through the Western Arctic (Inuvialuit) Claims Settlement Act. PCL is managed under the National Parks Act by Parks Canada, in consultation with the Inuvialuit Land Administration and the people of the hamlet of Tuktoyaktuk as a joint management regime (Parks Canada, 2020). However, even though PCL has been officially recognized for its undeniable cultural and geomorphological importance for more than 40 years, the site, especially as a whole, has not been the subject of many scientific studies until recent years.

The first study to mention Pingo Canadian Landmark by its name after its appointment as a site of national significance and a National Landmark was Mackay (1998). However, this study focused predominantly on Ibyuk Pingo, namely its stratigraphy, growth, and the development and evolution of the dilation cracks on its summit. Though PCL was not mentioned in many studies until recently, Ibyuk Pingo itself, given its prominence as the second largest of this type of landform in the world, has been covered in several scientific works. For example, Mackay (1998) points out that Ibyuk Pingo, formerly known as “Crater Summit Pingo”, has been subject to scientific study as far back as the 1950’s. That same study, as well as Müller (1962), states that the overburden above Ibyuk Pingo’s ice core is 15 m thick and is comprised of (from the surface downward) a 4 m layer of lake silts containing high contents of organic matter, a 2 m diamicton with glacially striated boulders, and 9 m layer of sand containing some remnants of driftwood logs. Also, regarding the currently drained lake that surrounds Ibyuk Pingo, the two previously mentioned studies state that the radiocarbon dating of organic matter present in Ibyuk Pingo’s overburden (such as driftwood, rootlets and even shells of mollusks, which were found in the uppermost silty sector of the overburden) indicates that lake was likely in existence from about 12,000 years ago to about 1650 years ago, which was the time after which its drainage occurred. Also, Mackay (1986a) and (1998) categorize Ibyuk Pingo (as well as the majority of the pingos located in the Tuktoyaktuk Peninsula area) as being a Closed or Hydrostatic system pingo, evidenced, for example, by the currently drained lake that surrounds it. Mackay (1986a) and (1998) also give insight into the summit crater and dilation cracks of Ibyuk Pingo, stating that they go as deep as 4.5 m into the overburden, and though this is still not enough to expose its ice core, exposure is bound to occur in the future (due to a combination of natural and anthropogenic forcing factors), and, eventually, Ibyuk Pingo will likely evolve into a pond, which will originate from what is now its

summit crater. This pond will have, at most, 15 m of depth (the maximum extent of Ibyuk Pingo's current overburden layer).

As for PCL, aside from some studies aimed at identifying possible periglacial landforms, including pingos and tundra polygons, on the surface of the planet Mars, which used examples of these landforms specifically from PCL to compare with those possibly found on the red planet (Soare et al., 2013, 2020), it was not until 2020 that the park truly started to appear as an object of study for several scientific papers. These have come to apply methods and technologies that were not available at the time of the works mentioned in the previous paragraph, and have come to provide new and insightful data regarding the park.

For example, in Lim et al. (2020a), helicopter-based photogrammetry was applied to evaluate the impact of a large storm event (which occurred on August 4th and 5th, 2019) on the coastline in several locations in the Mackenzie Delta area. One of these locations is Peninsula Point, which is a peninsula located in the northwestern part of PCL. More precisely, it is a 274,670 m^2 area with coastal cliffs and retrogressive thaw slumps where coastal retreat was quantified. The study estimated that 12,800 m^3 of material was eroded from this area just during this extreme storm event, being that the annual volumetric loss that occurred at this specific study area within the park was estimated to be of 44,522 m^3 (this value was reached by comparison with a UAV survey conducted a year earlier). It was also pointed out that, over that same one-year period, a maximum of approximately 8 m of coastal retreat occurred in some sectors, while as, associated just with the storm event, there were sectors where the cliffs retreated as much as 3.4 m. In another recent study, Lim et al. (2020b) also focused on Peninsula Point and quantified long-term shoreline retreat. This was done through the georeferencing and photogrammetric analysis of historic aerial imagery relative to the years of 1935, 1950, 1971, 1985, 1994, 2000, 2010 and 2018, being that a continuous retreat rate of 3.47 m/year was determined throughout the 83-year period (Figure 25). Additionally, this study also recurred to novel passive seismic surveys to evaluate vulnerability to subsidence. Given that higher ice contents close to the ground surface are typically associated with greater subsidence, the results pointed out remaining near-surface ice masses in the area, which are likely to be vulnerable to future subsidence (Figure 26).

In Parker (2021), Natural Resources Canada's CanCoast dataset (Manson et al., 2019) was examined to determine coastal sensitivities to climate change at 62 Parks Canada sites, including PCL. The referred dataset contained data regarding the Coastal Sensitivity Index (CSI), which, "by considering geomorphic conditions (e.g., coastal materials, slope, presence of ground ice) and environmental drivers (e.g., sea level change, wave height change including the effects of changing sea ice), (…) provides a generalized measure of an area's current

(2000's) and future (2090's) sensitivities to impacts such as erosion, flooding and inundation" (Parker, 2021). The CSI presents the following five classes of sensitivity (with the corresponding index values in parenthesis): Very Low (< -500); Low (-500 to -151); Moderate (-150 to 150); High (151 to 500); and Very High (> 500) (Manson et al. 2019). For the 2000's time period, PCL's 38.65 km coastline was characterized as having 7.88 km in the "High" sensitivity class, and 30.77 km in the "Very High" class. As for the 2090's time period, it was estimated that all 38.65 km of PCL's coast will belong to the "Very High" class. In terms of how much the calculated CSI values for PCL changed between the 2000's period to the 2090's period, this study stated that 2.8 km showed a decrease in sensitivity, 8.37 km showed a moderate increase (CSI increased by 1 to 500) and the remaining 27.48 km showed a large increase (CSI increased by > 500). Additionally, for each site, Parker (2021) presents values of Relative Sea Level Change for 2006 to 2020, which was -0,08 m at PCL, and for 2006 to 2100, which was +0,9 m at PCL.

Holland et al. (2023) took a geochemical approach to evaluate environmental change within PCL. Field work for this study consisted in the extraction of samples from a high-centered ice wedge polygon with lateral exposure, located 70 m from the shoreline (at the time of sampling, in July 2017). The main goals were to verify the presence of ion concentrations typically associated with marine aerosols in the sample taken from this coastal ice wedge, obtain radiocarbon dating for them, and ultimately evaluate the potential use of ice wedges as a marine aerosol archive. Summarily, it was concluded that the younger the ice, the greater the presence of the ionic concentrations associated with marine aerosols, especially throughout the late Holocene. This suggests that the distance between the ice wedge and the coast has progressively diminished, with the authors estimating a 1 km distance-to-coast reduction during the late Holocene.

Lastly, in Wolfe et al. (2021) and Wolfe et al. (2023), 2363 pingos in the Tuktoyaktuk Coastlands and adjacent areas of the Northwest Territories were identified and characterized, through an iterative process using the HRDEM (High Resolution Digital Elevation Model) created by Natural Resources Canada, satellite imagery from Google Earth Pro and ArcGIS Earth, and data relative to the surficial geology of the Tuktoyaktuk Coastlands, extracted from Rampton (1987) (Figure 27). Within the borders of PCL, this study identified 11 landforms as pingos (Figure 28), with Ibyuk pingo being pointed out for being "anomalously tall", at 49 m of height (considering only intact pingos with a height > 0.6 m, which was the case for 1993 pingos in this study, the average height was of 5.3 m). Ibyuk was also highlighted for its steep slopes, which according to the study can slightly exceed 67º (being that the average across all identified pingos was 6.4º).

In this context of growing interest in the site, the present dissertation, which also counts with state-of-the-art data and methods, shall provide a broad analysis of the landscape of PCL in an unprecedented level of detail, even in comparison to the other recent studies mentioned.

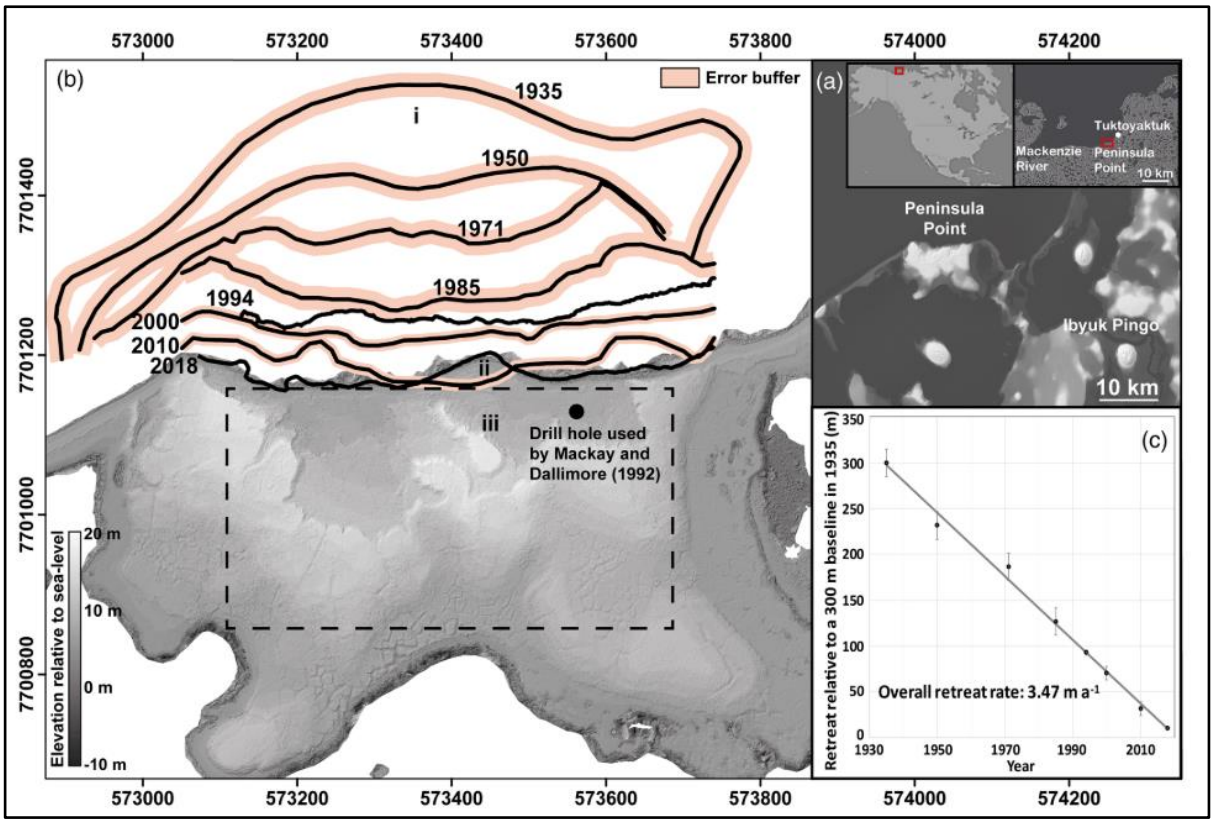

Figure 25 *– (a) shows the study area of Lim et al. (2020b) relative to the global (first inset) and regional (second inset) context. (c) was derived from the digitized shoreline positions shown in (b). The dashed box shows the survey area presented in Figure 26. A UTM reference scale is presented on the outer axes. Source: Lim et al. (2020b).*

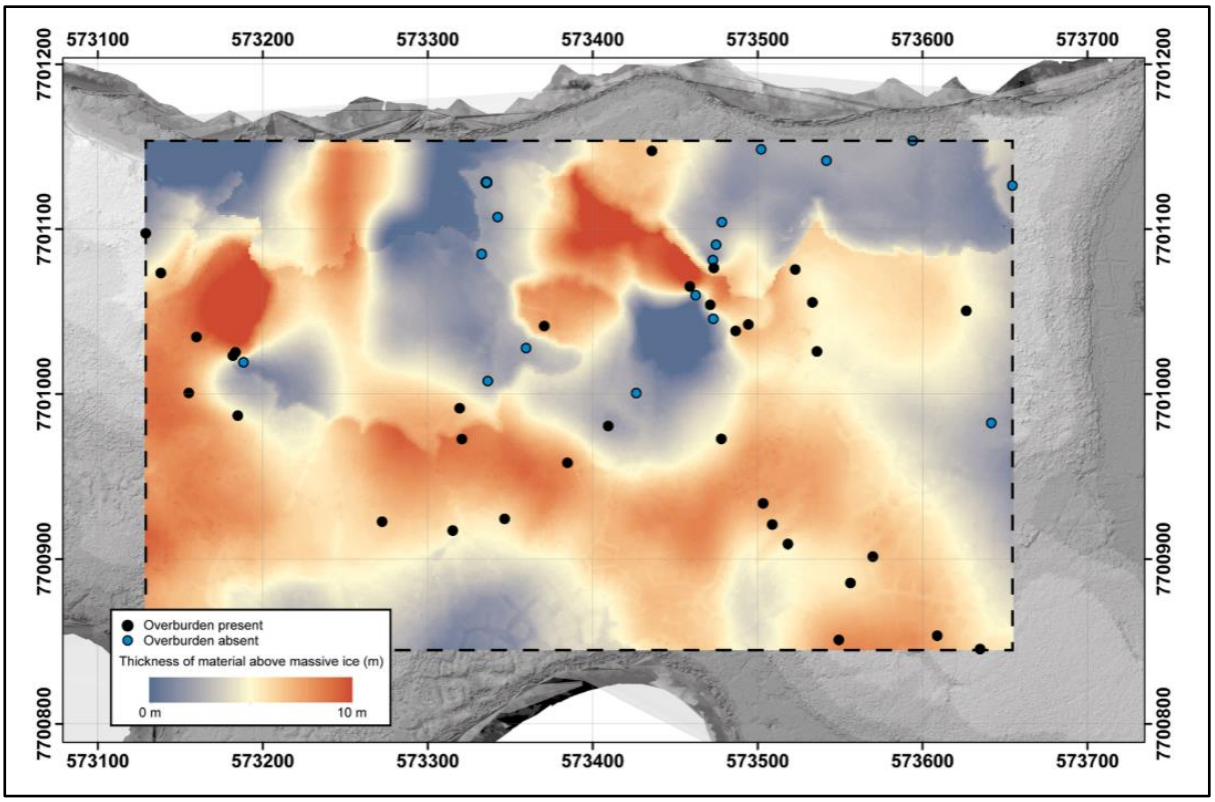

Figure 26 *– Surface to massive ice difference model created by Lim et al. (2020b), highlighting the organic-rich layer volumes. The areas in blue are those theoretically more susceptible to subsidence (as the massive ice is closer to the surface). The passive seismic signal measurement positions used, and respective classifications, are overlain. A UTM grid is overlain for scale in meters. Source: Lim et al. (2020b).*

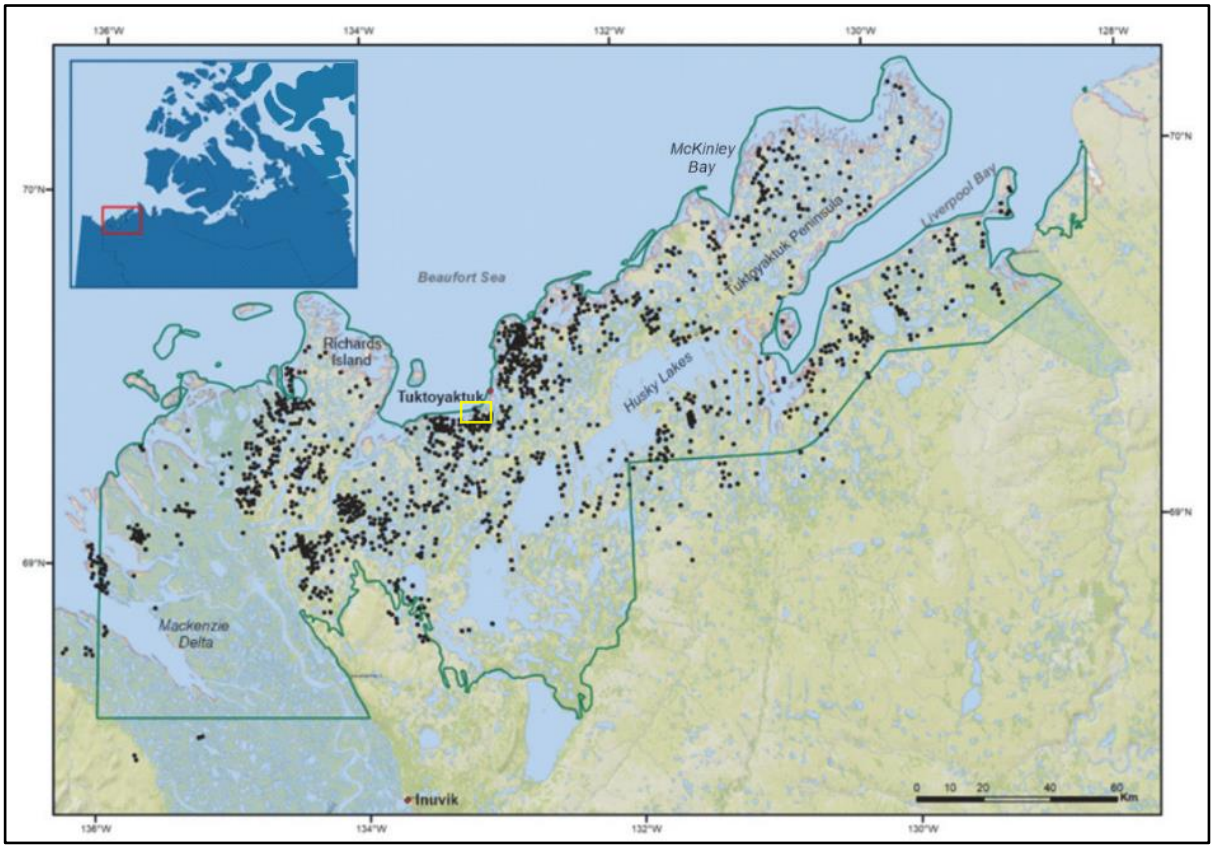

Figure 27 *– Study area of Wolfe et al. (2021) and Wolfe et al. (2023), showing the distribution of the 2363 pingos identified by these studies in the Tuktoyaktuk Coastlands and surrounding regions. Approximate location of PCL is signaled by the small yellow rectangle. Source: Adapted from Wolfe et al. (2021).*

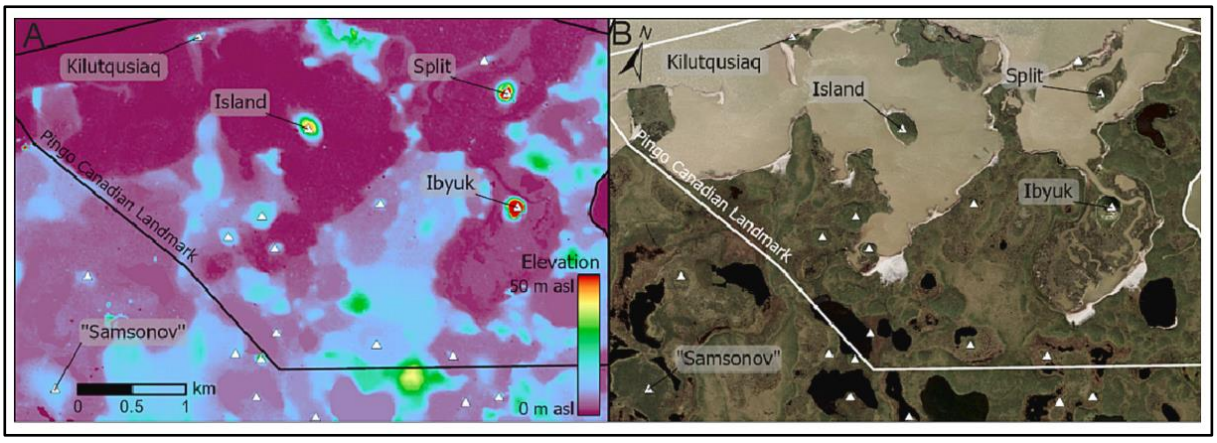

Figure 28 *– Example of the pingo mapping results of Wolfe et al. (2021) and Wolfe et al. (2023), obtained using (A) HRDEM and (B) satellite imagery, in the area of PCL, about 5 km southwest of Tuktoyaktuk, Northwest Territories. The four named pingos within PCL are shown. Source: Wolfe et al. (2023).*

3 – CHARACTERIZATION OF THE STUDY AREA

3.1 – Regional Geographic Framework

3.1.1 - Geology and Geomorphology

PCL is located in the southwest region of Tuktoyaktuk Peninsula, close to the Mackenzie River delta (Figures 29 and 30). The Tuktoyaktuk Peninsula is located north of the Arctic Circle (latitude: 68.8°N to 70.2°N and longitude 134.1°W to 129.3°W), in the Inuvialuit Settlement Region, located within the Inuvik region of the Northwest Territories (NWT), Canada (Figure 29). To the west of the Peninsula is Kugmalit Bay and the Mackenzie River Delta. To the north is the Beaufort Sea. To the east is Liverpool Bay, and to the south we find the Husky or Imaryuk Lakes area (formerly known as the Eskimo Lakes). The Peninsula is predominantly comprised of lowland tundra, dominated by ice-rich continuous permafrost landscapes, and containing many thermokarst lakes and tundra polygon networks (Mackay, 1977, 1978, 1979; Wolfe et al., 2021). Though the region is mostly flat, it is punctuated by periglacial landforms, such as ice cored domes of various sizes, being that this is the region with the highest concentration of pingos in the world (Mackay, 1998).

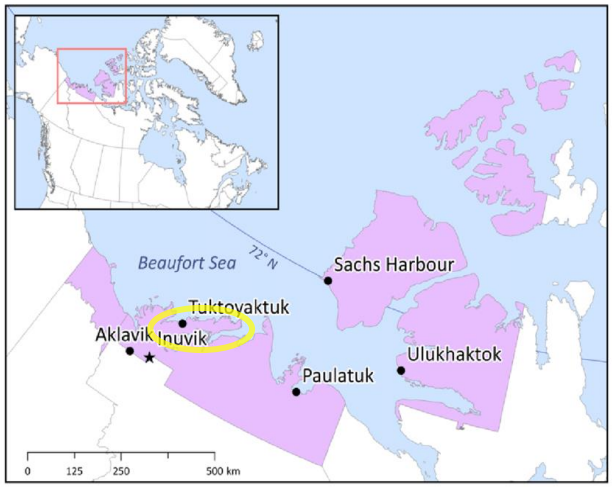

Figure 29 *- Location of the Inuvialuit Settlement Region (in purple) and its six communities. Tuktoyaktuk Peninsula is signaled by the small yellow oval. Source: Adapted from Kenny et al. (2018).*

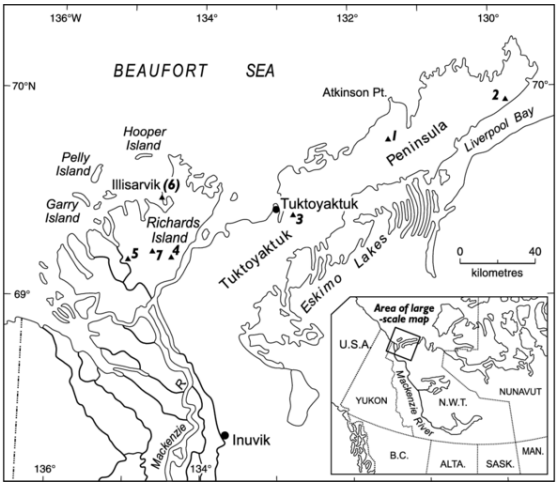

Figure 30 *- The Tuktoyaktuk Peninsula area. The numbers 1 to 7 refer to the sites of recently drained lakes. Source: Mackay & Burn (2002).*

As will be further discussed in the following sub-chapters, PCL has a diverse landscape, including from a geomorphological standpoint. It contains many of the characteristic landforms that can be found in the rest of Tuktoyaktuk Peninsula. Tundra polygon networks are well distributed throughout most of the park, and the landforms that most clearly stand out in the landscape are the pingo ice-cored hills, which give PCL its name (Figure 31). Parks Canada officially states that there are 8 pingos in the park (Parks Canada, 2020), but, as has been

mentioned, recently Wolfe et al. (2023) identified 11 of these landforms within PCL. In the present study's Geomorphological Map, 8 pingos were identified (as will be seen in the "Results" chapter). However, it should be noted that that map does not cover the entirety of the park (as will be explained in the "Data and Methods" chapter), and within the area that was mapped, a total of 75 "Ice Mounds" were identified, some of which could be considered incipient pingos or possibly even pingos. The larger and most well-known pingos of the park, and the only ones to have officially recognized names, are Peninsula Point (or Kilutqusiaq) Pingo, Island Pingo, Split Pingo, and the tallest of all, Ibyuk Pingo (with a height of 49 m) (Mackay, 1998; Wolfe et al., 2023).

From a geological standpoint, according to the surficial geology map of the Tuktoyaktuk Coastlands, created by Rampton (1987) for Parks Canada, the Tuktoyaktuk Peninsula is characterized by the following formations (Figures 32, 33 and 34): **Blanket and Rolling moraine deposits**, generally less than 1 m to 12 m thick, most likely dating from the Late Pleistocene, or more precisely, the Early Wisconsinian glaciation[1] (predominantly located in the southwest sector of the Peninsula, as well as on the inner coast along the Husky Lakes and Liverpool Bay, but also sparsely scattered throughout the rest of the Peninsula); **Lacustrine deposits of silt, sand, gravel and some peat and organic sediment**, generally 2 to 10 m thick, with ages ranging from the Early Wisconsinian, to the Late Wisconsinian[2], to the Holocene[3] (predominantly located in the southwest and central sectors of the Peninsula, but also present on the inner coast along the Husky Lakes and Liverpool Bay, and sparsely scattered throughout the rest of the Peninsula); **Glaciofluvial deposits associated with outwash from plains and valley trains**, generally 3 to 30 m thick, most likely dating from the Early Wisconsinian (predominantly located in the central and northeast sectors of the Peninsula, but also sparsely scattered throughout the rest of the Peninsula); **Eolian deposits of sand and silty sand** (generally 1.5 to 3 m thick) **with underlying Colluvial deposits of clay, silt, sand and angular pebble to boulder-sized clasts** (generally 0.5 to 3 m thick), dating from the Holocene (predominantly located in the northeast sector of the Peninsula); **Glaciofluvial ice contact deposits**, generally 5 to 20 m thick, most likely dating from the Early Wisconsinian (predominantly located on the inner coast along the Husky Lakes and Liverpool Bay); and, lastly, **Marine deposits of sand, gravel, silt, clay, minor peat and organic sediment**, generally more than 1 m thick, dating from the Holocene (located only along the Beaufort Sea coast, deposited at or near sea level, on beaches, bars and spits). As for the area of PCL specifically, it is predominantly covered by the **Lacustrine deposits of silt, sand,**

[1] Culmination of the Early Wisconsin: 100 ka BP.
[2] Culmination of the Late Wisconsin: 50 ka BP.
[3] Holocene epoch: 11.7 BP to Present Day.

gravel and some peat and organic sediment formation, but is also partially covered by the **Blanket moraine deposits** formation, and slightly by the **Marine deposits of sand, gravel, silt, clay, minor peat and organic sediment** formation.

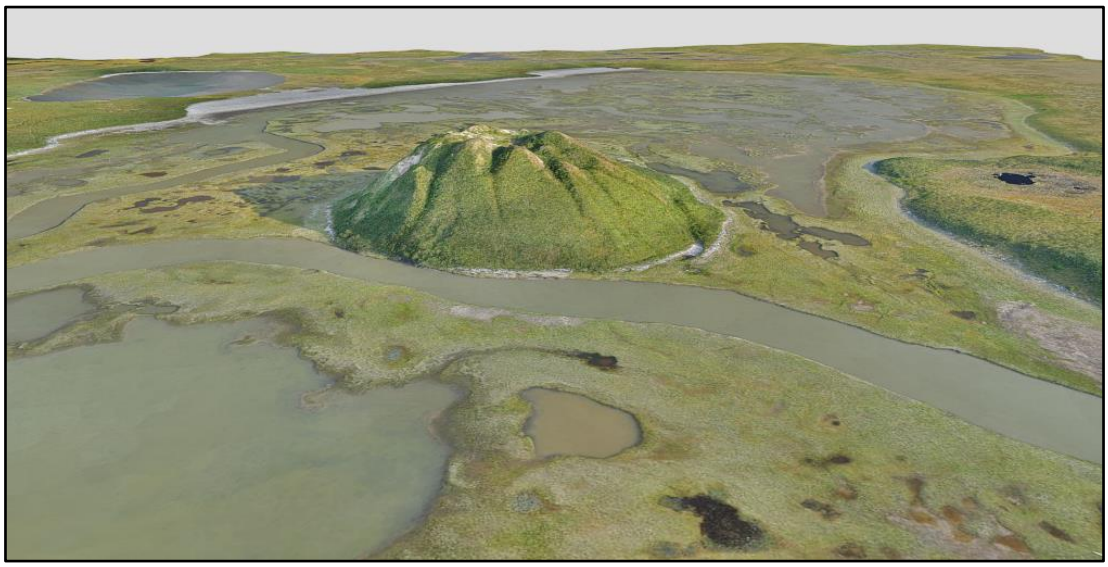

Figure 31 *- 3D model of PCL, presenting a view of Ibyuk Pingo's northern slopes, part of the drained lake that encompasses it, and surrounding areas. Source: Vieira (2020).*

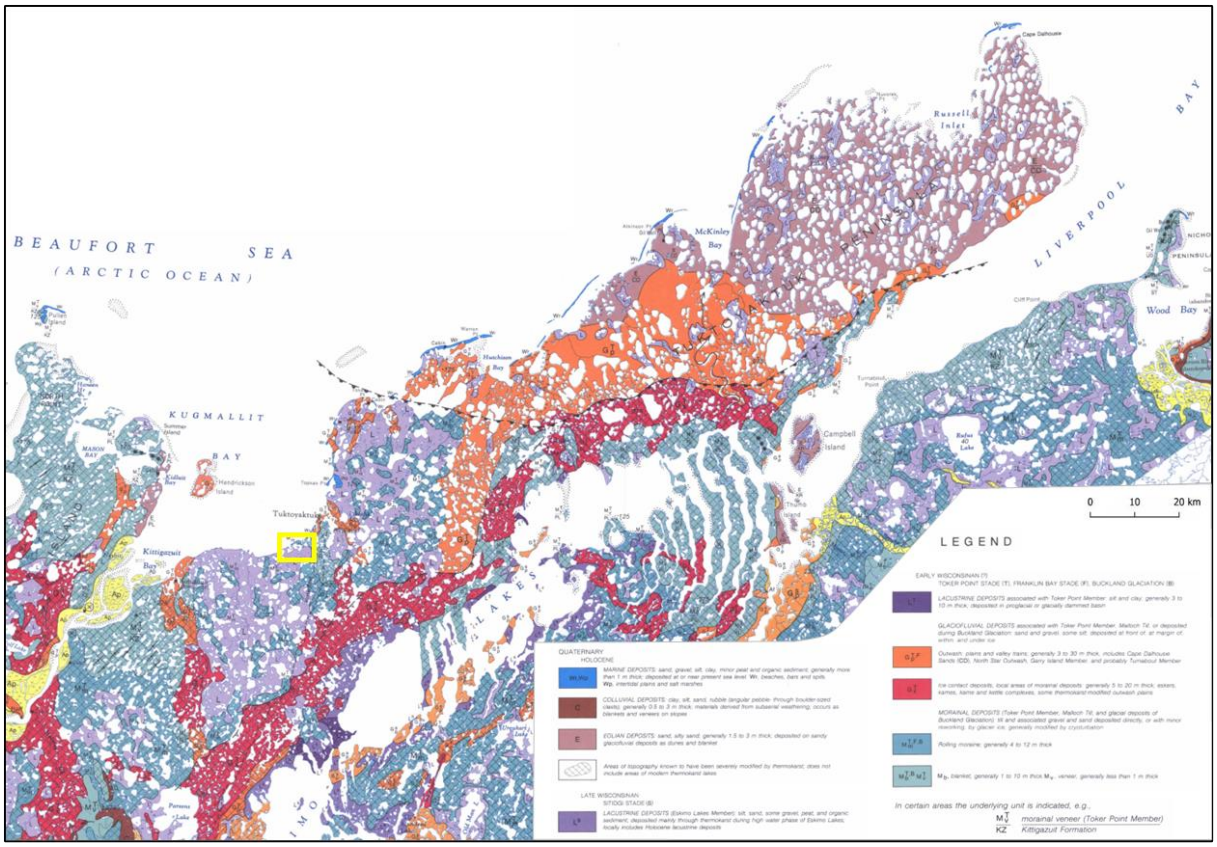

Figure 32 *– Surficial Geology of the Tuktoyaktuk Coastlands, focusing on the Tuktoyaktuk Peninsula. The general location of PCL is signaled by the small yellow rectangle. Source: Adapted from Rampton (1987).*

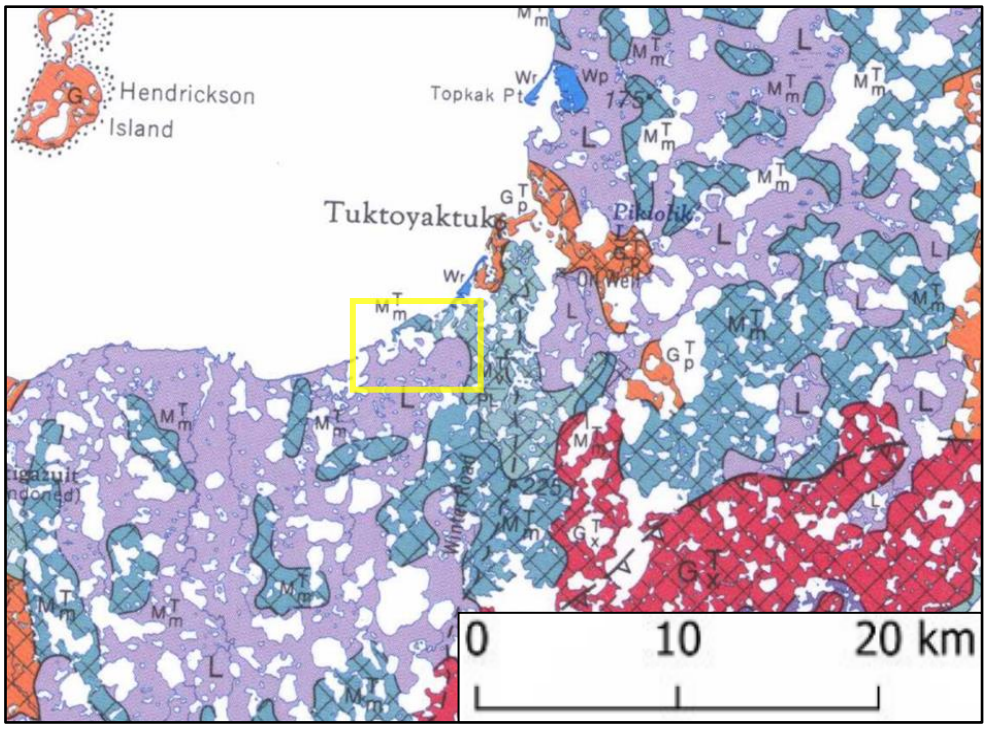

Figure 33 *- Surficial Geology of the Tuktoyaktuk Coastlands, focusing on PCL (general location signaled with yellow rectangle) and its surrounding areas. Same legend applies as for Figure 32. Source: Adapted from Rampton (1987).*

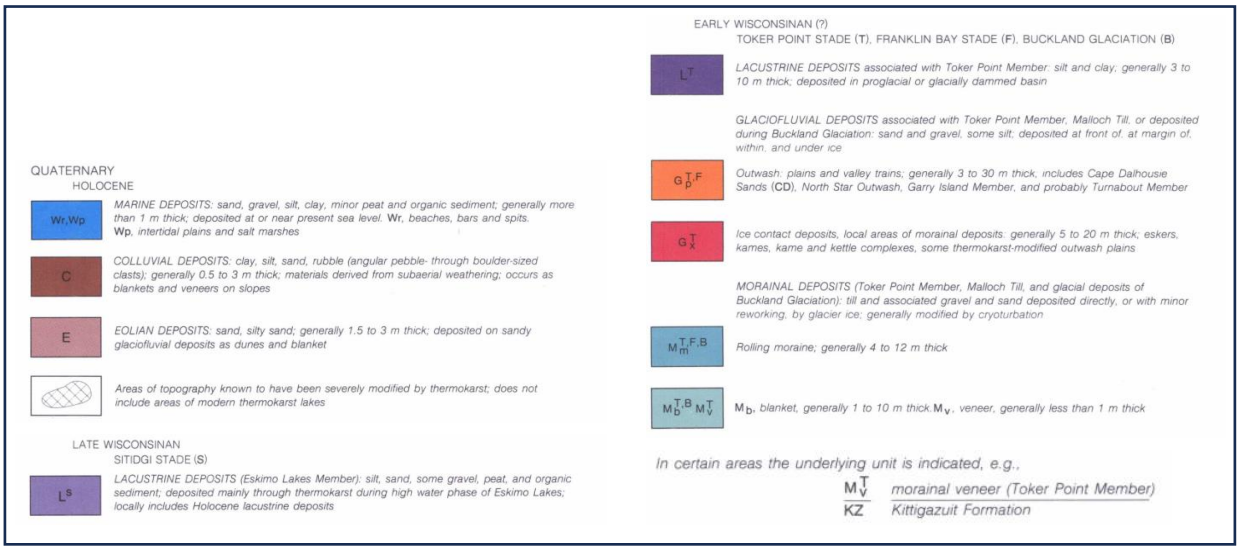

Figure 34 *– Enlarged version of the legend the applies to Figures 32 and 33. Source: Adapted from Rampton (1987).*

3.1.2 - Climate and Ocean Dynamics

According to the Köppen climate type classification system, the Tuktoyaktuk Peninsula is characterized by the **ET (Tundra)** climate type in its northeastern sector, and by the **Dfc**

(Continental Subarctic) climate type in its southwestern sector (which is where PCL is inserted) (Figure 35). The northeastern Tundra climate region is therefore typically characterized by extremely cold winters (with average temperatures of the coldest month often dropping below -30 ºC), and cool summers, with the warmest months registering monthly means greater than 0 °C, but less than 10 °C (average daily temperatures typically range from 5 °C to 15 °C in the summer). The southeastern Subarctic climate region is typically characterized by very cold winters (with average temperatures of the coldest month below 0 ºC), and 1 to 3 months of the year averaging above 10 ºC (Encyclopedia Britannica, 2009a, 2009b, 2009c; A. Peterson, 2016). As for the town of Tuktoyaktuk itself, the monthly mean of January is -27.2 ºC and that of July is 10.3 ºC. The thawing season (during which daily mean temperatures are positive) has an average duration of 55 days per year. The Tuktoyaktuk Peninsula registers relatively low levels of precipitation, as annual values typically range from 100 to 250 mm (Tuktoyaktuk counts with an annual average of 130 mm), without significant monthly differences, but with much of it falling as snow (56 cm/year is the average for Tuktoyaktuk) (Figure 36). Winds can be strong, especially during the winter months or during the occurrence of coastal storms, when they can reach > 50 km/h (French, 2007; Lim et al., 2020a).

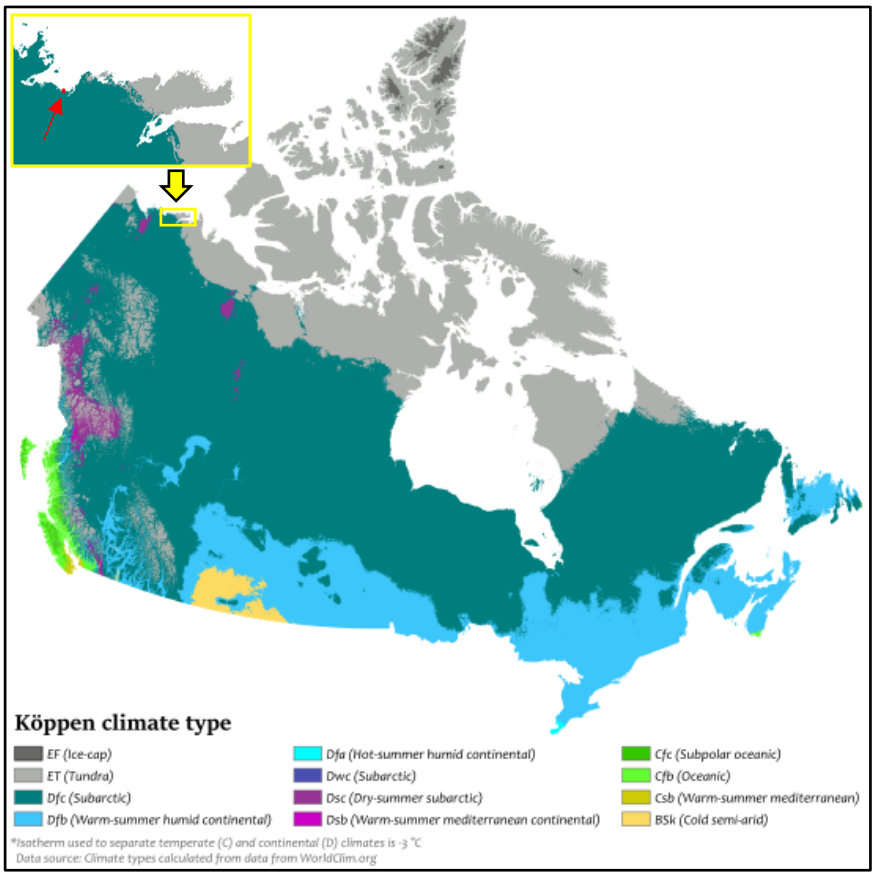

Figure 35 *- Köppen climate types of Canada. Approximate location of the Tuktoyaktuk Peninsula is signaled by the small yellow arrow and rectangle, and focused on in the large yellow rectangle. Within the large yellow rectangle, the approximate location of PCL is signaled with a small red arrow and dot. Source: Adapted from Peterson (2016).*

Figure 36 *- The landscape of PCL covered in snow. Ibyuk Pingo is in the front, Split Pingo is in the distance to the right, and Island Pingo is in the far distance to the left. Source: Saliqmiut - Tuktoyaktuk Centre for Arts and Culture (2022).*

Though localized current motions can be more complex (for example, due to wind patterns or small river inflows), currents generally flow from southwest to northeast along the Tuktoyaktuk Peninsula (Figure 37). The Mackenzie River, one of the largest rivers in North America, flows into the Beaufort Sea near the Tuktoyaktuk Peninsula, and the river discharges large volumes of freshwater, sediment, and nutrients into the coastal ocean. These are generally transported northeastward along the Tuktoyaktuk Peninsula, leading to the formation of deltaic and estuarine environments and influencing local marine ecosystems. Also, sea ice has a large impact on the ocean dynamics of the region, as it covers a substantial part of the coastal waters during much of the year, typically from October to June, with freezing usually beginning in the early fall, and breaking up and melting occurring in the late spring and summer. Together all these factors condition the development of coastal morphology (French, 2007; Timmermans & Toole, 2023).

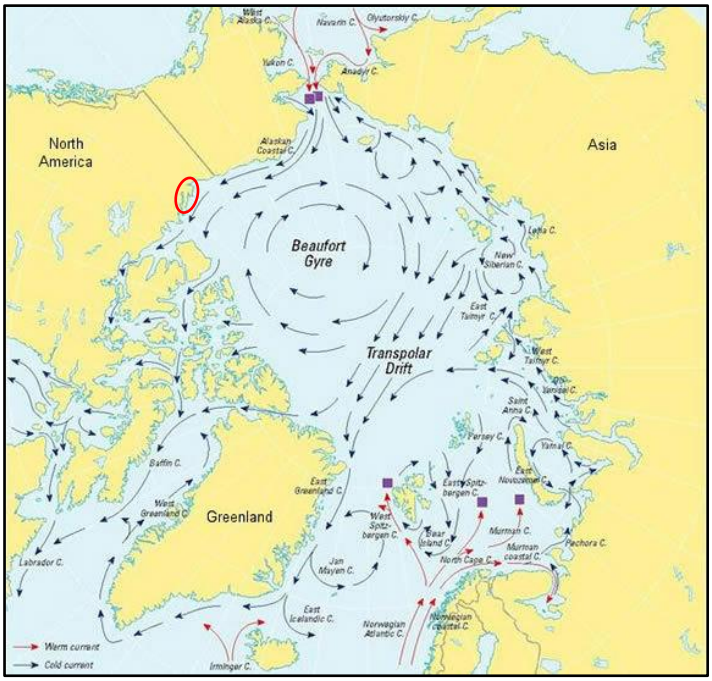

Figure 37 *- Arctic Ocean circulation. Tuktoyaktuk Peninsula is signaled by the small red oval. Source: AMAP - Arctic Monitoring and Assessment Programme (1998).*

At PCL specifically, according to Parker (2021) and Natural Resources Canada's CanCoast dataset (Manson et al., 2019), the Decadal Mean Wave Height for the 2000's is ≤ 0.25 m (corresponding to Sensitivity Class 1, the lowest on a scale of 5), while as for the 2090's it will be 0.26 m to 0.75 m (Sensitivity Class 2). However, as for the present-day tidal range, the same sources state that is ≤ 1 m, which falls into Sensitivity Class 5. Manson et al. (2019) refer that "flooding during storm surges is less likely to occur in areas with a large tide range and more likely to occur in areas with a small tide range", hence the very high sensitivity classification. Therefore, it can be discerned that flooding associated with storm events contribute greatly to the heterogeneity of PCL's landscape, leading to variations over time in the size and position of sand spits, beaches, and waterbodies, as well as to the deposition of driftwood along the coast, inundated basins, and at the base of pingos. The growth in intensity and frequency of storm events will lead to even harsher, and likely more permanent, changes in the landscape of this region. Also, in a warming climate, it can be expected that a reducing presence of sea ice throughout the year will lead to greater coastal erosion rates (especially when coupled with the more frequent occurrences of coastal storms), as the sea ice's mitigating effect on erosion will be diminished (Irrgang et al., 2018; Karjalainen et al., 2020; Lim et al., 2020a; Lim et al., 2020b; O'Rourke, 2017; Parker, 2021; Rantanen et al., 2022; Vermaire et al., 2013).

3.2 - Cultural Importance of Pingo Canadian Landmark

Though PCL's location is quite remote, there is a settlement only about 5 km northeast from the park, named Tuktoyaktuk (Figure 38), which can be translated as "place resembling a caribou", a named derived from legends that speak of a herd of caribou that waded into the ocean waters there and turned to stone. The rock formations resembling the petrified caribou are said to still be visible at low tide from the shore of the settlement. The hamlet of Tuktoyaktuk contained a population of 937 people in 2021, the vast majority of which belong to the Inuvialuit.

Figure 38 *- Welcome sign of the hamlet of Tuktoyaktuk (Left), and aerial view of the settlement (Right). Sources: AARoads (2019) (Left); Hamlet of Tuktoyaktuk (2024) (Right).*

The cultural value of PCL is indissociable from the Inuvialuit. They possess extensive traditional ecological knowledge, particularly related to Arctic wildlife, meteorology and climate patterns, and sustainable hunting, fishing and foraging practices. Some of their practices directly involve the landforms of the park as, for example, the pingos are sometimes used as vantage points, to gain a privileged view from above of the otherwise mostly flat landscape (Figure 39). Another key part of Inuvialuit culture is their language, Inuvialuktun, being that oral storytelling through it has resulted in the passing down through generations of historical events, myths, and cultural practices. The landscape is transversal to all those elements, and again, for example, pingos play a key role in folklore, such as in the "Story of the Great Flood", where one of these landforms was used as a refuge from the mythical natural disaster. Also still, Inuvialuit craftwork and art, including carvings, beadwork, and clothing made from animal hides and furs, is renowned both for its craftsmanship as well as its culturally symbolic value (Figure 40). These artworks sometimes depict stories, animals, and aspects of daily life, preserving cultural heritage. They continue to be created today, but older items are also found and are the subject of archaeological studies (Inuvialuit Regional Corporation, 2011, 2020; O'Rourke, 2017; Slaymaker, 2017; Walker, 2019).

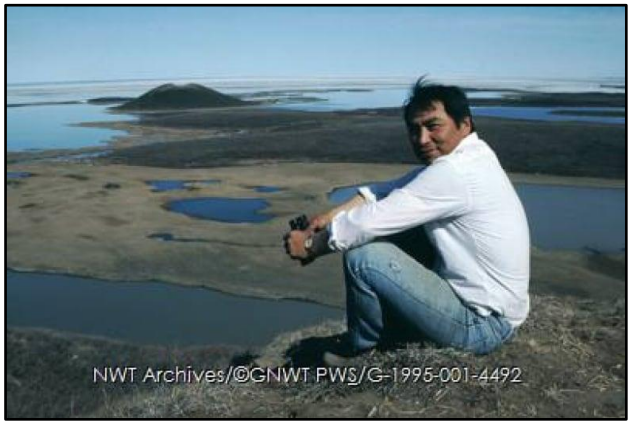

Figure 39 *- Randal Pokiak (1949-2020), first ever chair of the Inuvialuit Development Corporation and a lifelong advocate for Indigenous rights and traditional harvesting in the NWT, atop Ibyuk Pingo. Source: NWT Archives & Department of Public Works and Services (1987) in CBC News (2020).*

Figure 40 - *Examples of Inuvialuit artifacts. Top row, from left to right: Snow goggles; Bowl made from baleen; Needle case; Ladle. Bottom row, from left to right: Doll; Clothing toggle decorated with polar bear faces; Pendant or amulet; Harpoon head. Source: Inuvialuit Regional Corporation (2011).*

As the rich Inuvialuit traditions are intertwined with the land, in a context in which the land is at risk of gradually disappearing, those traditions are also at risk of vanishing. Coastal erosion is not only a threat to the landforms of PCL and the surrounding regions, but also to the infrastructure that is essential to the daily life of the inhabitants of these lands. With this, it is ever so important to take efforts to preserve both. Coastal erosion and the occurrence of storm events already have impacts on structures in Tuktoyaktuk (Figure 41), and measures are being taken to mitigate the risk, through means of the construction of coastal barriers (Government of Canada, 2023), and even relocation of homes (Lim et al., 2020a). As for PCL, having been declared a protected area under the Western Arctic (Inuvialuit) Claims Settlement Act (1984), and being currently managed under the Canada National Parks Act (2000), the Pingo Canadian Landmark Memorandum of Agreement (2001) and the Pingo Canadian Landmark Management Statement (2018), it benefits from a large group of conservational measures and regulations. For instance, the Western Arctic (Inuvialuit) Claims Settlement Act prohibits the exploration for, or extraction of, subsurface resources within the Pingo Canadian Landmark borders. Also, the site can only be visited by tourists who are accompanied by licensed guides, and visits take place solely along a wooden walkway constructed for that purpose that extends into the park. Also still, it is intended that PCL should only be accessed by boat or helicopter, but, as shall be pointed out later in this study, there is evidence that this measure is not always respected. Thus, the need to continue vowing for the conservation of the land, its people, and their culture continues in the region.

Figure 41 *- Waves caused by a storm in Tuktoyaktuk during the summer of 2019. Source: Cabin Radio (2023).*

4 - DATA AND METHODS

4.1 – General Considerations

Two major products created on behalf of this thesis are the Geomorphological Map and the Landcover Map. Both have as subject PCL, though, as shall be explained, it was not possible to characterize the entirety of the area of the park in the Geomorphological Map.

The Geomorphological Map was created mainly based on the ultra-high resolution (10 cm) Unmanned Aerial Vehicle (UAV) optical orthomosaic, obtained in the field in July 2019 by the team of CEG/IGOT - University of Lisbon and the Geological Survey of Canada. As for the ultra-high resolution (10 cm) UAV Digital Surface Model (DSM), it aided greatly in the elaboration of this map, namely through the products that were obtained based on it (for example, contour line maps and hillshade models). Also, the very-high resolution WorldView-2 scene, from July 2017, was used to complement the UAV data for some areas of the park that could not be covered by the UAV surveys. This commercial satellite imagery provided some additional information and was helpful in the elaboration of the Geomorphological Map, namely through the Landcover Map that was produced based on it, but also to fill some voids in the UAV data (as will be explained). All features present in the Geomorphological Map were manually digitized upon photointerpretation of the data mentioned.

The Landcover Map was created based on the very-high resolution (1.84 m multispectral imagery and 46 cm panchromatic imagery) WorldView-2 scene from July 2017, using a supervised classification analysis. The already described UAV orthomosaic aided in the elaboration of this map too, in the sense that it allowed to visualize some landscape features in even more detail than the commercial satellite scene (of course, this applies only to areas covered simultaneously by the UAV orthomosaic and the WorldView-2 scene). Namely, it was helpful in the control point identification step of the georeferencing process, which was necessary to apply to the purchased WorldView-2 satellite imagery, as well as in the step of the creation of training areas for the supervised classification.

The data used for the elaboration of the Geomorphological Map and Landcover Map, as well as the procedures associated with their creation are summarized in Figure 42, and shall be described in detail in the upcoming chapters.

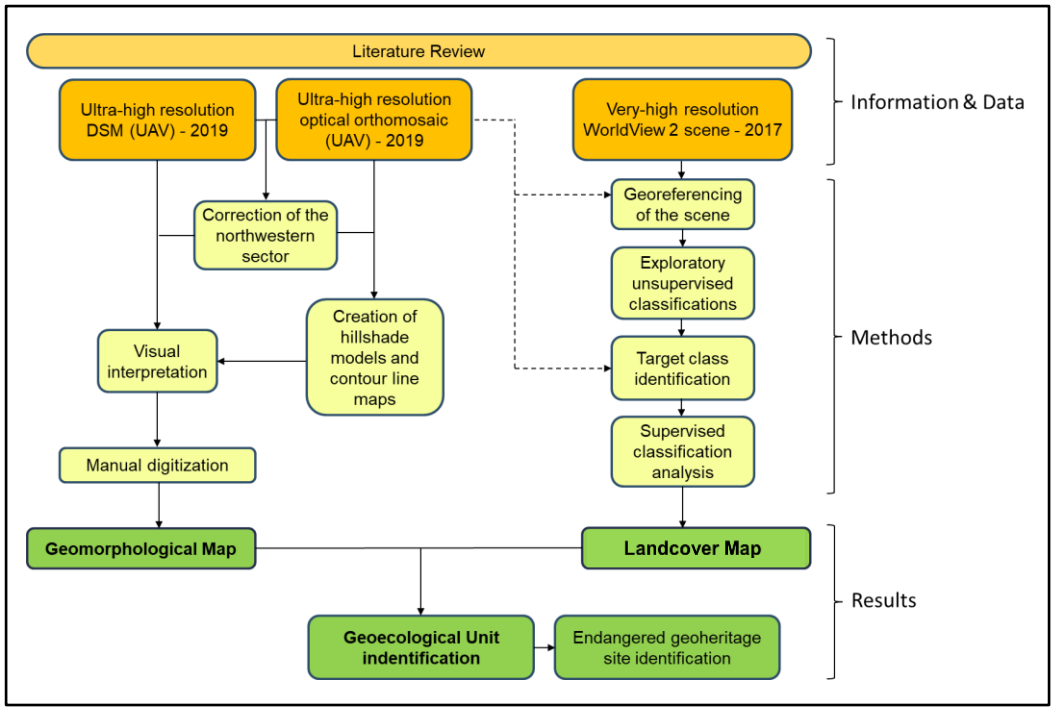

Figure 42 *– Flowchart depicting the data used (in orange) to create the main results of this dissertation (in green), as well as methods used (in yellow) to analyze the data and obtain the results.*

4.2 - Geomorphological Mapping

4.2.1 - UAV Orthomosaic and DSM

The UAV orthomosaic (Figure 43) and DSM (Figure 44) were both generated from a series of vertical photographs, taken on a field campaign that took place in the summer of 2019. Though I did not participate in it, both the main supervisor and co-supervisor of this thesis did. The original UAV flights which resulted in the data used in this study took place on July 29th, 30th and 31st of 2019. During these 3 days, a total of 17 flights were conducted, however, it was not possible to obtain a total coverage of the park, namely due to time constraints and logistical issues, such as difficult accessibility to the park (which, for conservational reasons, is to be accessed only by boat or helicopter), as well as difficult wind conditions. With these flights, about 65.34% of the area of the park (excluding coastal waters) was covered (See green outline in Figure 43 and 44). As for the UAV model used in this survey, it was a SenseFly ebee Plus RTK, equipped with a 20 megapixel S.O.D.A. camera (Figure 45). It should also be mentioned that, for these surveys, a Trimble R4 GPS base station for post-processing (PPK) of the aerial imagery was used, allowing a very accurate geolocation, even without using many ground control points (Figure 46). The software used in the postprocessing was Pix4Dmapper, being that the final orthomosaic was created based on a total of 8390 individual images, using 11 ground control points. As for the accuracy associated with the data obtained in this survey, the post-processing displayed a Root Mean Square Error of 0.035 m.

It should be clarified that, as I did not participate in the field campaign in which the surveys were conducted, I also did not perform any of the tasks associated with the post-processing of the raw imagery.

This already described UAV data does not, however, correspond to the totality of that which was analyzed to create the Geomorphological Map. This is because, still framed within the same field campaign, an additional survey was later conducted in the northwestern region of PCL by a team of the Geological Survey of Canada. This survey was conducted on the 9th of August, 2019, and the drone model used was a DJI Matrice 210 RTK, equipped with a 20 megapixel DJI ZenMuse X4S FC6510 camera (Figure 47). This survey allowed that, approximately, an additional 6.93% of the area of the park (excluding coastal waters) could be covered (see orange outline in Figure 43 and 44). Therefore, in total, the two drone surveys covered about 72.27% of the area of the park (excluding coastal waters). The geolocation of the orthomosaic and DSM associated with this second survey was also very good. However, a very slight adjustment of the positioning of the orthomosaic and DSM associated with the second survey was performed, so that they could align more perfectly with those of the first survey. This was done using the Freehand Raster Georeferencer plugin for QGIS. There was still an additional procedure that was necessary to apply to the DSM of the second drone survey, which was a correction to its altitude values. When comparing the DSM altitude values in the small regions where both the first and second survey overlapped (see black dotted areas in Figure 43 and 44), there appeared to be a somewhat consistent difference between them, with the altitudes of the second survey's DSM being (incorrectly) greater than those of the first. To correct this issue, first, precise and clearly identifiable locations were chosen (through visual interpretation of the orthomosaics) in the regions where both surveys overlapped. Then, with point features created on those locations, altitude values were extracted at them for each DSM. Next, the mean difference in altitude between the two DSMs at those points was calculated. Finally, given that the second survey's DSM had values that were incorrectly higher than those of the first survey, the mean difference was subtracted from the second survey's DSM values. With this, the second survey's DSM altitude values aligned much better with those of the first survey. Before these procedures, the mean difference in altitude between the DSMs of the first and second surveys was about 78.9 m, and after them it was approximately 0.1 m.

For the purpose of all analyses henceforth, the orthomosaic associated with the first survey and the one associated with the second survey were considered as one whole orthomosaic (and will be referred to as such from here forward), with the data of the first survey being superimposed upon that of the second in the areas where they overlap (see black dotted areas in Figure 43 and 44). The same is valid for the DSMs associated with the two surveys. However, it should also be mentioned that there were two areas of the park amidst the UAV

data that were covered by neither of the two surveys, with these two areas together corresponding to about 5.13% of the total area of PCL, excluding coastal waters (see magenta outline in Figure 43 and 44). In order to not have two “voids” of unmapped features surrounded by areas where features were mapped, it was decided that in these two areas, all features present would be digitized based on the visual analysis of the very-high resolution WorldView-2 scene. By using the commercial satellite image as a complement to the UAV data in these restricted areas, the final proportion of PCL’s extent (excluding coastal waters) covered by the Geomorphological Map was approximately 77.4%.

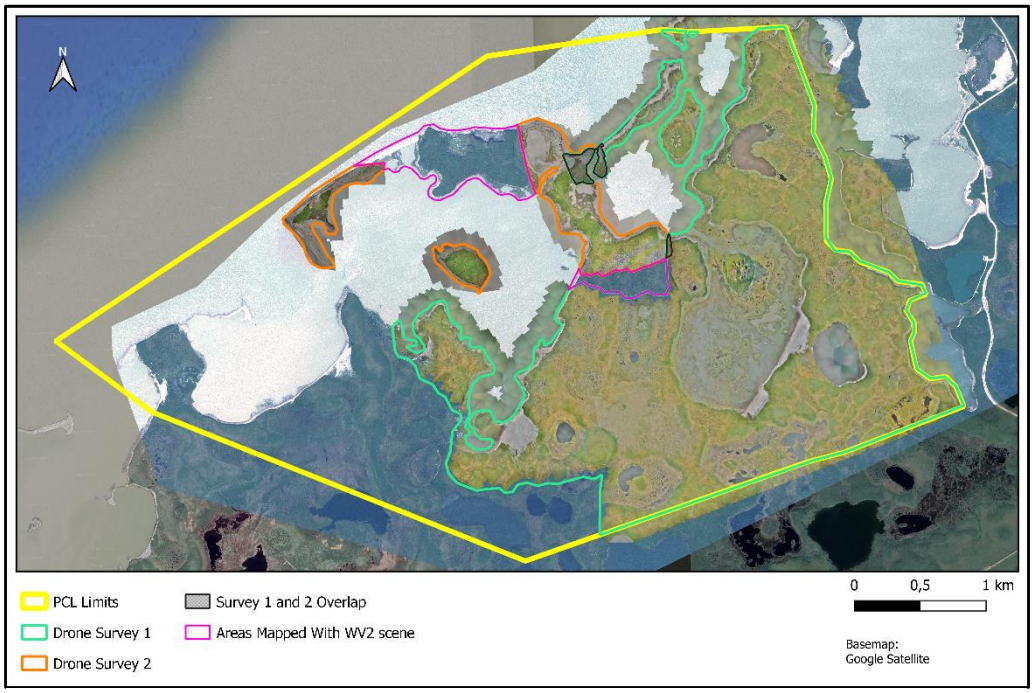

Figure 43 *– UAV orthomosaic, with the indication of the extent of PCL covered by UAV surveys 1 and 2, the areas where the two surveys overlap, and areas that were mapped using the WorldView-2 scene.*

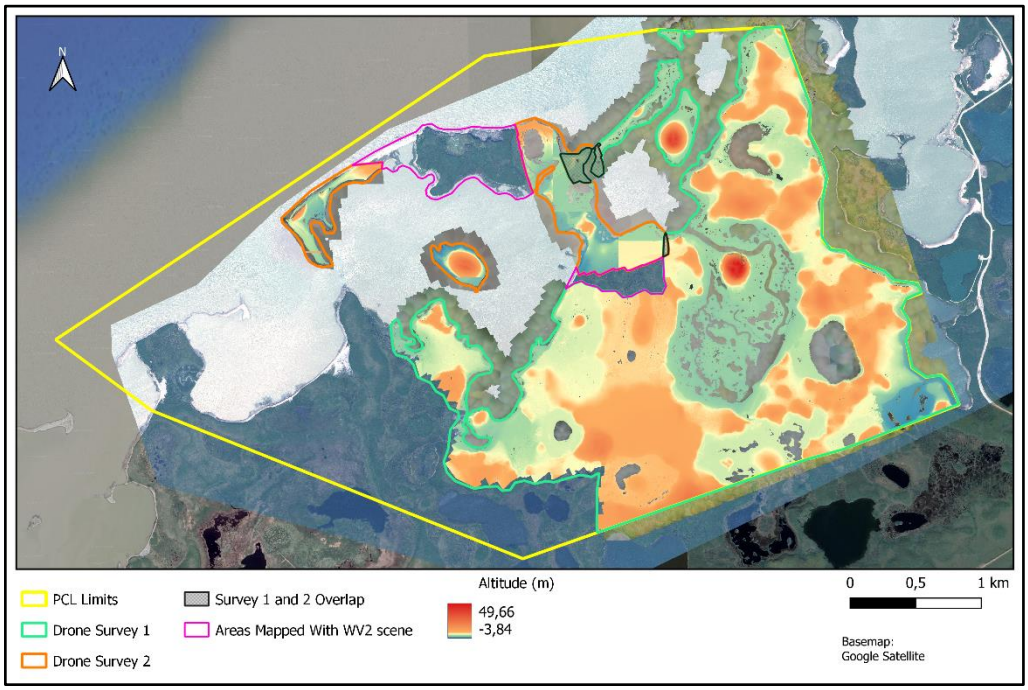

Figure 44 *- UAV DSM, with the indication of the extent of PCL covered by UAV surveys 1 and 2, the areas where the two surveys overlap, and areas that were mapped using the WorldView-2 scene.*

Figure 45 *- SenseFly ebee Plus RTK UAV model (Left), and its launch at PCL on behalf of the July 2019 field campaign of CEG/IGOT - University of Lisbon and the Geological Survey of Canada (Right). Source: Canada DroneTrader (2021) (Left); Photo by Vieira (2019) (Right).*

Figure 46 *- Trimble R4 GPS base station. Source: International Surveying Equipment (2024).*

Figure 47 *- DJI Matrice 210 RTK UAV model. Source: Arctic Drone Labs (2020).*

4.2.2 - Data Analysis Methods

The elaboration of the Geomorphological Map began with a visual analysis of the drone orthomosaic, with the objective of identifying the potential set of different landscape features that were to be included in the map. Previous study of literature regarding polar and periglacial geomorphology, as well as about the study area and the region in which it is inserted, aided in this initial procedure.

The original group of classes that were chosen were the following: “Pingos”; “Tundra Polygons”; “Lakes and Ponds”; “Driftwood Accumulations”; “Inundated Lake Basins”; and “Tourist Walkway”. However, as the mapping process carried on, more classes were considered necessary for a thorough representation of the landscape of the park, and were also added. These included the classes “Ancient Lake Basins”, “Vehicle Tracks”; “Seismic Lines”; “Ice Mounds”; “Sand”; “Cliffs”; and “Tundra Plains”. It was also decided to distinguish five sub-classes within the “Inundated Lake Basins” class and the “Ancient Lake Basins” class: “Large (Isolated) Wetland Lakes and Ponds”; “Wetlands”; “Wetlands with Lakes and Ponds”; “Dry Wetlands”; and “Dry Wetlands with Small Lakes and Ponds”. Also still, within the class “Pingos”, two sub-classes were added: “Pingo Craters and Dilation Cracks”; and “Pingo Surface Erosion”. With this, the final version of the map includes a set of twenty classes.

The ultra-high detail (10 cm resolution) of the UAV orthomosaic (and DSM) was a factor that significantly helped in the identification of all chosen landscape features, in the sense that it allowed all features to be mapped very precisely (Figure 48). Within the chosen GIS software for this task (QGIS), the mapping process was always conducted using large scale values, ranging from 1:1000 up to 1:50, in order to guarantee that the features were marked with high detail. Nevertheless, the scale values and other mapping techniques varied from class to class, depending on the nature of each class in question.

For the class “Pingos” (Figure 49), scales between 1:1000 and 1:500 were used to identify the borders of these landforms. Each pingo was marked as a polygon feature with a transparent fill. This way, what was marked on the map was the perimeter of each pingo. The identification of the pingos’ borders was done with the aid of the DSM derived hillshade models (namely, one created with a “Z Factor” of 1, an “Azimuth Value” of 300, and a “V Angle” of 40) (Figure 50) and contour line maps (namely, one with 1 m equidistance) (Figure 51). On these, the increment in elevation associated with the pingo landforms was quite noticeable, being that normally it was easy to determine very precisely where the pingos’ slopes began, and define their borders. In cases where it was less clear where the slopes started, visual proxies were used for the definition of the pingos’ borders, namely, noticeable changes in the vegetation (which tends to be lusher on the pingo slopes), or the limits of driftwood accumulations (being

that the deposition of driftwood difficultly occurs on pingo slopes). In total, 8 pingo landforms were found and included in this class.

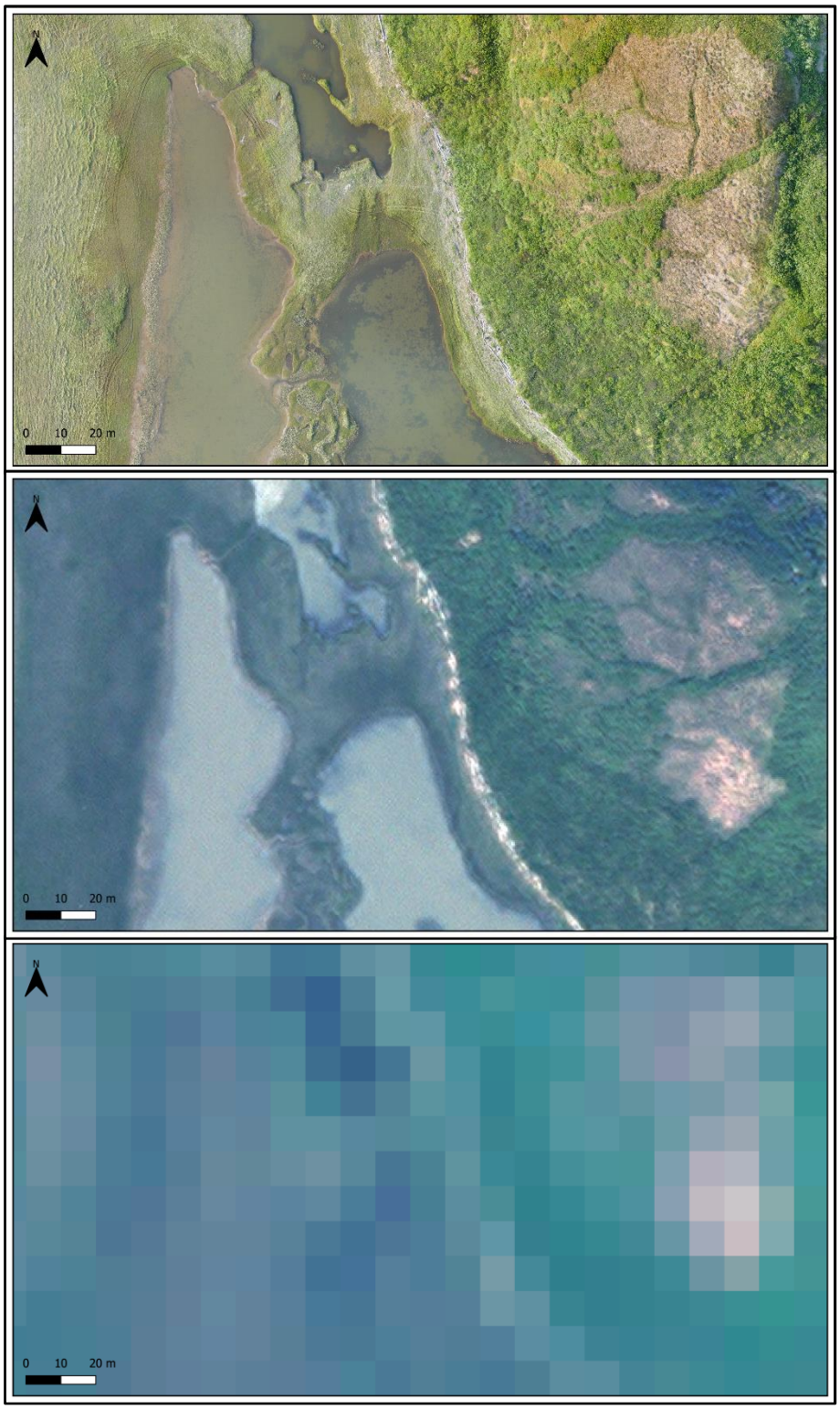

Figure 48 *– Comparison of the ultra-high resolution (10 cm) UAV imagery used for the Geomorphological Map (Top), with the very-high resolution (46 cm) pansharpened WorldView-2 scene (Middle), and with a georeferenced open access high resolution (10 m) Sentinel-2 true color composite (Bottom). All images refer to the exact same area, which is a portion of Ibyuk Pingo's eastern slopes, where, besides the natural features, vehicle tracks can be noticed (but only with UAV imagery), starting just above the map scale and leading up to the pingo's base.*

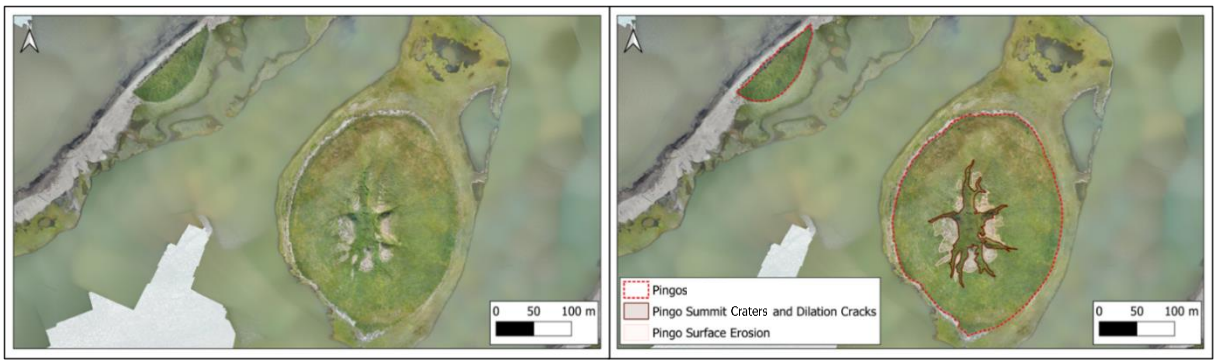

Figure 49 *– Examples of pingos digitized for the Geomorphological Map, in this case, Split Pingo (larger and to the right) and a smaller eroded pingo (to the left). Examples of the classes "Pingo Summit Craters and Dilation Cracks" and "Pingo Surface Erosion" are also shown.*

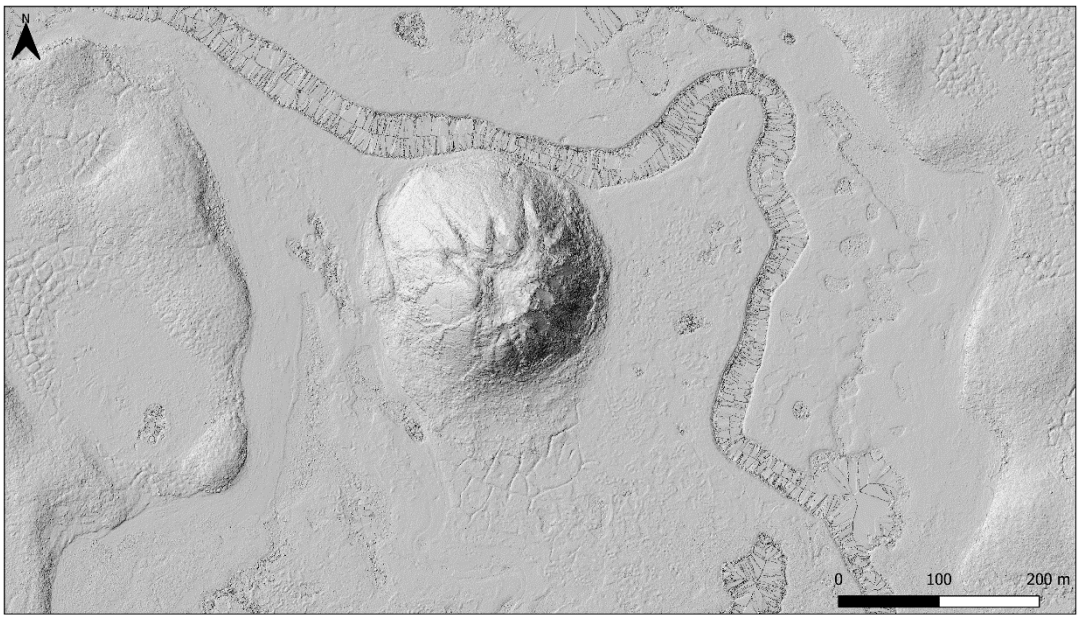

Figure 50 *– Hillshade model used as an aid in the elaboration of the Geomorphological Map. This view shows Ibyuk Pingo and its surroundings.*

Figure 51 *– Contour line map (1 m equidistance, with labels every 5 m), used as an aid in the elaboration of the Geomorphological Map. The view is the same as Figure 50.*

On some pingos, signs of the characteristic geomorphological dynamics that affect these landforms as they age were present, namely summit craters, dilation cracks, and surface erosion (Figure 49). These features were found and delineated on Pingos 1 (Ibyuk Pingo), 2 (Split Pingo), 3 (Island Pingo) and 7 (unnamed) (see Chapter 5.1 for pingo numbers). As the dilation cracks are typically extensions of the summit crater along the slope of the pingos, the craters and cracks were delineated together in the same class ("Pingo Summit Craters and Dilation Cracks", with 5 features identified), while as the patches of erosion present on the pingos' surface were attributed a separate class ("Pingo Surface Erosion", with 28 features identified). These classes were delineated as polygonal features, at scales of 1:250 to 1:100, as they required a more detailed view to identify. These two subclasses of the class "Pingos" overlap in certain spots, where surface erosion is present in the craters or cracks.

For the class "Tundra Polygons" (Figure 52), the scale normally used was 1:250. However, many times, in order to precisely delineate these features, even larger scales were used, like 1:100 or 1:50. This was done for smaller tundra polygons, namely those measuring less than about 15 m across, as well as in cases where the borders of tundra polygons were less clear. In these instances, the already mentioned hillshade models were very helpful, as in them these landforms were usually clearly noticeable. Each of these landforms were represented as polygonal features on the map, and it is important to mention that it was the tundra polygons themselves that were mapped, and not the ice wedges with which they are associated. In an initial stage, the process of mapping the ice wedges (as linear features) was begun, but it was later decided to not pursue that task, due to time constraint reasons and because it was considered that the mapping of the tundra polygons would provide sufficient data for the purposes and goals of this study. Given that a total of 14,518 tundra polygon features were identified and manually digitized, the "Tundra Polygons" class was the one which required the largest amount of time to map. Also, though tundra polygons can be quite varied in nature (something mentioned in the Literature Review section of this dissertation, and verified empirically throughout the mapping process), for the purposes of this study, tundra polygons were not distinguished into any type of sub-classes according to their morphology.

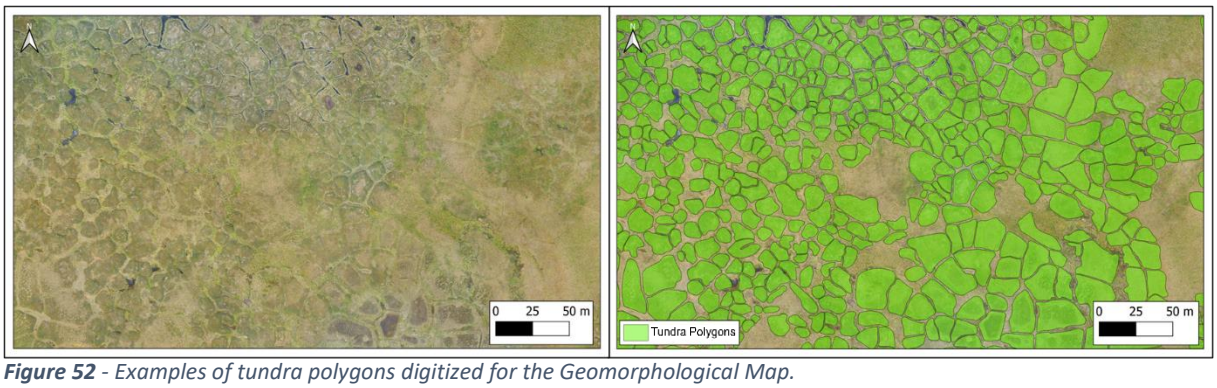

Figure 52 *- Examples of tundra polygons digitized for the Geomorphological Map.*

The “Lakes and Ponds” class represents the inland waterbodies existing within the park (Figure 53). PCL contains several larger lakes, being that these were mapped using a scale of 1:500. For smaller waterbodies, scales of 1:250 up to 1:50 were used. These larger scales were also applied for larger lakes in cases where the wet-dry line associated with the lake margin was difficult to discern (many times, due to the presence of hydrophytic vegetation). All lakes and ponds were mapped as polygonal features, with the borders of these polygons corresponding to the lake or pond margins. A total of 8593 waterbodies were digitized, being that the large majority of these were small waterbodies, located in the immediate vicinity of the larger lakes, and many times associated with the typical depressions of low-centered tundra polygons, or with ice wedges, which, as mentioned by French (2007) and Williams & Smith (1989), sometimes tend to develop into channel-like features.

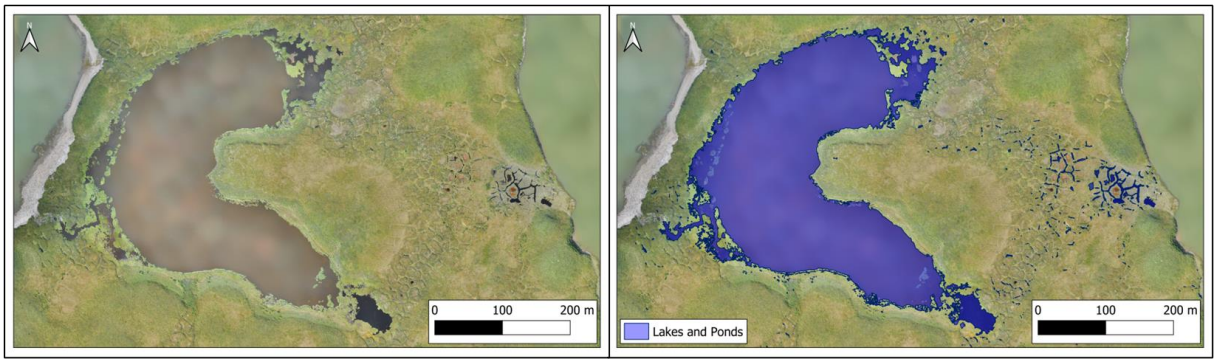

Figure 53 *- Examples of lakes and ponds digitized for the Geomorphological Map.*

In the class “Driftwood Accumulations” (Figure 54), these landscape features were mapped as polygonal elements, with a total of 90 polygons being digitized. The mapped driftwood accumulations were found to be somewhat varied in nature. Some had a very vast size, as well as a high density of driftwood, while others were much smaller and presented a much sparser distribution of driftwood. The smallest driftwood accumulation that was considered worthy of mapping contained roughly just a dozen logs (which varied in length between about 1 and 2 m). For the mapping of smaller accumulations like that, larger scales were used, such as 1:100, while the scales used for the biggest accumulations usually ranged from 1:1000 to 1:500. However, many of the mapped driftwood accumulations (especially the larger ones) presented not only portions on dry land, but also portions that were submersed. These submersed portions were included into the map (to the extent that they were still observable on the orthomosaic), being that larger scale values were used to map them due to their more difficult visibility.

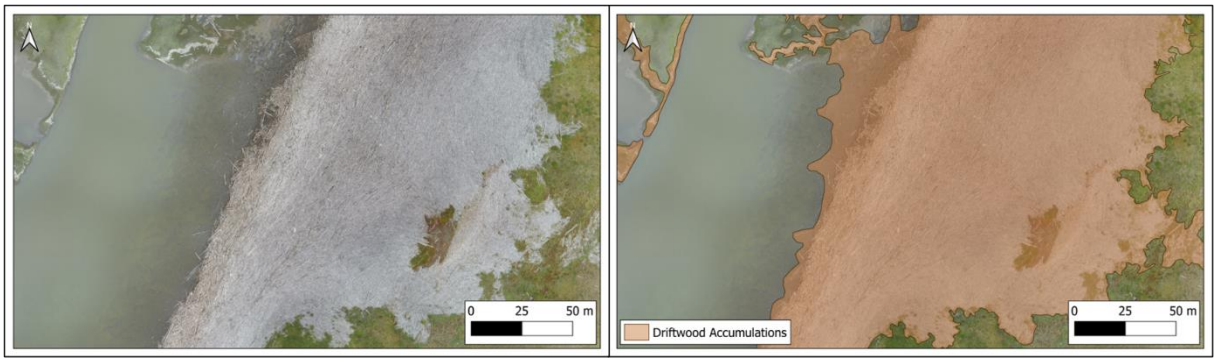

Figure 54 *- Examples of driftwood accumulations digitized for the Geomorphological Map.*

The “Inundated Lake Basins” class (Figure 55) corresponds to 2 polygonal features that encompass the extent of two now drained lakes located within the boundaries of the park which present signs of sometimes still being (at least partially) inundated. The larger one surrounds Ibyuk Pingo, while the smaller one is located near the southeastern limits of the park. The drained lakes are depressed in relation to their surrounding areas, something clearly noticeable in the DSM and hillshade models. Also, there is a clear change in vegetation between the depressed inundated lake basins and the more elevated areas that are contiguous to them. These factors aided in the process of identifying the margins of the drained lakes. To map these features, scales of 1:1000 to 1:500 were used.

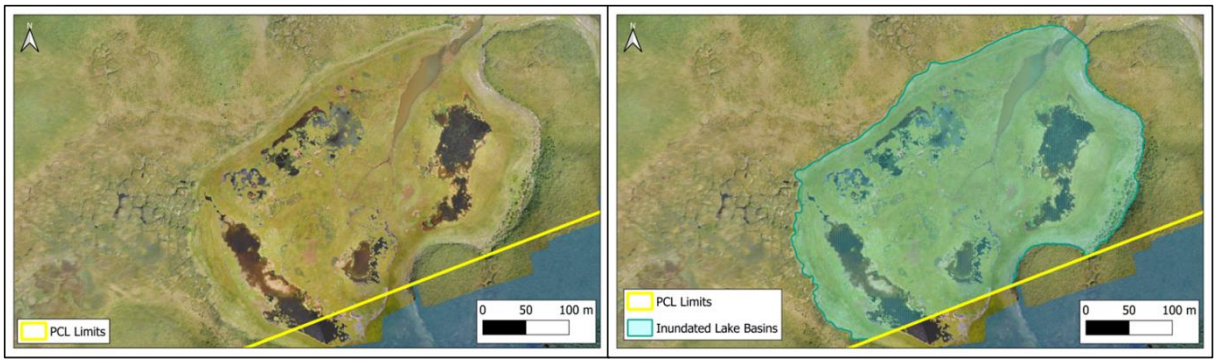

Figure 55 *– Example of an inundated lake basin digitized for the Geomorphological Map, in this case, the one located near the southeastern limits of the park.*

The “Ancient Lake Basins” class (Figure 56) comprises 4 features, that evidence signs of having once been lakes, but apparently have long been drained. They also do not show signs of recent and recurrent flooding (as is the case with the “Inundated Lake Basins”). Nevertheless, similarly to the “Inundated Lake Basins” these areas are also depressed in relation to their surroundings (as was evidenced in the DSM and hillshade models), and their vegetation was also distinct from those adjacent areas, typically being drier and less well developed. To delineate these features, the scales used were identical to those used for the “Inundated Lake Basins” (1:1000 to 1:500).

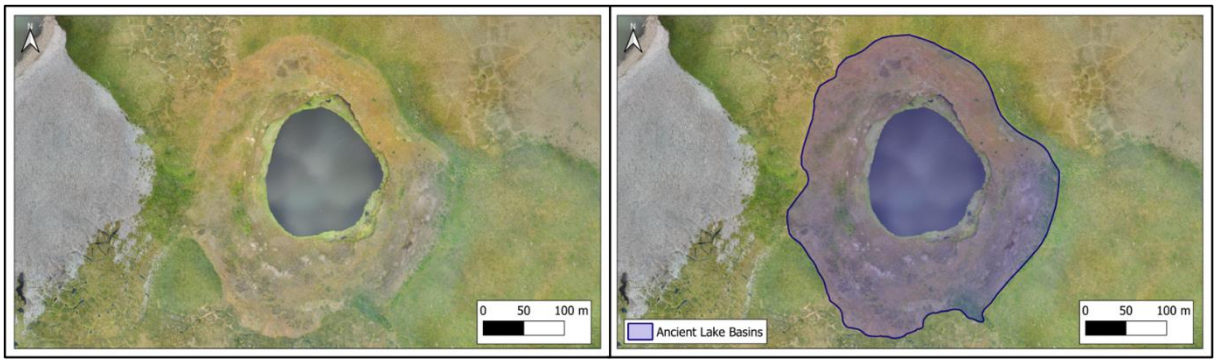

Figure 56 *- Example of an ancient lake basin digitized for the Geomorphological Map.*

The areas within the extent of the “Inundated Lake Basins” class are characterized by a great heterogeneity and are quite distinct from the remaining landscape of the park. For this reason, it was decided that these regions should be divided into subclasses. Though not characterized by such a high degree of heterogeneity, the “Ancient Lake Basins” class contained some areas that presented great similarity to those identified within the “Inundated Lake Basins”, and, therefore, it was decided that, when applicable, the same subclasses would be identified within that class too. With this, a total of five subclasses were digitized within the boundaries of these two classes, all consisting in polygonal features, being that this process involved an extensive interpretation of the landscape in these areas of the park (Figure 57). At the end of this process, QGIS’s vector geoprocessing tools were used to guarantee that there was no overlapping of these subclasses. Also, within the “Ancient Lake Basins”, some large lakes were found (as well as smaller lakes and ponds in their vicinity), and it was decided that all these waterbodies were to be included in the class “Lakes and Ponds” when they appeared to be perennial in nature. For the “Inundated Lake Basins” this was not done, as the lakes and ponds present within them seemed to be either ephemeral, or to have variable extents that most likely tend to be altered with the occurrence of flood events.

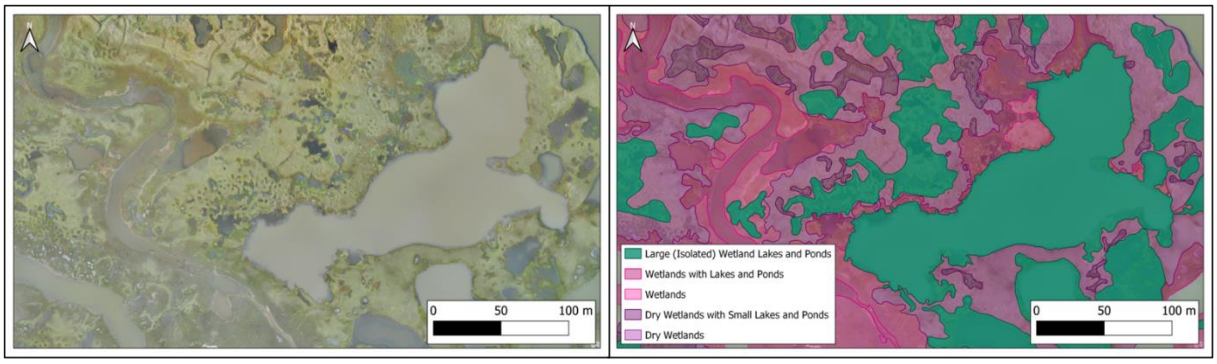

Figure 57 *- Examples of the five subclasses digitized within the “Inundated Lake Basins” and the “Ancient Lake Basins” classes for the Geomorphological Map. In this case, the view is of an area within the inundated lake basin that surrounds Ibyuk Pingo.*

The first of the five previously mentioned subclasses to be mapped was “Large (Isolated) Wetland Lakes and Ponds”, and it was only found within the “Inundated Lake Basins”

class. It was mapped first because its features were the most clearly distinguishable in comparison to those of the other subclasses. It was digitized using scales ranging from 1:500 to 1:250, depending on the size of the waterbodies and on how clearly identifiable their margins were. The waterbodies included in this class were those that were isolated, or not connected to the flows of coastal water that enter each basin (for the large basin surrounding Ibyuk Pingo this occurs at a sector of its northwestern margin, while as for the smaller basin the flow enters at a sector of its northeastern margin). Some smaller (but also isolated) waterbodies located in the immediate vicinity of larger ones were included into this subclass, but many waterbodies included in this subclass were relatively large, especially when compared to those that were included in the subclasses “Wetlands with Lakes and Ponds” and “Dry Wetlands with Small Lakes and Ponds”. This first subclass included a total of 61 polygonal features.

“Wetlands” and “Wetlands with Lakes and Ponds” were two more subclasses that were created. The first included a total of 58 polygonal features (and was only found in the “Inundated Lake Basins” class), while the latter included 47 of these features (and was also found in the “Ancient Lake Basins” class). As for the scales used for the digitization of these polygons, they ranged from 1:500 up to 1:100, in cases where landscape interpretation was more difficult. The areas included in these two classes have in common the fact that they are generally adjacent to the flow of coastal water that enters each basin, and present characteristics that indicate that they are frequently flooded (such as less developed vegetation, or muddy terrain). The main difference between these two classes is that the “Wetlands with Lakes and Ponds” subclass is characterized by possessing many small and medium waterbodies scattered across it, and tends to be muddier that that of the “Wetlands” subclass.

“Dry Wetlands” and “Dry Wetlands with Small Lakes and Ponds” were the other two subclasses also digitized. The first included a total of 68 polygonal features, and was found within the “Ancient Lake Basins” class, as well as the “Inundated Lake Basins” (though only within the larger of the inundated lake basins). The latter included 54 polygonal features, and was only found within the “Inundated Lake Basins”. Just like the two previously described subclasses, the scales used to digitize these were between 1:500 and 1:100, depending on how difficult the landscape interpretation was. These two subclasses have in common the fact that they both show signs of not being flooded as often as the others, being generally more distant from the flow of coastal water that enters the basin than the “Wetlands” and “Wetlands with Lakes and Ponds” subclasses. Their vegetation seems to be more developed than that present in those subclasses, and they also are much less muddy. What distinguishes the “Dry Wetlands” and the “Dry Wetlands with Small Lakes and Ponds” from each other is that the

latter is characterized by possessing many small waterbodies, which, in general, are inferior in size to those of the “Wetlands with Lakes and Ponds” subclass.

Next, the “Ice Mounds” class shall be mentioned (Figure 58). These periglacial landforms consist in relief elevations associated with frost heave processes, namely ice segregation. Another designation that was considered for this class was “incipient pingos”, as it is likely that, given the right conditions, many of these mounds will possibly evolve into pingos, and it is possible that some could already be considered pingos. However, as a clear criterion to differentiate “incipient pingos” from fully developed ones was not found in the literature, a more overarching designation, “Ice Mounds”, was decided upon. The UAV DSM played a great role in their identification, as sometimes they are difficult to notice when viewed directly from above by the naked eye, but can be easily detected with terrain elevation data. A total of 75 of these features were mapped, using scales of 1:500 to 1:250.

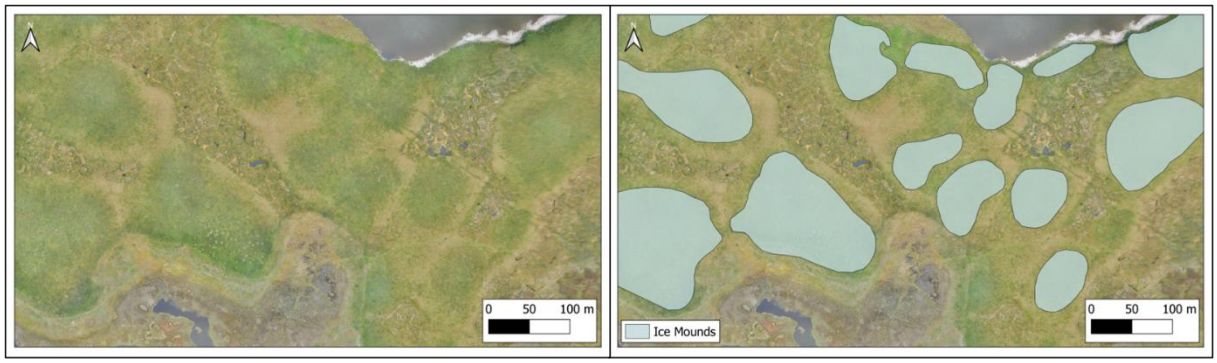

Figure 58 *- Examples of ice mounds digitized for the Geomorphological Map.*

Sand (Figure 59) was another class included in the Geomorphological Map, and it essentially corresponds to the sand spit located at Peninsula Point and some sandy beaches located along some sectors of the shore in PCL. 36 polygons were created for this class, and to do so scales of 1:250 to 1:100 were used.

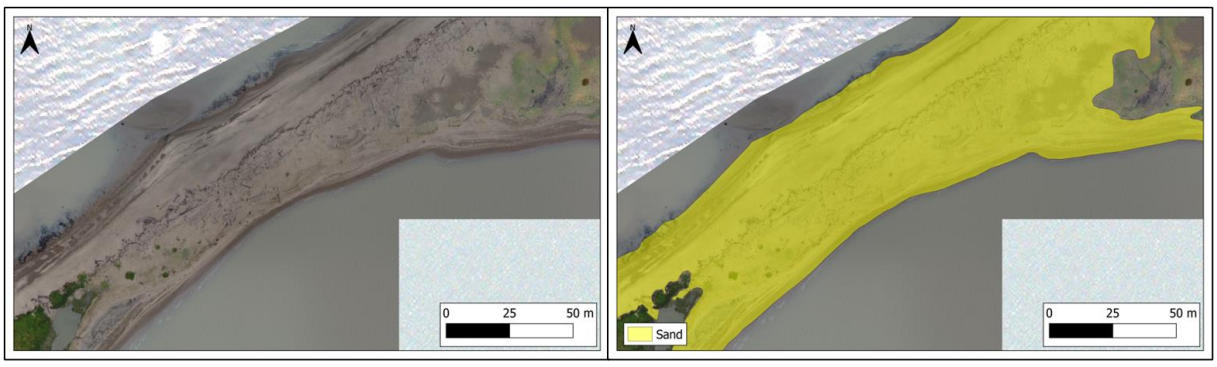

Figure 59 *– Example of the “Sand” class digitized for the Geomorphological Map.*

As mentioned in the “PCL in the Literature” chapter, at Peninsula Point there is a sector along the coast where coastal cliffs and retrogressive thaw slumps can be found. Besides this

area, another one with similar characteristics, though much smaller in extent, was also found at the northeasternmost tip of the park. These areas, given their geomorphological relevance, were also included into the map, as the class “Coastal Cliffs and Thaw Slumps” (Figure 60). To be more precise, the actual cliff scarps, the retrogressive thaw slumps, and any debris resulting from erosion located at their bases were incorporated into this class, while the class “Sand” was used to mark some areas that appeared to consist of debris-less beaches ahead of the cliffs and slumps (namely, at Peninsula Point). The “Coastal Cliffs and Thaw Slumps” class contains 2 polygonal features, and was mapped at scales of 1:500 to 1:250.

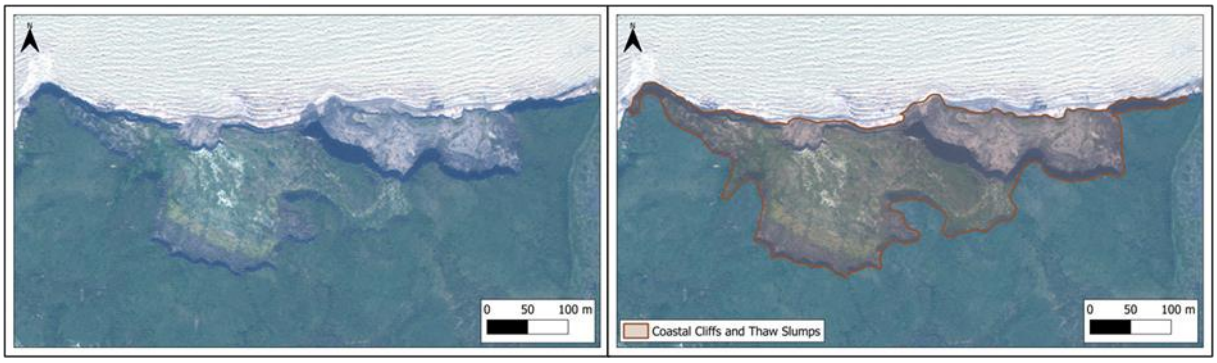

Figure 60 - Example of the “Coastal Cliffs and Thaw Slumps” class digitized for the Geomorphological Map, in this case, the one located at Peninsula Point.

The next class to be mentioned is the “Tourist Walkway” (Figure 61), which consists of a single polygonal feature. It represents the extent of the man-made boardwalk that exists in PCL, which, for conservational reasons, is intended to be the only area on which tourists can walk and visit the park. This infrastructure was digitized at a scale of 1:250.

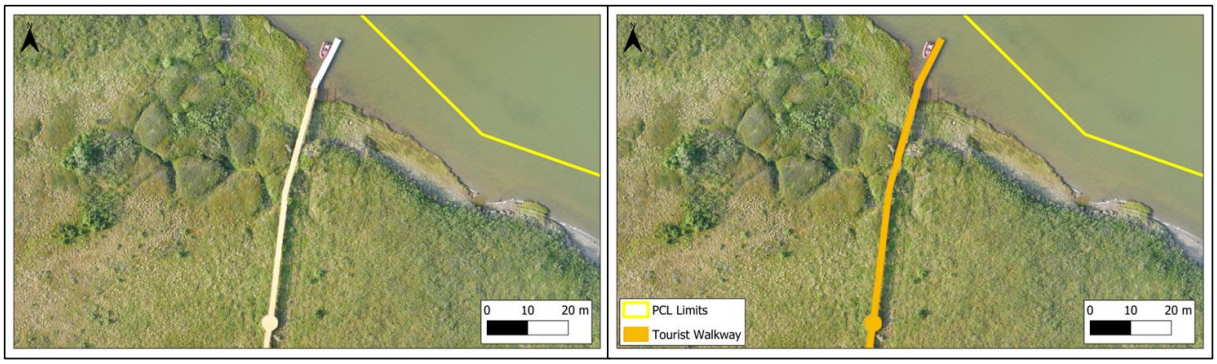

Figure 61 - Example of the “Tourist Walkway” class digitized for the Geomorphological Map.

Another anthropogenic feature that was represented corresponds to the “Vehicle Tracks” class, the only linear one included in the map (Figure 62). These consist in a large network of tracks left on the terrain by the circulation of motorized vehicles (most likely, ATVs, or all-terrain vehicles) within the boundaries of PCL, an activity that is supposed to be forbidden for conservational reasons. These vehicles typically leave a pair of tracks, being that the main method used for the mapping of these features consisted in tracing a single line approximately in the middle of those two tracks. This way, each one of the digitized lines was meant to

represent a pair of tracks left by a single vehicle. It should be said, however, that in some locations, the overlapping of tracks was so great that it was difficult to determine the exact middle of each pair of tracks. The approach applied in these cases was to digitize the lines along each individual track. Overall, 2201 linear features were traced, and the scales used ranged from 1:250 and 1:50. These very large scales were especially necessary in the areas where vehicle circulation had been intense, in order to guarantee the most correct mapping of the tracks even when they presented a high degree of overlapping.

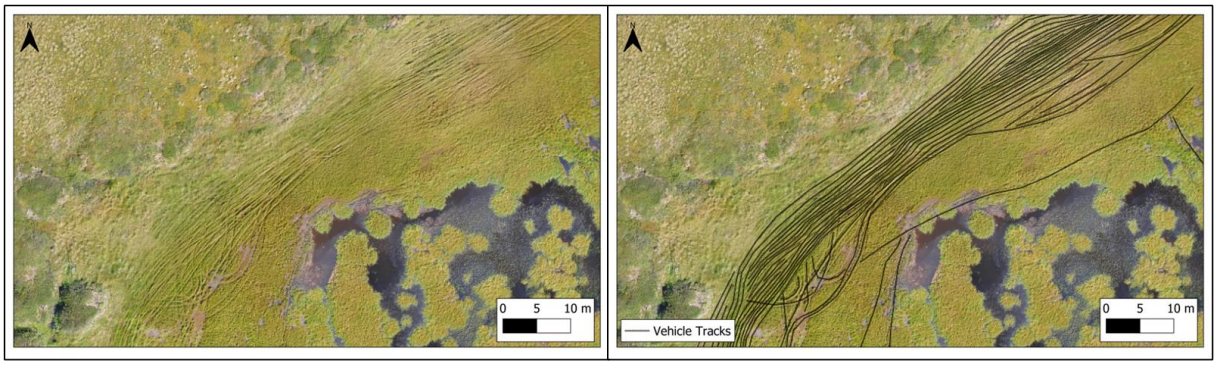

Figure 62 *- Examples of vehicle tracks digitized for the Geomorphological Map.*

The last feature of anthropogenic origin corresponds to the "Seismic Lines" class (Figure 63), which was mapped at a scale of 1:500. This feature is most likely associated with the seismic surveys developed on behalf of oil and gas exploration programs, such as those authorized by the former Canadian National Energy Board, in the 1960's and 1970's (Canada Energy Regulator, 2022). According to French (2007), these types of surveys took place in the Mackenzie Delta during this period, leading to significant impacts on the landscape and becoming a cause of human-induced thermokarst. Upon noticing this feature within the park, and after knowing those facts, it was decided that this class should be included into the map. This class initially comprised a single polygonal feature, but in the final version of the map, after all the features of every class were clipped by the boundaries of the park, it became comprised by 3.

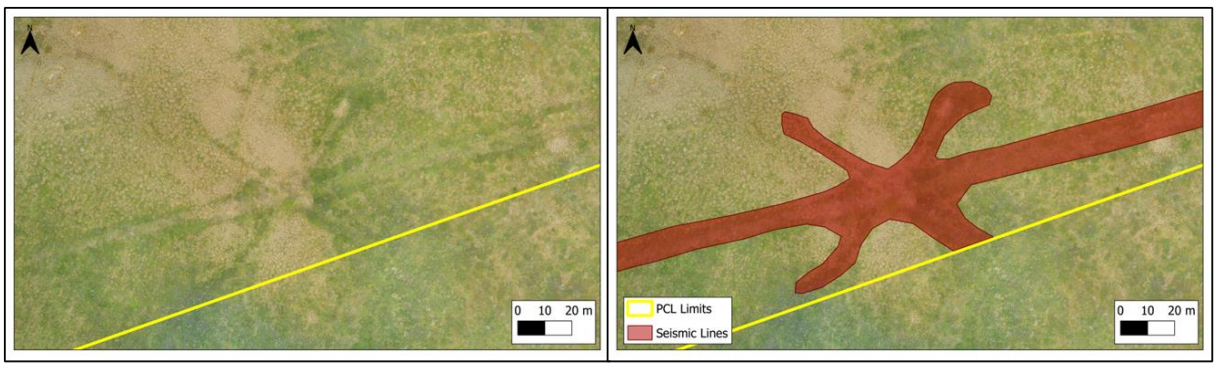

Figure 63 *- Example of the "Seismic Lines" class digitized for the Geomorphological Map.*

The final class to be described was also the last one to be created, and it is the “Tundra Plains” (Figure 64). This class corresponds to all the remaining terrain within the limits of the park (excluding coastal waters) that had not yet been covered by any of the other 19 already described classes and subclasses. With this, it was the only class that was not manually digitized, but instead obtained by starting with a polygon that covered the entirety of the park, and consecutively removing from this large polygon the areas covered by each one of the previously described classes (with the exception of the “Vehicle Tracks” class, as it was the only one in linear format). This was done with the “Difference” vector geoprocessing tool in QGIS. In addition, a shapefile consisting of the emersed land within PCL was used as a mask layer for the “Clip” vector geoprocessing tool (also in QGIS), in order to eliminate all coastal waters from that same polygon that started as the total extent of PCL (the process through which the emersed land polygon was obtained shall be described in Chapter 4.3.2). The final result of all these vector geoprocessing operations was the “Tundra Plains” class.

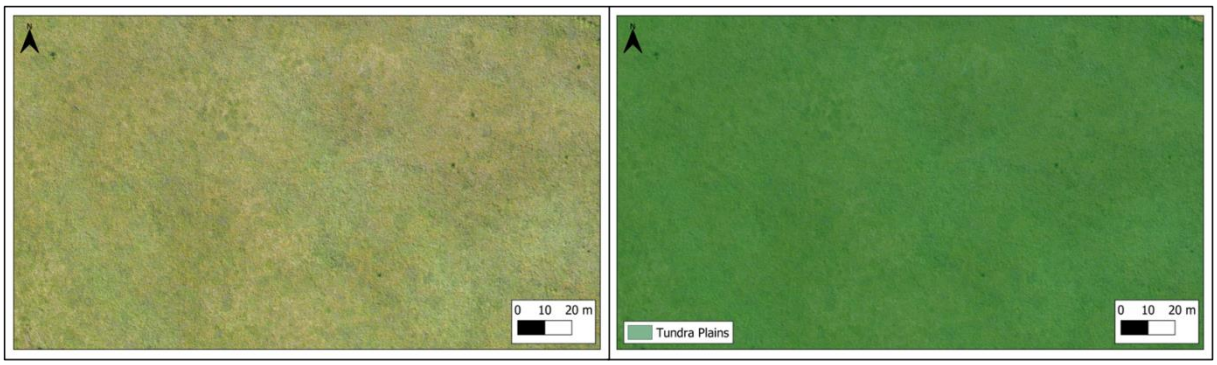

Figure 64 *- Example of the “Tundra Plains” class digitized for the Geomorphological Map.*

Also, it should be mentioned that after each class was considered as completely mapped, a visual sweep of the total extent of the park was done, in order to make sure that all the features that were to be digitized in each given class had truly been included in the map. If any feature had been originally missed, they were digitized at this stage.

4.3 - Landcover Mapping

4.3.1 - WorldView 2 Scene (Acquisition and Characteristics)

WorldView-2 is a commercial Earth observation satellite, owned by DigitalGlobe, a subsidiary of Maxar Technologies (Figure 65). The WorldView-2 mission was launched in October of 2009 and continues operational. It has a sun-synchronous orbit with a revisit time of up to 1.1 days, and circulates at an altitude of 770 km from the Earth’s surface. It presents 8 band multispectral imagery with 1.84 m spatial resolution, and panchromatic imagery with

46 cm spatial resolution. The spectral range of the 8 multispectral bands of WorldView-2 are as follows: 1. Coastal Blue (400-450 nm); 2. Blue (450-510 nm); 3. Green (510-580 nm); 4. Yellow (585-625 nm); 5. Red (630-690 nm); 6. Red Edge (705-745 nm); 7. NIR1 (770-895 nm); 8. NIR2 (860-1040 nm). This way, to obtain the RGB true-color composite that was used for visualizing the image, the bands used were Band 5 (as the Red band), Band 3 (as the Green band) and Band 2 (as the Blue band).

Figure 65 *- DigitalGlobe and Maxar Tech's WorldView-2 satellite. Source: Maxar Technologies (2021).*

One of the first procedures conducted was obtaining the pansharpened version of the WorldView-2 scene, through means of GIS software, in this case, QGIS (Figure 66). Therefore, the spatial resolution of the panchromatic band (46 cm) was used nearly always when working with the WorldView-2 imagery henceforth. The only instance in which the 1.84 m multispectral resolution was used was during the process of creating a land mask (which will be described ahead), as to do this it was necessary to perform calculations with several of the different multispectral bands.

Another procedure that was necessary to conduct before the elaboration of the Landcover Map was the georeferencing of the WorldVIew-2 scene (performed in QGIS). The reference imagery for this process was the already described very accurately geopositioned UAV orthomosaic. It should be mentioned that the WorldView-2 scene covers a larger area than that of the UAV imagery, extending beyond the limits of the park, and covering, for example, the nearby settlement of Tuktoyaktuk. However, with the UAV imagery being used as reference, all ground control points had to be created in the region that was covered simultaneously by the UAV imagery and the WorldView-2 scene. To guarantee the most accurate georeferencing possible, a large number of ground control points were created (62 points), spread across all this region where the two types of imagery overlapped (Figure 67). This region didn't contain any anthropogenic features besides the tourist walkway, which would have been easy choices for control points. This way, the very high detail of both types of imagery was crucial for the proper identification of control points in this landscape that almost

exclusively contained natural features. As for the parameters chosen in the QGIS Georeferencer, the “Transformation Type” was “Linear” and the “Resampling Method” was “Nearest Neighbor”. This georeferencing process presented a mean error of about 2.75 pixels, which corresponds to about 1.27 m.

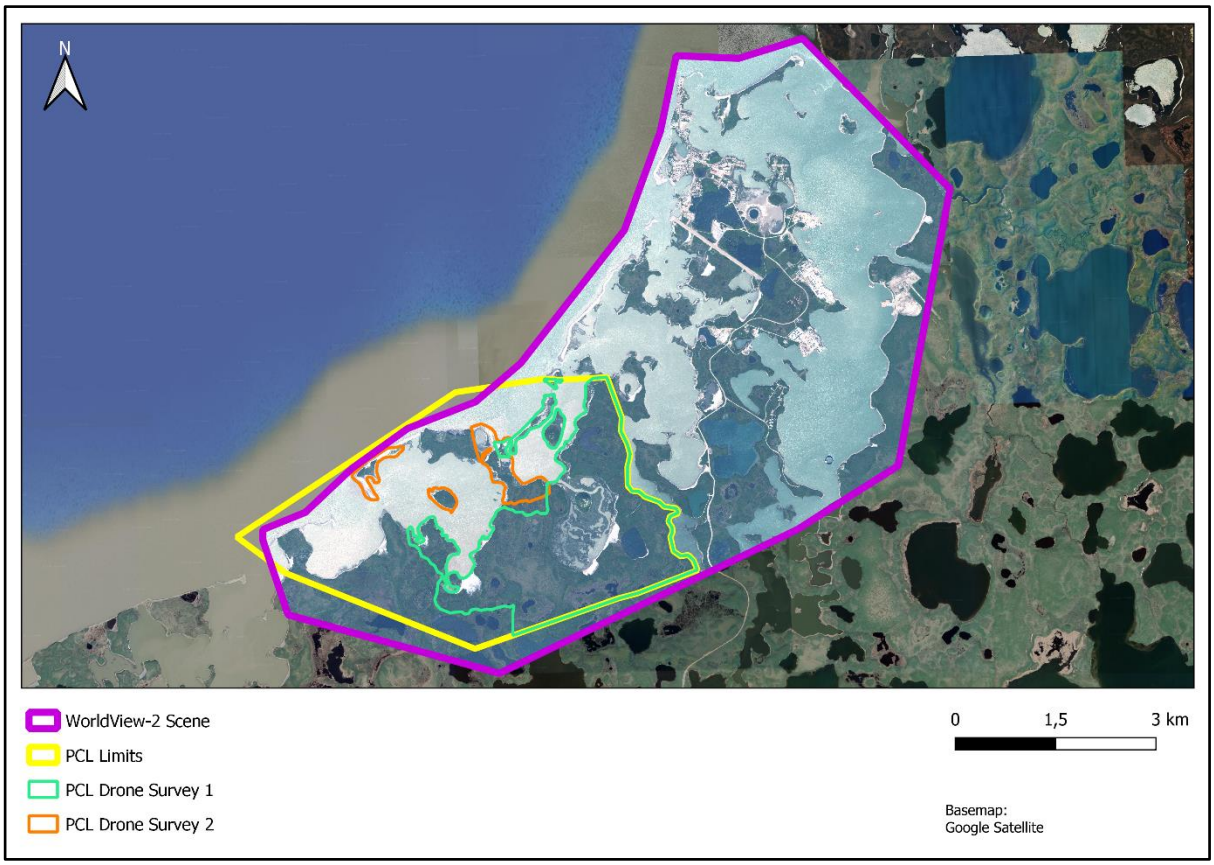

Figure 66 *- Pansharpened version of the WorldView-2 scene (after georeferencing), and comparison of its extent with that of the drone surveys used to create the Geomorphological Map, and with the limits of PCL. Note that the settlement of Tuktoyaktuk is present in the northeastern sector of the scene.*

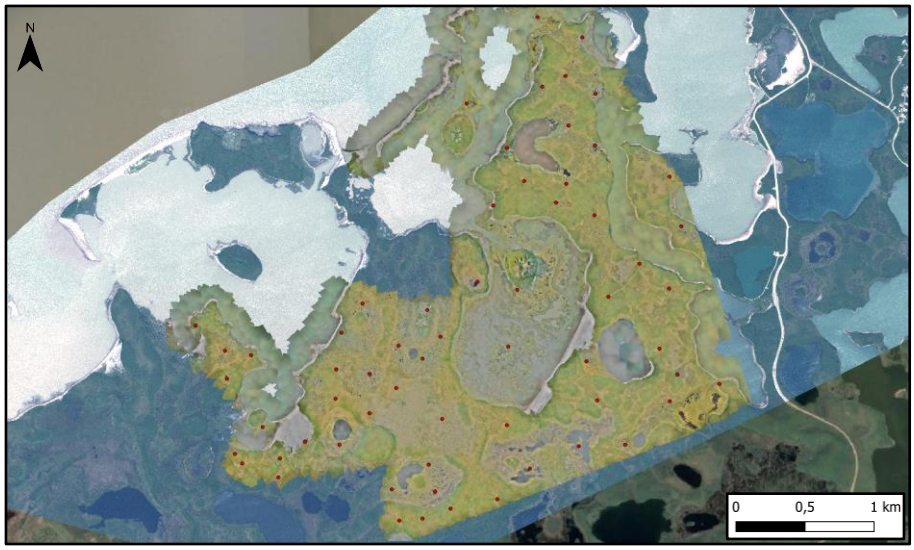

Figure 67 *– The 62 ground control points created in the georeferencing process (represented by small red dots).*

4.3.2 - Data Analysis Methods

The Landcover Map was created recurring to a supervised image classification analysis. However, before the final supervised classification was performed, a series of exploratory unsupervised classifications were conducted. The main purpose of this was to gain a better notion of the classes that could be chosen and integrated into the final supervised classification map. These analyses were conducted with ArcMap and QGIS, and included 20, 15, 10 and 5 class Isocluster unsupervised classifications, and 20, 15, 10 and 5 class K-Means unsupervised classifications. In truth, several other combinations of numbers of classes and classification methods were also tested, as well as different parameter values, but the before mentioned ones ended up being the most influential towards the decision of the final group of classes to be included into the supervised classification, as it was considered that they resulted in the best and most accurate representation of the variability of the landscape of the park.

It should also be mentioned that for some of the exploratory tests, all areas occupied by liquid water were included into the analyses, and they were conducted upon the whole WorldView-2 scene. It was, however, concluded that more appropriate results were obtained if pixels containing water were excluded from the analyses. Therefore, it was necessary to create a land mask. After consulting the literature, it was decided to calculate the Normalized Difference Water Index (NDWI), which, using the WorldView-2 multispectral bands, is done with the following formula: $NDWI = \frac{Coastal - NIR2}{Coastal + NIR2}$, according to Maglione et al. (2014) and Wolf (2012). Once this index was calculated, an iterative interpretation of its results was done, with the objective of determining the threshold value that most accurately distinguished the pixels between land and water. The threshold value chosen was 0.23, being that all values below or equal to 0.23 were classified as “land” and all values above 0.23 were classified as “water”. After this, a copy of the raster containing the NDWI results, but only with the pixels classified as “land”, was created. Then, the “Majority Filter” tool was used to clean up minor misclassifications in this “land” raster, which in most cases corresponded to individual pixels or very small groups of pixels that were classified as “water” according to the chosen threshold, even though there were truly land. As for the parameters chosen for the “Majority Filter” tool, they were “Circle” as the “Mode”, “1” as the “Radius” value, and “0” as the “Threshold” value. All these procedures were performed in QGIS, as well as the next step, which consisted in converting the “land” raster into vectorial format (Figure 68). Finally, the WorldView-2 scene was clipped using the “land” shapefile as a mask layer, in order to obtain a version of this scene without the pixels classified as water, and only those that correspond to emersed terrain. After conducting more exploratory tests to the version of the WorldView-2 scene containing only emersed land, it was decided that this version of the scene should also be clipped by a

shapefile corresponding to the extent of the areas covered by the UAV surveys that resulted in the orthomosaic and DSM. This was done in order to assure that the results were more befitting with the objectives of this study (which focuses on PCL as its study area, and not so much the surrounding areas that were also covered by the full scene), and to permit a more direct comparison with the Geomorphological Map. Therefore, the last exploratory unsupervised classifications (which were the most influential towards the decisions regarding the classes to be included into the final supervised classification), as well as the final supervised classification itself (which will be further described in the rest of this chapter and presented in the Results of this study), were conducted upon the WorldView-2 scene clipped by the land mask, as well as by the extent of the UAV orthomosaic and DSM (Figure 69).

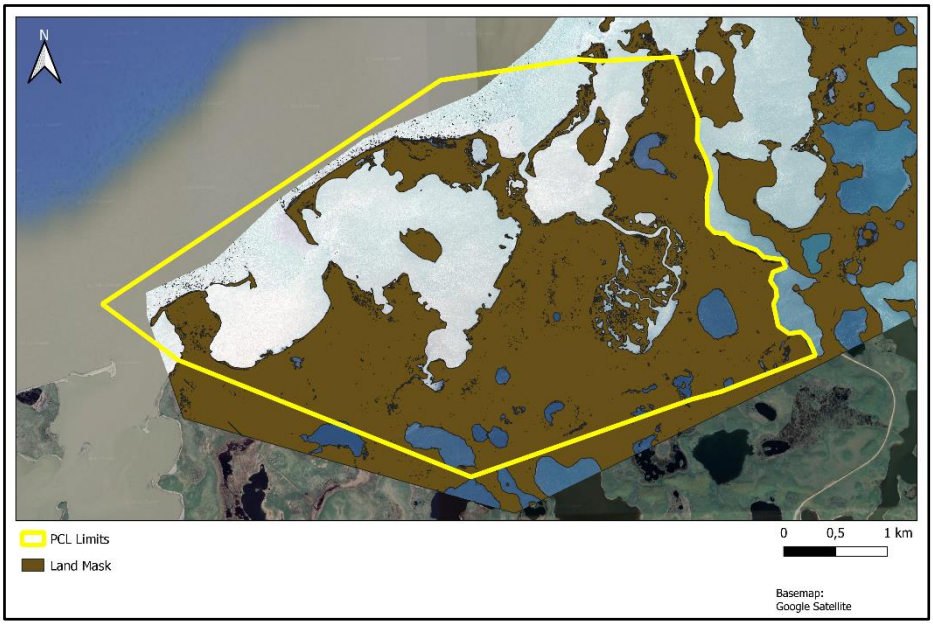

***Figure 68** – "Land" mask used to clip the WorldView-2 scene.*

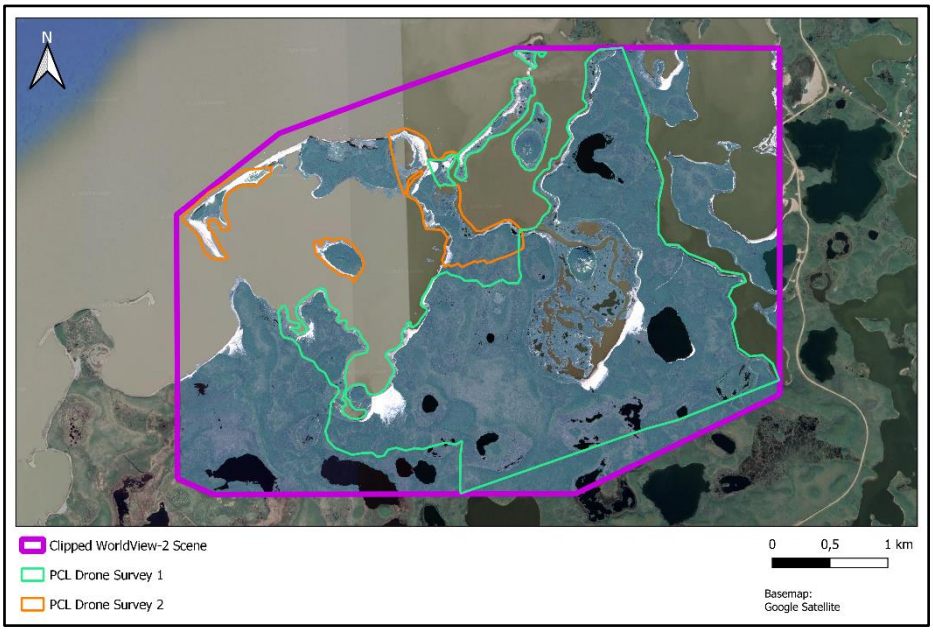

***Figure 69** – Final version of the WorldView-2 scene (clipped by the "land" mask and by the extent of the UAV surveys), which was used to create the Landcover Map.*

The final list of classes to be represented in the supervised classification map includes nine different landcover units: “High Shrub Tundra”; “Low Shrub Tundra”; “Dry Tundra”; “Inundated Tundra”; “Sand”; “Wet Sand and Mud”; “Bare Soil”; “Driftwood Accumulations”; and “Man-made Structures”. The choice to represent these classes, and give them these designations, was made after extensive visual analysis of the WorldView-2 scene and the exploratory unsupervised classifications, and also after consulting the literature.

Something that became very clear after doing those tasks was that the majority of the park is covered by vegetation, but this vegetation is not all homogeneous. For example, some areas of the park presented more developed vegetation communities than others, and some were drier than others. These different vegetation communities were distinguished relatively clearly in the exploratory unsupervised classifications, and, therefore, were considered important to be represented in the final supervised classification. With this, and considering that the predominant biome in this region of the world is the tundra, it was decided that the vegetation communities to be included as classes of the supervised classification map were: “High Shrub Tundra” (the most well developed vegetation community present in the park, containing well developed shrubs and very well developed herbaceous plants); “Low Shrub Tundra” (containing low shrubs and well developed herbaceous plants); and “Dry Tundra” (containing sporadic low shrubs and poorly developed herbaceous plants).

The exploratory unsupervised classifications were also able to point out, from the spectral data of the WorldView-2 imagery, that some areas within the park presented humid terrain, but were vegetated to some degree. These are areas that are prone to being flooded by the coastal waters, especially in the occurrence of storm surge events. Even though the majority of these areas present vegetation, these communities are not very developed. Considering these facts, it was decided that a class called “Inundated Tundra” was to be included in the supervised classification.

Nevertheless, not all the park is covered by vegetation, something that was translated correctly into the unsupervised classifications. Upon the analysis of those exploratory classifications, it was perceived that three main types of terrain within PCL could fall into this category: “Sand” (a class predominant along the coastline); “Wet Sand and Mud” (areas along the coastline in direct contact with the water, and also some areas contiguous with the class “Inundated Tundra” that present no vegetation and that are typically muddy); and “Bare Soil” (a class with little expression within the park, but that corresponds to areas of barren soil with no vegetation).

There were still other areas with very characteristic features, perceived by the unsupervised classifications, and included into the final Landcover Map. One of these was a

natural feature, and corresponds to the class “Driftwood Accumulations”. The tree branches and trunks that comprise these accumulations are sometimes of very considerable sizes, and the areas occupied by them within PCL are quite large as well. These areas were clearly distinguished in the unsupervised classifications, and therefore carried over into the supervised classification.

Finally, within the limits of PCL, there is only one structure that is of anthropogenic origin, which is the already mentioned tourist walkway. This feature’s spectral signature was unique enough to be distinguished clearly in the unsupervised classifications, and because of it, the class “Man-made Structures” was included into the final supervised classification.

Having prepared the WorldView-2 scene for analysis, and chosen the final group of nine target classes, the supervised classification was conducted. The software used for this task was ENVI (and in it, the “Classification Workflow” tool). In order to obtain the spectral signatures for each of the nine classes, several regions of interest, or training areas, were created (5 for each class). These regions of interest were well distributed across the already mentioned clipped version of the WorldView-2 scene, and an effort was made for them to be well representative of the variety of spectral signatures possibly associated with each class (Figure 70). With the training areas created, the ENVI supervised classification algorithm was finally ran, using the “Maximum Likelihood” method and “None” as the “Probability Threshold”. In the “Cleanup” step, the default settings were applied (“Smooth Kernel Size” of 3, and “Aggregate Minimum Size” of 9). Finally, the results were exported, both as a classification image (ENVI format) and in vectorial format (shapefile), and clipped by the extent of the Geomorphological Map.

Also, to assess the precision of the analysis, a confusion matrix was created for the final supervised classification, using ENVI software (Table 1). To do this validation process, five test areas (or “ground truth”) polygons were created for each of the nine classes. It was assured that they did not overlap with the training areas used to produce the results (in order to guarantee a more authentic appraisal of the algorithm’s performance). The pixels of the supervised classification results contained within the boundaries of each “ground truth” polygon were compared with the class associated with each polygon, and the results of that comparison are presented in Table 1. The Overall Accuracy of the supervised classification was high, 94.35%, which means that this percentage of the pixels contained within the boundaries of the “ground truth” polygons matched with their respective polygon’s class and were correctly classified. Amongst the classes with the highest accuracy are “Driftwood Accumulations”, with 99.81% of the test pixels of this class having been correctly classified, and “Man-made Structures” (100%). This means that the “Man-made Structures” class had an

Omission Error of 0% (within the test polygons of this class, no pixels of any other class we detected amongst the results). The classes for which the supervised classification algorithm performed less well overall were “Low Shrub Tundra” (89.75%) and “Wet Sand and Mud” (78.24%). However, even for those classes, the accuracy levels can still be considered high. It is also important to look at the Commission Error values, which evaluate how many pixels of a certain class incorrectly appeared in other classes. The “Bare Soil” class had the highest values in this error (31.98%), meaning that within the test polygons of other classes, there were several pixels that were incorrectly classified as being “Bare Soil”. Nevertheless, none of the classes presented very high omission or commission errors, and overall, it can be concluded that the results of the Landcover Map are of good quality. Lastly, regarding the Kappa Coefficient associated with the results of the supervised classification, it presented a value of 0.93. This statistic can vary from -1 to 1, with a value of 0 indicating that agreement between validation and classification is due to random chance, and a value of 1 indicating perfect agreement between validation and classification. Values below 0 are a sign of disagreement. According to the literature, 0.93 falls into the category of an “Almost Perfect” agreement between the final classification and the validation (McHugh, 2012).

Ground Truth (Pixels)											Comission (%)
Class	Bare Soil	Driftwood Accumulations	Dry Tundra	High Shrub Tundra	Inundated Tundra	Low Shrub Tundra	Man-made Structures	Sand	Wet Sand and Mud	Total	
Bare Soil	2072	0	74	1	84	0	0	0	815	3046	31,98
Driftwood Accumulations	19	7773	0	0	0	0	0	19	84	7895	1,55
Dry Tundra	96	0	12369	0	0	93	0	0	0	12558	1,51
High Shrub Tundra	0	0	0	8309	0	1460	0	0	0	9769	14,95
Inundated Tundra	17	0	0	229	14653	0	0	0	350	15249	3,91
Low Shrub Tundra	0	0	221	247	0	13604	0	0	0	14072	3,33
Man-made Structures	22	12	3	0	63	0	276	10	18	404	31,68
Sand	0	2	0	0	0	0	0	3510	32	3544	0,96
Wet Sand and Mud	10	1	0	0	44	0	0	0	4674	4729	1,16
Total	2236	7788	12667	8786	14844	15157	276	3539	5974	71267	
Ommission (%)	7,33	0,19	2,34	5,43	1,29	10,24	0,00	0,82	21,75		

Ground Truth (%)											Comission (%)
Class	Bare Soil	Driftwood Accumulations	Dry Tundra	High Shrub Tundra	Inundated Tundra	Low Shrub Tundra	Man-made Structures	Sand	Wet Sand and Mud	Total	
Bare Soil	92,67	0	0,58	0,01	0,57	0	0	0	13,64	4,27	31,98
Driftwood Accumulations	0,85	99,81	0	0	0	0	0	0,54	1,41	11,08	1,55
Dry Tundra	4,29	0	97,65	0	0	0,61	0	0	0	17,62	1,51
High Shrub Tundra	0	0	0	94,57	0	9,63	0	0	0	13,71	14,95
Inundated Tundra	0,76	0	0	2,61	98,71	0	0	0	5,86	21,4	3,91
Low Shrub Tundra	0	0	1,74	2,81	0	89,75	0	0	0	19,75	3,33
Man-made Structures	0,98	0,15	0,02	0	0,42	0	100	0,28	0,3	0,57	31,68
Sand	0	0,03	0	0	0	0	0	99,18	0,54	4,97	0,96
Wet Sand and Mud	0,45	0,01	0	0	0,3	0	0	0	78,24	6,64	1,16
Total	100	100	100	100	100	100	100	100	100	100	
Ommission (%)	7,33	0,19	2,34	5,43	1,29	10,24	0	0,82	21,75		

Table 1 *- Confusion Matrix of the results of the supervised classification. The highlighted values correspond to correct classifications. Commission and Omission Error values are also included (red cells correspond to higher errors).*

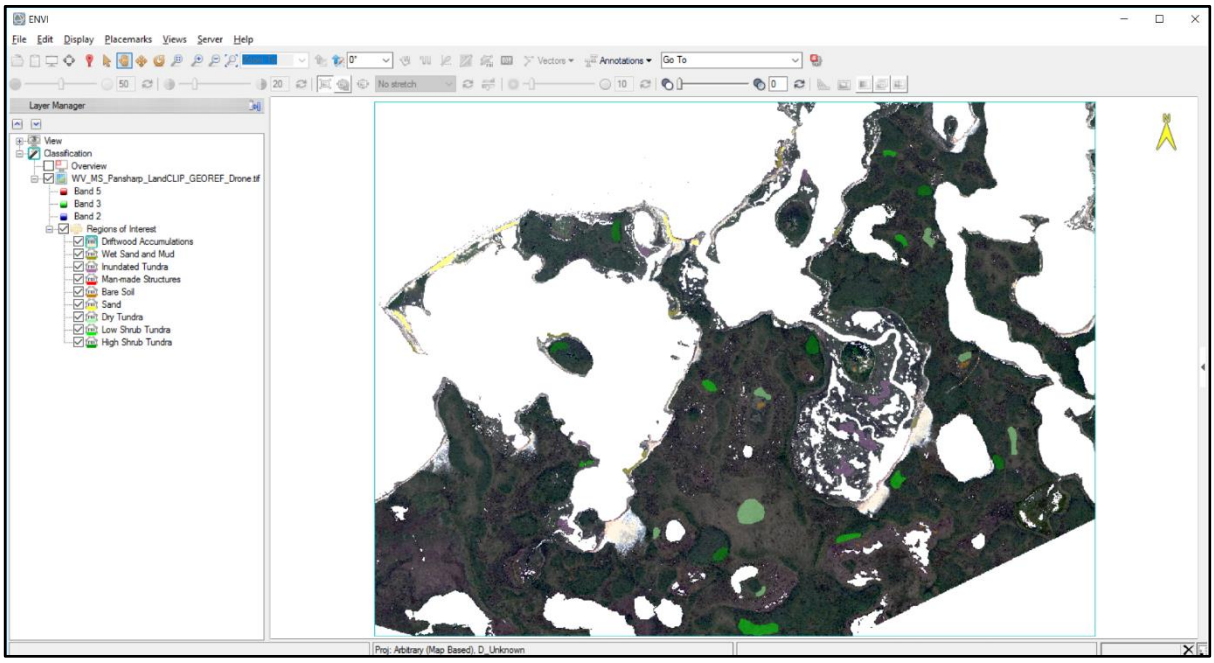

Figure 70 *– ENVI software that was used to create the supervised classification map. The regions of interest, or training areas created in the process are present in the image.*

5 – RESULTS

5.1 - Geomorphology

The Geomorphological Map comprises twenty classes and subclasses (Appendix Figure 1), and the mapping of them was done based on the UAV orthomosaic, with the WorldView-2 scene being used in some specific areas as described in Chapter 4.2.1 (Figures 43 and 44). The total area covered by the Geomorphological Map corresponds to about 77.4% (8.15 km^2) of the total area of the park (not including coastal waters). PCL presents a total area of about 16.56 km^2 including coastal waters, and 10.53 km^2 not including coastal waters. Being that the coastal waters incorporated into the park limits were not a focus of this study, all area-related calculations were done with the 10.53 km^2 value being considered as the "total area of PCL", and, from here onward, whenever the term "total area of the PCL" (or "total area of the park") is used, it shall refer to this value. It should be mentioned, however, that this 10.53 km^2 area does not consist solely of dry land, as it includes the several lakes and ponds, as well as the waters that inundate two lake basins. In the following paragraphs, each of the twenty classes and subclasses shall be described in more detail.

The class "Pingos" occupies in total 0.21 km^2, which corresponds to about 1.99% of the total area of the park (Figure 71). Eight pingos were identified and included into this map, and each were assigned a number, present in Table 2. To assign these numbers, the pingos were sorted by their height, and then labeled according to their rank in that order (with 1 being the highest and 8 the lowest). The four tallest pingos also have official designations recognized by Parks Canada that are included in Table 2 as well. Parks Canada officially reports eight of these landforms to exist within PCL, however, one of these eight exists near the southwestern limits of the park, in an area not covered by the UAV data, and therefore was not one of the eight pingos included in the map. This means that this map includes one pingo that is not officially accounted for by Parks Canada. It is Pingo 8, the small and eroded pingo located in the northwestern region of PCL, close to Pingo 2 (Split Pingo). Pingo 8 is both the lowest pingo (with its highest point located at 6.66 m above sea level) and the one which covers the smallest area (4160.46 m^2). As for the largest, and tallest, pingo in PCL, it is Pingo 1 (Ibyuk Pingo), which covers 55,989.8 m^2 and has a highest point located at 49.66 m above sea level. The maximum basal diameter of Ibyuk Pingo is about 307 m.

As for the subclass "Pingo Summit Craters and Dilation Cracks" it was present on Pingos 1 (Ibyuk Pingo), 2 (Split Pingo), 3 (Island Pingo) and 7, while as the subclass "Pingo Surface Erosion" was only found on Pingos 1 and 2 (Figure 71). Ibyuk and Split Pingos were also those where the area occupied by these classes were greater. On Ibyuk Pingo, 8530.33

m^2 (or 15.24%) of its surface is occupied by the “Pingo Summit Craters and Dilation Cracks” class, and 13,421.42 m^2 (or 23.97%) are occupied by the “Pingo Surface Erosion” class. On Split Pingo, 3837.31 m^2 (or 7.88%) of its surface corresponds to the “Pingo Summit Craters and Dilation Cracks” class, and 3376.09 m^2 (or 6.93%) correspond to the “Pingo Surface Erosion” class. On Island Pingo and Pingo 7, the “Pingo Summit Craters and Dilation Cracks” class occupies 2584.36 m^2 (or 4.44%) and 329.48 m^2 (or 2.45%) of their surface area, respectively.

Pingo	Area (m^2)	Highest Point (m)	Summit Crater and Dilation Crack Area (m^2)	Surface Erosion Area (m^2)
1 (Ibyuk Pingo)	55989,77	49,66	8530,33	13421,42
2 (Split Pingo)	48723,86	38,19	3837,31	3376,09
3 (Island Pingo)	58251,01	25,83	2584,36	-
4 (Peninsula Point Pingo)	7158,39	14,74	-	-
5	5662,77	12,13	-	-
6	18625,81	9,02	-	-
7	13471,78	8,02	329,48	-
8	4160,46	6,66	-	-
Mean	26505,48	20,53		

Table 2 *– Statistics related to the mapped pingos.*

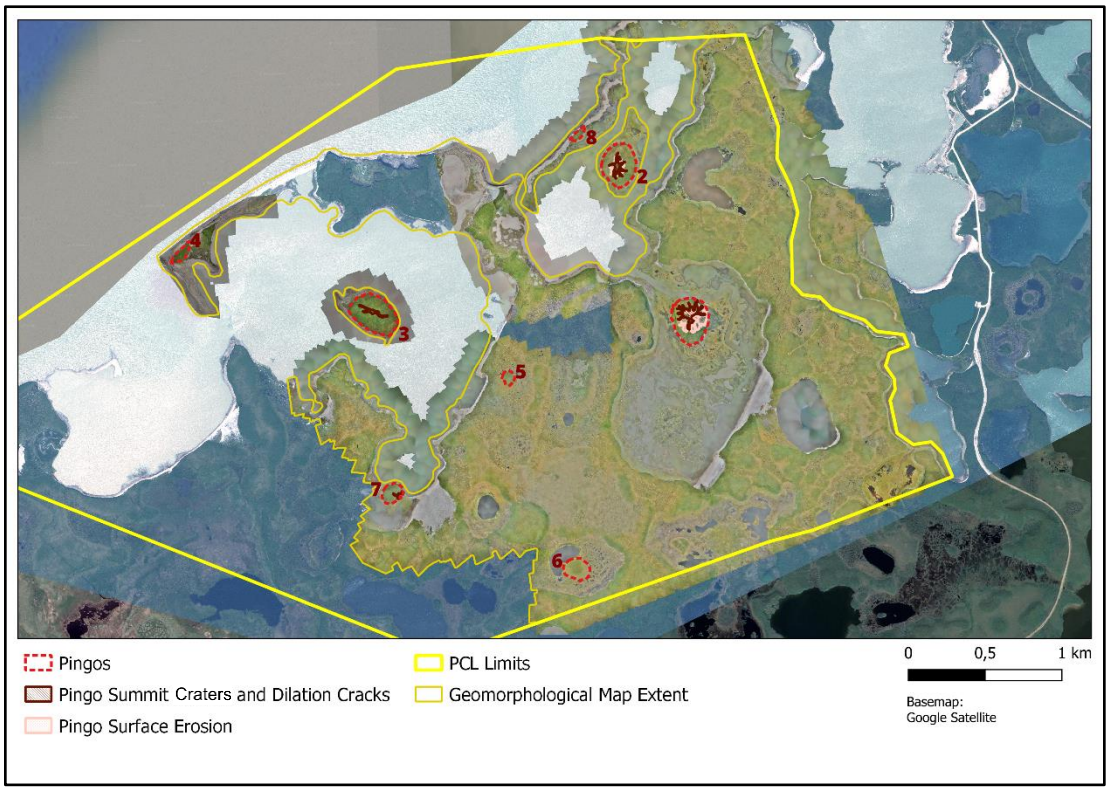

Figure 71 *– “Pingos”, “Pingo Summit Craters and Dilation Cracks” and “Pingo Surface Erosion” classes included into the Geomorphological Map.*

The class “Tundra Polygons” occupies in total 2.24 km^2, which corresponds to about 21.27% of the total area of PCL (Figure 72). Of all the map’s classes, this is the one which occupies the second largest relative portion of PCL. Nevertheless, these polygons can be distinct in nature. Some are well defined high-centered polygons, with the ice wedges between them forming a clear network, sometimes with the formation of small waterbodies in these depressions (Figure 73). In these cases, the polygons themselves are elevated, in some rare cases as high as 5 m above sea level. On these high-centered polygons, the vegetation usually consists of green, well developed shrubs. However, the low-centered variety of tundra polygons can also be found at PCL (Figure 74). These tend to be much drier, with vegetation that is mostly greenish-brown, yellow or brown. The troughs between these polygons (associated with ice wedges) are typically thin and were sometimes hard to notice. These types of polygons are characterized by their concave centers, which sometimes present small waterbodies. There are also some areas in PCL where the polygons and ice wedges seem to be degraded in a way that makes it difficult to clearly identify their borders. It was noticed that these “thermokarst” polygons, as called in some literature (French, 2007), occur typically in networks close to the shoreline or near waterbodies (Figure 75). As for size, the largest polygons usually exist in more elevated areas, and at the fringes of the more well developed networks of tundra polygons. These well developed networks consist of a large quantity of smaller and medium sized polygons, and are typically found in areas that are topographically depressed in relation to their surroundings (Figure 76). These networks can also be associated with higher ground ice contents, as denser networks imply not only more polygons, but also more ice wedges between them (Figure 77 and Appendix Figure 2).

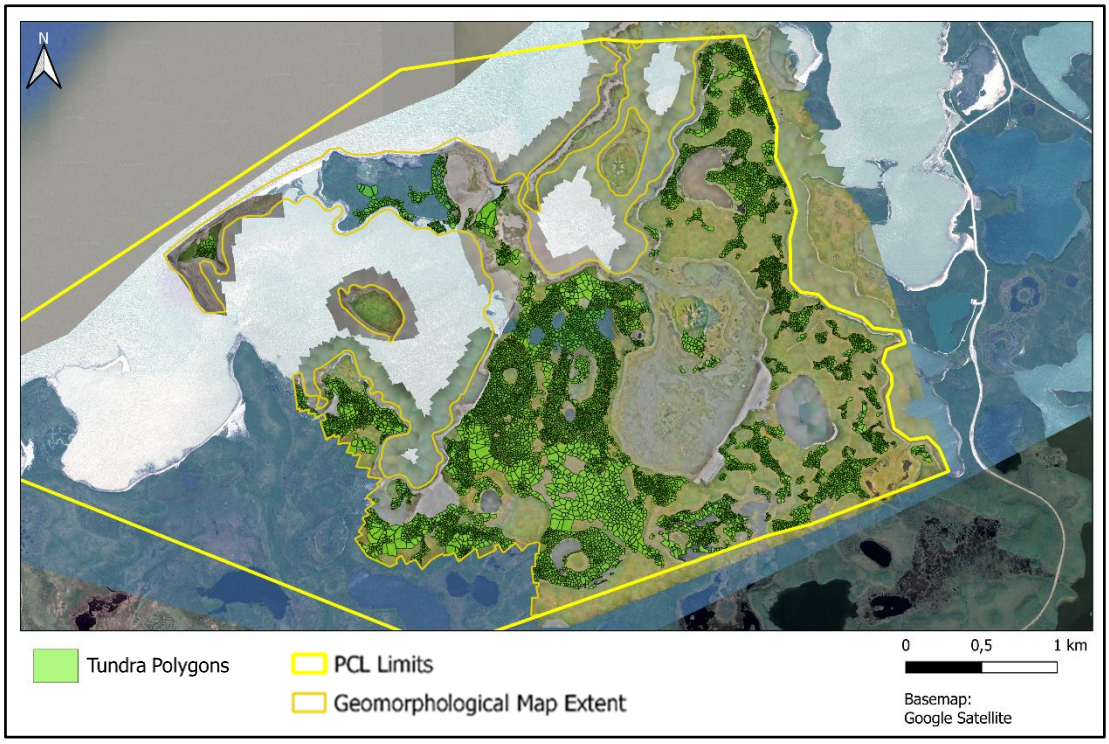

Figure 72 *– “Tundra Polygons” class included into the Geomorphological Map.*

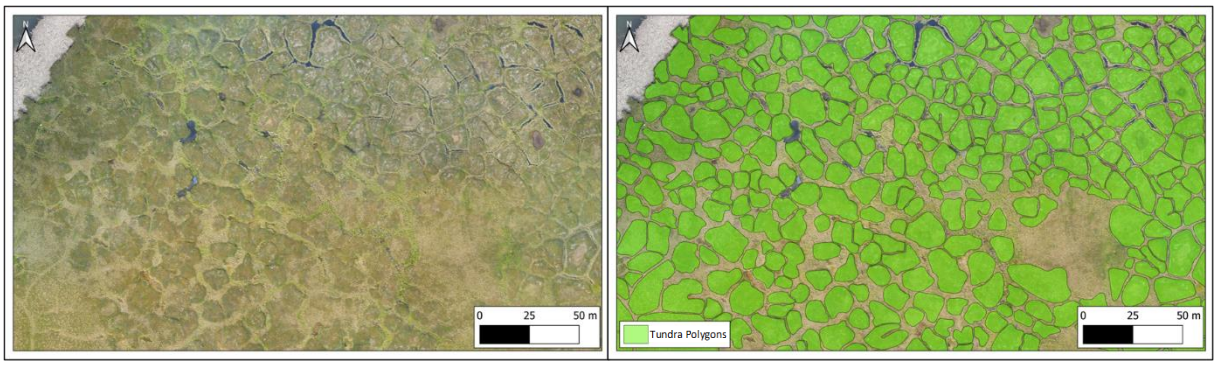

Figure 73 *– Examples of high-centered tundra polygons in PCL.*

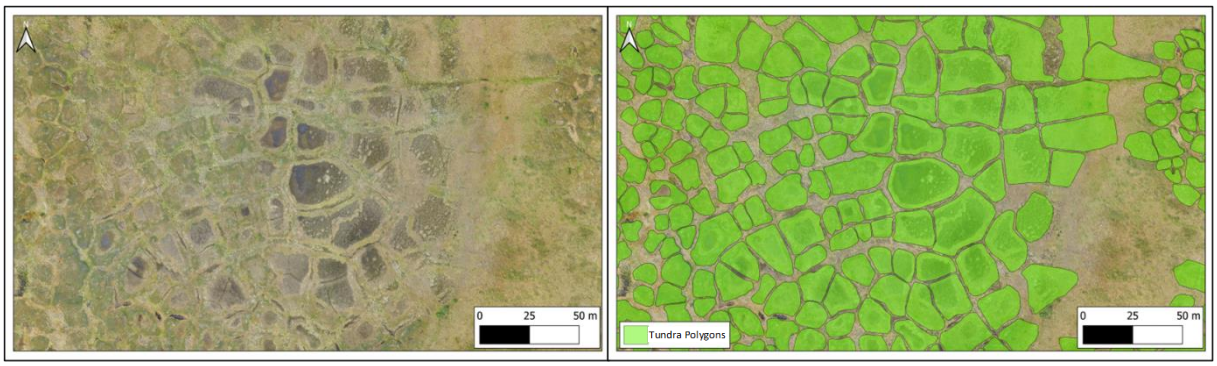

Figure 74 *– Examples of low-centered tundra polygons in PCL.*

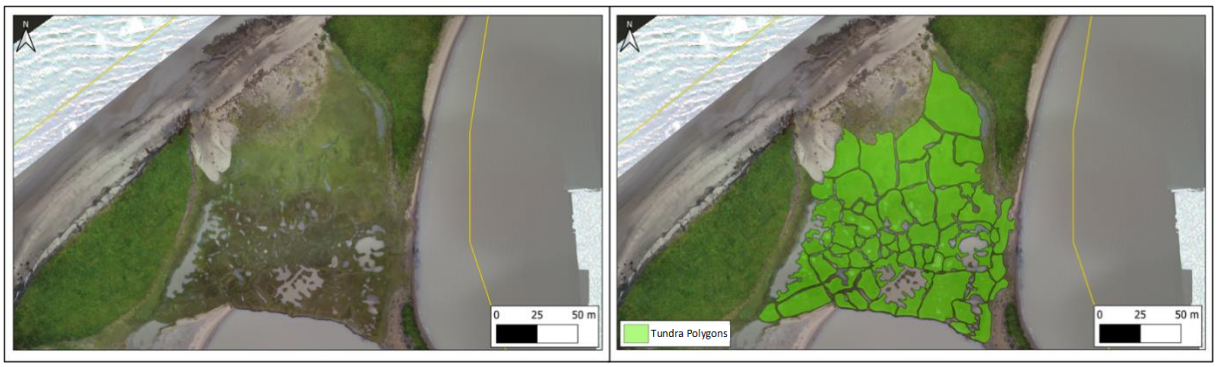

Figure 75 *– Examples of degraded, or "thermokarst" tundra polygons.*

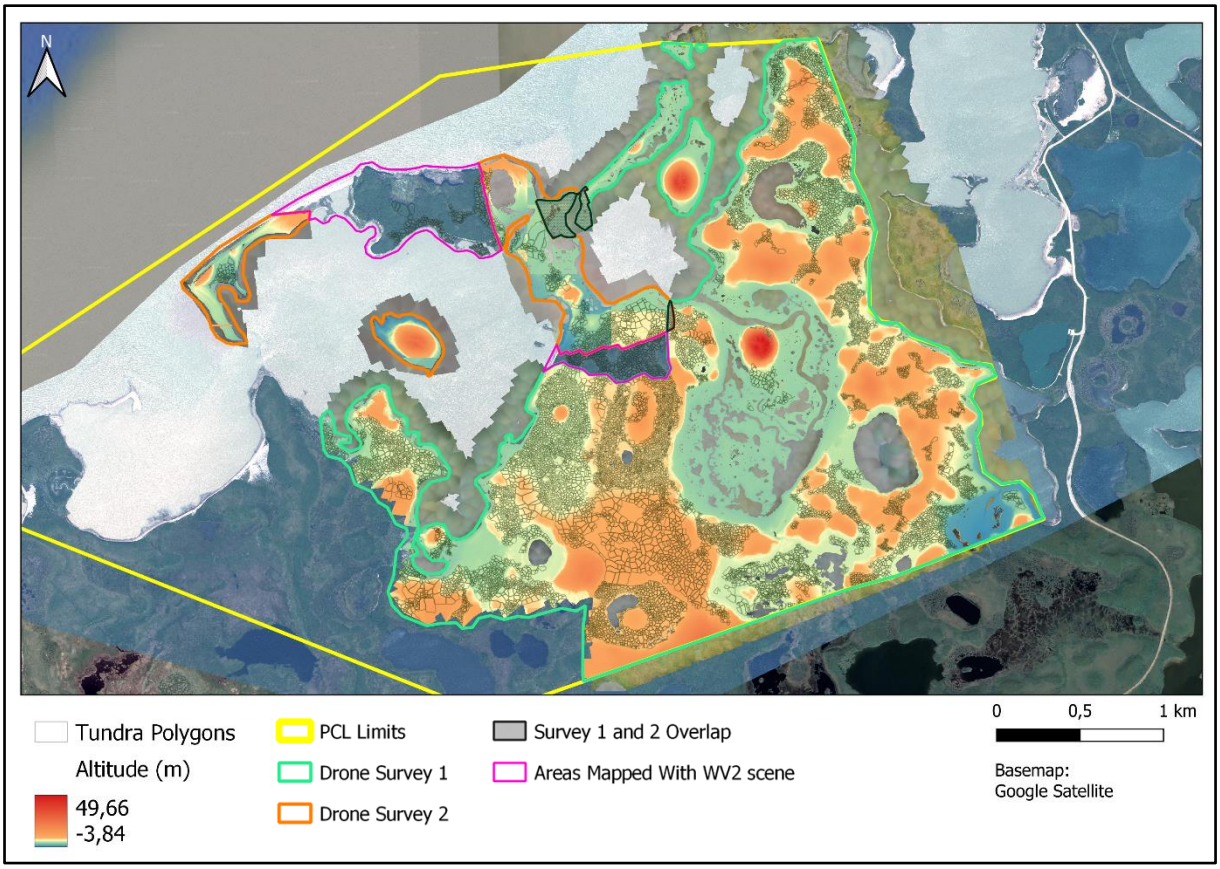

Figure 76 *– Comparison between "Tundra Polygon" class and DSM altimetric data.*

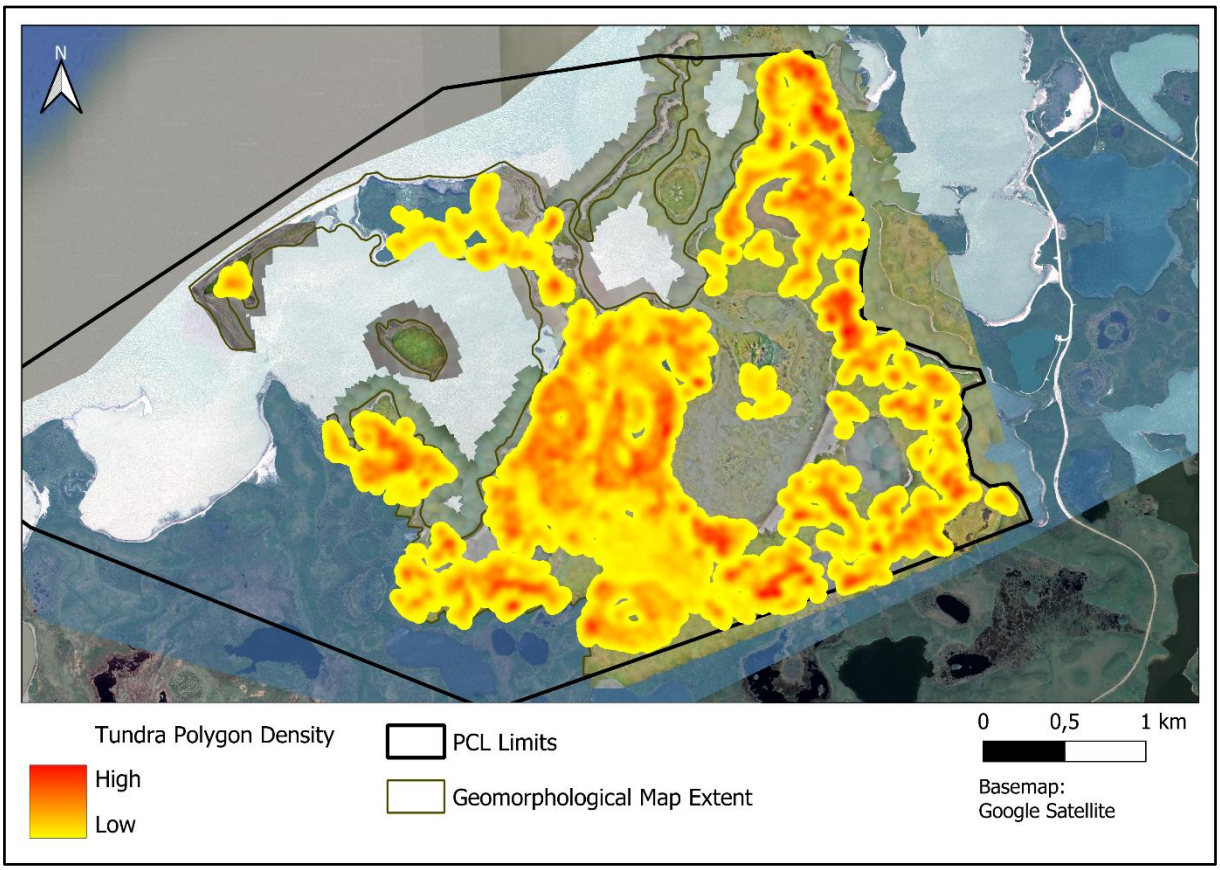

Figure 77 *– Heatmap indicating the areas of the Geomorphological Map where tundra polygon network densities are greater (in red). In can be inferred that these areas also contain high ground ice contents, associated with the ice wedges between the polygons.*

The “Lakes and Ponds” class occupies in total 0.39 km^2, which corresponds to about 3.7% of the total area of the park (Figure 78). As mentioned in the Data & Methods section, a very large number of waterbodies were identified and delineated, however the vast majority of these are small. Of the 8593 waterbodies digitized, there are only twenty with an area greater than 1000 m^2. Of these, only five have an area greater than 10,000 m^2, with the two largest lakes of the park being significantly larger than all the rest. The second largest one, located in the northeastern sector of PCL, just east of Split Pingo, has an area of 82,969.85 m^2. As for PCL’s largest isolated waterbody, it presents an area of 13,3005.49 m^2, and is located in the southeastern sector of the park, to the east of the large drained lake basin that surrounds Ibyuk Pingo. It should be mentioned that none of the waterbodies located within the limits of the “Inundated Lake Basins” were included into this class, as they were represented in their own specific subclass, “Large (Isolated) Wetland Lakes and Ponds”. Also, any waterbodies connected to the sea by flows of coastal water, even outside of the inundated lake basins, were not included in this class. However, “Lakes and Ponds” were digitized within the limits of the “Ancient Lake Basins” class, and in these cases, the current lakes seem to be remnants of the larger lakes that once filled the entirety of those basins.

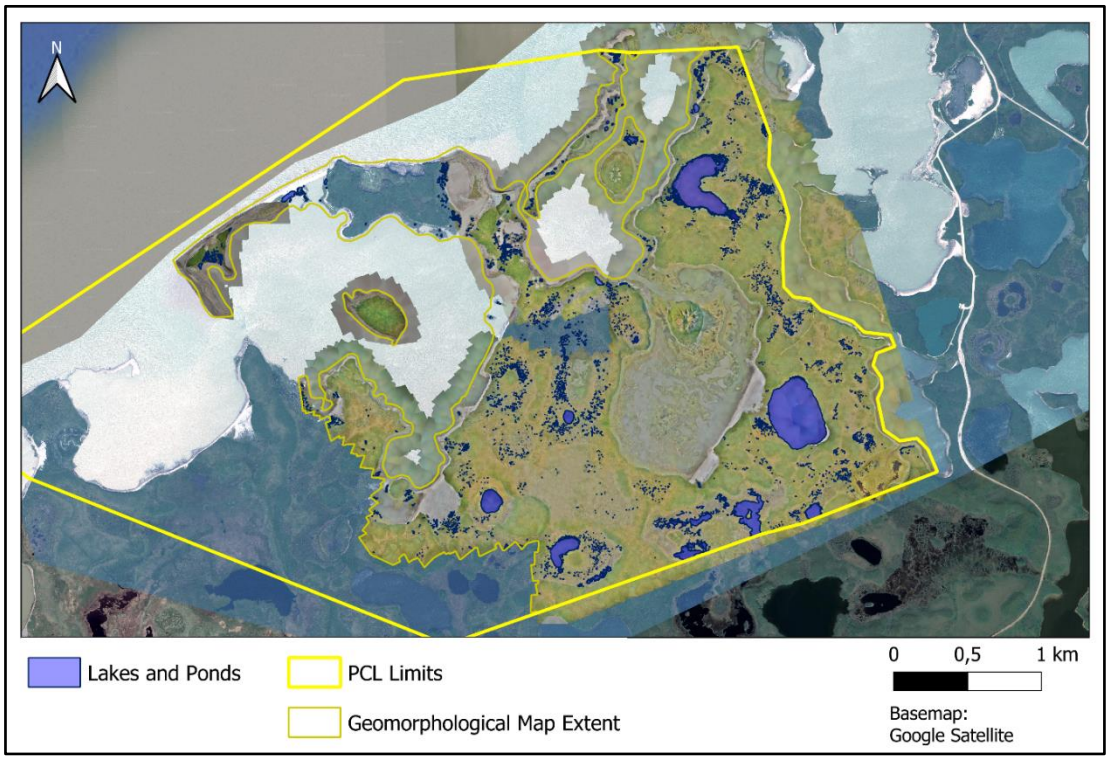

Figure 78 *- “Lakes and Ponds” class included into the Geomorphological Map.*

The “Driftwood Accumulations” class also occupies in total 0.39 km^2, corresponding again to about 3.7% of the total area of PCL (Figure 79). Some accumulations are of a very vast size, as well as a high density of driftwood, for example, those present along the southeastern margin of the inundated lake basin which surrounds Ibyuk Pingo. These logs are likely to originate from inland boreal forests located in the more continental regions of the

Canadian Arctic to the south, being transported upstream into the Beaufort Sea by the Mackenzie River and its tributaries, and then transported and deposited along the Tuktoyaktuk Peninsula's coast by ocean currents and sea ice (Dalaiden et al., 2018; Sendrowski et al., 2023). In PCL, layer upon layer of driftwood has been deposited by successive storms and flood events that have occurred throughout the decades. Other accumulations are much smaller in size, for example within the same basin, but away from the margins. Some present a much sparser distribution of driftwood, such as along the northern shore of Peninsula Point. As for the individual logs, they vary from less than 1 m to as much as almost 20 m in length. This landscape feature can also serve as a proxy for how far storm surge events have reached into the land of the park, as, for example, deposits of logs can be found along the shores of the large lake just east of the inundated basin that surrounds Ibyuk Pingo, indicating that in some more extreme events water overflows from that basin into the mentioned lake.

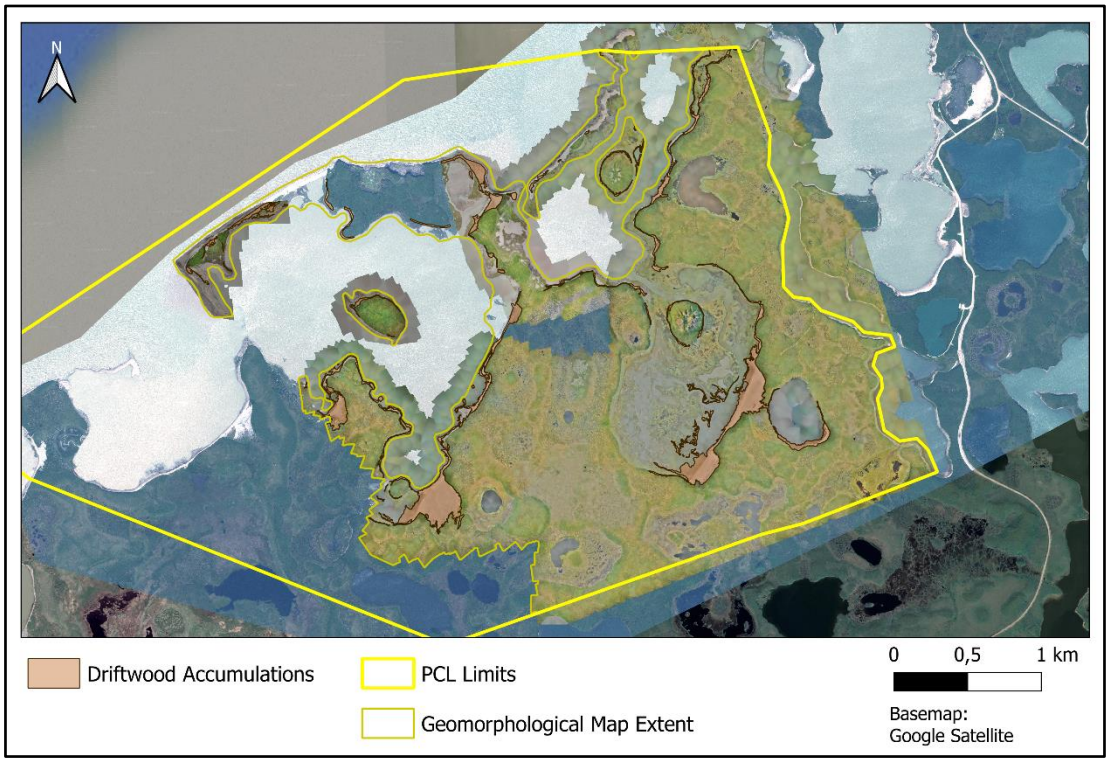

Figure 79 *- "Driftwood Accumulations" class included into the Geomorphological Map.*

The class "Inundated Lake Basins" occupies in total 1.22 km^2, which corresponds to about 11.59% of the total area of PCL (Figure 80). Of the two basins that comprise this class, the one located at the southeastern corner of the park is much smaller compared to the one that surrounds Ibyuk Pingo (the first has an area of 0.09 km^2, compared to the 1.13 km^2 of the latter). The class "Ancient Lake Basins" covers 0.65 km^2, representing 6.17% of the park (Figure 80). The main distinction between the "Inundated Lake Basins" and the "Ancient Lake Basins" is that the first show signs of recent flooding, while the latter seem to correspond to the relict extents of lakes that are now much smaller. Both classes do, however, present some sectors with similar landscapes and ecological characteristics, and for this reason both were

subclassified into the five subclasses shown in Figure 81, which will be described in the next paragraphs. In should be mentioned though that, of the five subclasses, only two were found within the areas covered by the “Ancient Lake Basins” (being those “Dry Wetlands” and “Wetlands with Lakes and Ponds”).

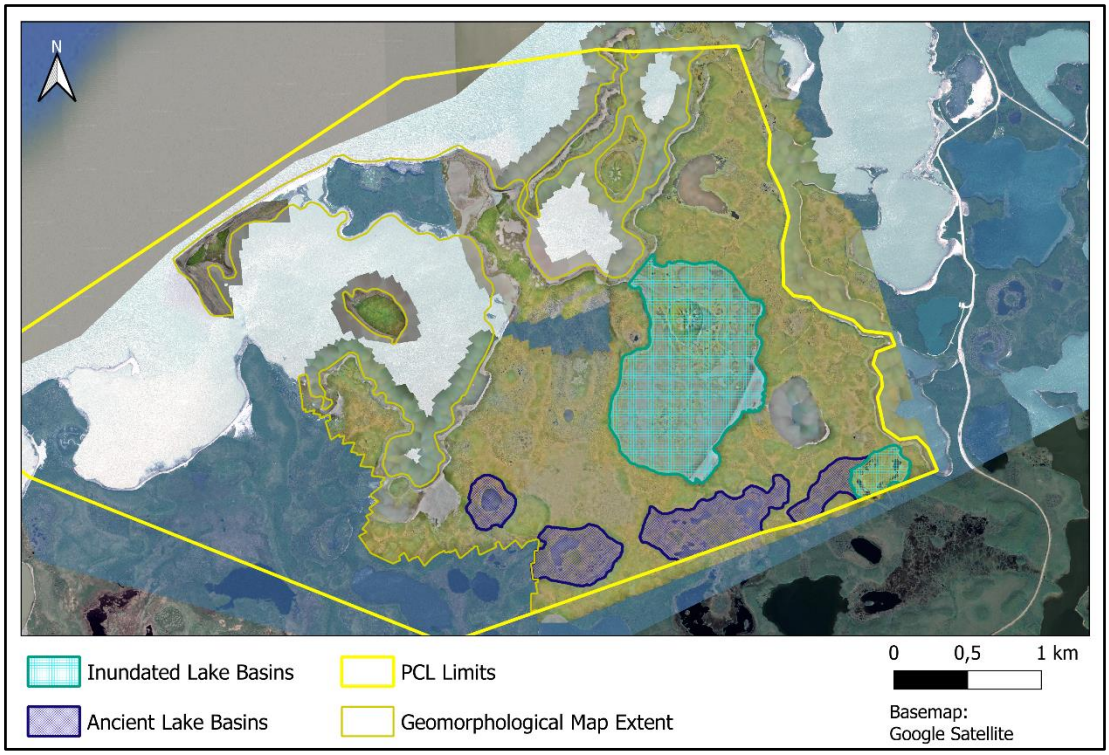

Figure 80 *- “Inundated Lake Basins” and “Ancient Lake Basins” classes included into the Geomorphological Map.*

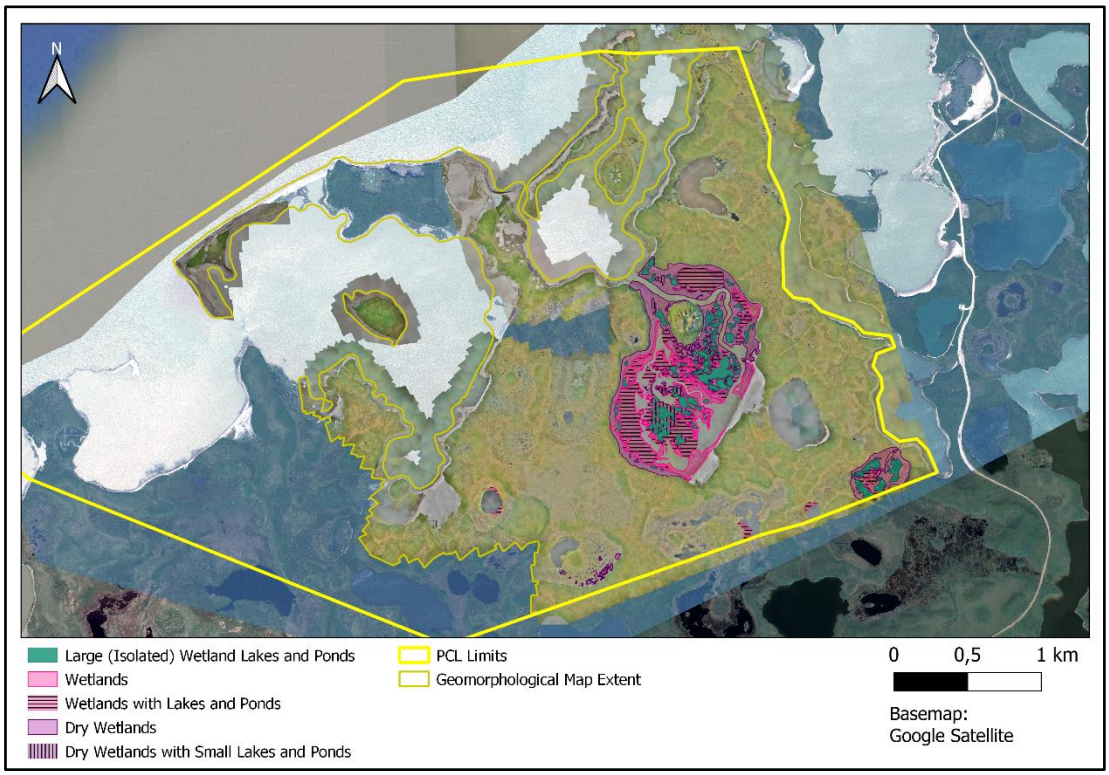

Figure 81 *- “Large (Isolated) Wetland Lakes and Ponds”, “Wetlands”, “Wetlands with Lakes and Ponds”, “Dry Wetlands” and “Dry Wetlands with Small Lakes and Ponds” subclasses included into the Geomorphological Map.*

The subclass “Large (Isolated) Wetland Lakes and Ponds” occupies in total 0.15 km^2, which corresponds to about 1.42% of the total area of the park. This class is comprised of waterbodies that are not connected to the flow of coastal water that enters the “Inundated Basins”. The largest of these waterbodies tend to have a light brown water coloration (possibly a sign of sediments or organic matter in suspension), while the smaller ones tend to be dark grayish-blue and many times with a much greater presence of hydrophytic vegetation, especially around the margins. Most of these waterbodies are relatively large, but some smaller ones located very close to the larger ones were also included in this unit. The larger waterbodies are associated with deeper depressions in the terrain, which are likely to retain water from floods.

The “Wetlands” subclass occupies in total 0.12 km^2, which equals to about 1.14% of the total area of the park. This class corresponds to areas of the basin that appear to be frequently flooded (close to the coastal water that enters the basin). The vegetated areas present within it are less developed than in the “Dry Wetlands” unit and have a dark green/greenish-brown coloration. This unit also includes many muddy areas.

The subclass “Wetlands with Lakes and Ponds” occupies in total 0.24 km^2, which corresponds to about 2.28% of the total area of PCL. It includes areas that appear to be frequently flooded (usually being close to the flows of coastal water that enter the basins) and that have many small and medium sized waterbodies. The vegetation here is identical to that of the “Wetlands” unit (not very developed and with dark green/greenish-brown coloration). Most waterbodies tend to be dark grayish-blue and many times present hydrophytic vegetation, especially around the margins. The larger waterbodies tend to have a light brown coloration away from the margins. Some areas where the waterbodies are very shallow appear to have a light gray/white coloration. Just like the “Wetlands” class, this unit includes many muddy areas, especially near the waterbodies.

The subclass “Dry Wetlands” occupies in total 0.33 km^2, which corresponds to about 3.13% of the total area of the park. This makes it the subclass with the largest representation within the “Inundated Lake Basins” and “Ancient Lake Basins” classes. This unit includes areas of the basins that do not appear to be frequently flooded. Its vegetated areas are not greatly developed, but more so than in the “Wetlands” unit. These areas have a green or light green coloration. More well developed vegetation formations, also of a light green coloration, present on slightly elevated locations that appear scattered throughout the areas that seem to be frequently flooded (corresponding to the “Wetlands” and “Wetlands with Lakes and Ponds” classes), were also included into the “Dry Wetlands” class.

The “Dry Wetlands with Small Lakes and Ponds” subclass occupies in total 0.04 km^2, which corresponds to about 0.38% of the total area of PCL. Of the five subclasses, it is therefore the one that covers the smallest area. It includes areas that do not appear to be frequently flooded, but that contain many small and some medium sized waterbodies. The vegetation of this unit is identical to that of the “Dry Wetlands” unit (more developed than the vegetation of the “Wetlands” unit and mostly of a green or light green coloration), though the areas closest to the waterbodies are frequently of the same greenish-brown coloration as seen in the “Wetlands with Lakes and Ponds” unit. Most of the waterbodies belonging to this class tend to be dark grayish-blue and many times present hydrophytic vegetation, especially around the margins. The larger waterbodies tend to have a light brown coloration away from the margins, similarly to the “Wetlands with Lakes and Ponds” unit.

The class “Ice Mounds” covers an area of 0.6 km^2, representing 5.7% of the area of PCL (Figure 82). The average maximum height of the “Ice Mounds” included in the map was 8.83 m, being that the tallest element in this class was 17.93 m. It is possible that some of these mounds are incipient pingos, though clear dimensional thresholds were not found in the literature to distinguish these from fully developed pingos. In truth, several of the landforms included in this class, could even possibly be considered fully developed pingos. However, it was decided not to give them that designation as, nor are they officially recognized as pingos by Parks Canada, nor do they present the typical morphological characteristics associated with these landforms (a conical hill, with a circular or oval footprint on the terrain when seen from above). The difficulty in finding clear criteria to categorize these landforms is what ultimately led to them being defined with the “catch-all” term “Ice Mounds”.

The “Sand” class has a total area of 0.33 km^2, which represents 3.13% of the total area of the park (Figure 83). These areas essentially correspond to beaches located along most of PCL’s coast, and the sand spit that extends from Peninsula Point. This class is likely to be dynamic in nature, in the sense that its extent varies over time as a consequence of tidal activity and storm events. This is particularly true for the sandspit that extends from Peninsula Point, something that is noticeable in older areal imagery of the park, as will be seen in Chapter 6.2 and 6.4. It should also be noted that this class has more expression on the coastal sectors that are more exposed to the Beaufort Sea, and less so on the inner, more sheltered coastal sectors of the park.

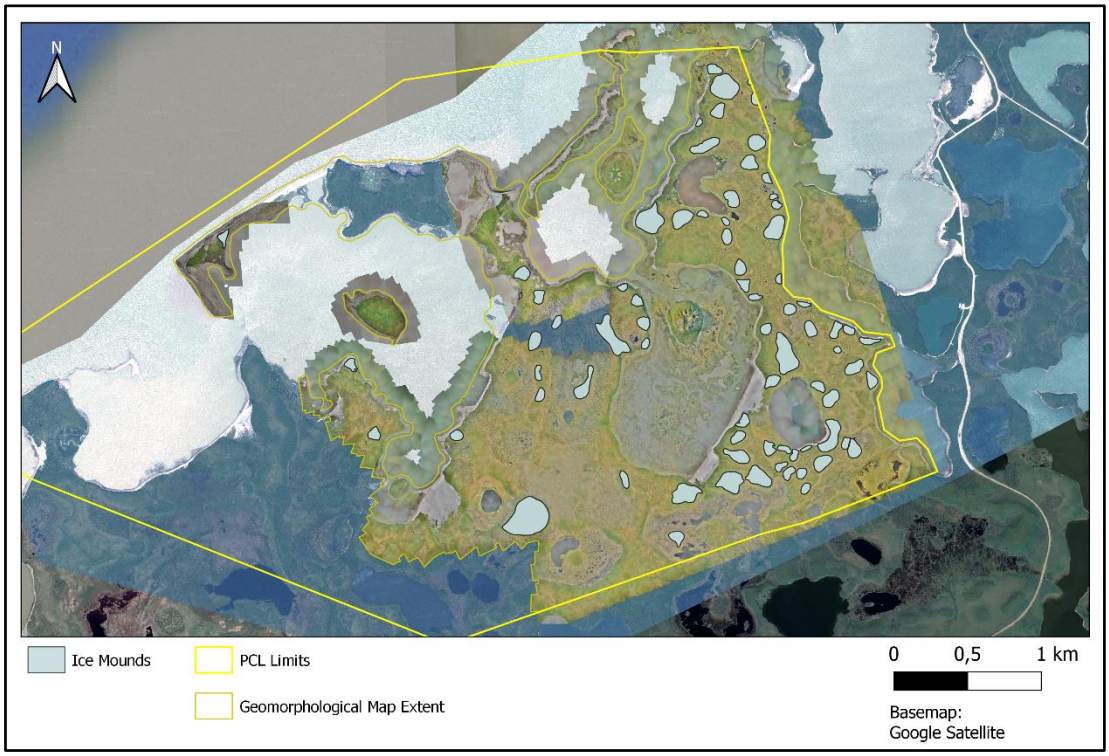

Figure 82 *- "Ice Mounds" class included into the Geomorphological Map.*

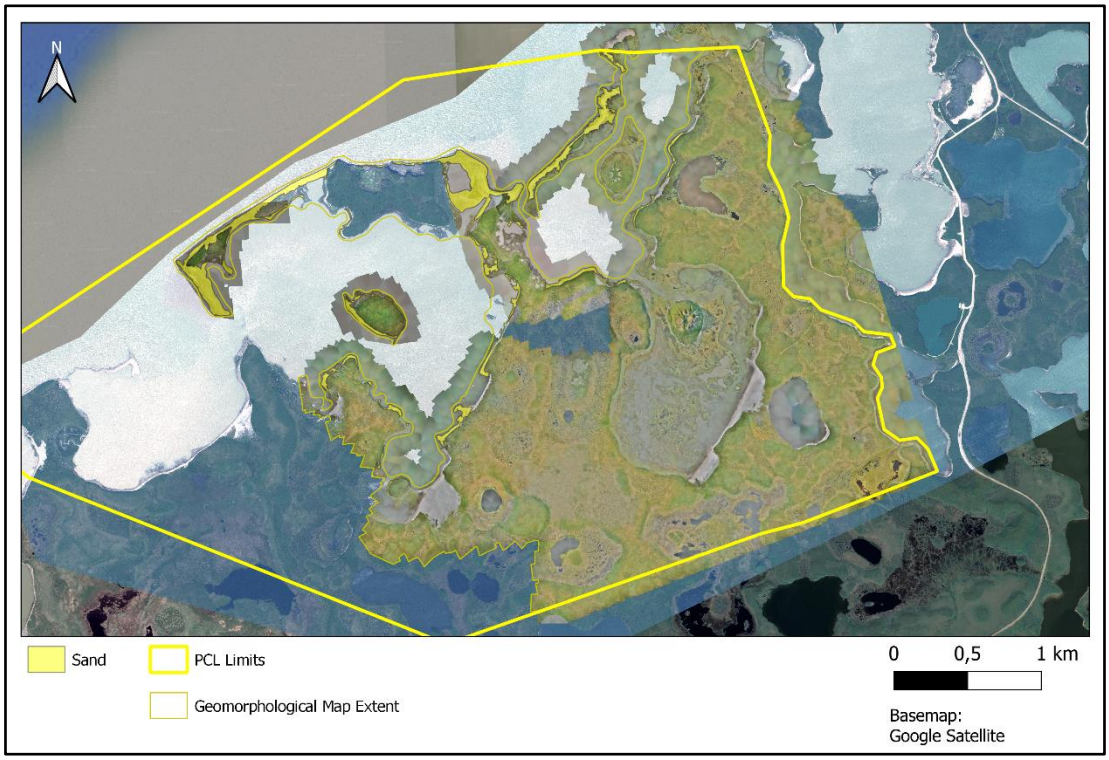

Figure 83 *- "Sand" class included into the Geomorphological Map.*

The “Coastal Cliffs and Thaw Slumps” class covers an area of 0.07 km^2, or 0.66% of PCL (Figure 84). This class encompasses two distinct sectors, one on Peninsula Point (much larger in size, with an area of 67,422.75 m^2) and one at the northeastern tip of the park limits (much smaller, with an area of only 1155.36 m^2). According to the UAV DSM data used in this study, the cliffs in the northeastern sector of PCL first present a 3 m drop, followed by a sector of bluffs with a gradual increase in altitude (likely to be relict retrogressive thaw slumps), followed then by another cliff face of roughly 2 m. Here, retreat seems to be relatively inactive, as vegetation is well developed and the soil seems relatively undisturbed. The same can not be said for the larger cliff sector at Peninsula Point. This sector, as mentioned in Chapter 2.3, was the subject of the recent studies of Lim et al. (2020a) and Lim et al. (2020b). Though the drone altimetric data was not available for this area of PCL, these studies refer that these cliffs can be higher than 20 m, and are in active regression. Lim et al. (2020a) refers that due to a single storm event that occurred in August of 2019 “lower elevation (< 20 m) cliffs recorded an average recession of 3.3 m, whereas higher (> 20 m) cliffs receded by an average of 1.75 m”. Inland from the exposed permafrost cliffs, retrogressive thaw slumps can be found. Though they seem to still be active, retreat rates there are likely to be much more gradual when compared to the cliffs. Still referring to the previously mentioned study, it states that, in relation to the same storm event, “the thaw-slump complexes remained relatively unaffected” and “debris flow fans were generally more resistant to storm erosion than the ice-rich cliffs”.

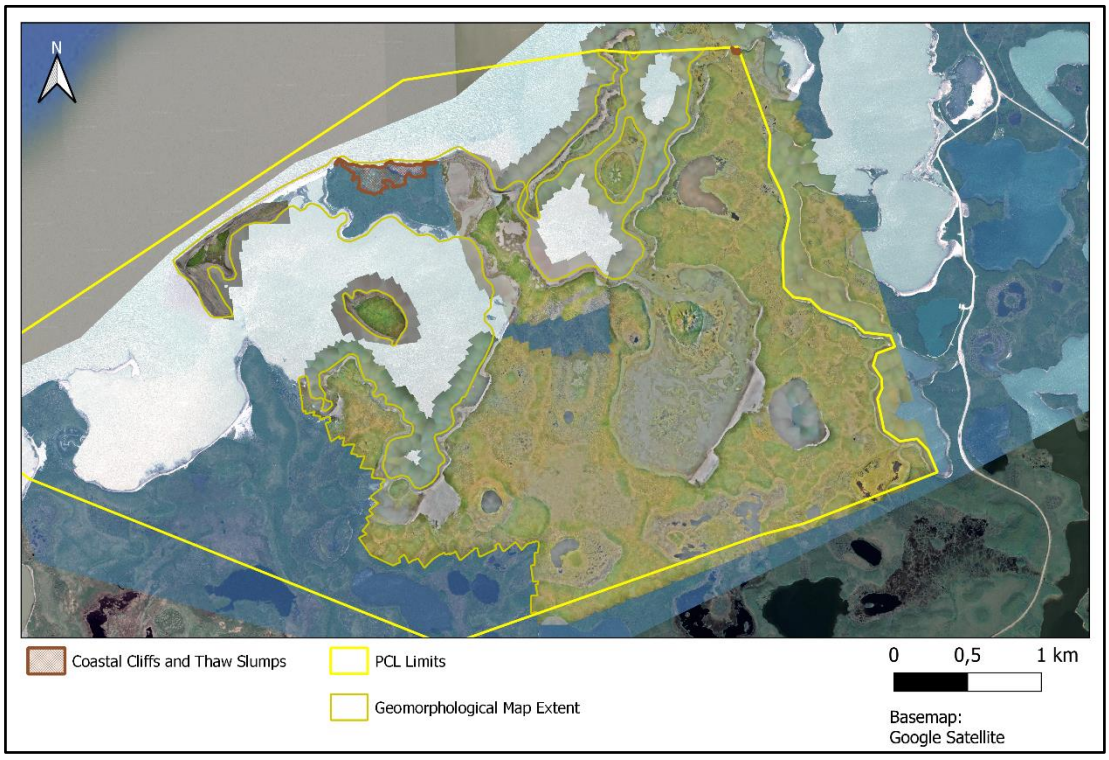

Figure 84 *- “Coastal Cliffs and Thaw Slumps” class included into the Geomorphological Map.*

The “Tourist Walkway” class occupies in total 0.001 km^2, which corresponds to about 0.01% of the total area of the park (Figure 85). This class is clearly the one with the smallest representation within the park. Though it is also possible to visit the park by canoe or kayak, following different routes established for that purpose, the walkway is intended to be the only portion of the park where tourists can visit PCL on foot. This is to preserve the natural landscape of the park as much as possible, being that Ibyuk Pingo and several other pingos can still be clearly viewed from the walkway. However, as we will see, the reality is that this isn’t the only area were humans circulate on the land of the park.

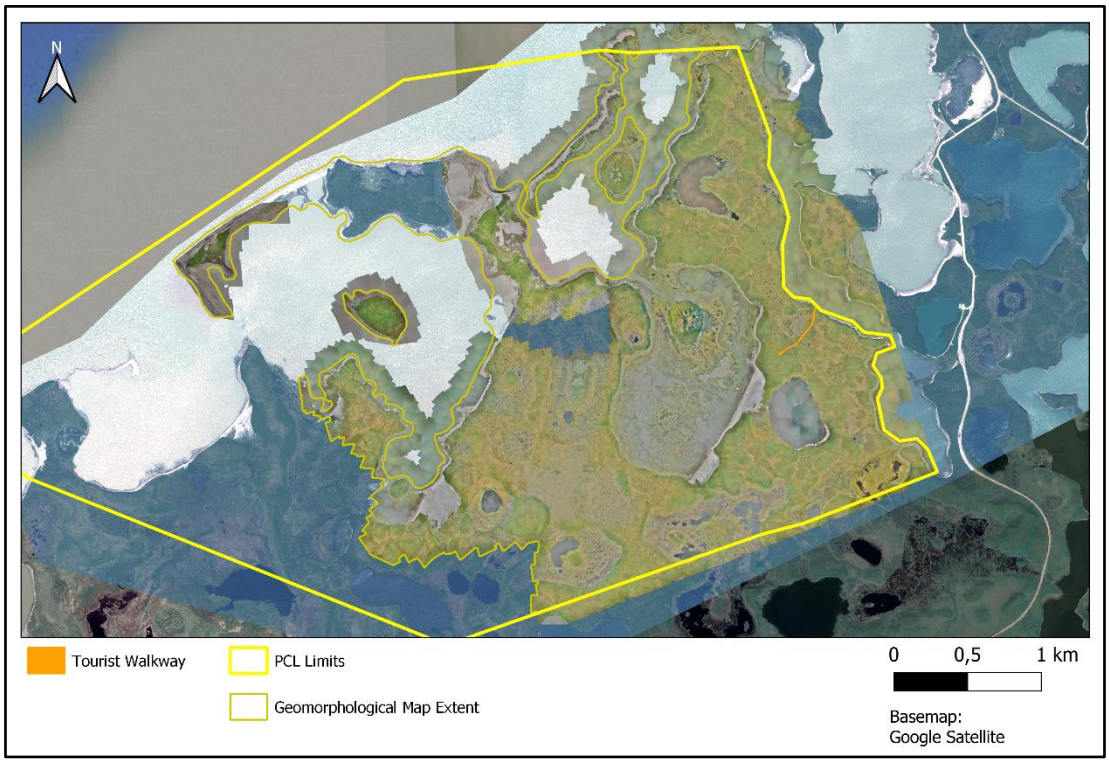

Figure 85 *- “Tourist Walkway” class included into the Geomorphological Map.*

The class “Seismic Lines” occupies in total 0.01 km^2, which corresponds to 0.09% of the total area of the park (Figure 86). This feature is located near the southern limits of PCL. According to Canada Energy Regulator (2022) and French (2007), these features likely date back to the 1960’s and 1970’s. Also according to French (2007), clearance of vegetation and other surface level disturbances of the terrain, even small ones, are a very common human-induced cause of thermokarst. In the case of these seismic lines, which are rather large features, the impact on the landscape is quite noticeable, even when observing the orthomosaic of the park at higher resolution. However, given that the disturbances were already created about 55 to 65 years ago, the vegetation there has since regrown. In truth, the vegetation along these former seismic lines is amongst the most well developed within the park. This could be because the thermal disturbances associated with the seismic lines did indeed lead to the formation of thermokarst as suggested by French (2007), and consequently to the formation of depressions in the terrain, where water potentially accumulated. This,

combined with the initial aeration of the topsoil associated with the disturbances may have facilitated the development of vegetation.

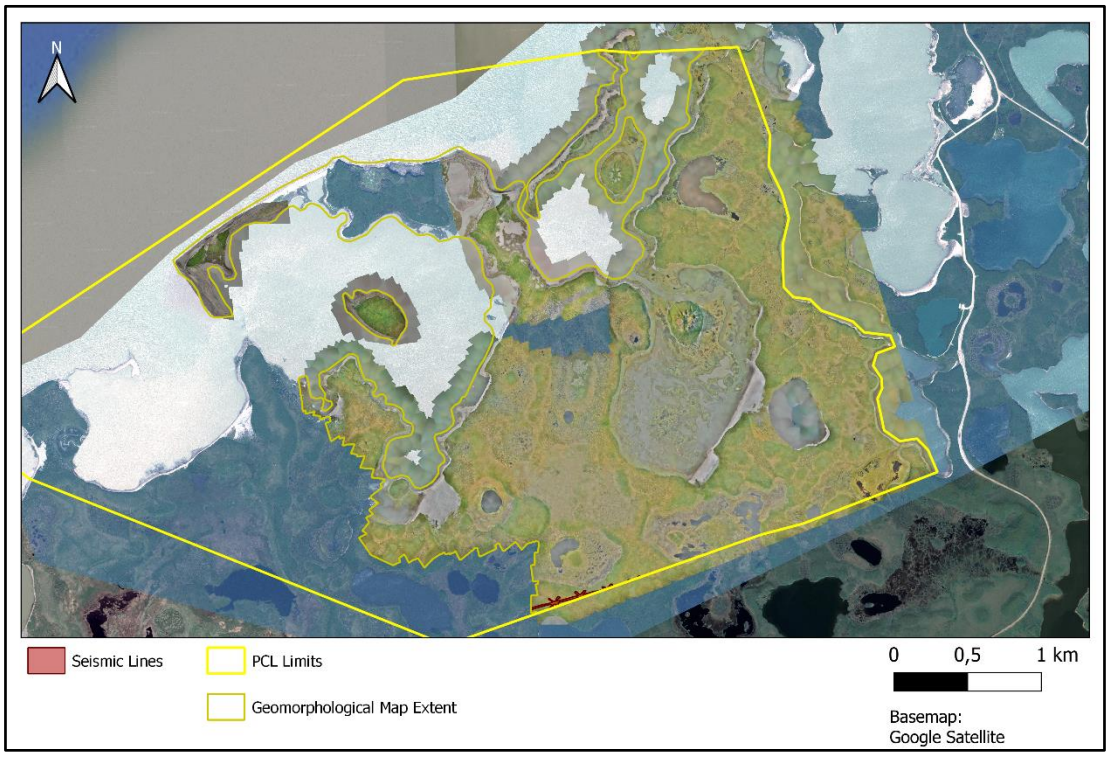

***Figure 86** - "Seismic Lines" class included into the Geomorphological Map.*

The "Vehicle Tracks" are the only linear type feature in this map (Figure 87). This way, it was not possible to directly determine the area occupied by these features, but instead it was possible to determine the total length of them, which was 113.53 km. To roughly estimate the extent of terrain occupied by the tracks, a 1 m buffer was created around these linear features, and then the "Dissolve" vector geoprocessing tool was applied to those buffers. This way, it was possible to determine, that approximately 0.16 km^2 were covered by these tracks, corresponding to about 1.52% of the total area of PCL. These tracks are likely to be left predominantly by ATVs. A vehicle of this type was spotted by the team of CEG/IGOT - University of Lisbon and the Geological Survey of Canada during the field campaign of 2019, when much of the data used in this study was obtained. Similarly to the previously mentioned seismic line features, these features also constitute a man-induced influence on the landscape of PCL. The tracks are clearly having a negative impact on the vegetation, with signs of recent and continuous degradation visible in the UAV orthomosaic. Naturally, in the areas where circulation is more frequent and intense, the impacts on the land are greater (Figure 88 and Appendix Figure 3). Some tracks even lead up to Ibyuk Pingo, suggesting that the occupants of the vehicles climb its slopes.

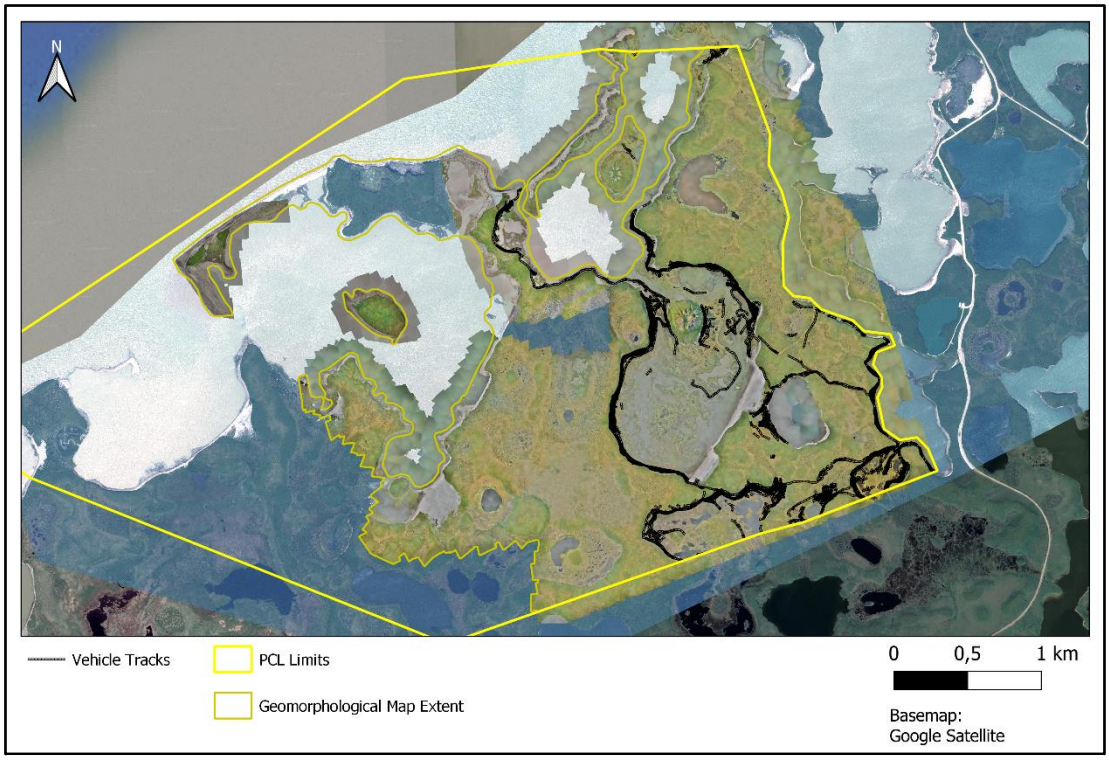

***Figure 87** - "Vehicle Tracks" class included into the Geomorphological Map.*

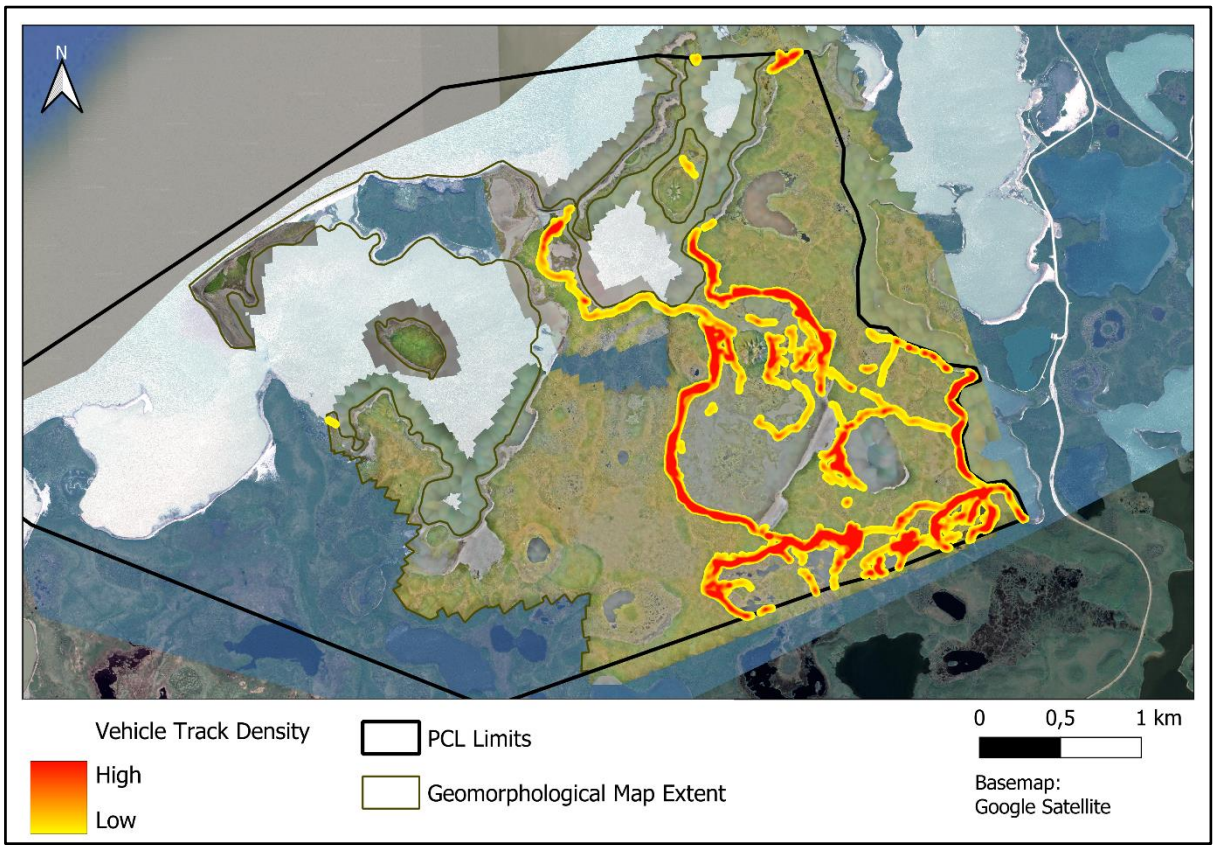

***Figure 88** - Heatmap showing the areas where the vehicle track network densities are greater (in red). It can be inferred that these areas are where the impacts of vehicle circulation on the terrain and vegetation are greater.*

The “Tundra Plains” is the class that occupies the largest area, 2.53 km^2, which corresponds to 24.03% of PCL (Figure 89). These areas of the park are generally flat, with an average altitude of 1.47 m above sea level. Some of these plains may be flooded during the occurrence of storm surge events, but generally they do not present signs of this occurring often. They are deprived of notable geomorphological features, and are predominantly covered by shrub and herbaceous tundra vegetation.

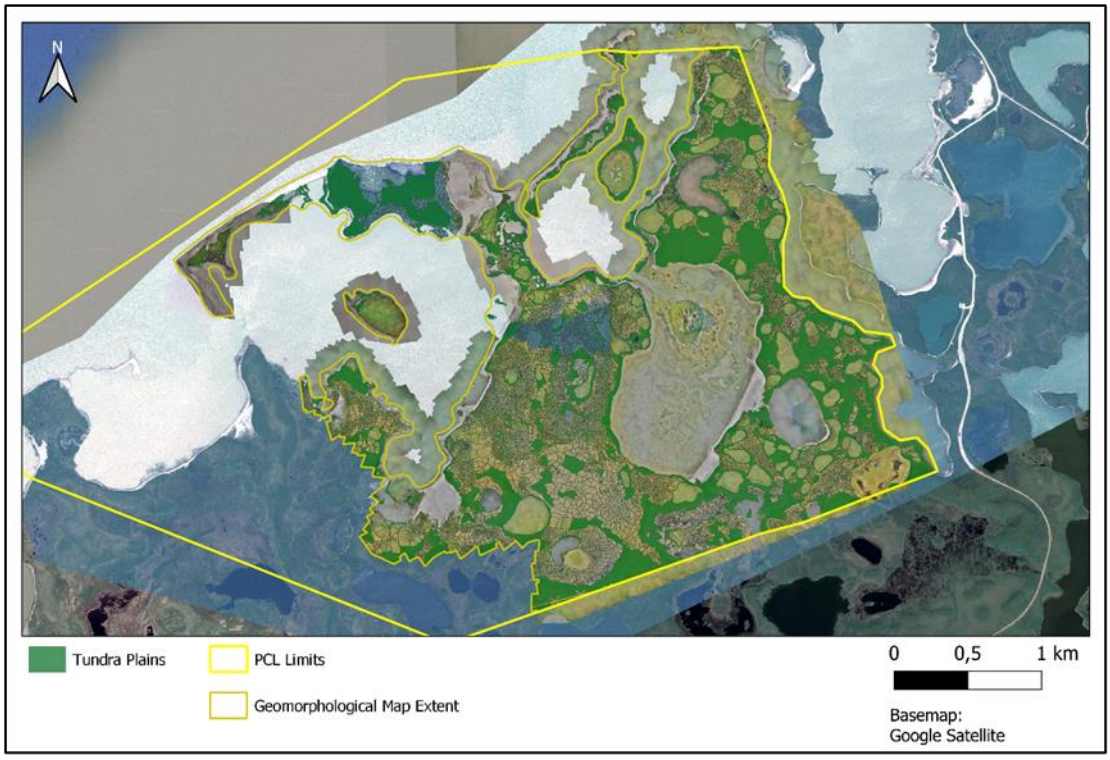

Figure 89 *- “Tundra Plains” class included into the Geomorphological Map.*

A summary of the geographical statistics regarding the areas of the twenty classes and subclasses of the Geomorphological Map are presented in Table 3 and Figure 90. In conclusion, it can be stated that the three classes with highest representation in the portion of PCL that was mapped are “Tundra Plains” (24.03%), “Tundra Polygons” (21.27%) and “Inundated Lake Basins” (11.59%). Those with the smallest representation are “Pingo Summit Craters and Dilation Cracks” (0.19%), “Pingo Surface Erosion” (also 0.19%), “Seismic Lines” (0.09%), and “Tourist Walkway” (0.01%).

GEOMORPHOLOGICAL MAP			
Class	Number of Features	Total Area (km2)	% of PCL's Total Area (not including costal waters)
Pingos	8	0,21	1,99
Pingo Summit Craters and Dilation Cracks	5	0,02	0,19
Pingo Surface Erosion	28	0,02	0,19
Tundra Polygons	14518	2,24	21,27
Lakes and Ponds	8593	0,39	3,70
Driftwood Accumulations	90	0,39	3,70
Inundated Lake Basins	2	1,22	11,59
Ancient Lake Basins	4	0,65	6,17
Large (Isolated) Wetland Lakes and Ponds	61	0,15	1,42
Wetlands	58	0,12	1,14
Wetlands with Lakes and Ponds	47	0,24	2,28
Dry Wetlands	68	0,33	3,13
Dry Wetlands with Small Lakes and Ponds	54	0,04	0,38
Ice Mounds	75	0,60	5,70
Sand	36	0,33	3,13
Coastal Cliffs and Thaw Slumps	2	0,07	0,66
Tourist Walkway	1	0,001	0,01
Seismic Lines	3	0,01	0,09
Vehicle Tracks	2201	0,16	1,52
Tundra Plains	15	2,53	24,03
TOTAL AREA OF PCL NOT INLCUDING COASTAL WATERS (km2)	10,53		

Table 3 *- Statistics regarding the areas of the classes and subclasses of the Geomorphological Map.*

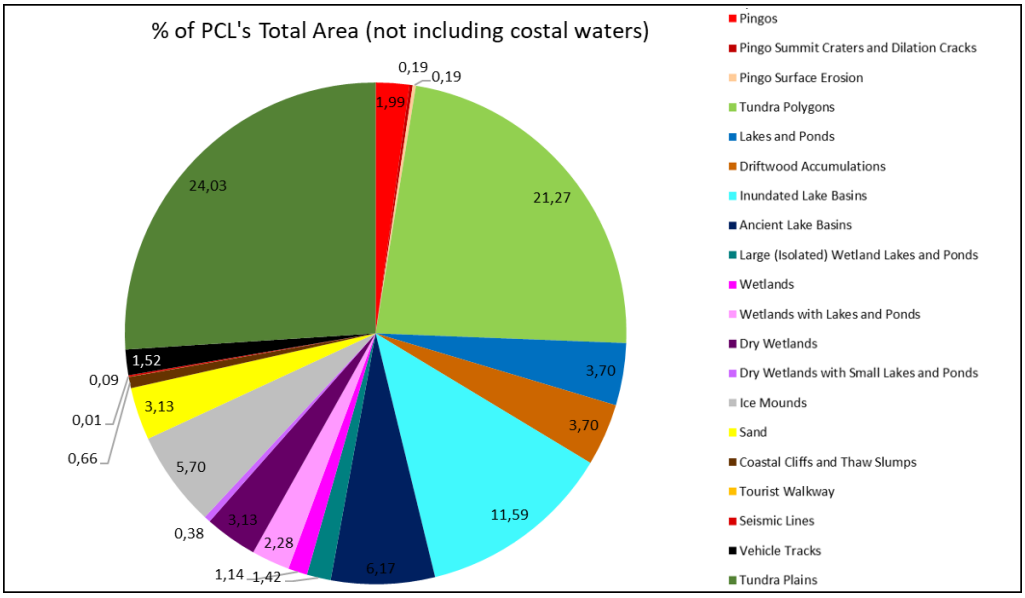

Figure 90 *– Pie chart with the relative proportion of each class and subclass of the Geomorphological Map in relation to the total area of PCL.*

5.2 - Landcover Units

As has been mentioned, a supervised classification over a WorldView-2 scene was performed on the same extent of the park as the Geomorphological Map. Therefore, for comparative descriptions, the "total area of the park" will again correspond to 10.53 km^2 (as the coastal waters within its limits were also not incorporated into the supervised classification). In the following paragraphs, each of the nine classes that were included into this supervised classification Landcover Map (Appendix Figure 4) shall be described in more detail.

The class "High Shrub Tundra" occupies in total 1.94 km^2, which corresponds to about 18.42% of the total area of the park (Figure 91). The vegetation of this class is the most

developed of the park, being that it is mainly comprised of well developed shrubs and very well developed herbaceous plants. Even though these areas are those at which vegetation is more developed in the park, it should be reminded that the climatic context in which PCL is inserted (as described in Chapters 2.1 and 3.1.2) does not provide ideal conditions for great plant development. With this, some examples of species that may be found in these areas include dwarf birches (*Betula nana*), dwarf arctic willows (*Salix arctica),* heath (plants of the *Erica* genus), Labrador tea (plants of the *Rhododendron* genus), crowberry plants (*Empetrum nigrum*), cranberry plants (subgenus *Oxycoccus* of the genus *Vaccinium*) and cloudberry plants (*Rubus chamaemorus*) (Pingo Canadian Landmark Memorandum of Agreement, 2001).

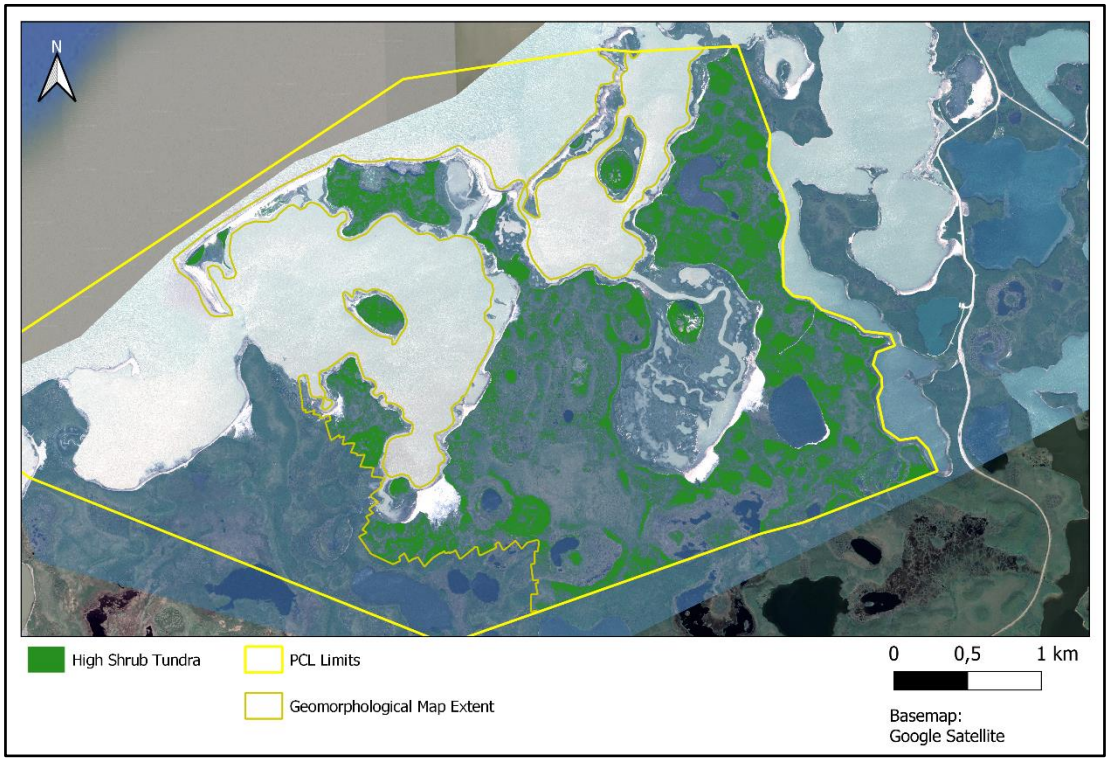

***Figure 91** - "High Shrub Tundra" class included into the Landcover Map.*

The class "Low Shrub Tundra" occupies in total 2.45 km^2, which corresponds to about 23.3% of the total area of PCL (Figure 92). It is, therefore, the class with the largest representation within the borders of PCL. This vegetation community mostly consists of low shrubs and well developed herbaceous plants. Therefore, of the previously mentioned species mentioned, those that can be expected to be most commonly found in these areas are the heath, Labrador tea, Crowberry, Cranberry and Cloudberry plants (Pingo Canadian Landmark Memorandum of Agreement, 2001). However, communities of these species are likely to be less developed than in the areas occupied by "High Shrub Tundra" class.

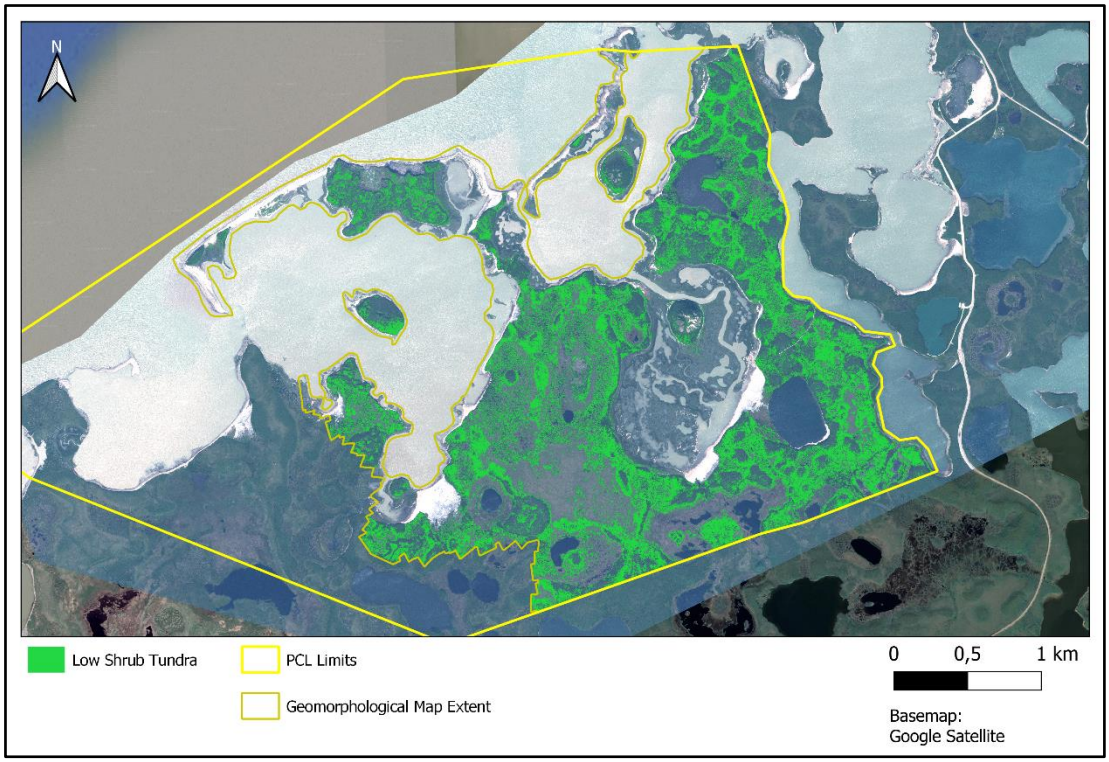

***Figure 92** - "Low Shrub Tundra" class included into the Landcover Map.*

The "Dry Tundra" class occupies in total 1.11 km^2, which corresponds to about 10.58% of the total area of the park (Figure 93). This vegetation community essentially contains sporadic low shrubs and poorly developed herbaceous plants. The species found there are likely to be similar to those of the "Low Shrub Tundra", but less developed and sparser. Also, this unit seems to be located in areas that are more topographically depressed than the "High Shrub Tundra" and "Low Shrub Tundra" classes, but that are not inundated frequently as occurs with the areas occupied by the "Inundated Tundra" class.

The "Inundated Tundra" class occupies in total 1.04 km^2, which corresponds to about 9.84% of the total area of PCL (Figure 94). This class consists of areas that are prone to being flooded by the coastal waters, especially in the occurrence of storm surge events, being that these areas typically correspond to depressions in the terrain. Even though most of these areas present vegetation, these communities are not very developed, and essentially correspond to poorly developed herbaceous plants and hydrophytic vegetation. Also, the terrain in these areas is very humid, and contains many muddy areas. The drained lake basin that surrounds Ibyuk Pingo was almost entirely classified as belonging to this unit.

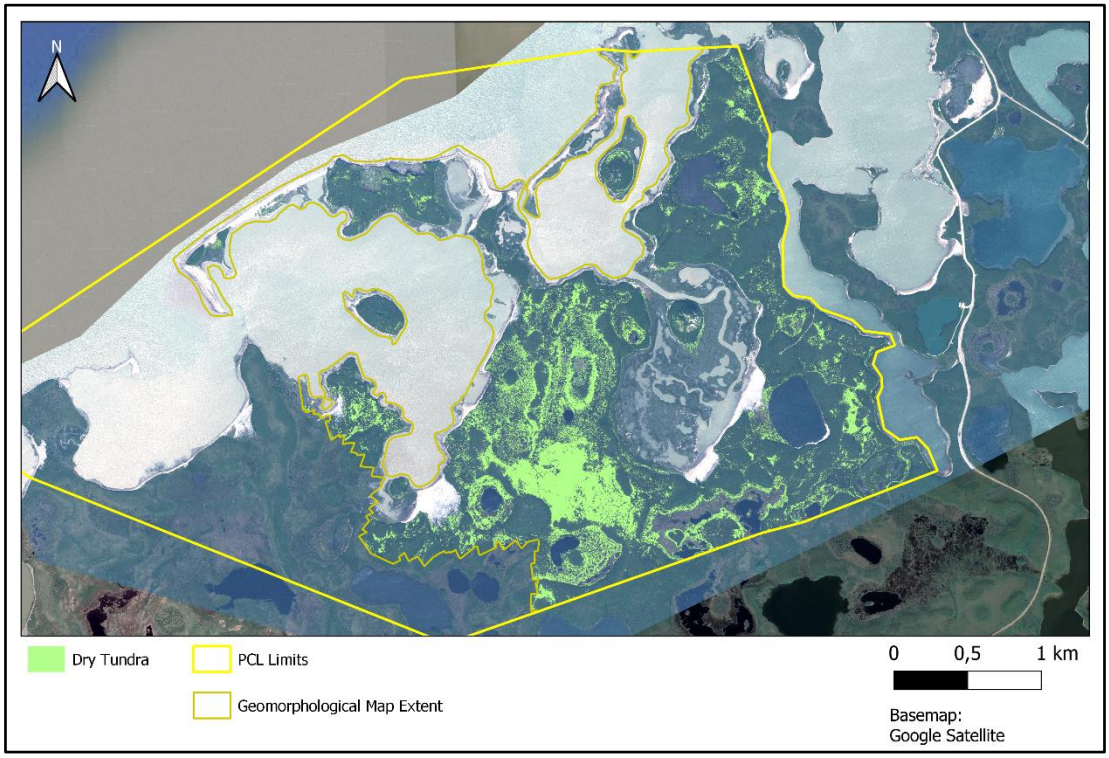

Figure 93 *- "Dry Tundra" class included into the Landcover Map.*

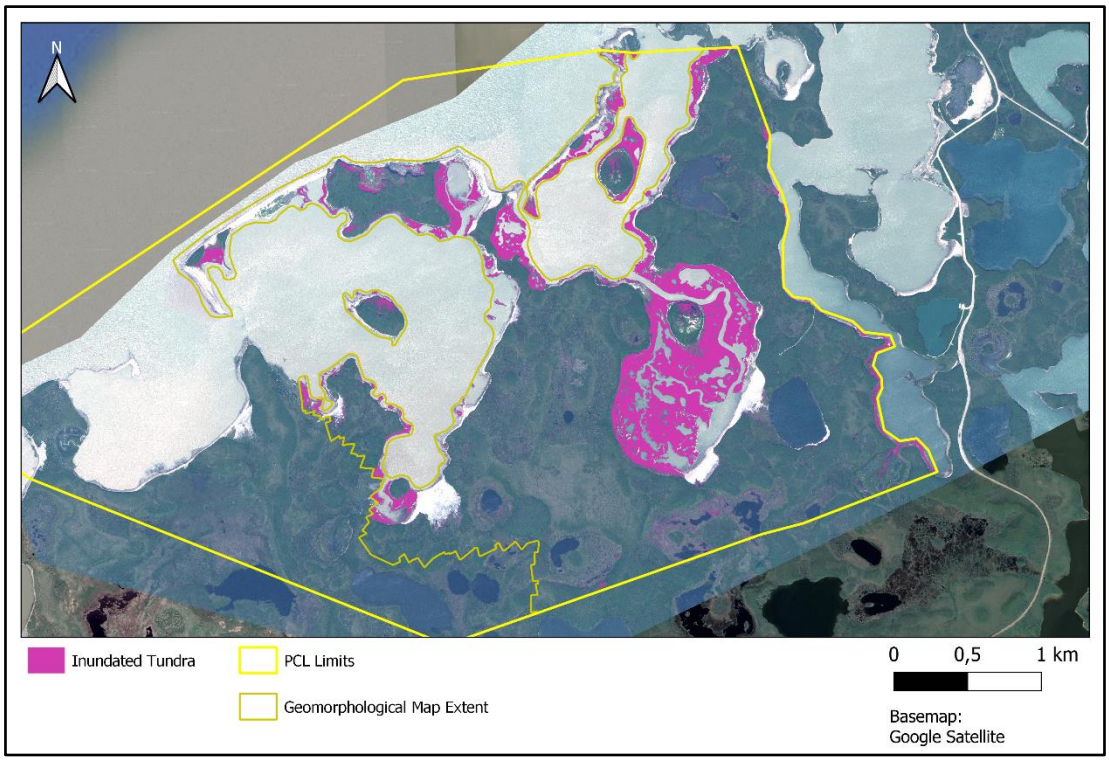

Figure 94 *- "Inundated Tundra" class included into the Landcover Map.*

The class “Bare Soil” occupies in total 0.55 km^2, which corresponds to about 5.2% of the total area of PCL (Figure 95). This class corresponds to areas of barren and dry soil with no vegetation, predominantly located in topographically depressed sections of the park. It can be noticed that some areas that should have been classified as “Wet Sand and Mud” were misclassified as this class (Table 1).

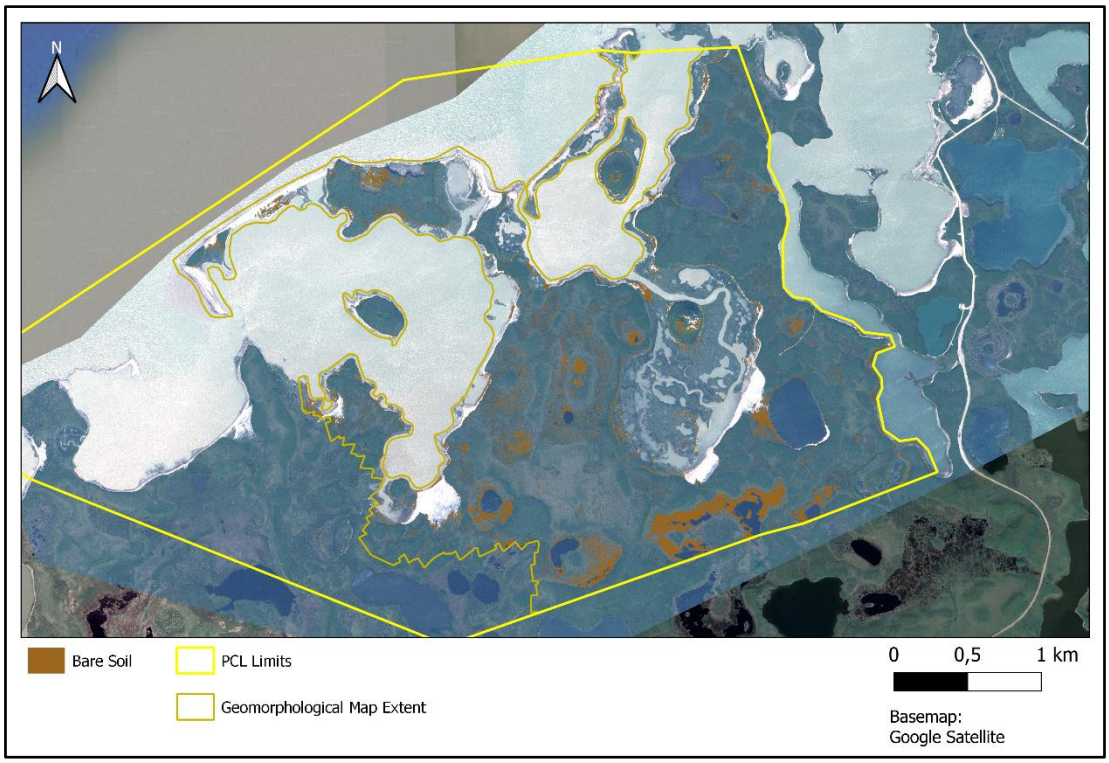

Figure 95 *- “Bare Soil” class included into the Landcover Map.*

The class “Sand” occupies in total 0.09 km^2, which corresponds to about 0.85% of the total area of the park (Figure 96). This class is predominantly located along the coastline, and corresponds to beach sand (namely, the drier sand, not directly in contact with the coastal waters). When comparing the “Sand” class of the Landcover Map with the “Sand” class of the Geomorphological Map, we see that in the Landcover Map it corresponds to a smaller area (0.09 km^2 compared to the 0.33 km^2 of the Geomorphological Map). This is due to the fact that the supervised classification algorithm attributed pixels located within the areas classified as “Sand” in the Geomorphological Map to other landcover units. Looking back at the Confusion Matrix associated with the results of this analysis (Table 1), it is expected that those other landcover units were mostly “Driftwood Accumulations” and “Man-made Structures”, whose spectral signatures are likely to be similar to that of the “Sand”.

The “Wet Sand and Mud” class occupies in total 0.20 km^2, which corresponds to about 1.86% of the total area of the park (Figure 97). These are areas along the coastline in direct contact with the water, and also some areas contiguous with the class “Inundated Tundra” that present no vegetation and that are typically muddy.

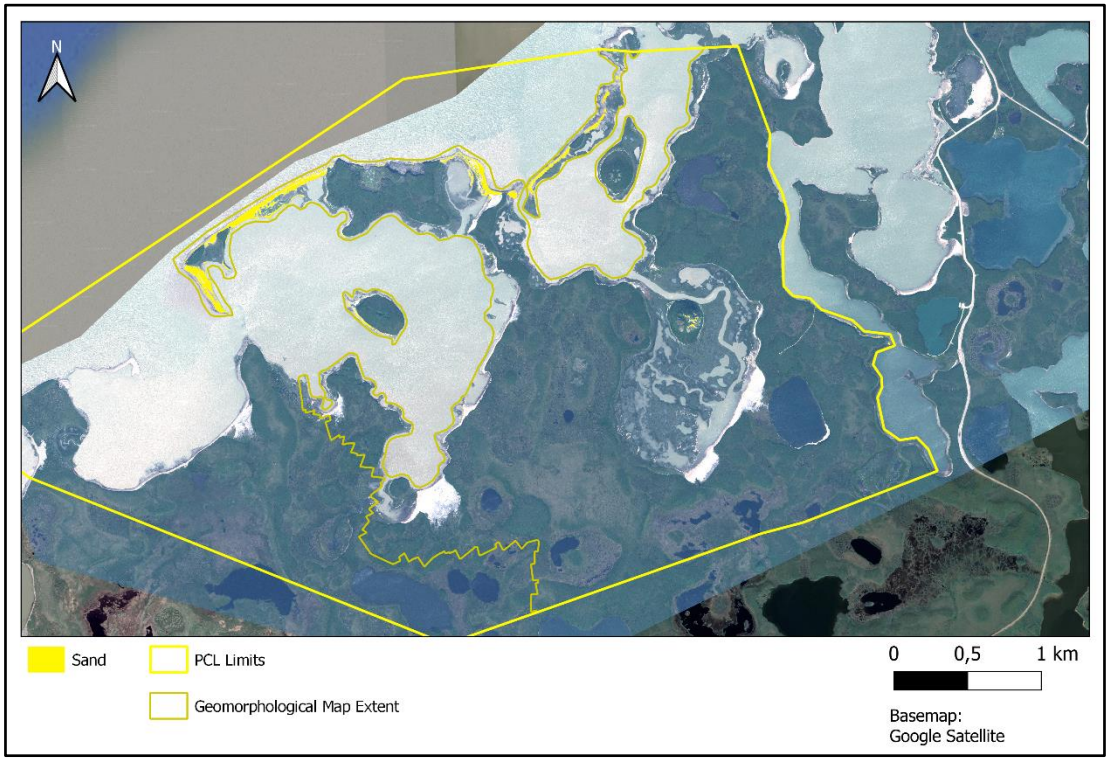

Figure 96 *- “Sand” class included into the Landcover Map.*

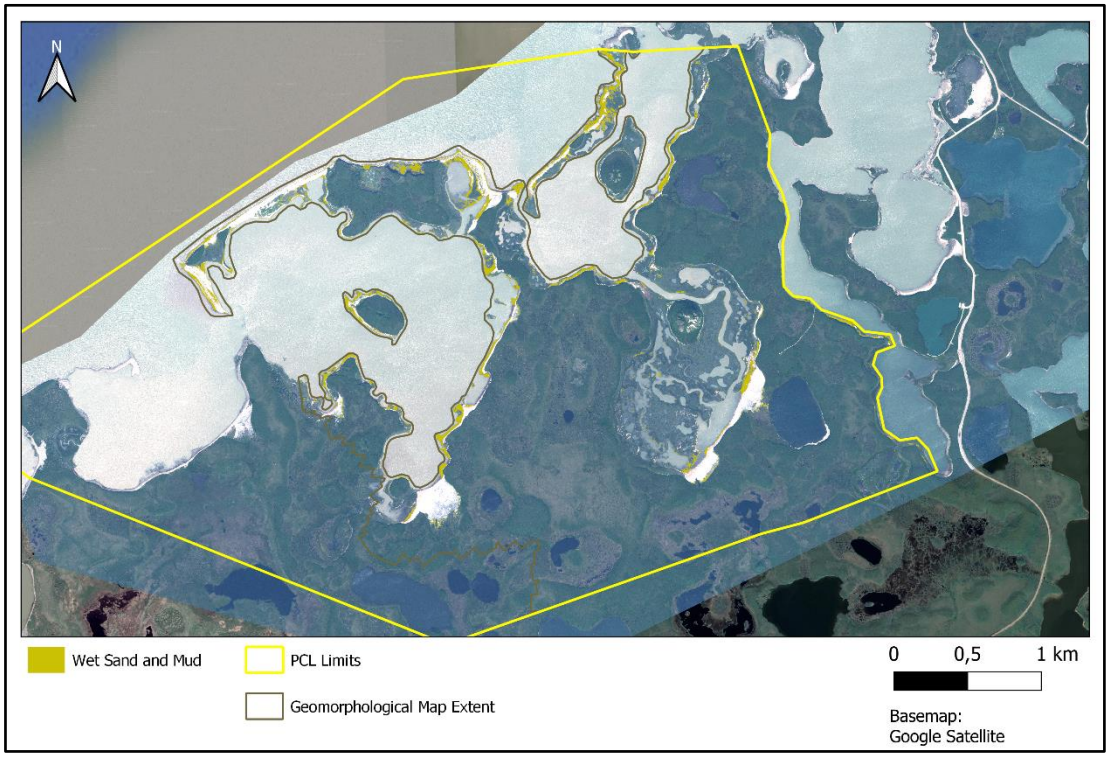

Figure 97 *- “Wet Sand and Mud” class included into the Landcover Map.*

The class “Driftwood Accumulations” occupies in total 0.22 km^2, which corresponds to 2.09% of the total area of PCL (Figure 98). Just as the “Sand” class, this one is present in both the Geomorphological Map and the Landcover Map, and again, in each they present somewhat different extents, being that in the supervised classification results, the class covers a slightly smaller area (0.22 km^2, compared to the 0.39 km^2 of the Geomorphological Map). This could be because in the manual digitization performed for the Geomorphological Map, submerged portions of the driftwood accumulations were included (to the extent that that they were visually perceivable in the UAV orthomosaic). It is likely that these portions of the driftwood accumulations were not classified as such, falling into the “Wet Sand and Mud”, “Sand”, and “Man-made Structures” classes (Table 1), or not being classified at all, given that areas with water pixels were excluded from this analysis using a “Land” mask (Figure 68).

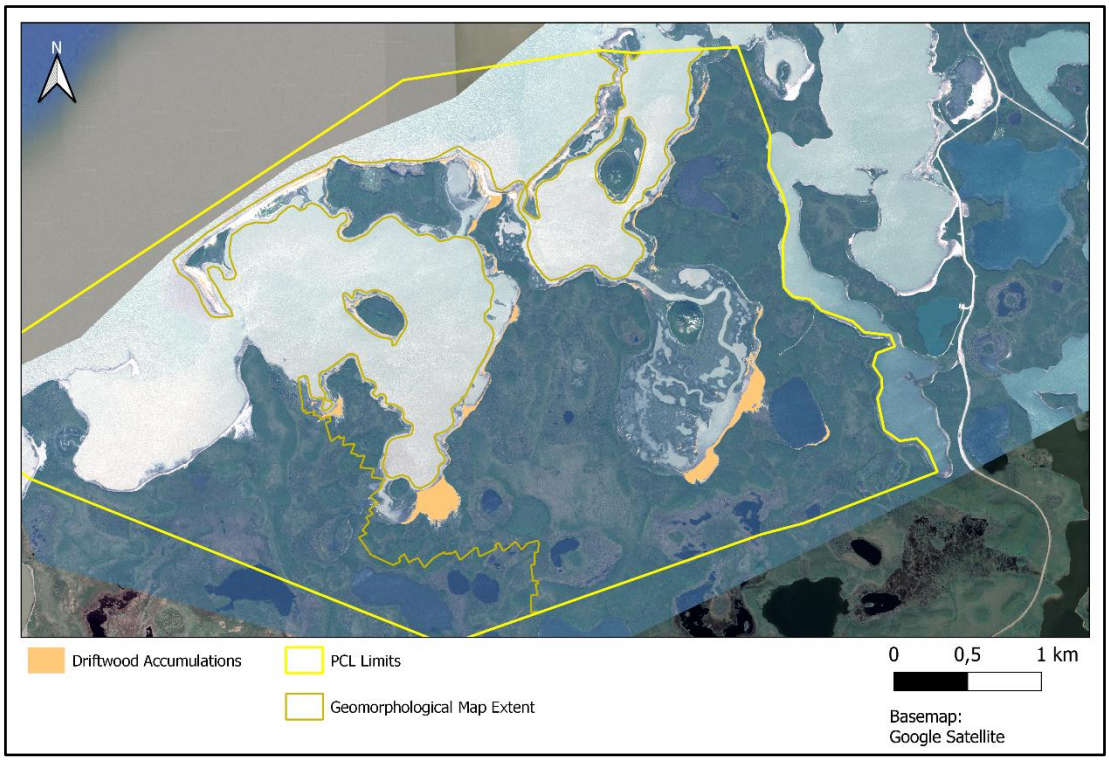

Figure 98 *- “Driftwood Accumulations” class included into the Landcover Map.*

The class “Man-made Structures” occupies in total 0.14 km^2, which corresponds to about 1.30% of the total area of the park (Figure 99). Within the limits of PCL, in reality the only feature within the park that should correspond to this class is the tourist walkway, and it was correctly classified as such by the supervised classification algorithm. However, considering that the walkway only covers an area of 0.001 km^2 (as mentioned int the description of the Geomorphological Map) the remaining areas that were included into this class by the algorithm correspond to misclassifications, and are likely to have been attributed to areas that should have been classified as other units, such as “Inundated Tundra”, “Wet Sand and Mud”, “Bare Soil”, “Driftwood Accumulations” and “Sand” (Table 1) .

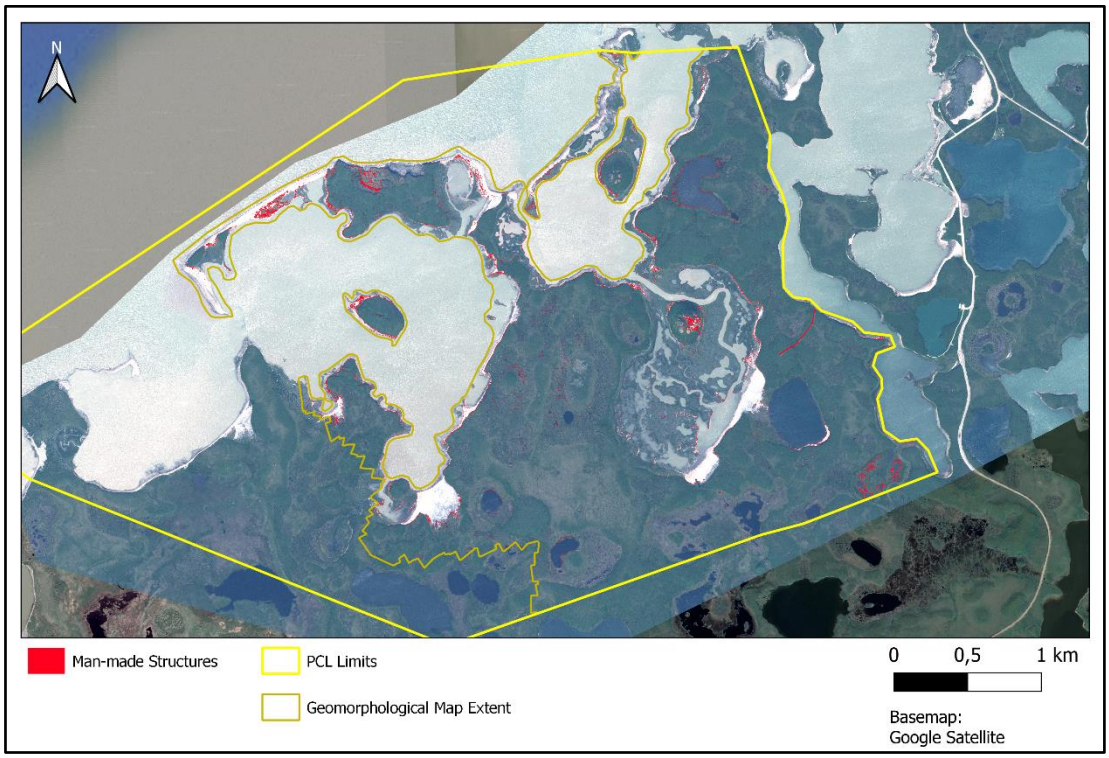

***Figure 99** - "Man-made Structures" class included into the Landcover Map.*

Some statistics regarding the areas of the nine classes of the Landcover Map are presented in Table 4 and Figure 100. In sum, the three classes with highest representation in the portion of the park that was mapped are "Low Shrub Tundra" (23.30%), "High Shrub Tundra" (18.42%) and "Dry Tundra" (10.58%). Those with the smallest representation are "Wet Sand and Mud" (1.86%), "Man-made Structures" (1.3%), and "Sand" (0.85%).

LANDCOVER MAP		
Class	Total Area (km2)	% of PCL's Total Area (not including costal waters)
High Shrub Tundra	1,94	18,42
Low Shrub Tundra	2,45	23,30
Dry Tundra	1,11	10,58
Inundated Tundra	1,04	9,84
Bare Soil	0,55	5,20
Sand	0,09	0,85
Wet Sand and Mud	0,20	1,86
Driftwood Accumulations	0,22	2,09
Man-made Structures	0,14	1,30
TOTAL AREA OF PCL NOT INLCUDING COASTAL WATERS (km2)	10,53	

***Table 4** - Statistics regarding the areas of the classes of the Landcover Map.*

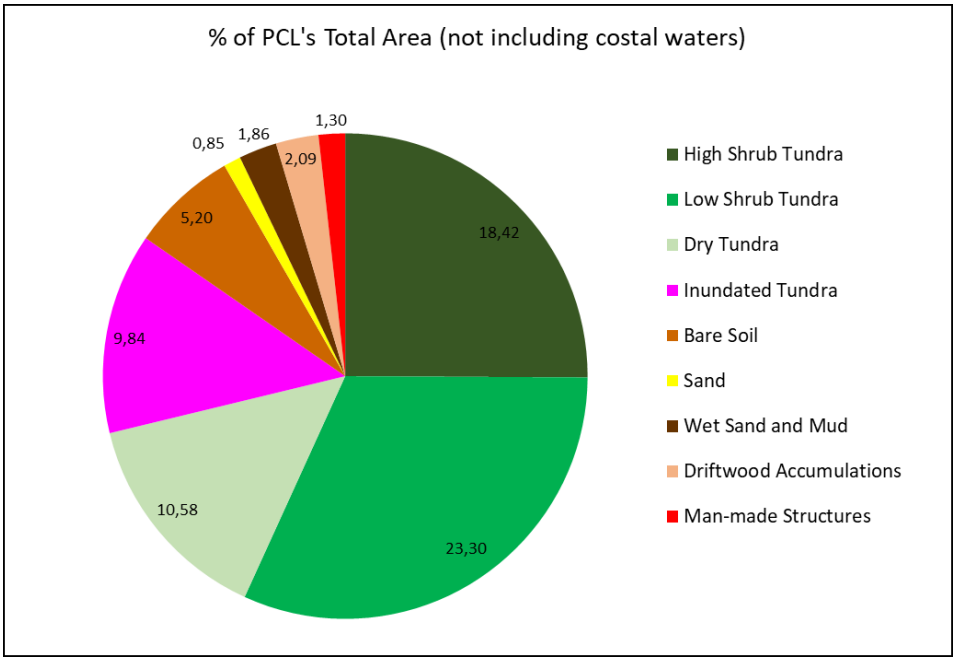

Figure 100 *- Pie chart with the relative proportion of each class of the Landcover Map in relation to the total area of PCL.*

6 – PINGO CANADIAN LANDMARK'S GEOECOLOGICAL UNITS AND THE STUDY AREA IN THE CONTEXT OF CLIMATE CHANGE

6.1 - Introduction

The main purpose of this subchapter is to provide an overarching interpretation of the results, which are compiled in a Geoecological Map, as well as to assess the status of the park in terms of its susceptibility to the impacts of climate change.

Climate change on a global scale is an undeniable reality (IPCC, 2014, 2021, 2023), and its impacts are being felt in the Arctic more than practically any other region of the world (Cohen et al., 2014; Davy et al., 2018; Rantanen et al., 2022; Screen & Simmonds, 2010; Stjern et al., 2019; You et al., 2021). These impacts have been widely reported and studied within the Arctic and in the region of the Tuktoyaktuk Peninsula, where PCL is located. Raising air and sea temperatures (with associated degradation of permafrost and ground ice), increases in the frequency and magnitude of storm events (with associated coastal erosion and storm surge flooding), and the reduction of the protection offered by sea ice, are all factors to be expected in this ever so more evident context of climate change (Holland et al., 2023; Irrgang et al., 2018; Karjalainen et al., 2020; Lim et al., 2020a; Lim et al., 2020b; O'Rourke, 2017; Parker, 2021; Vermaire et al., 2013). These factors, coupled with the negative feedback cycles that they can trigger (Figure 101), and the continuous anthropogenic emission of greenhouse gases (amongst other forcing factors associated with human activity), result in a very unfavorable scenario for the preservation of the characteristic landforms and ecology of the Arctic, as well as for its inhabitants.

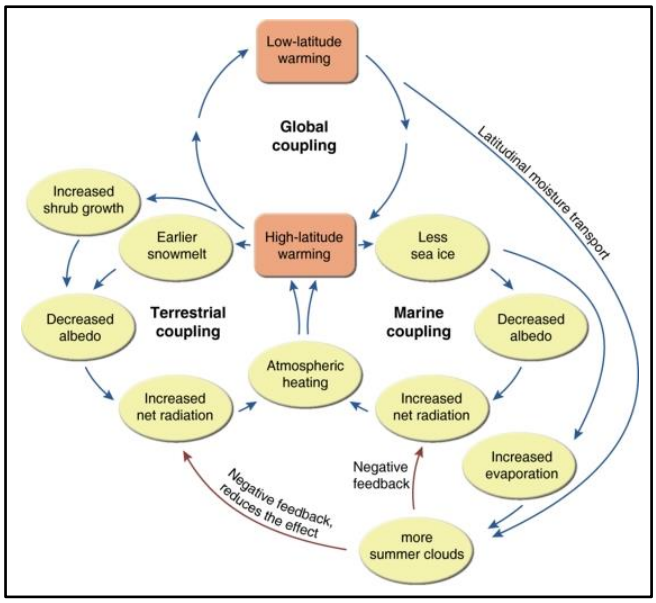

***Figure 101** - Examples of climate feedback cycles associated with climate change and warming in the Arctic. Source: GRID-Arendal (2016).*

6.2 - Coastal Changes in Pingo Canadian Landmark

One of the most noticeable effects of climate change is coastal erosion. Though this was not the major focus of this dissertation, some work was done to assess how PCL is impacted by coastal processes. Aerial photos, dating from 1950, 1967, 1972, 1985, 2000 and 2004 were compared with the present-day (2017) landscape and coastline of PCL, in order to visualize changes. The photographs of 1950, 1967, 1972 and 1985 were obtained from the Earth Observation Data Management System (EODMS) of Natural Resources Canada (NRCAN), and were chosen as they were the images that presented the lowest cloud coverage in each decade that they belonged to. Unfortunately, images with low cloud coverage were not available for the 1990's. To allow comparisons with the WorldView-2 scene, these images were georeferenced (with the QGIS Georeferencer, using 7 to 10 ground control points for each image). Those of 2000 and 2004 were supplied (already georeferenced) by Dustin Whalen (NRCAN). Shorelines were manually digitized (using the wet-dry line as the proxy) within the borders of PCL for each of those aerial photographs, as well as for the 2017 WorldView-2 scene, at a scale of 1:500 to 1:1000 (depending on how clearly visible the wet-dry line of the coast was). The results are displayed in Figure 102. Though no quantitative analyses were performed using these shorelines, the coastal retreat, and even erosion of landforms such as pingos, was evident upon a simple visual analysis. Figures showing each aerial photo and comparing the shoreline of the respective year with those of 1950 and 2017 are presented in the Appendix (Appendix Figures 6 to 12).

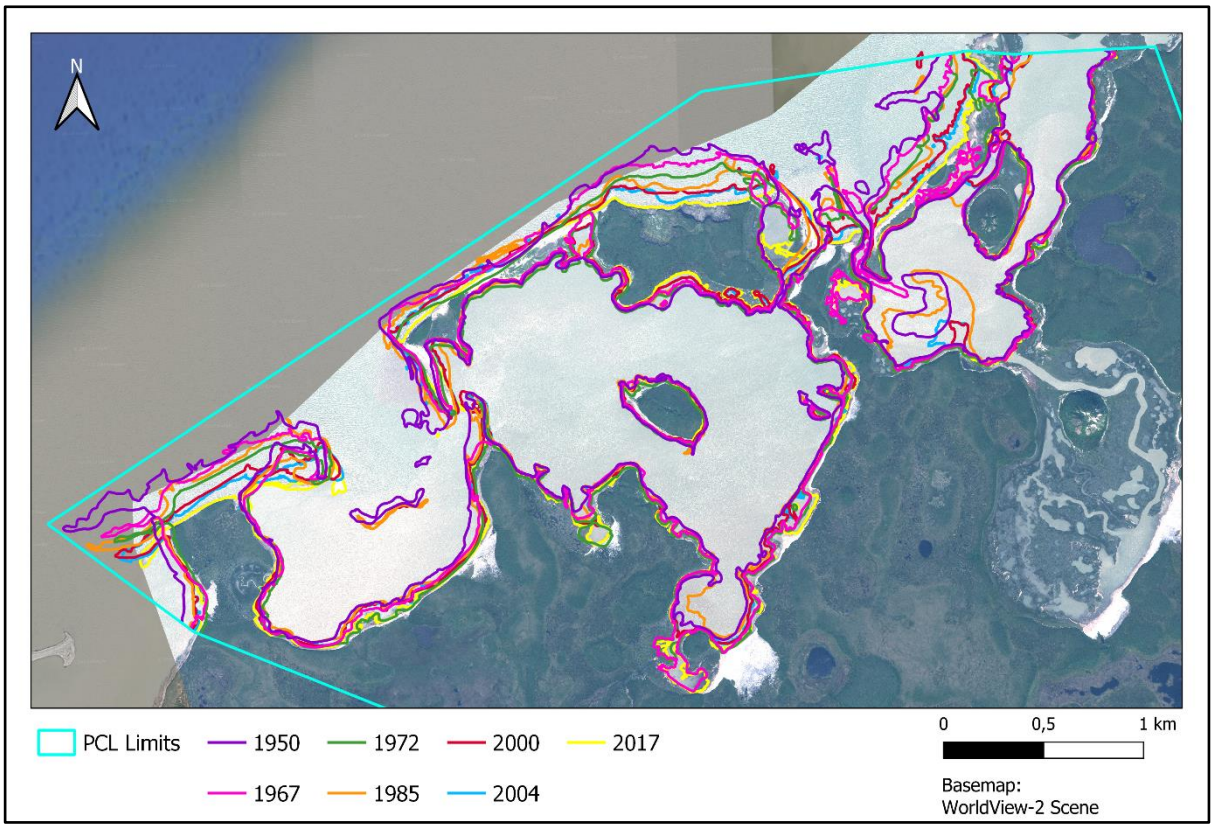

Figure 102 *– Coastlines digitized using archived aerial photos ranging from 1950 to 2004, and the 2017 WorldView-2 scene.*

6.3 – Geomorphology and Landcover Comparison

A summary of the standout results regarding an overlap analysis that was conducted (using the “Overlap Analysis” vector analysis tool in QGIS) to compare the Geomorphological and the Landcover maps, is shown in Tables 5 and 6. Summarily, this analysis calculated for each class of the Geomorphological Map the area (in m^2) occupied by each of the landcover units, but also, it calculated for each landcover unit the area (in m^2) occupied by each of the classes of the Geomorphological Map. This analysis helped to understand the relations between the two maps and to establish connections between geomorphology and landcover units within PCL. With this, it aided in the elaboration of the Geoecological Map. The complete results of the overlap analysis are presented in the Appendix (Appendix Tables 1 and 2).

In most cases, classes that were intended to represent similar features and landscapes throughout the park truly did have high degrees of overlap. Amongst the classes of the Geomorphological Map, the cases where this was most evident are, for example, the “Pingo Surface Erosion” class (highest overlap with the “Bare Soil” landcover unit), “Driftwood Accumulations” class (highest overlap with the “Driftwood Accumulations” unit), the “Inundated Lake Basins” class and all five of its subclasses (highest overlap with the “Inundated Tundra” unit), and the “Tourist Walkway” class (highest overlap with the “Man-made Structures” unit). Amongst the classes of the Landcover Map, the same can be said for example for the “Inundated Tundra” unit (highest overlap with the “Inundated Tundra Basins” class of the Geomorphological Map), the “Sand” and “Wet Sand and Mud” units (highest overlap with the “Sand” class), and “Driftwood Accumulations” (highest overlap with the “Driftwood Accumulations” class). An interesting fact to note is that the areas of the Geomorphological Map occupied by the class “Vehicle Tracks” presented their highest degree of overlap with the “Bare Soil” landcover unit, which is indicative of the negative and degrading impact that the circulation of these vehicles has upon the terrain and vegetation communities of PCL.

Geomorphological Map Class	Main Landcover Unit
Pingos	High Shrub Tundra
Pingo Summit Craters and Dilation Cracks	High Shrub Tundra
Pingo Surface Erosion	Bare Soil
Tundra Polygons	Low Shrub Tundra
Lakes and Ponds	Man-made Structures
Driftwood Accumulations	Driftwood Accumulations
Inundated Lake Basins	Inundated Tundra
Ancient Lake Basins	Bare Soil
Large (Isolated) Wetland Lakes and Ponds	Inundated Tundra
Wetlands	Inundated Tundra
Wetlands with Lakes and Ponds	Inundated Tundra
Dry Wetlands	Inundated Tundra
Dry Wetlands with Small Lakes and Ponds	Inundated Tundra
Ice Mounds	High Shrub Tundra
Sand	Driftwood Accumulations
Coastal Cliffs and Thaw Slumps	Bare Soil
Tourist Walkway	Man-made Structures
Seismic Lines	High Shrub Tundra
Vehicle Tracks	Bare Soil
Tundra Plains	Low Shrub Tundra

Table 5 – *For each class of the Geomorphological Map (left column), the class from the Landcover Map with which it had the highest overlap is indicated (right column).*

Landcover Unit	Main Geomorphological Map Class
High Shrub Tundra	Tundra Plains
Low Shrub Tundra	Tundra Plains
Dry Tundra	Tundra Polygons
Inundated Tundra	Inundated Lake Basins
Bare Soil	Tundra Plains
Sand	Sand
Wet Sand and Mud	Sand
Driftwood Accumulations	Driftwood Accumulations
Man-made Structures	Tundra Plains

Table 6 *- For each class of the Landcover Map (left column), the class from the Geomorphological Map with which it had the highest overlap is indicated (right column).*

6.4 – A Geoecological Map of Pingo Canadian Landmark as a Synthesis of the Relationships Between Geomorphology and Vegetation Communities

Considering that Geoecology can be defined as “the study of the multifaceted relationships between substrate and biota” (Rajakaruna & Boyd, 2014), geoecological units can be understood as being regions that present homogeneous characteristics in terms of geomorphology, geology and vegetation. Taking into account the results of the Geomorphological Map, the altimetric data associated with the UAV DSM, the results of the Landcover Map, as well as the data regarding the impacts of coastal erosion on PCL, a synthesis map representing the main geoecological units of PCL was prepared (Figures 103 and 104 and Appendix Figure 5).

The Geoecological Map was created through manual digitization, at a scale of 1:1000. It consists of five units: “Pingos”; “Highland Tundra”; “Lowland Tundra”; “Inundated Tundra”; and “Coastal Tundra”. It was decided that the term “Tundra” would be universal to nearly all classes, as it is the prevalent biome in which the study area is inserted.

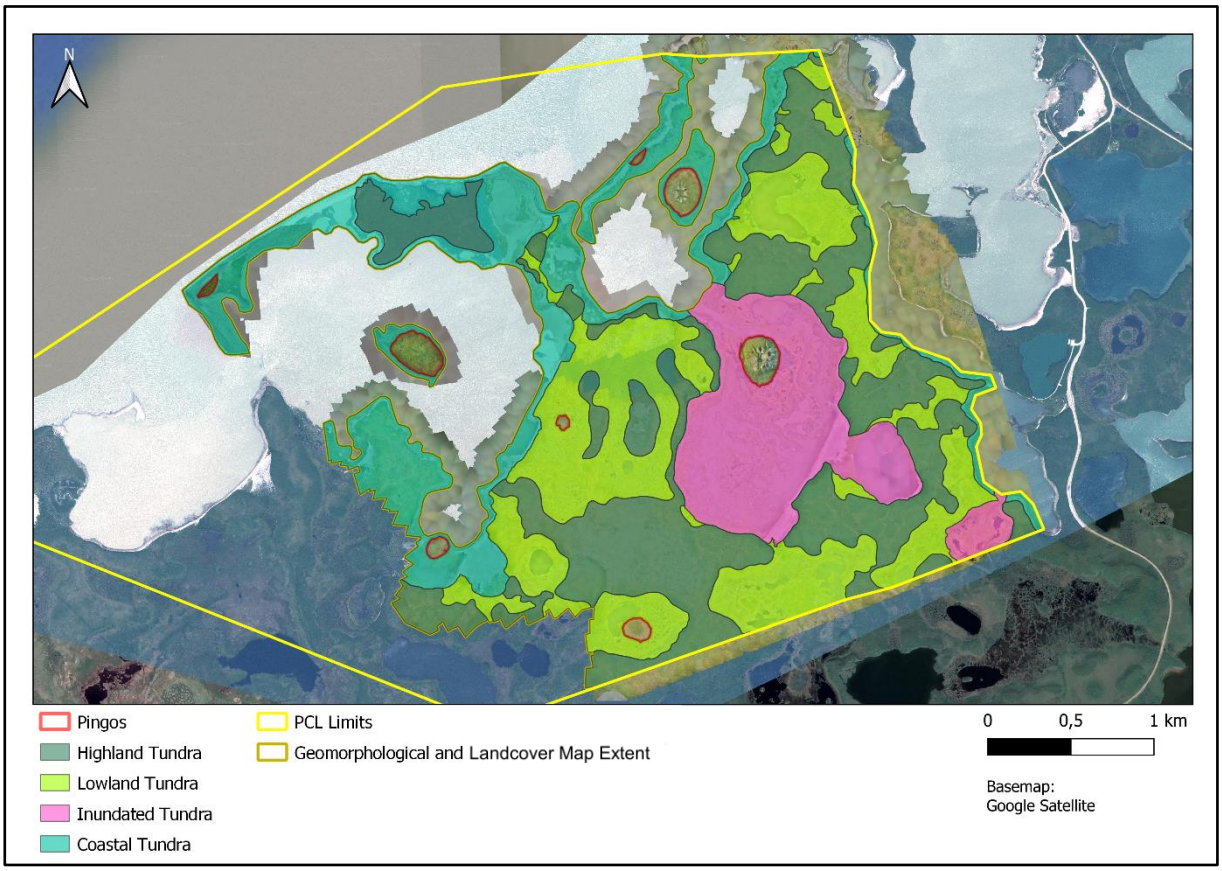

Figure 103 *– Geoecological Map of Pingo Canadian Landmark.*

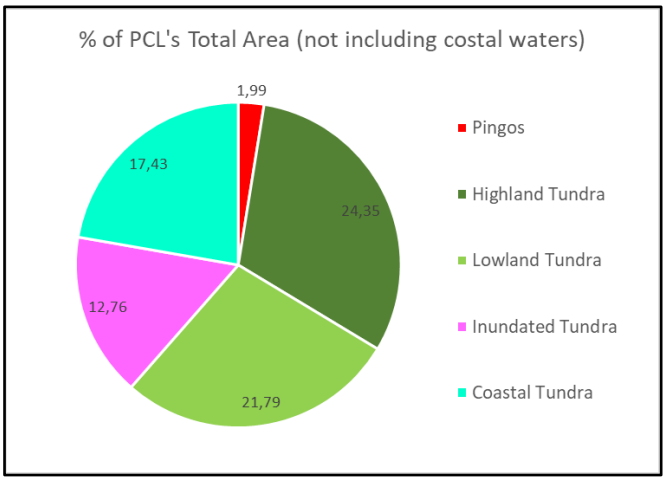

Figure 104 *- Pie chart with the relative proportion of each class of the Geoecological Unit Map in relation to the total area of PCL.*

The “Pingos” unit consists of the eight landforms that were presented in the Geomorphological Map, which cover 1.99% of the total area of the park. It was decided to

include the class “Pingos” into this map, given their uniqueness and unmatched prominence on the landscape within PCL. When compared with the results of the Landcover Map, the area corresponding to the “Pingos” was characterized by having its highest overlap with the “High Shrub Tundra” class (Table 5), but also presented a high overlap with the “Low Shrub Tundra” class (Appendix Table 1). It can therefore be concluded that pingos are amongst the areas of the park where conditions for vegetation development are best, with the exception of some spots on the summits of the highest pingos, where erosion associated primarily with wind action and precipitation can be noticed. One factor that may benefit the development of plants on the pingos is nutrient and moisture availability in the pingo overburden. Though pingos are located in permafrost regions, their overburden does not consist of frozen ground (as it is part of the active layer), and it usually is rich in organic matter. Also, though height may be a prejudicial factor to vegetational development in the case of the summits of tall pingos, in general, the slopes of these hill landforms benefit from better sunlight exposure (which is particularly important in this region of the globe, where sunlight is limited during a considerable portion of the year) and thinner snow cover than the surrounding areas, which are factors that also favor plant growth (Holmes et al., 1968; Mackay, 1979, 1998; Müller, 1962).

The “Highland Tundra” unit covers 24.35% of the area of PCL, making it the dominant Geoecological Unit. It corresponds to areas within the park that are topographically elevated in relation to their surroundings. Though this unit has large extensions that are predominantly flat, it is also within its boundaries that nearly all of the “Ice Mound” features included into the Geomorphological Map can be found. As for its association with the tundra polygon networks that can be found throughout the park, though some more dense networks do exist, they are typically small in extent, and most tundra polygons found here are large, forming much less dense ice wedge networks. Also, the tundra polygons found here are predominantly of the high-centered type. In terms of vegetation communities found here, for the most part they are associated with the “High Shrub Tundra” and “Low Shrub Tundra” units, however in some sectors the “Dry Tundra” is also present.

The “Lowland Tundra” unit covers 21.79% of the area of the park, and corresponds to areas that are topographically depressed when compared to the “Highland Tundra” unit, but not as much as the “Inundated Tundra”. For example, the areas corresponding to the “Ancient Lake Basins” class of the Geomorphological Map were translated into this geoecological unit. Here we can find the most dense networks of tundra polygons, and consequently, of ice wedges in the soil. Though the quantity of ice associated with each wedge may vary (for example, according to their age, as older wedges are thicker and contain more ice), these areas with denser tundra polygon and ice wedge networks are likely to have high ground ice contents. Being that these areas are topographic depressions, runoff of precipitation water is

facilitated, leading to the infilling of thermal contraction cracks in the soil, and triggering the cyclical process associated with the formation of ice wedges, as described in Chapters 2.1 and 2.2.2. The channel-like features associated with excessive runoff accumulation between polygons mentioned in the literature, and included into the Geomorphological Map as part of the “Lakes and Ponds” class, are common in this region as well (Barry & Gan, 2011; French, 2007; Williams & Smith, 1989). Though this is the geoecological unit where the most well developed tundra polygon networks can be found, it is also here that we find the most examples of tundra polygons in their less advanced state of evolution (low-centered tundra polygons, sometimes with small waterbodies in their centers). Still, the vast majority of the polygons in this unit are of the high-centered type. As for the presence of vegetation communities, more developed shrubs exist in some spots, such as on some high-centered tundra polygons, but the prevailing classes from the Landcover Map are “Low Shrub Tundra”, “Dry Tundra” and “Bare Soil”.

The “Inundated Tundra” covers 12.76% of PCL, and essentially corresponds to the extents of the “Inundated Lake Basins” of the Geomorphological Map. It was also decided to include the large lake just east of the inundated basin that surrounds Ibyuk Pingo and the large driftwood accumulations found on its margins, as these deposited logs indicate that coastal floods have breached into this lake in the past. The driftwood accumulations, which were present in both the Geomorphological Map and the Landcover Map, were in many cases used as a proxy to help identify the maximum extent of these flooded areas. The predominant class from the Landcover Map found here is the “Inundated Tundra”, though it should be mentioned that this class was much more prevalent within the larger inundated basin that surrounds Ibyuk Pingo than the smaller one located near the southeastern limits of PCL. The smaller basin is likely to be flooded less frequently, given its more sheltered position in relation to the Beaufort Sea.

Lastly, we have the “Coastal Tundra” geoecological unit. It represents 17.43% of the area of the park, and essentially corresponds to all areas that have immediate contact with coastal waters within PCL. These areas are closely related to the “Sand” and “Coastal Cliffs and Thaw Slumps” classes of the Geomorphological Map and the “Sand” and “Wet Sand and Mud” classes of the Landcover Map. However, some other features can be found here, such as tundra polygons, which in many cases are heavily degraded and could be classified as “thermokarst polygons”. Also, five of the eight Pingos are located amidst this unit. As will be portrayed in Figure 105, it is within this unit that we find the sectors of the park that are most likely to be susceptible to coastal erosion.

6.5 – Assessment of Recent Coastal Erosion and Anthropogenic Impacts in Pingo Canadian Landmark

It was also decided to create a map that would point out specific areas within PCL where susceptibility to coastal erosion and storm surge events (and consequently, to climate change) are likely to be highest, as well as areas where direct negative man-induced impacts on the landscape are most intense (Figure 105). This map was created by manual digitization (at scales of 1:2000 to 1:3000), and contains four classes, representing areas of "High Human Impact", "High Susceptibility to Coastal Erosion", and pingo landforms that present "Susceptibility to Coastal Erosion" and "Susceptibility to Storm Surges". Regarding the areas presented as having "High Susceptibility to Coastal Erosion", it should be pointed out that no quantitative analysis specifically of shoreline change was conducted to further substantiate this designation. Rather, its portrayal is based on the extensive interpretation of the remote sensing data used in this study, the subsequent results that were obtained with that data, as well as information present in the literature (as presented in Chapters 2 and 3).

The "High Susceptibility to Coastal Erosion" class, is primarily associated with the "Coastal Tundra" geoecological unit. However, other, more specific, criteria were taken into account during the creation of this class. Given the conclusions provided in Lim et al. (2020a) and Lim et al. (2020b), it was decided that the study area of those research projects, which was incorporated into the "Coastal Cliffs and Thaw Slumps" class of the Geomorphological Map, would be considered one of the areas of high susceptibility to coastal erosion. Additionally, the shorelines digitized for 1950, 1967, 1972, 1985, 2000, 2004 and 2017 (Figure 102 and Appendix Figures 6 to 12) were also taken into consideration, as visual analysis of the shoreline evolution throughout that 67-year period allow to identify some general trends regarding where coastal retreat was most dramatic. Finally, the tundra polygon heatmap (Figure 77 and Appendix Figure 2) was also very helpful, having been used as a proxy to identify areas where ground ice content (and therefore susceptibility to erosion) are likely to be higher. In the end, a total of 0.98 km^2 were included into this class, representing 9.21% of the park. Within these areas, special attention was given to pingos, considering their unique geoheritage value. Using the same nomenclature as presented in Table 2 and Figure 71, Island Pingo (Pingo 3), Peninsula Point Pingo (Pingo 4), Pingo 7 and Pingo 8 are found to be located within the area of "High Susceptibility to Coastal Erosion". Particular attention should be allocated to Peninsula Point Pingo and Pingo 8, as it is clearly visible that their ice cores have already been exposed, making them especially prone to degradation and erosion. Figure 106 shows the drastic changes verified at these sites between 1950 and 2017. Despite being located within the Coastal Tundra geoecological unit, it was decided not to attribute the same

class of “High Susceptibility to Coastal Erosion” to Split Pingo (Pingo 2), due to its height and the good state of preservation of its overburden (which helps protect it from the effects of wave action associated with coastal storms). It was however classified as a site likely to be affected by storm surge events, and the same was attributed to Ibyuk Pingo (Pingo 1). Given the current circumstances, storm surges do not necessarily present a great threat to the preservation of these two largest pingos in the park. However, for each pingo in the park, it is expected that at some point in the future, they will commence a process of subsidence and eventually collapse. This, coupled with the continuous retreat of the coastline that is to be expected in coming decades, will result in all these landforms becoming prone to disappearing from the landscape.

Lastly, we have areas of “High Human Impact”, where anthropogenic activity has produced clear negative impacts on the landscape of PCL, namely by means of vehicle circulation. As already mentioned, the vehicles predominantly used for this clandestine activity are most likely ATVs such as the one that was seen and caught on photo by the team of CEG/IGOT - University of Lisbon and the Geological Survey of Canada, illegally circulating within the park limits (Figure 107). The areas of more intense circulation, and therefore of greatest impact on the land and vegetation, were identified recurring to the vehicle track heatmap presented in Figure 88 and Appendix Figure 3. The main established routes are primarily associated with the borders of the “Inundated Lake Basins” and “Ancient Lake Basins” from the Geomorphological Map. Some tracks even lead up to the base of Ibyuk Pingo, suggesting that these individuals may then proceed to climb the landform upon arriving at it.

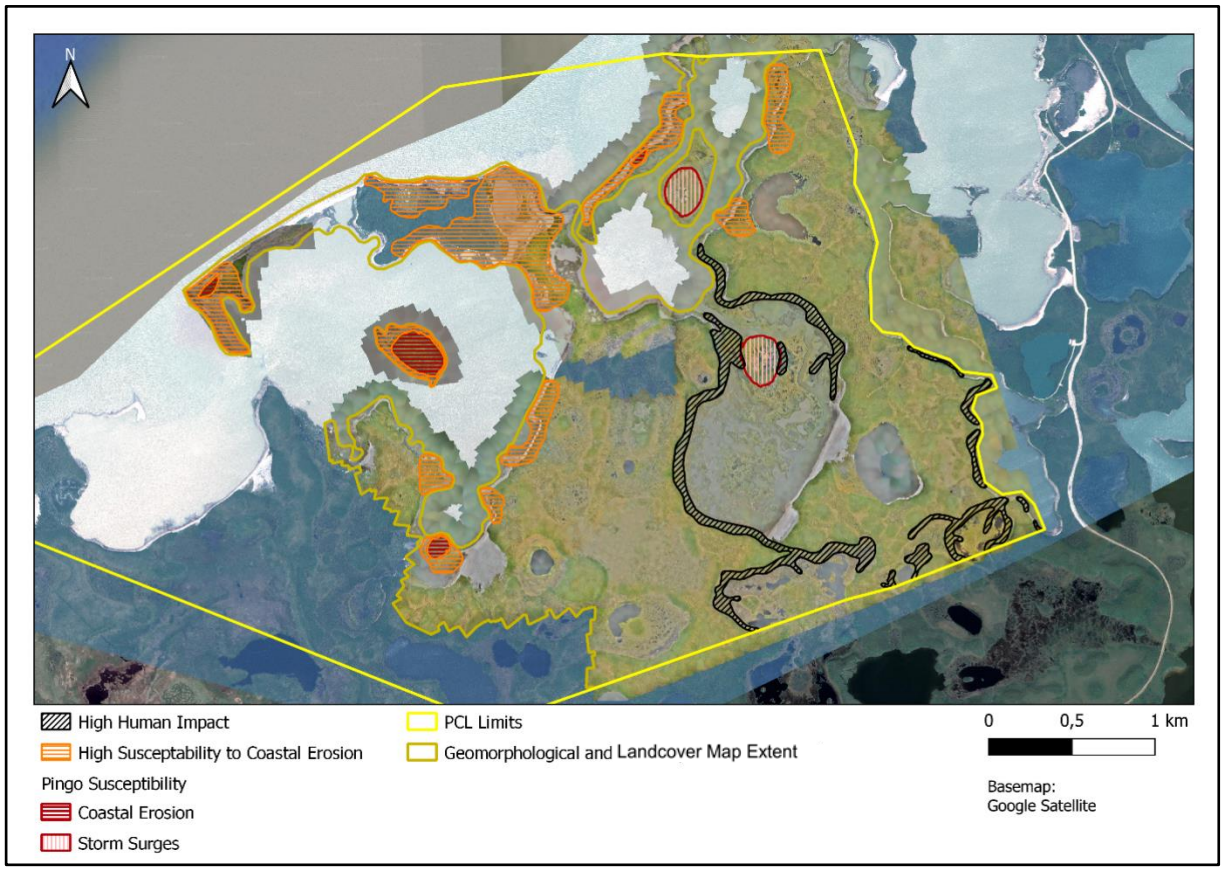

Figure 105 *– Areas within PCL where susceptibility to coastal erosion is likely to be highest, and areas where anthropogenic impacts are most evident.*

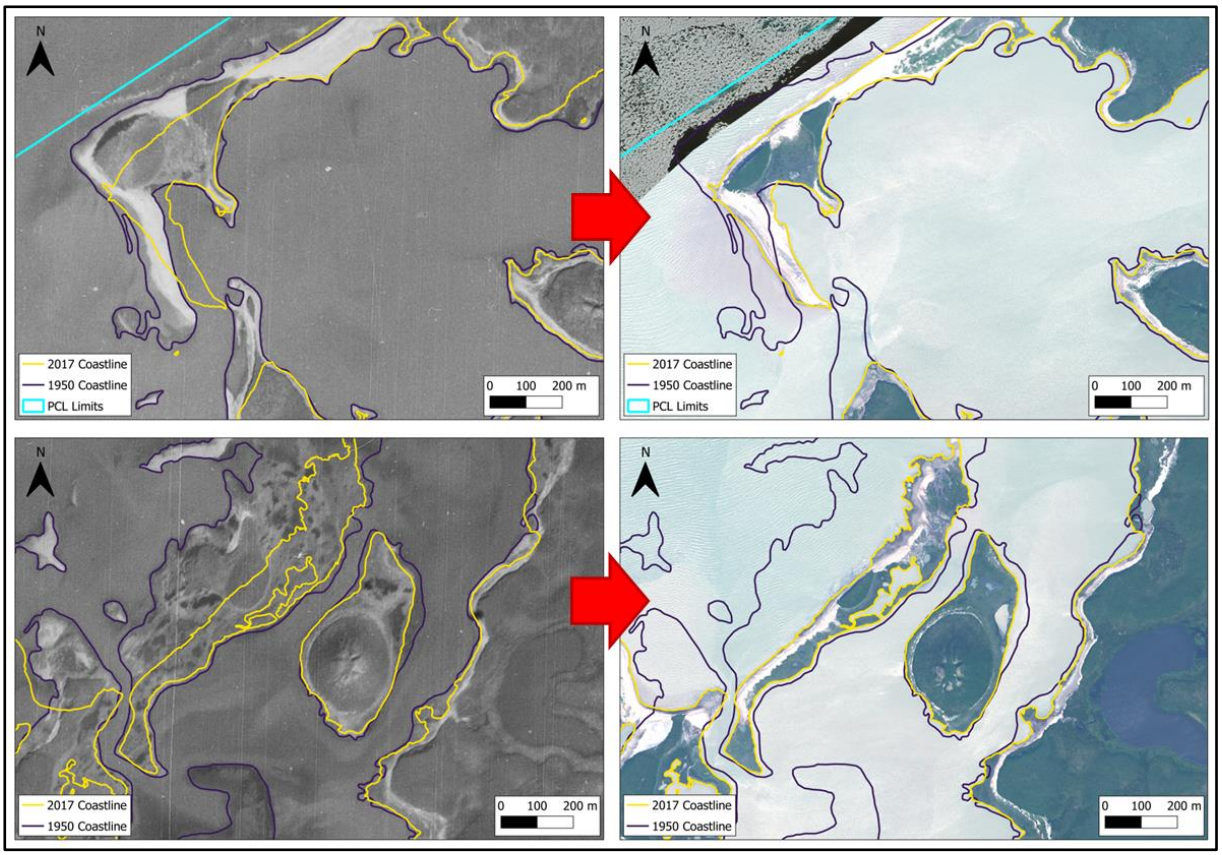

Figure 106 *– Top row shows the comparison of the landscape at the extremity of Peninsula Point between 1950 (top left) and 2017 (top right). Note the erosion of Peninsula Point Pingo (Pingo 4). Bottom row shows the comparison of the landscape near Split Pingo (Pingo 2) between 1950 (bottom left) and 2017 (bottom right). Note the erosion of Pingo 8 (just west of Split Pingo).*

Figure 107 *– ATV viewed by the team of CEG/IGOT - University of Lisbon and the Geological Survey of Canada during the field campaign of July 2019.*

7 - CONCLUSION

When this research project began, several objectives were set, branching over a wide scope of different geographical fields. This allowed to achieve a complete and thorough understanding of the landscape of Pingo Canadian Landmark.

Regarding the main goals of this study, using remote sensing data of very high spatial and spectral resolutions, it was possible to provide a detailed characterization of the landscape at PCL, as well as a good understanding of its geoecological dynamics (always supported by scientific literature). Also, it was understood how important being able to work with data of extreme quality can be. The ultra-high resolution UAV orthomosaic and DSM, as well as the very-high resolution multispectral and panchromatic commercial satellite imagery used throughout this study were key in the achievement of the highly detailed results. Both these sources of data also exemplify how important both field work and remote sensing can be for the elaboration of good scientific research. Even in remote areas, one does not necessarily invalidate the other, and in truth, they can complement each other very well.

As for the more specific objectives that were set, scientifically based precision cartography was produced for the park, in the form of the Geomorphological Map of PCL with twenty classes and subclasses (Chapters 4.2 and 5.1 and Appendix Figure 1), which was analyzed and interpreted in order to diagnose the recent (2017 and 2019) state of the landscape of the park with a great level of detail. Geographical Information Systems were widely used throughout that process, as well as for the creation and analysis of another major product of this research project, the Landcover Map (Chapters 4.3 and 5.2 and Appendix Figure 4). Unsupervised, and ultimately, supervised classification methods were applied to WorldView-2 satellite imagery, resulting in the clear identification of nine spectrally distinct landcover units within the park. Finally, after an overarching analysis and interpretation of all major results reached on behalf of the study, an additional division of the park into five homogeneous sectors in terms of geomorphology and vegetation, called geoecological units (“Highland Tundra”, “Lowland Tundra”, “Inundated Tundra”, “Coastal Tundra” and “Pingos”), was accomplished (Chapter 6.4 and Appendix Figure 5). Additionally, all the achieved results (together with the consultation of the literature) helped point out areas and landforms within PCL that are most likely to be affected by climate change, as well as areas where human activity is currently producing negative impacts on the land (Chapter 6.5).

However, as is frequently the case in scientific pursuits, there is always room for improvement and expansion of knowledge. Regarding the Geomorphological Map, an effort was made so that the attention to detail employed in the creation of this cartography was very

high. This not only allowed a characterization of the landscape of PCL in unprecedented detail, but was also important for the calculation of very precise geographical statistics regarding the landscape of the park. For some units (for example, “Inundated Lake Basins”, “Ancient Lake Basins” and “Seismic Lines”), perhaps even more detail could have been employed, but the scales of digitization that were used were still sufficient to fulfill the goals of this study. Further, a more in-depth analysis could be conducted regarding some of the classes. For example, it would be interesting to provide a more detailed distinction of the different “Ice Mounds” based on their height and morphology, or to subdivide the “Tundra Polygons” class into subclasses such as “High-centered Polygons”, “Low-centered Polygons” and “Thermokarst Polygons”, or even add a linear class to the map called “Ice Wedges” to represent these features that exist between each tundra polygon. These would, however, be very laborious tasks, considering the quantity of “Tundra Polygon” features that were manually digitized on behalf of this map (14,518). Also, of course, it would have been ideal if the entirety of PCL had been covered by ultra-high UAV data. However, given the difficulty and logistical challenges associated with obtaining this data in such a remote part of the globe, as well as the conservational measures that are employed to protect the park, the data that was collected by the team of CEG/IGOT - University of Lisbon and the Geological Survey of Canada was an extremely important asset to this study. This data covered about 72.27% of the area of the park, 77.4% when combined with the very-high detail WorldView-2 scene, which was more than sufficient to reach a very good understanding and description of PCL’s landscape. Perhaps, an attempt could have been made to map the remaining 22.6% of the parks area by recurring to the WorldView-2 scene. However, despite the very-high resolution of that imagery (46 cm), this approach could compromise the uniformity of the overall detail of the map, being that some features would not be as easily discernable as in the UAV imagery, or not noticeable at all, as is the case of the “Vehicle Tracks” class. This very important feature would not even be noticed had it not been for the ultra-high resolution (10 cm) of the UAV orthomosaic.

As for the Landcover Map, its results were also very satisfactory, which can be attested by the Overall Accuracy value of 94.35% that was obtained. However, as described previously in Chapters 4.3.2 and 5.2, the supervised classification algorithm had more difficulty in correctly identifying some classes than others. For example, the classes “Wet Sand and Tundra” and “Low Shrub Tundra” presented the highest Omission Errors, meaning that they were those which the algorithm most misclassified as being other units. In the case of the “Low Shrub Tundra” the Omission Error was 10.24% (having been predominantly confused with the “Dry Tundra” and “High Shrub Tundra” classes). In the case of the “Wet Sand and Tundra” class, the Omission Error was 21.75% (having been predominantly confused with the “Bare Soil” and “Inundated Tundra” classes). On the other hand, with the highest Commission Errors,

we have the classes “Man-made Structures” (31.68%) and “Bare Soil” (31.98%), which were those that the algorithm attributed most times to areas where they should not have been. Nevertheless, in any supervised classification, some level of inaccuracy is expected to occur, and overall, the quantity of misclassifications in the analysis is not high. An effort was made to achieve this during the process of creating training areas for the supervised classification algorithm. One minor hindrance that can be reported though was the unavailability of an option within the ENVI software to export those training areas in either raster or vectorial format (which would have allowed for a better representation of them then that which is presented in Figure 70).

Another way to further develop the study and understanding of the landscape of PCL would be by performing a more in-depth comparison of its current state with its past states. To do this, quantitative analyses of coastal retreat using the archived aerial photos and the shorelines digitized upon them (Figure 102 and Appendix Figures 6 to 12) can be conducted with Digital Shoreline Analysis System (DSAS) software. Also still, further crossing of the 2019 UAV DSM with the results obtained and presented in this study, allied with a similar approach using altimetric data from a prior date (if available) could provide interesting information regarding geomorphological dynamics, such as terrain subsidence and pingo growth and collapse, or even climatological dynamics, through the evolution of driftwood accumulations.

Though even more extensive results could have been attained, it can be considered that the initial set of goals were met to a satisfying degree. Throughout the elaboration of this research project, it has become evident that PCL shows great geomorphological significance, as many of its landforms, such as tundra polygons, ice wedges, ice mounds and pingos, only exist in permafrost environments and form under specific conditions. It was also shown that PCL is quite diverse from a biogeographical standpoint, with various vegetation communities spread throughout the park, in accordance with a straight relationship that they form with the park's geomorphology, as well as the climatic framework in which it is inserted. Allied to its scientific value, the landscape of PCL is also of great cultural value to the Inuvialuit. For all these reasons, it is ever so important to look after this site and advocate for its conservation, especially in the context of climate change that is upon us, with particular preponderance in the Arctic. Much scientific evidence points to a rise in frequency and magnitude of erosion and permafrost degradation, linked to increased marine storms and higher air and sea temperatures, which on one hand is very worrying, but on the other is also a sign that this matter has caught the attention of the scientific community for quite some time now, and is being adequately studied by a large variety of scientific branches and through a multitude of approaches. Only this way, with founded information backed by credible scientific sources, can correct decisions be made at conservational and even political levels. In this respect, it is hoped

that, besides the purely scientific value of the results and conclusions that this study has produced, the work developed on behalf of this project can also contribute to a better understanding of the landscape of PCL, and consequently aid in its management.

BIBLIOGRAPHY

AARoads. (2019). *Inuvik-Tuktoyaktuk Highway (NT 10) Trip Report*. Https://Www.Aaroads.Com/Forum/Index.Php?Topic=24301.0.

Allaby, M. (2015). A Dictionary of Ecology. In *Oxford - A Dictionary of Ecology* (5th ed.). Oxford University Press. https://doi.org/10.1093/acref/9780191793158.001.0001

AMAP - Arctic Monitoring and Assessment Programme. (1998). *AMAP Assessment Report: Arctic Pollution Issues*.

Arctic Drone Labs. (2020). *DJI Matrice 210 RTK V2*. Https://Www.Arcticdronelabs.Com/Our-Fleet/Dji-Matrice-210-Rtk-V2.

Barry, R. G., & Gan, T.-Yew. (2011). Frozen ground and permafrost. In *The global cryosphere : past, present and future* (1st ed., pp. 165–189). Cambridge University Press.

Cabin Radio. (2023). Ottawa will spend $54M to defend Tuktoyaktuk's shoreline. Https://Cabinradio.ca/138154/News/Environment/Climate/Ottawa-Will-Spend-54m-to-Defend-Tuktoyaktuks-Shoreline/.

Canada DroneTrader. (2021). *Sensefly eBee - Fixed Wing UAV - RTK enabled*. Https://Canada.Dronetrader.Com/Ads/Sensefly-Ebee-for-Sale-Fixed-Wing-Uav-Rtk-Enabled-Spare-Parts-and-Accessories.

Canada Energy Regulator. (2022). *CER Fact Sheet: NEB's Role in Arctic Offshore Seismic Exploration*. Https://Www.Cer-Rec.Gc.ca/En/about/North-Offshore/Archive/Publications/Fact-Sheet-Nebs-Role-in-Arctic-Offshore-Seismic-Exploration.Html.

Canada National Parks Act (2000).

CBC News. (2020). "All his wisdom will be missed": Lifelong Inuvialuit advocate dies at 71. Https://Www.Cbc.ca/News/Canada/North/Randal-Boogie-Pokiak-Inuvialuit-Obituary-1.5680097.

Cohen, J., Screen, J. A., Furtado, J. C., Barlow, M., Whittleston, D., Coumou, D., Francis, J., Dethloff, K., Entekhabi, D., Overland, J., & Jones, J. (2014). Recent Arctic amplification and extreme mid-latitude weather. *Nature Geoscience*, *7*(9), 627–637. https://doi.org/10.1038/ngeo2234

Costa, B. (2022). *Remote Sensing Analysis of Recent Coastal Change and Controlling Factors in Tuktoyaktuk Peninsula (Beaufort Sea Coast, Canada)* [Master's degree, Universidade de Lisboa]. https://repositorio.ul.pt/handle/10451/52111

Dalaiden, Q., Goosse, H., Lecomte, O., & Docquier, D. (2018). A model to interpret driftwood transport in the Arctic. *Quaternary Science Reviews*, *191*, 89–100. https://doi.org/10.1016/j.quascirev.2018.05.004

Davy, R., Chen, L., & Hanna, E. (2018). Arctic amplification metrics. *International Journal of Climatology*, *38*, 4384–4394. https://doi.org/10.1002/joc.5675

Eisner, W. R., & Peterson, K. M. (1998). High-resolution pollen analysis of tundra polygons from the North Slope of Alaska. *Journal of Geophysical Research: Atmospheres*, *103*(D22), 28929–28937. https://doi.org/10.1029/98JD01462

Encyclopedia Britannica. (2009a). Continental Subarctic Climate. In *Encyclopedia Britannica*. https://www.britannica.com/science/continental-subarctic-climate

Encyclopedia Britannica. (2009b). Köppen Climate Classification. In *Encyclopedia Britannica*. https://www.britannica.com/science/Koppen-climate-classification/World-distribution-of-major-climatic-types

Encyclopedia Britannica. (2009c). Tundra Climate. In *Encyclopedia Britannica*. https://www.britannica.com/science/tundra-climate

Encyclopedia Britannica. (2016). Pingo. In *Encyclopedia Britannica*. https://www.britannica.com/science/pingo

French, H. (2007). *The Periglacial Environment* (3rd ed.). John Wiley & Sons Ltd. https://doi.org/10.2307/j.ctt1w6tb9v.3

French, H., & Harbor, J. (2013). The Development and History of Glacial and Periglacial Geomorphology. In *Treatise on Geomorphology* (Vol. 8). Elsevier Ltd. https://doi.org/10.1016/B978-0-12-374739-6.00190-1

Gamesby, R. (2012). *Periglacial Landforms*. Https://Www.Coolgeography.Co.Uk/A-Level/AQA/Year%2012/Cold%20environs/Periglaciation/Periglacial%20landforms.Htm.

Government of Canada. (2023). *The Government of Canada invests to protect Tuktoyaktuk from coastal erosion*. Https://Www.Canada.ca/En/Housing-Infrastructure-Communities/News/2023/07/the-Government-of-Canada-Invests-to-Protect-Tuktoyaktuk-from-Coastal-Erosion.Html.

Grechishchev, S. (1970). *Basis of method for predicting thermal stresses and deformations in frozen soils*. https://doi.org/https://doi.org/10.4224/20359113

GRID-Arendal. (2016). *Climate feedbacks - The connectivity of the positive ice/snow albedo feedback, terrestrial snow and vegetation feedbacks and the negative cloud/radiation feedback*. https://www.grida.no/resources/5261

Grosse, G., Romanovsky, V., Nelson, F. E., Brown, J., & Lewkowicz, A. G. (2010). Why permafrost is thawing, not melting. *Eos - Transactions, American Geophysical Union*, *91*(9), 87–88. https://doi.org/10.1029/2010EO090003

Hamlet of Tuktoyaktuk. (2024). *Hamlet of Tuktoyaktuk Website - Home*. Https://Tuktoyaktuk.Ca/.

Hargitai, H., & Soare, R. (2014). Ice Wedge Polygon. In *Encyclopedia of Planetary Landforms*. Springer, New York, NY. https://doi.org/10.1007/978-1-4614-9213-9_193-1

Harris, S. A., French, H. M., Heginbottom, J. A., Johnston, G. H., Ladanyi, B., Sego, D., & Everdingen, R. O. (1988). *Glossary of permafrost and related ground-ice terms*. https://nrc-publications.canada.ca/eng/view/ft/?id=69fb8993-1baa-4225-b33a-6a02341d383d

Holland, K. M., Porter, T. J., Criscitiello, A. S., & Froese, D. G. (2023). Ion geochemistry of a coastal ice wedge in northwestern Canada: Contributions from marine aerosols and implications for ice-wedge paleoclimate interpretations. *Permafrost and Periglacial Processes*, *34*(2), 180–193. https://doi.org/10.1002/ppp.2184

Holmes, G. W., Hopkins, D. M., & Foster, H. L. (1968). Pingos in Central Alaska. In *U.S. Geological Survey Bulletin - Contributions to General Geology* (Vols. 1241-H). http://137.229.113.30/webpubs/usgs/b/text/b1241h.pdf

International Surveying Equipment, Inc. (2024). *Trimble R4 GPS GNSS with recon data collector*. Https://Www.Usasurveyingsupplies.Com/Index.Php?Route=product/Product&product_id=93.

Inuvialuit Regional Corporation. (2011). *Taimani – At That Time: Inuvialuit Timeline Visual Guide* (C. Arnold, W. Stephenson, B. Simpson, & Z. Ho, Eds.; 2nd ed.). Inuvialuit Regional Corporation. https://irc.inuvialuit.com/document/taimani-time-inuvialuit-timeline-visual-guide

Inuvialuit Regional Corporation. (2020). *IRC Heritage Sites*. Https://Irc.Inuvialuit.Com/about-Irc/Culture/Heritage-Sites/.

IPCC. (2014). *Summary for Policymakers - Climate Change 2014: Synthesis Report. Contribution of Working Groups I, II and III to the Fifth Assessment Report of the Intergovernmental Panel on Climate Change*. Gian-Kasper Plattner. https://archive.ipcc.ch/pdf/assessment-report/ar5/syr/AR5_SYR_FINAL_SPM.pdf

IPCC. (2021). *Summary for Policymakers - Climate Change 2021: The Physical Science Basis. Contribution of Working Group I to the Sixth Assessment Report of the Intergovernmental Panel on Climate Change*. https://www.ipcc.ch/report/ar6/wg1/chapter/summary-for-policymakers/

IPCC. (2023). *Summary for Policymakers - Climate Change 2023: Synthesis Report*. https://www.ipcc.ch/report/ar6/syr/downloads/report/IPCC_AR6_SYR_SPM.pdf

Irrgang, A. M., Lantuit, H., Manson, G. K., Günther, F., Grosse, G., & Overduin, P. P. (2018). Variability in Rates of Coastal Change Along the Yukon Coast, 1951 to 2015. *Journal of Geophysical Research: Earth Surface*, *123*, 779–800. https://doi.org/10.1002/2017JF004326

Karjalainen, O., Luoto, M., Aalto, J., Etzelmüller, B., Grosse, G., Jones, B. M., Lilleøren, K. S., & Hjort, J. (2020). High potential for loss of permafrost landforms in a changing climate. *Environmental Research Letters*, *15*(10). https://doi.org/10.1088/1748-9326/abafd5

Kenny, T.-A., Wesche, S. D., Fillion, M., MacLean, J., & Chan, H. M. (2018). Supporting Inuit food security: A synthesis of initiatives in the Inuvialuit Settlement Region, Northwest Territories. *Canadian Food Studies / La Revue Canadienne Des Études Sur l'alimentation*, *5*(2), 73–110. https://doi.org/10.15353/cfs-rcea.v5i2.213

Kim, J. S., & Yethiraj, A. (2008). The effect of salt on the melting of ice: A molecular dynamics simulation study. *Journal of Chemical Physics*, *129*(12), 124504. https://doi.org/10.1063/1.2979247

Lachenbruch, A. (1962). Mechanics of Thermal Contraction Cracks and Ice-Wedge Polygons in Permafrost. *Special Paper of the Geological Society of America*, *70*, 1–65. https://doi.org/10.1130/SPE70-P1

Lachenbruch, A. (1966). Contraction theory of ice-wedge polygons: A qualitative discussion. *First International Conference on Permafrost*, 63–71. https://www.permafrost.org/wp-content/uploads/ConferenceMaterials/01st-International-Conference-on-Permafrost-Proceedings-Lafayette-Indianna-1966.pdf

Lim, M., Whalen, D., J. Mann, P., Fraser, P., Berry, H. B., Irish, C., Cockney, K., & Woodward, J. (2020a). Effective Monitoring of Permafrost Coast Erosion: Wide-scale Storm Impacts on Outer

Islands in the Mackenzie Delta Area. *Frontiers in Earth Science*, *8*. https://doi.org/10.3389/feart.2020.561322

Lim, M., Whalen, D., Martin, J., Mann, P. J., Hayes, S., Fraser, P., Berry, H. B., & Ouellette, D. (2020b). Massive Ice Control on Permafrost Coast Erosion and Sensitivity. *Geophysical Research Letters*, *47*(17). https://doi.org/10.1029/2020GL087917

Mackay, J. R. (1977). Pulsating Pingos, Tuktoyaktuk Peninsula, N.W.T. *Canadian Journal of Earth Sciences*, *14*(2), 209–222. https://doi.org/10.1139/e77-023

Mackay, J. R. (1978). Sub-pingo water lenses, Tuktoyaktuk Peninsula, Northwest Territories. *Canadian Journal of Earth Sciences*, *15*(8), 1219–1227. https://doi.org/10.1139/E78-130

Mackay, J. R. (1979). Pingos of the Tuktoyaktuk Peninsula Area, Northwest Territories. *Géographie Physique et Quaternaire*, *33*(1), 3–61. https://doi.org/https://doi.org/10.7202/1000322ar

Mackay, J. R. (1986a). Growth of Ibyuk Pingo, Western Arctic Coast, Canada, and some implications for environmental reconstructions. *Quaternary Research*, *26*(1), 68–80. https://doi.org/10.1016/0033-5894(86)90084-0

Mackay, J. R. (1986b). The first 7 years (1978-1985) of ice wedge growth, Illisarvik experimental drained lake site, western Arctic coast. *Canadian Journal of Earth Sciences*, *23*(11), 1782–1795. https://doi.org/10.1139/e86-164

Mackay, J. R. (1998). Pingo growth and collapse, Tuktoyaktuk Peninsula area, western arctic coast, Canada: A long-term field study. *Geographie Physique et Quaternaire*, *52*(3), 271–323. https://doi.org/10.7202/004847ar

Mackay, J. R., & Burn, C. R. (2002). The first 20 years (1978-1979 to 1998-1999) of active-layer development, Illisarvik experimental drained lake site, western Arctic coast, Canada. *Canadian Journal of Earth Sciences*, *39*(11), 1657–1674. https://doi.org/10.1139/e02-068

Maglione, P., Parente, C., & Vallario, A. (2014). Coastline extraction using high resolution WorldView-2 satellite imagery. *European Journal of Remote Sensing*, *47*(1), 685–699. https://doi.org/10.5721/EuJRS20144739

Manson, G. K., Couture, N. J., & James, T. S. (2019). *CanCoast 2.0: data and indices to describe the sensitivity of Canada's marine coasts to changing climate*. https://doi.org/10.4095/314669

Maxar Technologies. (2021). *Maxar Reaffirms its Commitment to Preserving the Space Environment*. Https://Blog.Maxar.Com/Space-Infrastructure/2021/Maxar-Reaffirms-Its-Commitment-to-Preserving-the-Space-Environment.

McHugh, M. L. (2012). Interrater reliability: the kappa statistic. *Biochemia Medica*, *22*(3), 276–282. https://doi.org/10.11613/BM.2012.031

McRoberts, E. C., & Morgenstern, N. R. (1975). Pore Water Expulsion during Freezing. *Canadian Geotechnical Journal*, *12*(1), 130–141. https://doi.org/10.1139/t75-012

Müller, F. (1962). Analysis of Some Stratigraphic Observations and Radiocarbon Dates from Two Pingos in the Mackenzie Delta Area, N.W.T. *Arctic*, *15*(4), 278–288. https://doi.org/10.14430/arctic3582

NWT Archives, & Department of Public Works and Services. (1987). *Randal Pokiak on top of a pingo in 1987*.

O'Neill, H. B., Roy-Leveillee, P., Lebedeva, L., & Ling, F. (2020). Recent advances (2010–2019) in the study of taliks. *Permafrost and Periglacial Processes*, *31*(3), 346–357. https://doi.org/10.1002/PPP.2050

O'Rourke, M. J. E. (2017). Archaeological site vulnerability modelling: The influence of high impact storm events on models of shoreline erosion in the Western Canadian arctic. *Open Archaeology*, *3*(1), 1–16. https://doi.org/10.1515/opar-2017-0001

Parker, S. (2021). *Coastal Sensitivity Index Summaries for Parks Canada Administered Sites*.

Parks Canada. (2020). *Pingo Canadian Landmark - National Historic Sites*. Https://Www.Pc.Gc.ca/En/Lhn-Nhs/Nt/Pingo.

Peterson, A. (2016). *Köppen climate types of Canada*. Https://Pt.m.Wikipedia.Org/Wiki/Ficheiro:Canada_K%C3%B6ppen.Svg.

Peterson, K. M., & Billings, W. D. (1980). Tundra Vegetational Patterns and Succession in Relation to Microtopography near Atkasook, Alaska. *Arctic and Alpine Research*, *12*(4), 473. https://doi.org/10.2307/1550495

Pingo Canadian Landmark Management Statement (2018).

Pingo Canadian Landmark Memorandum of Agreement (2001).

Rajakaruna, N., & Boyd, R. (2014). Geoecology. In *Oxford Bibliographies*. https://doi.org/10.1093/obo/9780199830060-0125

Rampton, V. N. (1987). *Surficial Geology, Tuktoyaktuk Coastlands, District of Mackenzie, Northwest Territories*. https://doi.org/10.4095/125160

Rantanen, M., Karpechko, A. Y., Lipponen, A., Nordling, K., Hyvärinen, O., Ruosteenoja, K., Vihma, T., & Laaksonen, A. (2022). The Arctic has warmed nearly four times faster than the globe since 1979. *Communications Earth and Environment*, *3*(168), 1–10. https://doi.org/10.1038/s43247-022-00498-3

Rowley, T., Giardino, J. R., Granados-Aguilar, R., & Vitek, J. D. (2015). Periglacial Processes and Landforms in the Critical Zone. In *Developments in Earth Surface Processes* (Vol. 19, pp. 397–447). Elsevier. https://doi.org/10.1016/B978-0-444-63369-9.00013-6

Saliqmiut - Tuktoyaktuk Centre for Arts and Culture. (2022). *Land of the Pinguqsaaryuit*. Https://Www.Saliqmiut.Com/Video-Gallery/v/Fkn946h9kxyflz72s43ryrdy7kppmc.

Screen, J. A., & Simmonds, I. (2010). The central role of diminishing sea ice in recent Arctic temperature amplification. *Nature*, *464*(7293), 1334–1337. https://doi.org/10.1038/nature09051

Sendrowski, A., Wohl, E., Hilton, R., Kramer, N., & Ascough, P. (2023). Wood-Based Carbon Storage in the Mackenzie River Delta: The World's Largest Mapped Riverine Wood Deposit. *Geophysical Research Letters*, *50*(7). https://doi.org/10.1029/2022GL100913

Sharma, V. K. (2010). Introduction to process geomorphology. In *Introduction to Process Geomorphology*. CRC Press - Taylor & Francis Group. https://doi.org/10.1201/b15108

Slaymaker, O. (2017). *Landscapes and Landforms of Western Canada* (O. Slaymaker, Ed.). Springer International Publishing. https://doi.org/10.1007/978-3-319-44595-3

Soare, R. J., Conway, S. J., Pearce, G. D., Dohm, J. M., & Grindrod, P. M. (2013). Possible crater-based pingos, paleolakes and periglacial landscapes at the high latitudes of Utopia Planitia, Mars. *Icarus*, *225*(2), 971–981. https://doi.org/10.1016/j.icarus.2012.08.041

Soare, R. J., Conway, S. J., Williams, J.-P., Gallagher, C., & Keown, L. E. M. (2020). Possible (closed system) pingo and ice-wedge/thermokarst complexes at the mid latitudes of Utopia Planitia, Mars. *Icarus*, *342*, 113233. https://doi.org/10.1016/j.icarus.2019.03.010

Stjern, C. W., Lund, M. T., Samset, B. H., Myhre, G., Forster, P. M., Andrews, T., Boucher, O., Faluvegi, G., Fläschner, D., Iversen, T., Kasoar, M., Kharin, V., Kirkevåg, A., Lamarque, J. F., Olivié, D., Richardson, T., Sand, M., Shawki, D., Shindell, D., … Voulgarakis, A. (2019). Arctic Amplification Response to Individual Climate Drivers. *Journal of Geophysical Research: Atmospheres*, *124*(13), 6698–6717. https://doi.org/10.1029/2018JD029726

Sturtevant, P. M., Lestak, L., Manley, W. F., & Maslanik, J. (2004). Coastal Erosion Along the Chukchi Coast Due to an Extreme Storm Event at Barrow, Alaska. In V. Rachold, H. Lantuit, N. Couture, & W. Pollard (Eds.), *Arctic Coastal Dynamics - Report of the 5th International Workshop* (pp. 114–118). McGill University, Montreal, Canada. https://www.researchgate.net/publication/242132406_COASTAL_EROSION_ALONG_THE_CHUKCHI_COAST_DUE_TO_AN_EXTREME_STORM_EVENT_AT_BARROW_ALASKA

Timmermans, M.-L., & Toole, J. M. (2023). The Arctic Ocean's Beaufort Gyre. *Annual Review of Marine Science*, *15*(1), 223–248. https://doi.org/10.1146/annurev-marine-032122-012034

Vermaire, J. C., Pisaric, M. F. J., Thienpont, J. R., Courtney Mustaphi, C. J., Kokelj, S. V., & Smol, J. P. (2013). Arctic climate warming and sea ice declines lead to increased storm surge activity. *Geophysical Research Letters*, *40*(7), 1386–1390. https://doi.org/10.1002/grl.50191

Vieira, G. (2020). *Pingo Canadian Landmark Simplified 3D Mesh*. Https://Sketchfab.Com/3d-Models/Pingo-Canadian-Landmark-1-8b0e1f9f388040d885e854e8f6da08c2.

Walker, J. (2019). *Living Tradition: Supporting the Inuvialuit Community of Tuktoyaktuk Through Productive Cultural Space* [Master's Degree Thesis, Dalhousie University]. https://dalspace.library.dal.ca//handle/10222/75439

Warburton, J. (2013). Patterned Ground and Polygons. In R. Giardino & J. Harbor (Eds.), *Treatise on Geomorphology* (Vol. 8, pp. 298–312). Academic Press. https://doi.org/10.1016/B978-0-12-374739-6.00213-X

Western Arctic (Inuvialuit) Claims Settlement Act (1984).

Williams, P. J., & Smith, M. W. (1989). *The Frozen Earth*. Cambridge University Press. https://doi.org/https://doi.org/10.1017/CBO9780511564437

Wolf, A. F. (2012). Using WorldView-2 Vis-NIR multispectral imagery to support land mapping and feature extraction using normalized difference index ratios. *Algorithms and Technologies for Multispectral, Hyperspectral, and Ultraspectral Imagery XVIII (Proceedings of SPIE Defense, Security, and Sensing)*, *8390*. https://doi.org/10.1117/12.917717

Wolfe, S. A., Morse, P. D., & Behnia, P. (2021). Spatial distribution of pingos in the Tuktoyaktuk coastlands and adjacent areas , Northwest Territories. *Geological Survey of Canada*. https://doi.org/https://doi.org/10.4095/328305

Wolfe, S. A., Morse, P. D., Parker, R., & Phillips, M. R. (2023). Distribution and morphometry of pingos, western Canadian Arctic, Northwest Territories, Canada. *Geomorphology*, *431*, 108694. https://doi.org/10.1016/j.geomorph.2023.108694

Wolter, J., Lantuit, H., Wetterich, S., Rethemeyer, J., & Fritz, M. (2018). Climatic, geomorphologic and hydrologic perturbations as drivers for mid- to late Holocene development of ice-wedge polygons in the western Canadian Arctic. *Permafrost and Periglacial Processes*, *29*(3), 164–181. https://doi.org/10.1002/ppp.1977

You, Q., Cai, Z., Pepin, N., Chen, D., Ahrens, B., Jiang, Z., Wu, F., Kang, S., Zhang, R., Wu, T., Wang, P., Li, M., Zuo, Z., Gao, Y., Zhai, P., & Zhang, Y. (2021). Warming amplification over the Arctic Pole and Third Pole: Trends, mechanisms and consequences. In *Earth-Science Reviews* (Vol. 217, pp. 1–25). Elsevier. https://doi.org/10.1016/j.earscirev.2021.103625

APPENDIX

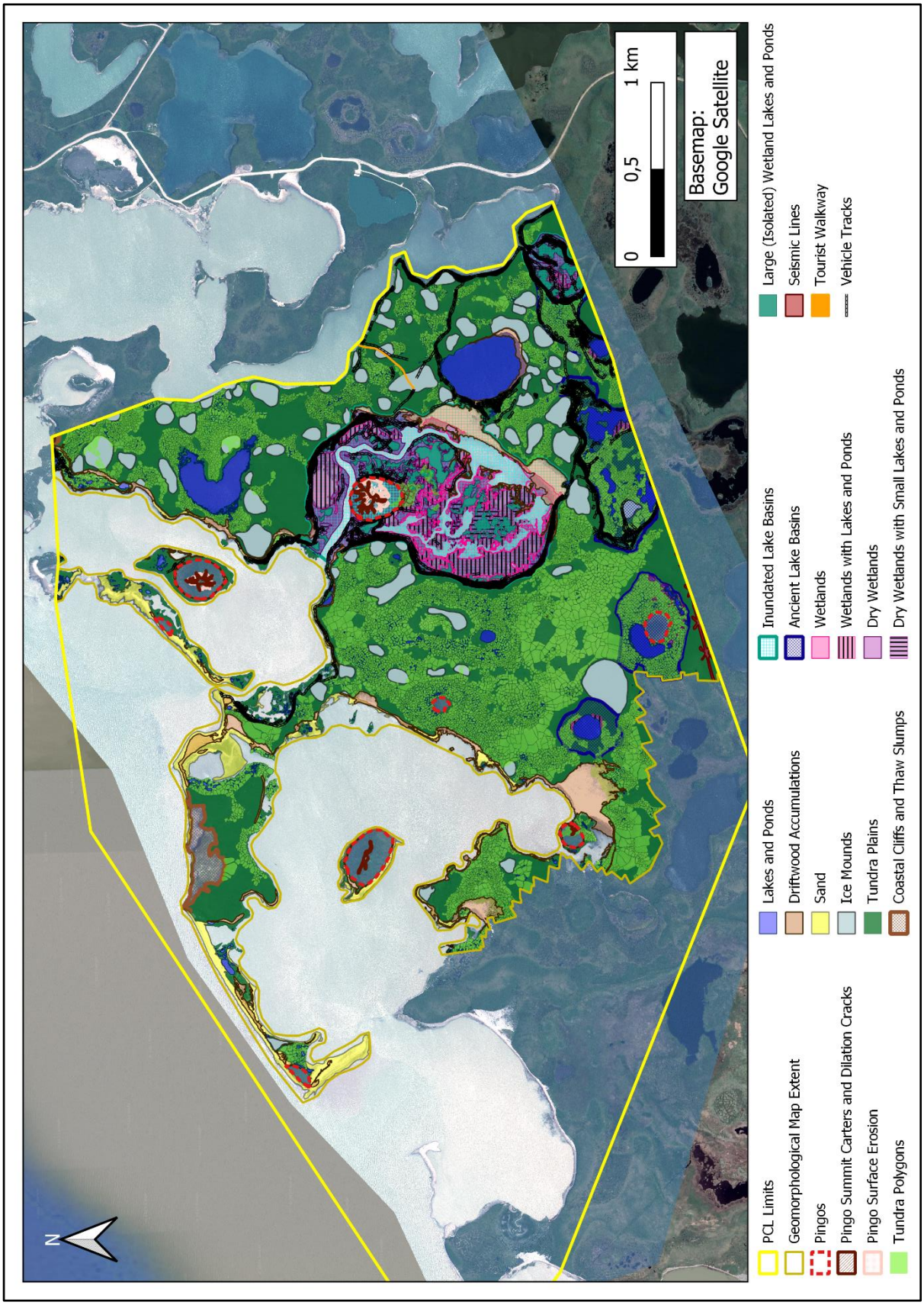

***Appendix Figure 1** – Geomorphological Map of Pingo Canadian Landmark.*

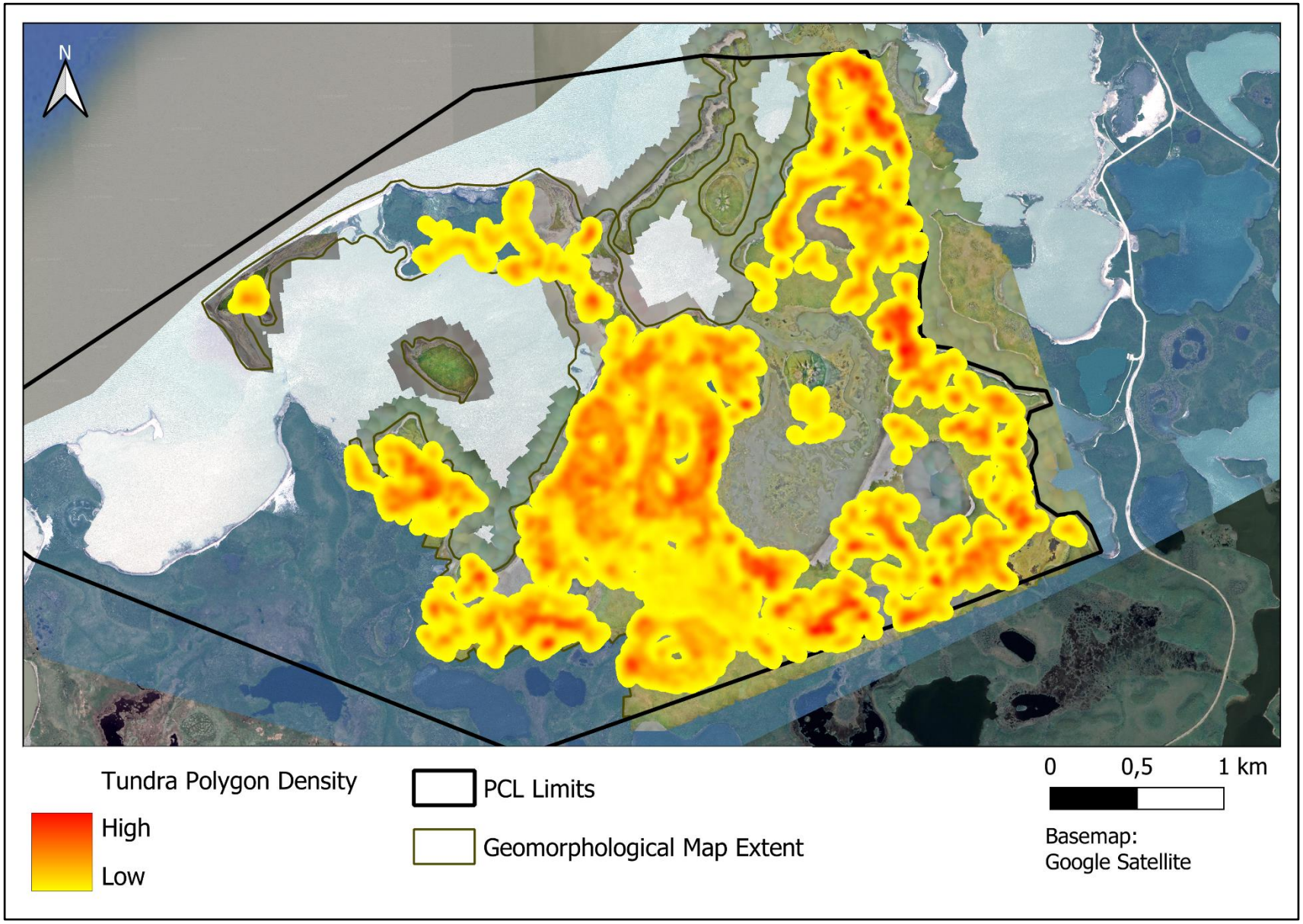

Appendix Figure 2 *– Tundra polygon heatmap of PCL (enlarged version of Figure 77).*

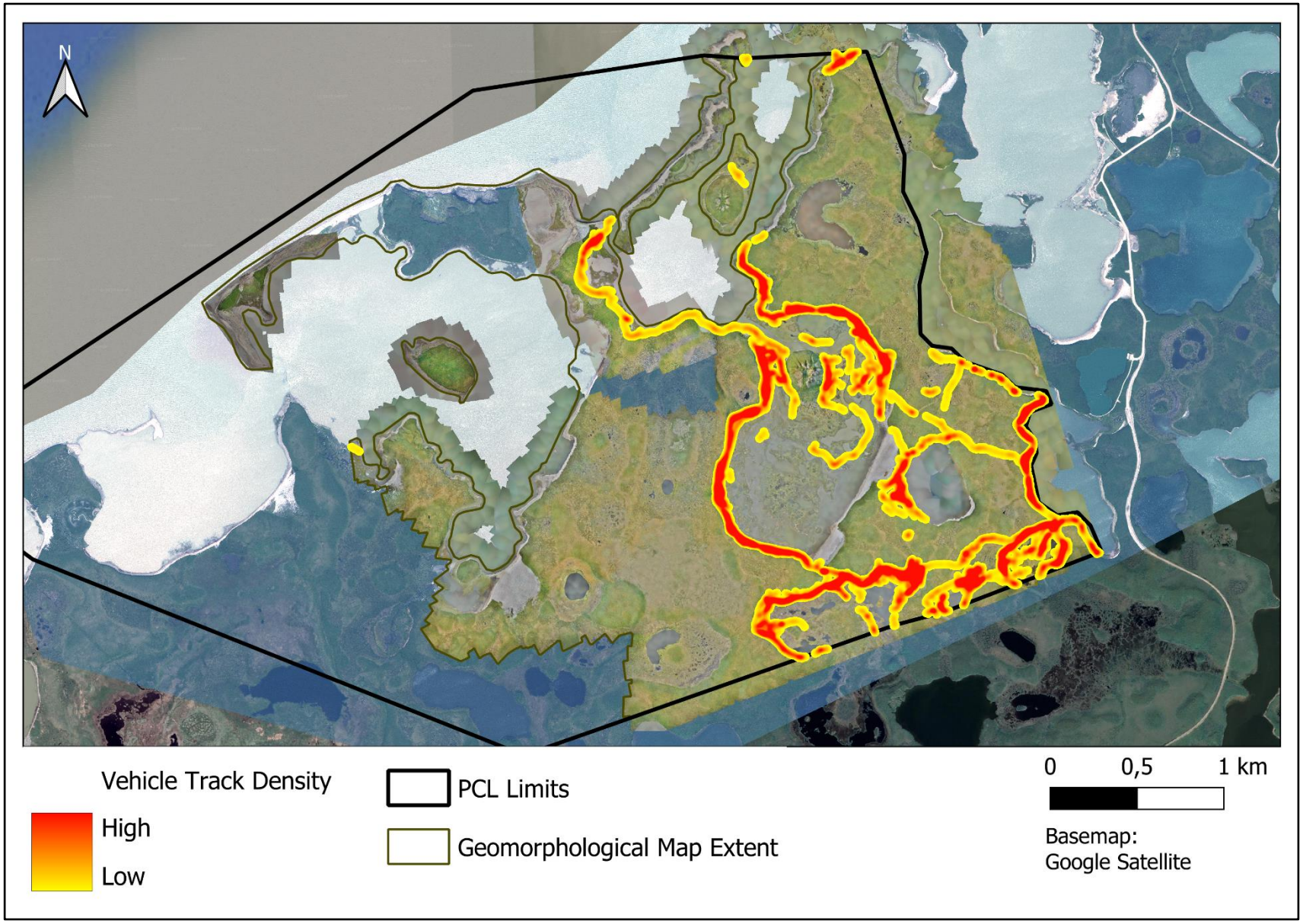

Appendix Figure 3 *– Vehicle track heatmap of PCL (enlarged version of Figure 88).*

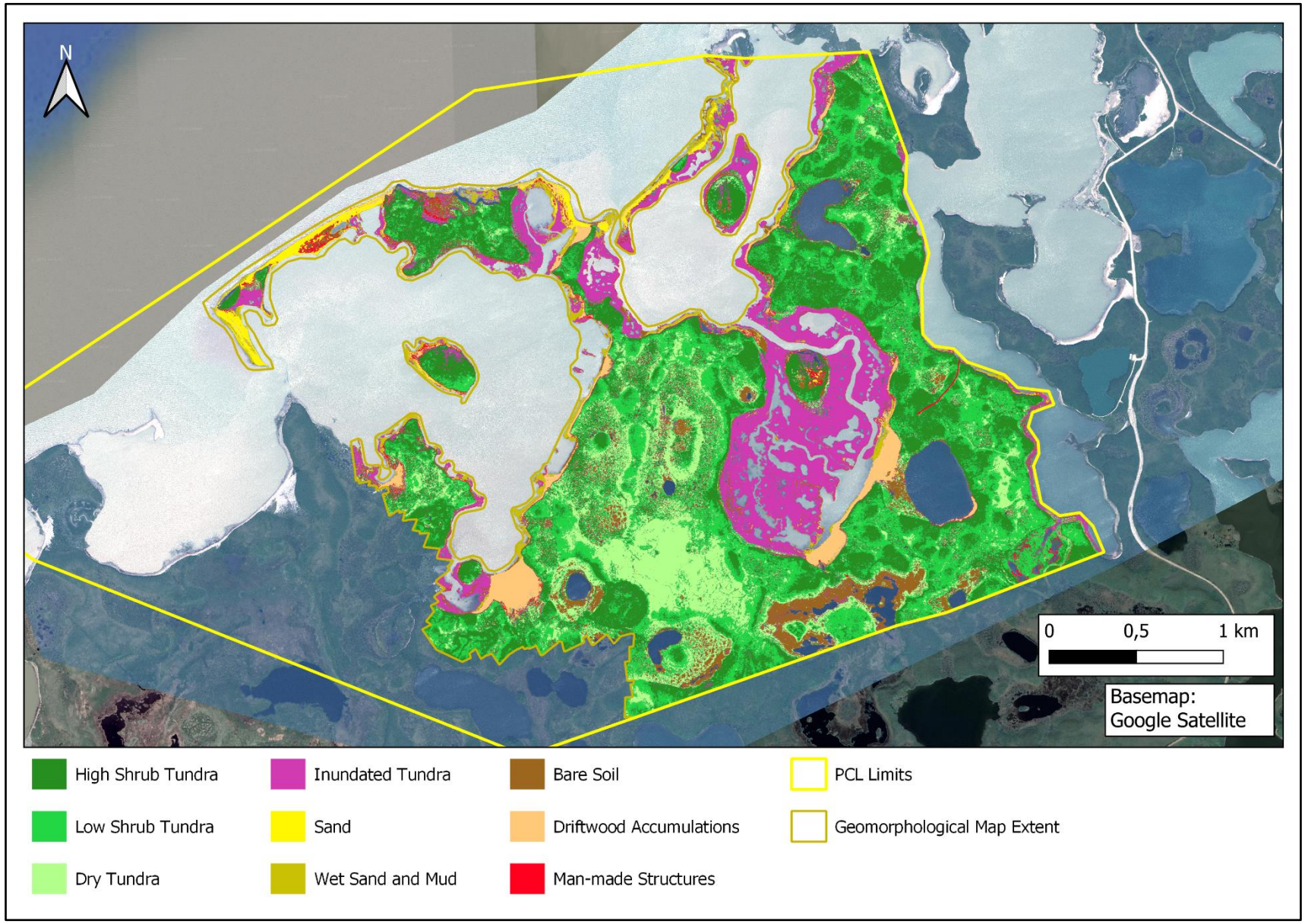

Appendix Figure 4 *– Landcover Map of Pingo Canadian Landmark.*

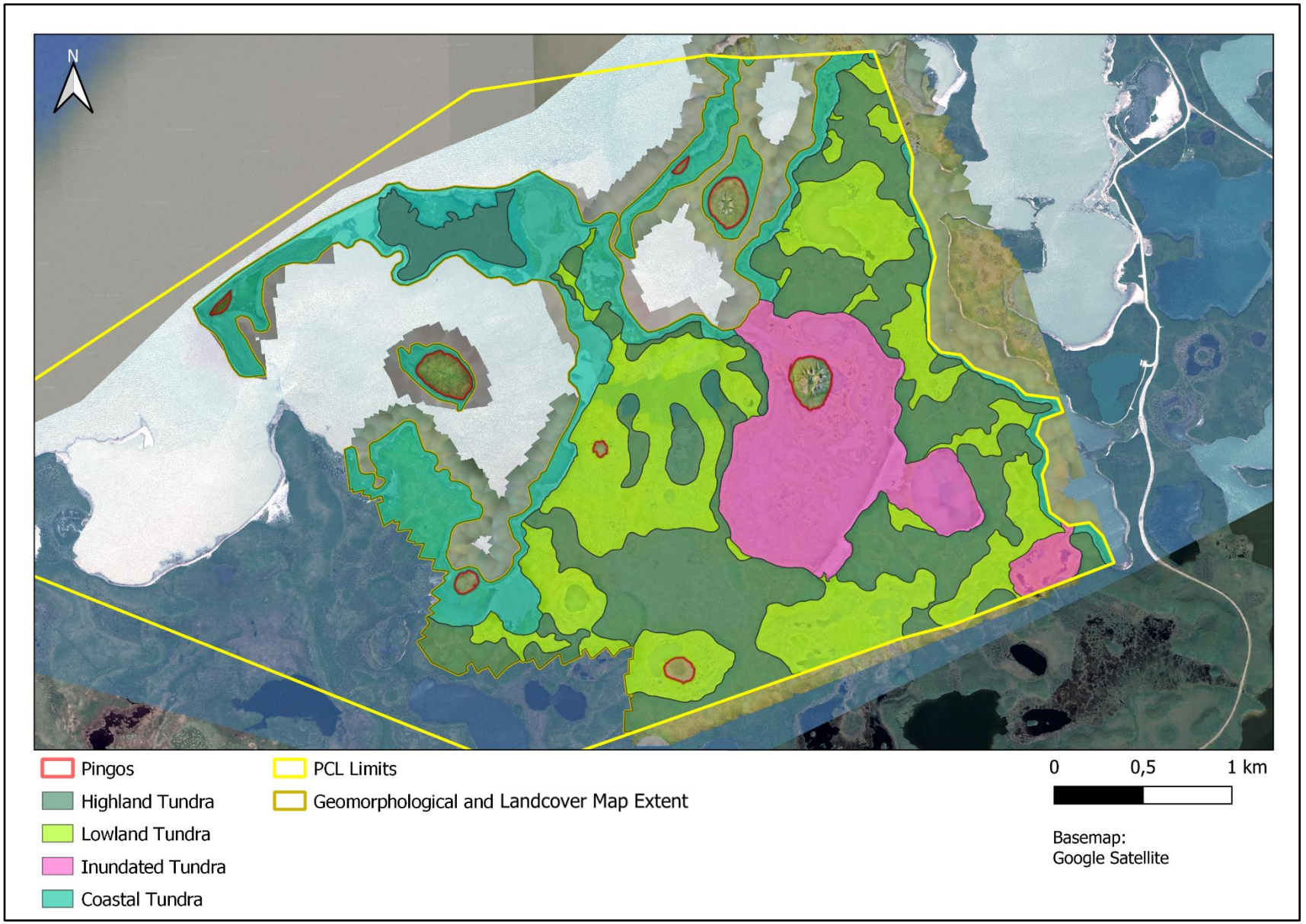

Appendix Figure 5 – *Geoecological Map of Pingo Canadian Landmark.*

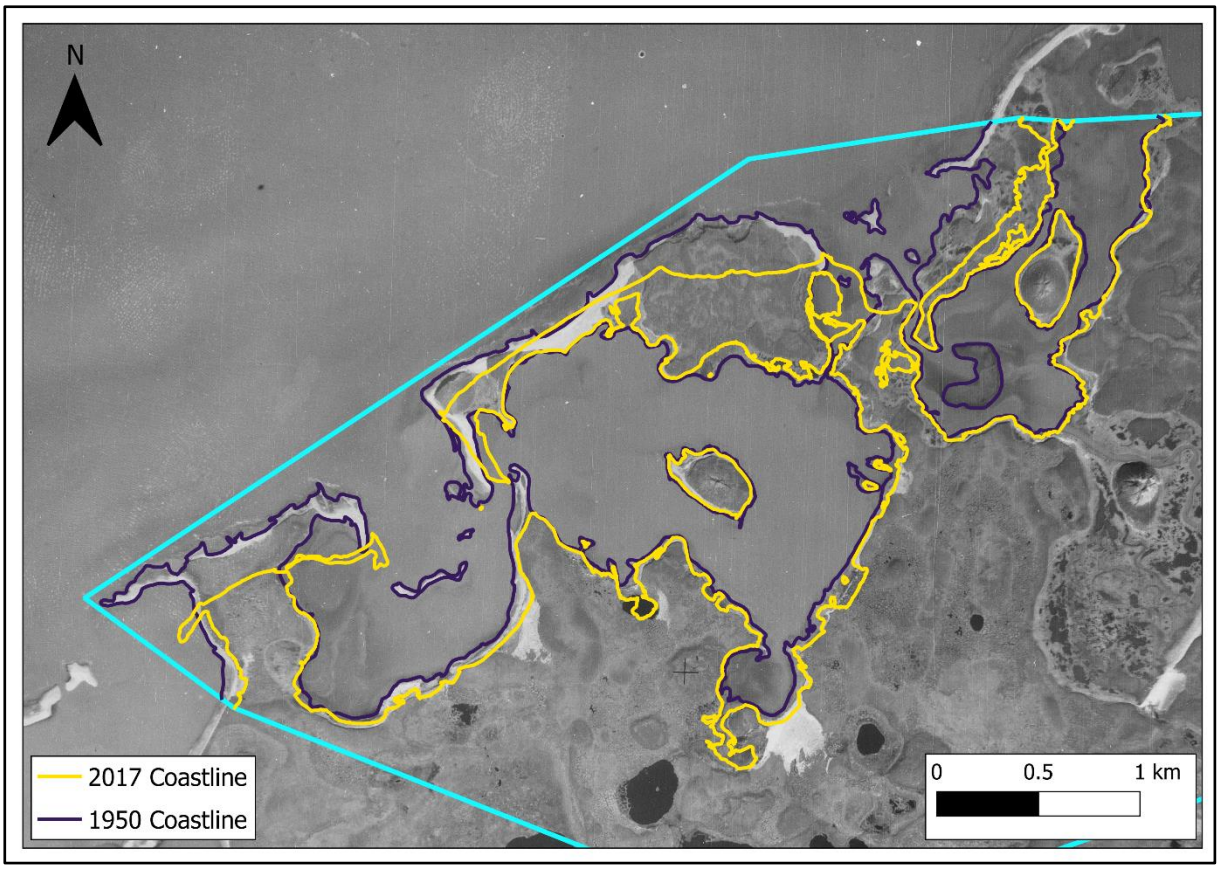

Appendix Figure 6 *– 1950 aerial photo, with coastlines of 1950 and 2017.*

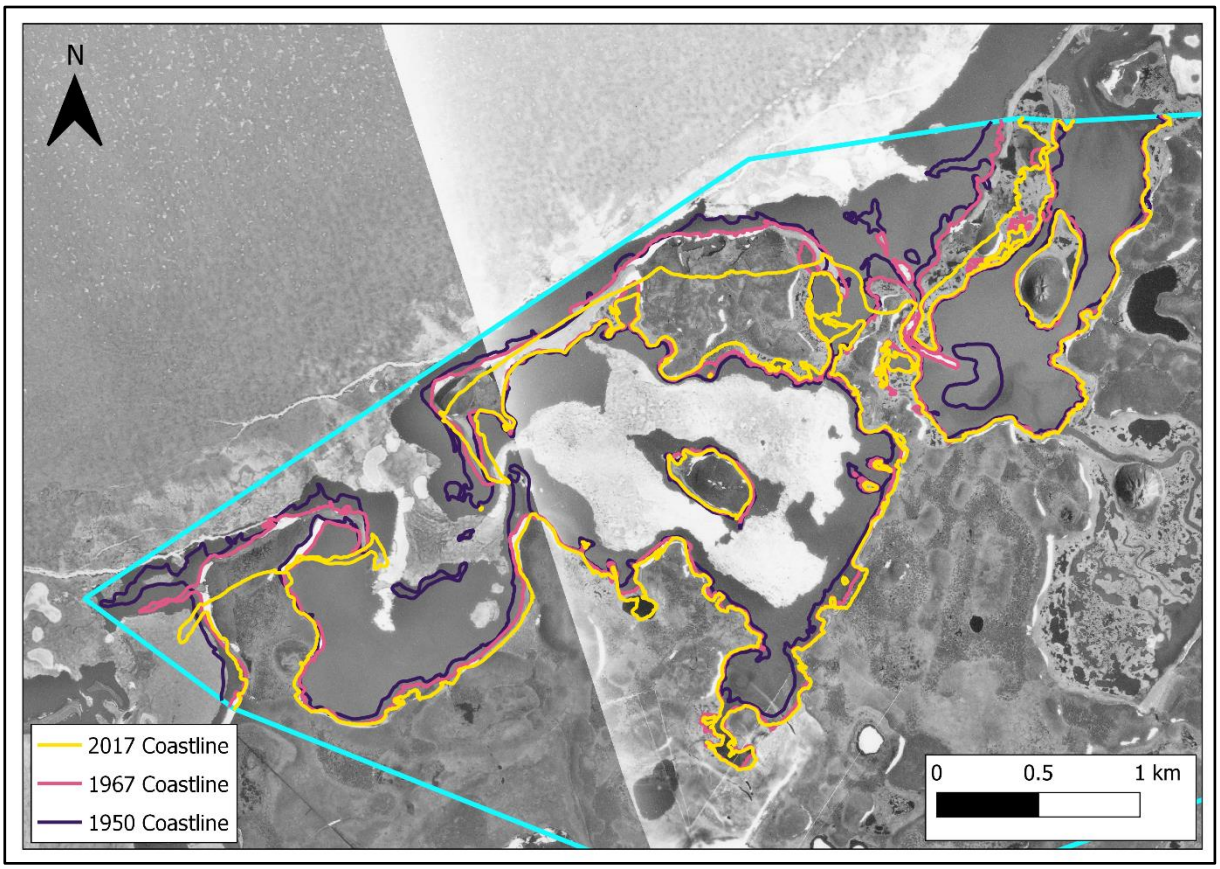

Appendix Figure 7 *– 1967 aerial photo, with coastlines of 1950, 1967 and 2017.*

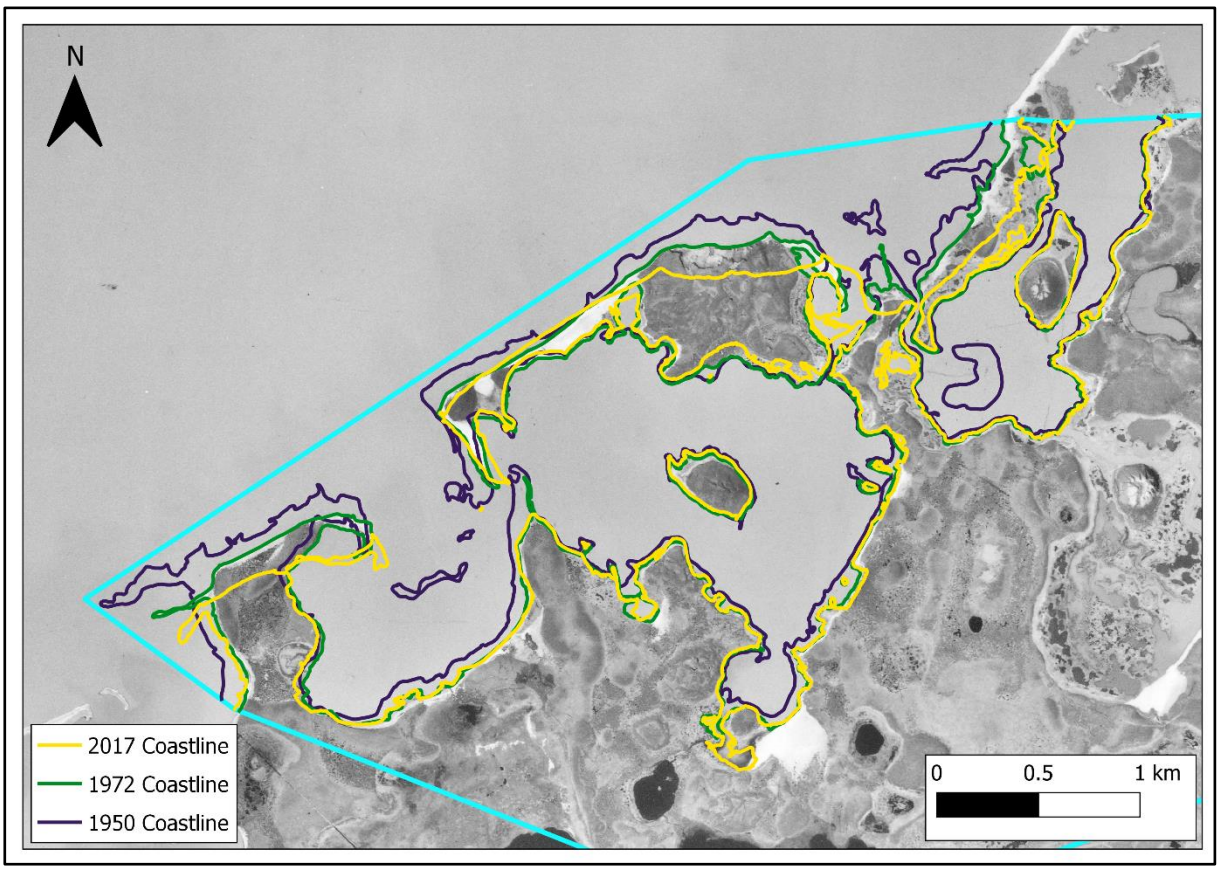

Appendix Figure 8 *- 1972 aerial photo, with coastlines of 1950, 1972 and 2017.*

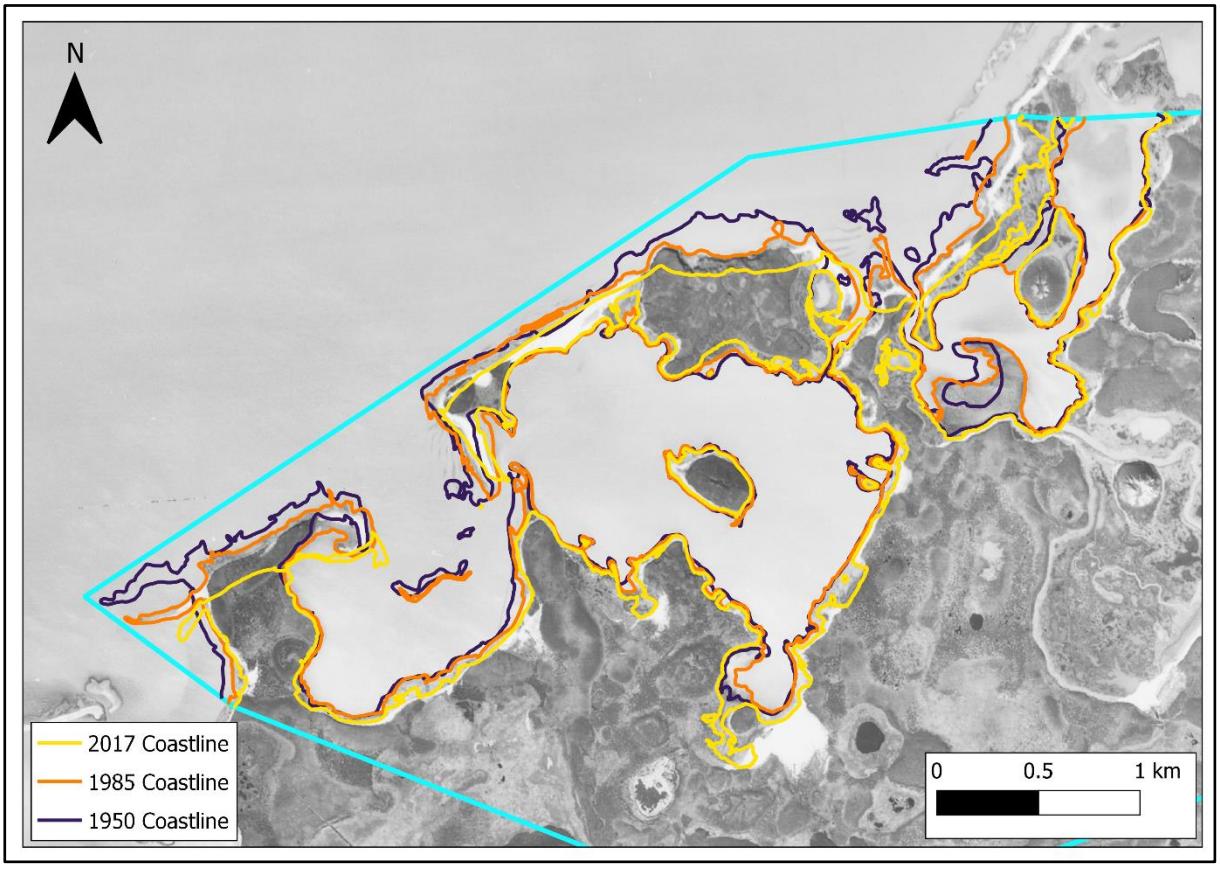

Appendix Figure 9 *- 1985 aerial photo, with coastlines of 1950, 1985 and 2017.*

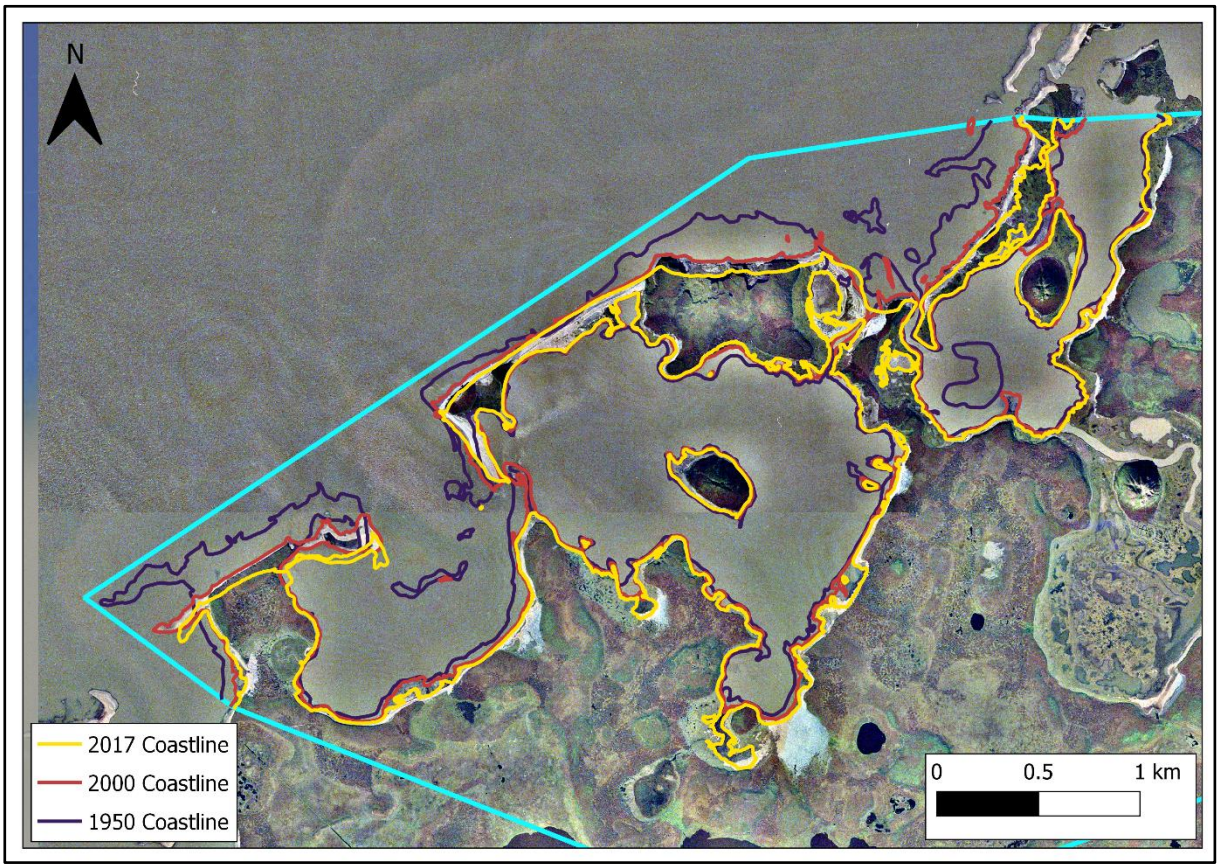

Appendix Figure 10 *- 2000 aerial photo, with coastlines of 1950, 2000 and 2017.*

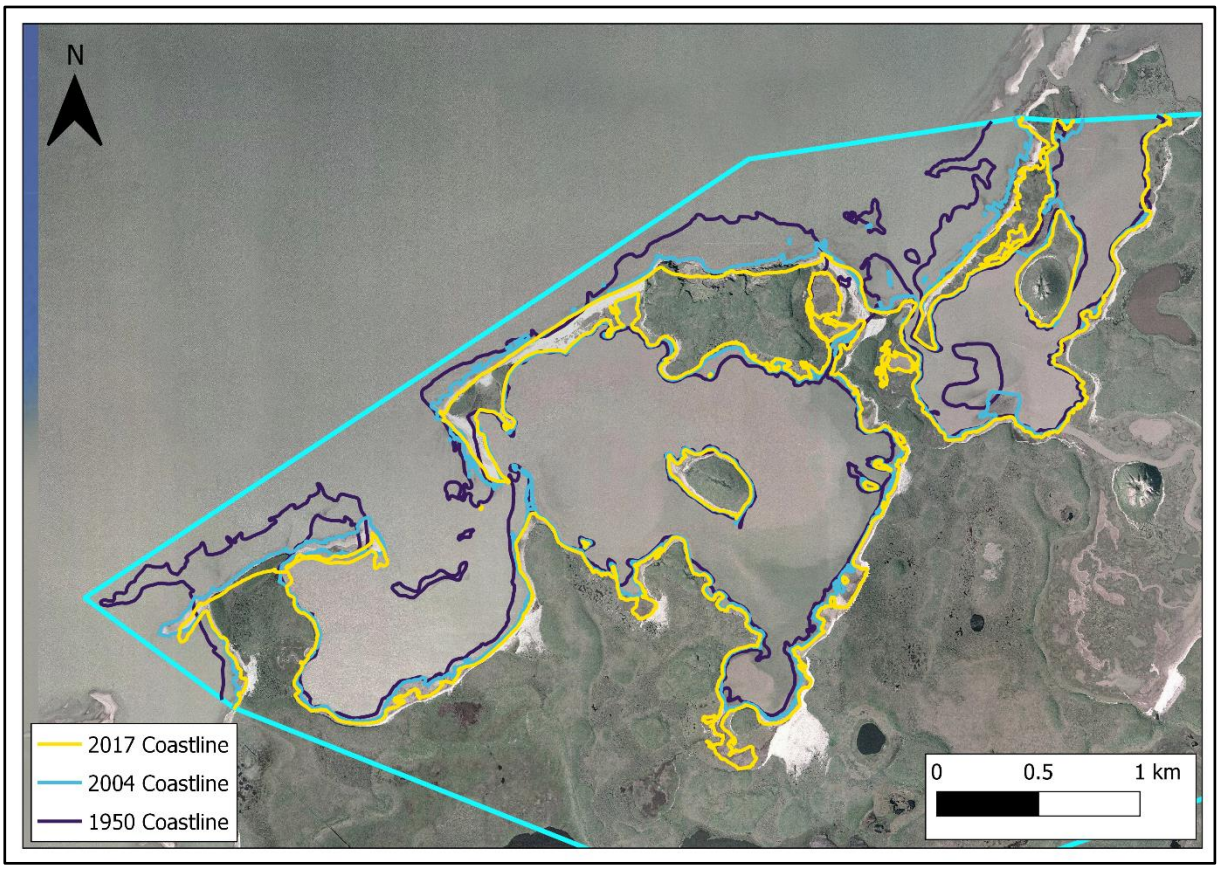

Appendix Figure 11 *– 2004 aerial photo, with coastlines of 1950, 2004 and 2017.*

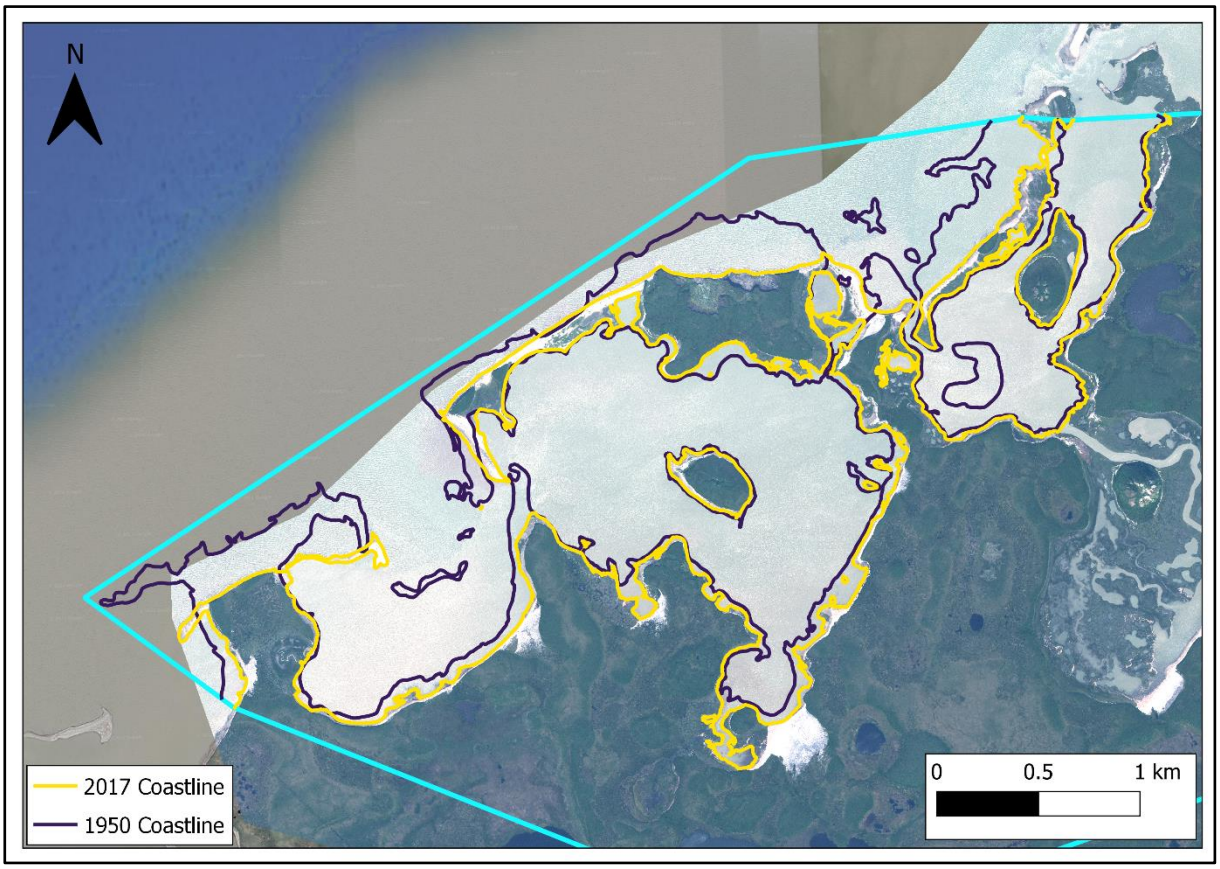

Appendix Figure 12 *– 2017 WorldView-2 scene, with coastlines of 1950 and 2017.*

Class Names	Pingos	Pingo Summit Craters and Dilation Cracks	Pingo Surface Erosion	Tundra Polygons	Lakes and Ponds	Driftwood Accumulations	Inundated Lake Basins	Ancient Lake Basins	Large (Isolated) Wetland Lakes and Ponds	Wetlands	Wetlands with Lakes and Ponds	Dry Wetlands	Dry Wetlands with Small Lakes and Ponds	Ice Mounds	Sand	Coastal Cliffs and Thaw Slumps	Tourist Walkway	Seismic Lines	Vehicle Tracks	Tundra Plains
High Shrub Tundra	169418,2	12030,8	7459,5	1451049,0	35060,1	34698,5	176950,7	202105,0	32942,1	3226,0	20840,4	70752,3	2803,9	540596,6	4741,2	18480,6	75,7	8066,2	46714,5	1576295,2
Low Shrub Tundra	133090,4	6335,1	6019,8	1720859,5	7922,3	39432,1	153310,6	307231,8	14524,1	2002,3	14104,5	86097,3	1642,7	530028,2	4601,6	17342,5	162,3	7018,5	66646,4	1863171,0
Dry Tundra	52146,7	3538,8	5238,2	1525303,8	4293,2	40897,4	123911,3	355534,0	7352,6	3372,8	12133,7	81836,9	2461,1	31611,4	6036,5	23952,5	0,0	1829,3	83562,9	1095382,3
Inundated Tundra	65710,8	6747,9	9403,4	315714,9	74171,0	129856,3	680581,1	164574,2	90511,5	84778,1	160371,6	255421,5	40307,4	33598,0	56930,1	53748,6	6,2	641,5	93818,1	562198,1
Bare Soil	50683,5	7825,7	14433,8	826286,2	76620,4	194826,8	298445,9	404425,9	18067,4	39211,4	46547,6	136252,7	12427,0	11835,3	73934,7	59830,9	61,7	634,0	105356,4	1135578,9
Sand	2895,9	411,5	1971,5	578,3	551,5	45802,2	11848,1	0,0	0,0	1238,5	0,0	990,6	0,0	0,9	124620,3	11,3	0,0	0,0	436,9	7792,8
Wet Sand and Mud	4057,2	794,0	2112,2	33019,4	3216,6	138661,6	143179,4	1069,8	1984,3	31101,5	24900,1	32826,0	1411,2	68,5	178178,5	16081,9	0,0	0,0	10337,5	89565,5
Driftwood Accumulations	3514,3	389,2	1400,4	17137,3	3395,6	249288,7	104980,4	0,0	174,4	16891,2	3751,7	13690,2	246,4	0,0	195865,9	22010,2	0,0	0,0	3144,5	30984,2
Man-made Structures	40384,7	7434,4	9718,6	137964,8	98497,6	211335,5	253749,0	57604,8	56322,0	24708,1	41315,0	61118,1	11060,1	6408,2	110440,4	51712,8	625,2	0,0	12464,4	393499,9

Appendix Table 1 *– Results of the overlap analysis. In this case, we can see for each class of the Geomorphological Map (columns) the extent in which it overlapped with each class of the Landcover Map (rows). Green cells indicate higher degrees of overlap. All values presented are in* m^2.

Class Names	High Shrub Tundra	Low Shrub Tundra	Dry Tundra	Inundated Tundra	Bare Soil	Sand	Wet Sand and Mud	Driftwood Accumulations	Man-made Structures
Pingos	169418,2	133090,4	52146,7	65710,8	50683,5	2895,9	4057,2	3514,3	40384,7
Pingo Summit Craters and Dilation Cracks	12030,8	6335,1	3538,8	6747,9	7825,7	411,5	794,0	389,2	7434,4
Pingo Surface Erosion	7459,5	6019,8	5238,2	9403,4	14433,8	1971,5	2112,2	1400,4	9718,6
Tundra Polygons	1451049,0	1720859,5	1525303,8	315714,9	826286,2	578,3	33019,4	17137,3	137964,8
Lakes and Ponds	35060,1	7922,3	4293,2	74171,0	76620,4	551,5	3216,6	3395,6	98497,6
Driftwood Accumulations	34698,5	39432,1	40897,4	129856,3	194826,8	45802,2	138661,6	249288,7	211335,5
Inundated Lake Basins	176950,7	153310,6	123911,3	680581,1	298445,9	11848,1	143179,4	104980,4	253749,0
Ancient Lake Basins	202105,0	307231,8	355534,0	164574,2	404425,9	0,0	1069,8	0,0	57604,8
Large (Isolated) Wetland Lakes and Ponds	32942,1	14524,1	7352,6	90511,5	18067,4	0,0	1984,3	174,4	56322,0
Wetlands	3226,0	2002,3	3372,8	84778,1	39211,4	1238,5	31101,5	16891,2	24708,1
Wetlands with Lakes and Ponds	20840,4	14104,5	12133,7	160371,6	46547,6	0,0	24900,1	3751,7	41315,0
Dry Wetlands	70752,3	86097,3	81836,9	255421,5	136252,7	990,6	32826,0	13690,2	61118,1
Dry Wetlands with Small Lakes and Ponds	2803,9	1642,7	2461,1	40307,4	12427,0	0,0	1411,2	246,4	11060,1
Ice Mounds	540596,6	530028,2	31611,4	33598,0	11835,3	0,9	68,5	0,0	6408,2
Sand	4741,2	4601,6	6036,5	56930,1	73934,7	124620,3	178178,5	195865,9	110440,4
Coastal Cliffs and Thaw Slumps	18480,6	17342,5	23952,5	53748,6	59830,9	11,3	16081,9	22010,2	51712,8
Tourist Walkway	75,7	162,3	0,0	6,2	61,7	0,0	0,0	0,0	625,2
Seismic Lines	8066,2	7018,5	1829,3	641,5	634,0	0,0	0,0	0,0	0,0
Vehicle Tracks	46714,5	66646,4	83562,9	93818,1	105356,4	436,9	10337,5	3144,5	12464,4
Tundra Plains	1576295,2	1863171,0	1095382,3	562198,1	1135578,9	7792,8	89565,5	30984,2	393499,9

Appendix Table 2 *- Results of the overlap analysis. In this case, we can see for each class of the Landcover Map (columns) the extent in which it overlapped with each class of the Geomorphological Map (rows). Green cells indicate higher degrees of overlap. All values presented are in m².*